UNIVERSITY OF LONDON THESIS

Degree PhD Year 2006 Name of Author BAHRA Amar Singh

NEWTON'S METHOD

IN

STATIC FORCE INFERENCE

FROM

REDUNDANT SPACE FRAME DYNAMICS

AMAR SINGH BAHRA

Doctoral Thesis Presented for the Degree of *Doctor of Philosophy*

University College London
April 2006

ProQuest LLC
789 East Eisenhower Parkway
P.O. Box 1346
Ann Arbor, MI 48106-1346

Numero pondere et mensura Deus omnia condidit.

——— Newton

Grau, teurer Freund, ist alle Theorie
Und grün des Lebens goldner Baum.

——— Goethe

Abstract

This thesis is concerned with inferring static, self-equilibrating, axial forces in redundant space frames from knowledge of their natural frequencies and associated mode shapes. Accordingly, it is necessary to have a mathematical description of the physical frame in an eigenproblem parameterised with variables accounting for load. Newton's method provides an iterative means of minimising the difference between the eigenvalues and eigenvectors and the measured frequencies and mode shapes they respectively represent; forces are thus inferred from the converged eigenproblem. Rather than updating all member forces, models are formulated on force distributions and scalars relating to the extent of loading form the updating parameters. Enforcing such equilibrium constraints beneficially minimises the order of Newton's method. For multiply redundant frames, it is necessary to formulate the model on a number of force distributions and any state of equilibrium can be described by their linear superposition. The ways in which load affects the dynamic characteristics are investigated thoroughly. Frequencies are shown to coalesce and exchange places in the spectrum, leading to non-smooth functions since the eigenvalues are numerically ordered. Mode tracing strategies, which utilise eigenvector consistency across coalescence points to conserve function smoothness, are investigated. This consistency, however, is observed to deteriorate if the eigenvalues exhibit veering. Measures facilitating mode tracing when consistency is deficient are explored. Special treatment is required at eigenvalue degeneracy in order to observe eigenpair differentiability, which is

necessary for Newton's method. Numerical simulations demonstrate success of force identification in a variety of contexts. Newton's method is effectively applied to identify load in actual, physical frames with single and multiple force distributions. Offset and length parameters supplement load to stabilise and improve the accuracy of solution. For complicated frames, it is shown that starting iteration in the eigenvector, as well as eigenvalue, neighbourhood is crucial for convergence to result.

Contents

List of Figures

List of Tables

Prologue

The purpose of this thesis has been to thoroughly investigate the prospect of identifying axial forces in space frames, solely from knowledge of their vibration modes. It is intended to be of benefit to those who seek to know the state of static loading, perhaps for reasons of monitoring structural integrity or for improving a mathematical model's description of a structure. Self-equilibrating, axial forces can easily develop in redundant frames due to a number of causes, such as non-uniform thermal fields or even lack-of-fit at fabrication. By inferring load from the actual physics of a frame, advantages are held over direct measurement methods using strain gauges, whose configuration relies on a load datum that cannot always be known. The work here outlined therefore holds much promise in providing a physically more sound means of identifying static load in space frames.

The foundation for such a concept to be successful is the assumption that the natural frequencies are significantly dependent upon loading, so that their magnitudes at different loaded states are capable of uniquely signifying the sizes of the axial forces that caused them to be what they are. It is necessary therefore to model the frequencies as functions of load. Due to the complexities of space frames, explicit functions of load cannot be determined; the frequencies can, however, be approximated at discrete values of load using finite element models. Solution of such models equates to determining the eigenvalues, which relate to the frequencies, of an eigenproblem parameterised with distributions of axial force; the associated eigenvectors

are capable of describing the mode shapes in which the modes oscillate.

The ways in which static, axial force distributions affect the dynamics of frames is a relatively unexplored area of research. Ch. 1 and Ch. 5 go some way into exploring such effects and it is found that there exist similarities between the dynamic, global system as a whole and the individual systems of the constituent beam members. Of particular note is that the fundamental global mode vanishes at the onset of buckling of the first member, just as the fundamental mode of a single beam vanishes at its Euler buckling load. Ch. 1 also surveys the complicated manner in which frames load statically and how this influences the dynamic characteristics.

Having a finite element model parameterised on load is simply not enough to identify axial forces and some means of bringing the model eigenvalues to closer agreement with a set of measured frequencies is needed so that the forces can be inferred. Newton's method[1] provides an iterative means for doing so, based on approximating the unknown eigenvalue functions as first order functions using their magnitudes and gradients. Effectively, the eigenvalue functions are modelled as their tangents and the problem is solved for the root of the tangent, some value of load. Repetition progressively takes iterates closer to the root of an actual, generally non-linear eigenvalue function if iteration is started in the neighbourhood of this root. For a single eigenvalue, λ, dependent upon a single load parameter, p, Newton's method

[1]Newton (1711), *De analysi per aequationes numero terminorum infinitas, 1669*, and Newton (1736), *Methodus fluxionum et serierum infinitarum, 1664-1671.*

evaluates progressive iterates as

$$p^{k+1} = p^k - \frac{\lambda(p^k)}{\lambda'(p^k)},$$

which can be illustrated as shown in the following figure.

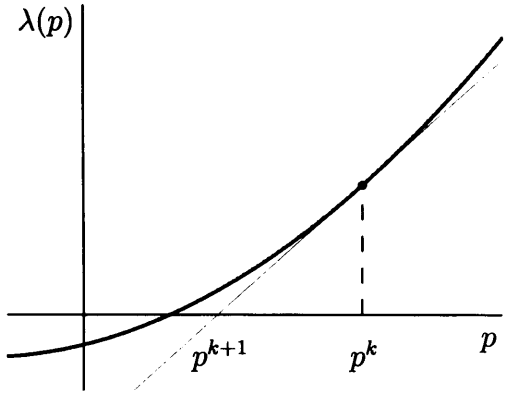

Newton's description of the method actually differs greatly from the modern implementation shown above. The method outlined in Newton's manuscripts does not even evaluate successive iterates p^{k+1} but computes a complicated sequence of polynomials. Although the modern method derives in a natural way from Newton's fundamental theorem of calculus, as shown in the course of this thesis, Newton failed to notice the connection with calculus and viewed the method as purely algebraic. A simplified description of Newton's original method, using successive iterates p^{k+1} instead of polynomial computations, was given independently by Raphson (1690); the modern iteration is therefore sometimes referred to as the Newton-Raphson method.

Considerable advancement in using Newton's method to identify frame loading is herein demonstrated compared to work by Greening (1999), upon which present work is founded. Formerly, the strategy was to update the

finite element model using all the frame member forces as updating parameters; in order to greatly reduce the number of updating parameters, and thus facilitate iteration and reduce computational cost, the notion of equilibrium constraints has been introduced. That is to say, *a priori* knowledge of the way forces distribute in a frame requires only one updating parameter that accounts for the extent of loading in a particular distribution. Such a concept is further seen to lend itself to describing the equilibrium of frames with multiple force distributions through the linear superposition of these distributions. The problem formulation is described in Ch. 2.

Another development from former frame load identification has been to overcome the problem of frequencies exchanging places in the spectrum. This is problematic because the eigenvalues that relate to the frequencies are numerically ordered and, due to this exchanging phenomenon, form non-smooth functions of load, which is detrimental to iteration. The consistencies of eigenvectors are used to trace out the true, smooth eigenvalue functions amongst a landscape of intersecting, overlapping functions. It is therefore necessary to know not only the frequencies of a frame, but also to extract its associated mode shapes so that the tracing of modes can be performed. How much the mode shape consistency can be relied upon throughout iteration is thoroughly investigated and it is found that veering of the eigenvalues is a mechanism by which it can greatly deteriorate. Mode tracing is outlined in Ch. 4 and its validity is investigated therein. Some strategies that potentially strengthen consistency, and thus aid mode tracing, are suggested and

explored in Ch. 4 and Ch. 7, one attempting to predict what the eigenvectors will become at the next iterate and another artificially tagging experimental frequencies with 'stronger', mathematical eigenvectors.

Since, under the influence of loading, frequencies exchange spectral positions, eigenvalues are coalesced at discrete load values. Function discontinuity at points of eigenvalue coalescence means that evaluation of the eigenpair derivatives there needs particular attention for differentiability to be observed. At coalescence, eigenvalues have equal magnitudes and so are degenerate or 'repeated'; their associated eigenvectors exist in a degenerate space, that is to say, their dimensions 'stick together'. The physical interpretation is a repeated frequency with mode shapes that are a number of distinct mode shapes superimposed. Degeneracy associated with transitorily coalesced eigenvalues has herein been overcome to make differentiability observable, as described in Ch. 3, through methods from the literature that anticipate the separation of the eigenvectors into distinct spaces along with the eigenvalue separation as load varies. Other, more intricate forms of eigenvalue degeneracy are also dealt with.

The proposed method of force identification has been implemented in a variety of numerical simulations, in Ch. 5, and on real, physical space frames possessing single and multiple distributions of axial force, in Ch. 6 and Ch. 7, respectively. Results are very encouraging and show that an unconstrained Newton's method is capable of converging upon force distributions and equilibrium states generated by multiple force distributions. The accuracy of

axial force identification is shown not to be affected by the number of force distributions required to describe equilibrium, with constraint of the solution being provided by the overall equilibrium state itself.

The load parameters of iteration schemes for real, physical frames have been supplemented with physically meaningful parameters that account for the effective lengths of the frame members. These are the member lengths themselves and joint offset parameters describing the finite lengths of the beams within the joints that oscillate as rigid bodies. The supplementary parameters are seen to stabilise convergence and provide a more accurate solution to the sought level of load.

Issues particular to more complicated frames, with a greater number of frame members, are noted and strategies to aid iteration are suggested. For such structures, mode shape consistency greatly, and rapidly, deteriorates away from the root, which encumbers the necessary tracing of modes. Starting iteration in both the eigenvalue and eigenvector neighbourhood is shown to be crucial. Successful convergence in such instances has been demonstrated, but finding more robust, global convergence methods that are less dependent on where iteration is started is deemed the main thrust for future work in the area of force identification.

Summaries of some of the work undertaken can be found in two papers: Bahra and Greening (2005a) and Bahra and Greening (2005b).

Acknowledgments

Thanks are firstly due to Dr Paul Greening for overseeing the work towards this thesis during the past few years. I would also like to acknowledge the following people:

> Jaafar Abdelhalim; Professor James Croll; Dr John Eyre; Professor Michael Friswell; Laurent Giampellegrini; Oliver Jones; João Filipe Rio; Tristan Robinson; Malcolm Saytch; Richard Sharp; Kenny Kataoka Sorenson.

I am grateful to the Engineering and Physical Sciences Research Council for their research funding.

Nomenclature

$\mathbb{R}$	real, Euclidean space
γ	coefficient describing how much an eigenvector contributes to a coupled mode shape
δ	Kronecker delta
ϵ	strain
η	offset, the length of the rigid portion of a flexural beam element, m
θ	phase angle, radians
λ	eigenvalue
$\boldsymbol{\lambda}$	m-tuple of eigenvalues
$\overline{\boldsymbol{\lambda}}$	m-tuple of eigenvalue differences, $\boldsymbol{\lambda}(\mathbf{p}^k) - \boldsymbol{\lambda}(\mathbf{p}^{\circledR})$
ξ	damping factor
ρ	density, kgm^{-3}
σ	singular value
ϕ	element of an eigenvector, degree of freedom
$\boldsymbol{\phi}$	eigenvector
$\boldsymbol{\varphi}$	left eigenvector
$\boldsymbol{\psi}$	arbitrary eigenvector at degeneracy
ω	circular frequency, 2πHz
$\boldsymbol{\Gamma}$	transformation matrix transforming $\boldsymbol{\psi}$ to their distinct-space, adjacent eigenvectors
$\overline{\boldsymbol{\Gamma}}$	transformation matrix numerically combining a set of eigenvectors to align with a single, root eigenvector
$\boldsymbol{\Theta}$	binary permutation matrix
$\boldsymbol{\Lambda}$	diagonal matrix of degenerate eigenvalues
$\boldsymbol{\Sigma}$	diagonal matrix of singular values
$\boldsymbol{\Phi}$	eigenvector matrix
$\boldsymbol{\Psi}$	matrix of arbitrary eigenvectors at degeneracy
automac	modal assurance criterion of a set of eigenvectors specifically amongst themselves
b	number of frame joints
c	general constant
crossmac	modal assurance criterion of a set of eigenvectors specifically with eigenvectors at some other parameter state
d	degree of eigenvalue degeneracy, eigenvalue multiplicity
e	normalised member force, element of $\mathbf{E}$

f	member force, N
$\mathbf{f}$	ℓ-tuple of member forces f_i, $i = 1, 2, \ldots, \ell$
i	vector designation, matrix row designation
j	matrix column designation
k	iteration number
l	beam effective length, m
ℓ	number of frame members
m	number of eigenvalue functions upon which Newton's method is formulated, number of functions of a linear set of equations
mac	modal assurance criterion
$\overrightarrow{mac}$	modal assurance criterion with the k^{th} iterate eigenvector forward-cast
$\overleftarrow{mac}$	modal assurance criterion with the $(k+1)^{th}$ iterate eigenvector backward-cast
n	dimensionality of Newton's method, degree of frame static redundancy
p	force parameter, P normalised to the lowest Euler buckling load
p_E^+	normalised positive buckling load, unity
p_E^-	normalised negative buckling load, the ratio of P_E^- to P_E^+
$\mathbf{p}$	n-tuple of force parameters p_i, $i = 1, 2, \ldots, n$
Δp	scalar Newton progression
$\Delta \mathbf{p}$	multidimensional Newton progression
p_{u_i}	force parameter, factor upon the i^{th} left singular vector of $\overline{\mathbf{E}}$
$\mathbf{p}_u$	n-tuple of force parameters p_{u_i}, $i = 1, 2, \ldots, n$
poc	pseudo-orthogonality check
r	modal designation
s	number of modes in the root subset
t	number of modes at the current iterate subset used to pair those in subset S
u	displacement
$\mathbf{u}$	left singular vector
$\mathbf{v}$	right singular vector
xor	cross-orthogonality, cross-mass-orthogonoality
$\overrightarrow{xor}$	cross-orthogonality with the k^{th} iterate eigenvector forward-cast
$\overleftarrow{xor}$	cross-orthogonality with the $(k+1)^{th}$ iterate eigenvector backward-cast
A	cross-sectional area, m^2
$A(\omega)$	accelerance, dB

$\mathbf{A}$ total stiffness matrix, $\mathbf{K} + \mathbf{G}$
$\mathbf{B}$ total mass matrix, equivalent to $\mathbf{M}$
D number of pre-buckled rigid body modes
E Young's modulus of elasticity
$\mathbf{E}$ equilibrium matrix
$\overline{\mathbf{E}}$ reduced, full rank equilibrium matrix
$\mathbf{G}$ geometric stiffness matrix
$\mathbb{G}$ geometric stiffness matrix shell, $\frac{1}{P}\mathbf{G}$, $P \neq 0$
$\mathbf{H}$ diagonal matrix whose elements are the reciprocals of the Jacobian column norms
I second area moment, m^4
$\mathbf{I}$ identity matrix
J St Venant torsional stiffness — for a circle, equal to the polar second area moment, m^4
$\mathbf{J}$ Jacobian matrix
$\mathbf{K}$ structural stiffness matrix
L beam length, m
$\mathbf{M}$ mass matrix
N order of eigenproblem, number of finite element model degrees of freedom
P force parameter, factor upon a distribution of axial force
P_E fundamental Euler buckling load, N
P_E^+ Euler load when a frame is loaded such that the member to buckle at the lowest value $|P|$ is in compression
P_E^- Euler load when a frame is loaded such that the member to buckle at the lowest value $|P|$ is in tension
$\mathcal{P}$ pencil, $\mathbf{A} - \lambda\mathbf{B}$
$\overline{\mathcal{P}}$ manipulated pencil — q.v. Eq$^{\underline{\mathrm{n}}}$ 3.33-3.34
$\mathbf{Q}$ matrix defined as $\mathbf{K}' - \lambda\mathbf{M}'$
S root subset of eigenvectors
T current iterate subset of eigenvectors
$\mathbf{T}$ coordinate transformation matrix of direction cosines
$\mathbf{U}$ left singular vector matrix
$\overline{\mathbf{U}}$ matrix of the first n columns of $\mathbf{U}$
$\mathbf{V}$ right singular vector matrix
$\mathbf{W}$ modal mass matrix

$'$ derivative
(n) n^{th} derivative
$*$ well-converged root quantity

$+$	generalised matrix inverse
$\dagger$	Moore-Penrose matrix inverse
e	'elemental', in opposition to 'global'
k	iteration number
T	transpose
R	analogous, mathematical root quantity
®	experimentally determined root quantity
Я	ambiguous, mathematical root quantity

$\lvert \quad \rvert$	vector modulus
$\lVert \quad \rVert_2$	Euclidean vector norm
$\lVert \quad \rVert_\infty$	infinity vector norm
$\longrightarrow$	set permutation, mapping
diag	diagonalise a zero matrix with a set of ordered elements
length	length of a vector, number of vector elements
range	range of a matrix, the space spanned by its columns
rank	matrix rank, the number of linearly independent matrix columns
trace	matrix trace, the sum of its diagonal elements

Note on subscripts:

Matrices, their columns and elements are designated in the following manner.

(Reference is never made to the rows of a matrix.)

$\mathbf{A}_i$	The i^{th} matrix of a set of matrices $\mathbf{A}_1, \mathbf{A}_2, \ldots$ &c.
$\mathbf{a}_j$	The j^{th} column vector of a matrix $\mathbf{A}$
a_{ij}	The scalar at the i^{th} row and j^{th} column of a matrix $\mathbf{A}$, mutually

Note on eigenvector lengths used in consistency evaluation:

Firstly, eigenvectors, say $\boldsymbol{\phi}^k$ and $\boldsymbol{\phi}^{®}$, used in a consistency evaluation, such as $mac(\boldsymbol{\phi}^k, \boldsymbol{\phi}^{®})$, are by definition of equal length. This length is therefore limited by the number of degrees of freedom available in the smaller of the two eigenvectors. Typically, $length(\boldsymbol{\phi}^{®}) < length(\boldsymbol{\phi}^k)$ because only a small

proportion of the degrees of freedom are measured for a physical frame. This is not hereafter stated, as the lengths of eigenvectors are inferable from the limiting number of degrees of freedom. If, however, the total number of eigenvector elements used to evaluate consistency is less than the total available, this *is* stated — for example, if only $\frac{N}{10}$ degrees of freedom out of a total N available are used, the dimensions of the eigenvectors are indicated, e.g., $mac(\boldsymbol{\phi}^{\circledR}_{\frac{N}{10}\times 1}, \boldsymbol{\phi}^{\boldsymbol{k}}_{\frac{N}{10}\times 1})$.

Note on units:

Frequently throughout the thesis, reference is made to values without stating their units. All units conform to the *Système International* and are shown in the Nomenclature.

Chapter 1

Axial Force Influence on Space Frame Dynamics

The effects of axial load on the vibrations of single beams are first described to give an appreciation of how constituent frame members behave in isolation. Some classic results are derived. Discussion and findings from the literature are presented, which focus, in terms of both static and dynamic behaviour, on the complexity of having beams coupled within frames. However, it is found that some analogy can be drawn between the characteristics of the constituent members and of a frame as a whole, such as the Euler buckling load coinciding with the fundamental frequency vanishing.

1.1 Dynamics of Axially Loaded Beams

The dynamics of axially loaded bars have been understood for some time; Lord Rayleigh (1877) in his Theory of Sound published detailed derivations from elemental forces and energies the equations governing the longitudinal, torsional and transverse vibrations of bars. It was there shown that the longitudinal and torsional vibrations can be described by the one-dimensional wave equation,

$$\frac{\partial^2 u}{\partial t^2} = c^2 \frac{\partial^2 u}{\partial x^2}, \tag{1.1}$$

where u, t, and x are respectively displacement, time and distance along the bar; c is a constant. The transverse vibrations were separately described through appreciation of the balance of potential and kinetic energies.

The work was extended to include the effects of longitudinal tension, most notably the raising of the natural frequencies. A thorough and comprehensive account of the effects of axial load on beam dynamics can be found in more recent papers: Shaker (1975), Bokaian (1988) and Bokaian (1990). These give closed form analytical and numerical solutions to the effects of both tensile and compressive axial load on the frequencies and mode shapes of beams with various boundary conditions. It is worth, at this point, reviewing the most basic of these findings.

The free motion of a beam can be described by the familiar differential equation

$$EI\frac{\partial^4 u}{\partial x^4} + P\frac{\partial^2 u}{\partial x^2} + \rho A\frac{\partial^2 u}{\partial t^2} = 0, \tag{1.2}$$

where E is Young's modulus, I the second area moment, P axial force (positive when compressive), ρ density and A the cross-sectional area. At frequency ω, it may be assumed that the beam vibrates in simple harmonic motion $u(x,t) = \overline{u}(x)\sin\omega t$, and thus the time-dependency of Eq$^{\underline{n}}$ 1.2 can be eliminated:

$$EI\frac{d^4\overline{u}}{dx^4} + P\frac{d^2\overline{u}}{dx^2} - \rho A\omega^2\overline{u} = 0, \tag{1.3}$$

or, defining the non-dimensional parameters

$$\xi = \frac{x}{L},\ p = \frac{PL^2}{\pi^2 EI} \text{ and } \Omega^2 = \frac{\rho AL^4}{EI}\omega^2, \tag{1.4}$$

$$\frac{d^4\overline{u}}{d\xi^4} + \pi^2 p\frac{d^2\overline{u}}{d\xi^2} - \Omega^2\overline{u} = 0. \tag{1.5}$$

The solution to Eq$^{\underline{n}}$ 1.5 is of the form $\overline{u} = Ue^{\alpha\xi}$, U constant, which is satisfied by the four roots of the bi-quadratic equation

$$\alpha^4 + \pi^2 p\alpha^2 - \Omega^2 = 0, \tag{1.6}$$

viz.,

$$\alpha_1 = \pm\left(-\frac{\pi^2 p}{2} + \left(\left(\frac{\pi^2 p}{2}\right)^2 + \Omega^2\right)^{\frac{1}{2}}\right)^{\frac{1}{2}} \tag{1.7}$$

and

$$\alpha_2 = \pm\left(-\frac{\pi^2 p}{2} - \left(\left(\frac{\pi^2 p}{2}\right)^2 + \Omega^2\right)^{\frac{1}{2}}\right)^{\frac{1}{2}}. \tag{1.8}$$

For brevity, it has been assumed that both the end conditions and mode shapes are symmetric about the beam centre at $x = 0$. The results, therefore, will be restricted to such modes.

Results for particular boundary conditions are now established. For the case of simple supports, the cosinusoidal solution $\overline{u} = U\cos(2n-1)\pi\xi$, U constant and n the frequency number, which satisfies the conditions of zero end displacement and curvature, substituted into Eq$^{\underline{n}}$ 1.5 gives the frequency equation

$$\Omega_n = (2n-1)\pi^2\left((2n-1)^2 - p\right)^{\frac{1}{2}}. \tag{1.9}$$

Eq$^{\underline{n}}$ 1.9 shows that for a simply supported beam, the natural frequencies are parabolic functions of the axial load. It is clear, and a point worth noting, that $\Omega_n \rightarrow 0$ as $p \rightarrow (2n-1)^2$, showing that the n^{th} frequency vanishes when $P_n = \frac{\pi^2 EI}{L^2}(2n-1)^2$, i.e., at the n^{th} Euler buckling load. Of course, only instability at $n = 1$ has any physical significance, the cases when $n > 1$ being purely of academic interest.

For a fixed-fixed beam, consider that the modes, which are restricted to being symmetric, are expressible as the even functions

$$\overline{u} = U_1\cos\alpha_1\xi + U_2\cos\alpha_2\xi, \tag{1.10}$$

which, when subjected to the boundary conditions $\overline{u}\left(\pm\frac{1}{2}\right) = d\overline{u}\left(\pm\frac{1}{2}\right)/dx = 0$, lead to the frequency equation

$$\alpha_1\tanh\frac{\alpha_1}{2} - \alpha_2\tanh\frac{\alpha_2}{2} = 0. \tag{1.11}$$

The approach for a free-free beam is identical, except that the boundary conditions are more involved. Since both ends are free, it is obvious that the bending moments there, and therefore curvatures, are zero: $d^2\overline{u}\left(\pm\frac{1}{2}\right)/dx^2 =$

0. The transverse force at the ends, however, is comprised of the shear force, $EI\,(d^3\overline{u}/dx^3)$ and the axial force component $P\,(d\overline{u}/dx)$. Hence the boundary constraints on Eq$^{\underline{n}}$ 1.10, for a free-free beam, are

$$\frac{d^2\overline{u}\left(\pm\frac{1}{2}\right)}{dx^2} = 0 \text{ and } \frac{d^3\overline{u}\left(\pm\frac{1}{2}\right)}{d\xi^3} + \pi^2 p \frac{d\overline{u}\left(\pm\frac{1}{2}\right)}{d\xi} = 0, \tag{1.12}$$

giving

$$\alpha_1^3 \tanh\frac{\alpha_2}{2} - \alpha_2^3 \tanh\frac{\alpha_1}{2} = 0. \tag{1.13}$$

Solution of these equations establishes the load-frequency loci of Fig. 1.1, such as are found in Shaker (1975), Bokaian (1988) and Bokaian (1990). These references further include other boundary conditions, combinations of boundary conditions, analysis of non-symmetric modes and the variations of the mode shapes with respect to axial force. Note that for a beam with simple supports, the Euler and vibration modes are of the same form so that there is no disturbance to the mode shape and the load-frequency relation is perfectly parabolic; the remaining relations are near parabolic. The frequency-load figure shows that for free-free and simple-simple boundary conditions, the frequencies of the beams vanish at the same load, a consequence of both having the same fundamental Euler load. For fixed-fixed boundary conditions, the fundamental Euler load is fourfold larger with the frequency seen to vanish at a value of $p = 4$. At zero load, a simply supported beam has non-dimensional frequency $\Omega = \pi^2$, with fixed-fixed and free-free beams both having non-dimensional frequency $\Omega = 22.373$.

Stephen (1989) uses the exact results of Bokaian to test the upper bound

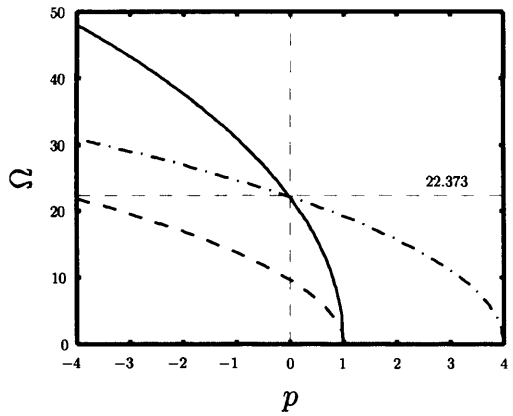

Figure 1.1: Classic beam frequency-load loci for three boundary conditions: ——— free-free; · — · — · — · fixed-fixed; — — — — simple-simple.

approximation to the fundamental frequencies of beams with various boundary conditions, as given by the Rayleigh quotient, and the lower bound approximation as given by the equation of Galef (1968):

$$\omega(P)^2 \approx \omega(0)^2 \left(1 - \frac{P}{P_E}\right), \tag{1.14}$$

where ω, P and P_E are respectively fundamental frequency, load and Euler buckling load. The author finds that the shortfalls in both the upper and lower bound approximations may be attributed to the dissimilarity between the static buckling and fundamental vibration modes of the beams, with the error increasing closer to buckling. Consequently, the upper and lower bound solutions coincide with each other and with the exact solution for the case of a simply supported beam since its buckling and vibratory mode shapes are identical.

Laura (1992) notes that following Bokaian's treatment of axially loaded Euler-Bernoulli beams, no effort has been made to account for the dynamics of axially loaded Timoshenko beams, which further account for shear

deformation as well as rotary inertia. Abrahamovich (1992) then develops the characteristic equations for the natural frequencies of compressed Timoshenko beams subject to ten different sets of boundary conditions. Only combinations of simple and hinged supports admit closed form solutions. For these boundary conditions, the given theory indicates that the ω^2-load relations are similar to what is indicated by the Euler-Bernoulli theory, but that a slight non-linearity is present, which increases with the radius of gyration of the beam (i.e., as the shear deformations of the beam become more significant).

Extensive research into axially loaded beams has revealed interesting phenomena. Liu et al. (1996) discover the fundamental mode of a tensed, free-free beam, previously overlooked, which is essentially the result of axial tension transforming the pitching rigid body mode into a strain mode; the frequency and mode shape of this mode are determined analytically and confirmed using a finite element formulation. Virgin and Plaut (1993) study the *forced* linear vibrations of a beam under tensile and compressive axial load with various boundary conditions. It is found that axial compression decreases the magnitudes of the frequencies and increases the vibration amplitude. The dynamics of the post-buckled state of a perfectly symmetric beam are studied by Virgin (1985), who shows that the ω^2-load relation initially following buckling is also linear but has a slope of -2 times that of the pre-buckled beam. Przybylski (2000) extends the work of Tomski et al. (1998) to analyse the effects of prestress on the vibrations of a two member

column excited by a follower force (an axial force that remains tangential to a deflected member). Amongst the findings are that prestress alters the instability mechanism under external load from flutter to divergence and that, although it acts to lower the critical external load, prestress may be used as a means of passive vibration control. Naguleswaran (2004) investigates the dynamics of a prismatic, Euler-Bernoulli beam subject to a linearly varying axial force with a constant component, and with a variety of boundary conditions, and finds that the Euler load and the vanishing of the fundamental frequency are again coincident.

Laura et al. (1983) find success in using polynomial functions to approximate the transverse vibrations of axially loaded, continuous beams with concentrated masses at span-wise locations. Jensen (2000) shows that high frequency, axial vibrations of an axially loaded, simply supported beam can increase its Euler load, although the beam may assume stable, buckled equilibria.

Knowing the frequency-load relations for a variety of boundary conditions, it is natural to want to utilise this for identifying the axial force in a beam. The identification of axial force in struts through inference from observed natural frequencies is outlined by Stephens (1936) and, exacting this, Lurie (1951), who also seeks to determine the degree of end fixity. Sundararajan (1992) contributes by proposing a simple secant method, utilising the quasi-linear ω^2-load relation of beams (linear for a simply supported beam), of approximating the fundamental frequency of an axially loaded beam, or

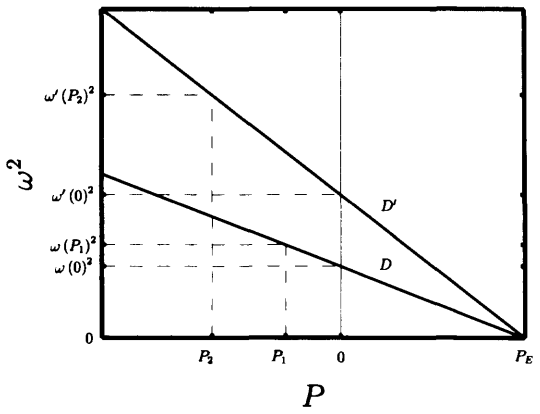

Figure 1.2: Frequency identification of mass-modified structures, as suggested by Sundararajan (1992): D, original structure; D', modified structure; ———— approximating functions.

other simple structure, by using a reference structure of the same stiffness distribution and therefore the same Euler buckling load. The method is suitable for estimating frequency values at loaded states of a structure that has been modified in terms of its mass distribution from an original structure, provided there is knowledge of the frequencies at zero load for both structures and that a further frequency is known for the original structure at some loaded state. This is illustrated by Fig. 1.2, from which it can be appreciated that the fundamental frequency approximation is

$$\omega'(P_2)^2 \approx \omega'(0)^2 + \frac{\omega'(0)^2 P_2}{\omega(0)^2 P_1}\left(\omega(P_1)^2 - \omega(0)^2\right). \tag{1.15}$$

Although not stated by Sundararajan, Eq$^{\underline{n}}$ 1.15 can alternatively be formulated as a force identification method:

$$P_2 \approx \frac{\omega(0)^2 P_1\left(\omega'(P_2)^2 - \omega'(0)^2\right)}{\omega'(0)^2\left(\omega(P_1)^2 - \omega(0)^2\right)}. \tag{1.16}$$

Such means of force identification are appealing in that they are passive and effective, but they do not analogise in an obvious way to intricate assem-

blies of members in frameworks, where there can exist severe distortions to the ω^2 loci due to dynamic system coupling. Not having closed form solutions or simple, approximating models necessitates the use of finite element models for force identification in more complex structures, such as space frames, as outlined in this thesis.

1.2 Static and Kinematic Effects of Variation in Frame Member Lengths

In many engineering fields, aerospace, civil, mechanical and oceanic alike, beams exist collectively in space frames. Changes in member lengths may be imposed on a frame without axial forces developing if it is statically determinate. The effect here is to alter the structural geometry as there are no redundant members restraining the movement of the structure. Indeed, such geometric alterations are prescribed to statically determinate frames such as antenna reflectors, where shape precision is of the utmost importance.

Utku et al. (1991) discuss the employment of actuators for incremental geometry control in determinate frames. The authors note that for small length adjustments, such as prevention of deviation from a desired geometry, piezoelectric or heat actuators suffice, whereas for situations requiring greater movement, hydraulic actuators are necessary. The study includes an example of one of the points of a crane moving along a prescribed trajectory, with two of the ten members forming the structure being length-adjustable. Haftka (1984), and later Haftka and Adelman (1985), investigate static shape

control by the prescription of forces and temperatures to members. The example of a beam shows that the effectiveness of actuation decreases rapidly as the wavelength of geometrical disturbance decreases, while for a tetrahedron module antenna finite element model a factor fifty reduction in thermal distortion is achieved by having seven of the four hundred and twenty rod members as controls. In two related works, Bushnell (1979a) and Bushnell (1979b), an attempt is made to control the surface shape of an axisymmetric shell using force actuators and actuators that produce self-equilibrating couples, indicating that the latter are more suitable for mirror reflector surface control.

It is in statically indeterminate or redundant frames that member strains generate force distribution throughout the structure, and the objectives for inducing these may be static or dynamic in nature. However, as Hanaor (1988) indicates, indeterminate structures can themselves be divided into kinematically determinate and kinematically indeterminate classes, and although prestress can be induced by virtue of their static indeterminacy, the latter class of structures, which includes cable networks and tensegrity structures, rely on prestress for geometric integrity and possess infintessimal mechanisms. Hanaor goes on to develop an algorithm for the design and optimisation of prestressed structures of both classes. An interesting study by Tarnai (1980) shows that a class of cyclically symmetric frame that is statically and kinematically determinate can, through pure geometry change, become prestressable even with the conservation of topology.

Stressless geometry control of redundant frames is still a possibility, as is demonstrated by Ramesh et al. (1991), but as the authors note the redundancy is computationally prohibitive to the objective.

As mentioned in many of these studies, including that of Hanaor and Levy (1985), a large proportion of space structures are designed for very small external load, meaning that self-equilibrating, internal member forces may become the dominant design consideration.

As well as for geometry control, a number of algorithms have been developed for optimising indeterminate space frames with static equilibrium or stability constraints. Hanaor (1988) suggests an algorithm derived from the flexibility method with the objective of optimising prestress effects on structural capacity, i.e., the amount of external load a structure can withstand. The formulation is intended for frames whose design is governed by the buckling of a critical member. N.B. As acknowledged by Cilley (1900), if weight is to be the objective function, then it is clear that an optimised structure will be determinate, that is to say a frame needs the minimum number of members to prevent it from becoming mechanistic, and in a complete state of stress (i.e., use is made of all members to resist an external load). Spillers and Levy (1984), however, discover that this is also true in their force optimisation results for a prestressed, *redundant* truss with two loading conditions, but note that without prestress the optimal design for the indeterminate frame is not in a state of complete stress. Essentially, this suggests that prestress helps, when the structure is externally loaded, in a way that relieves

otherwise over-stressed members and utilises the redundancies; without pre-stress, this extra structural strength is not utilised. Holnicki-Szulc (1979) and Levy and Hanaor (1991) show similar findings for singly-loaded trusses with, respectively, network theory and realisability theorems.

Notwithstanding the fact that static determinacy is synonymous with optimal design for static criteria, many structures are redundant for other reasons. Hanaor and Levy (1985) and Levy and Hanaor (1991) state that the minimum number of bars that need to be prestressed in an indeterminate structure in order to realise an optimum force system is equal to the number of redundant bars it comprises. Băluţ and Gioncu (1990) identify, in their discussion of geometrical tolerance effects on space frame behaviour, that prestress and the degree of redundancy are closely related. Indeed, as Greene (1983) and Hanaor and Levy (1985) state,

> **Axiom 1.2.1** 'The number of linearly independent force distributions in a statically indeterminate frame is equal to the degree of internal redundancy.'

Hanaor and Levy also discuss the way in which prestress enhances space truss design through utilisation of the compressive capacity of nominally tensile members. The objective of maximising the overall elastic limit load capacity through imposing lack-of-fit is investigated as well as the consequent minimisation of weight. It is decided that prestress should be provided through straining just a nominated set of redundant members. It is seen that the lack-of-fit pattern, i.e., the locations of the strained redundancies, suggested

by the algorithm therein is generally asymmetric, even for symmetric frames experiencing symmetric external forces, although the resulting, induced force distribution may well be symmetric. For fundamentally different patterns of imposed lack-of-fit, very similar force distributions result, whereas displacements are significantly different. The nature of these straining patterns, and the force distributions they induce, are later discussed in the following chapter and are exemplified in Ch. 5, and Ch. 7. There is the possibility of doubling the load capacity or halving the structural weight by imposing lack-of-fit; Holnicki-Szulc (1979) previously provided similar findings. Importantly, Spillers and Levy (1984) note that

> **Axiom 1.2.2** 'Any state of equilibrium can be realised through the prescription of member forces.'

Băluţ and Gioncu (1990) show that effects due to the existence or natural onset of lack-of-fit can be relieved by adjustable joints, but that there is a limit to the degree of accommodation that can be provided.

As Alpay and Utku (1973) indicate, loading of space structures may be random and non-deterministic. Greene (1983) uses an approach to evaluate the effects of random member length changes on the geometric accuracy and force distribution in antenna trusses statistically. Many deterministic, linear finite element analyses are performed with each member length error generated randomly per evaluation, in a Monte Carlo study. The resulting statistical properties are then used, with comparison to an ideal truss state, to appreciate the accuracy that can be met. Among the conclusions are

that a greater number of truss members decreases geometrical error whilst increasing the residual member forces, which is in concordance with concepts outlined hitherto, i.e., that a greater number of members is prohibitive to geometric control. Also, as the number of members increases, the static behaviour of the antennae tends to that of an equivalent continuum structure. (If the reader is interested, Rong et al. (2000) demonstrate the behaviour of a continuum structure, under dynamic constraints, as material is progressively taken away from it.) Similarly, Hedgepeth (1982) uses a statistical approach for the appreciation of random member imperfection errors and shows that for a very general class of structure the mean-square surface distortion is proportional to the sum of the inverse square of the vibration frequencies of the structure with an appropriately chosen mass distribution.

1.3 Dynamic Effects of Load in Space Frames

Dynamic control is of great importance in space structures, where varying thermal fields and a lightly damped environment, combined with the structural properties of light weight and high flexibility, call for adaptive structures. That is to say, such structures must be able to adjust their properties in order to withstand a variety of factors. Prestressing as a vibration controlling measure has received attention in the literature amongst other methods, such as those that modify the stiffness, mass and damping of a frame. It is appealing, perhaps due to the fact that the inherent properties of a skeletal frame can be utilised for control as opposed to having to alter the structural

form through the addition of structural components or dampers. Such alternatives would be particularly difficult for structures in space and prestress offers a means of remotely manipulating frames.

Using a finite element analysis, Natori and Iwasaki (1987) inspect the geometric and dynamic adaptiveness of indeterminate frames formed by the tessellation of octet[1] modules, and determinate frames created from them by the systematic removal of redundant members. Global curvatures in such frames, one module in amplitude, are achieved by length deviation in either the top and bottom members or the diagonal members, the former being analogous to bending and the latter shearing, with the bending effect having the greatest bearing on vibration frequencies. Unlike with a determinate frame, the actuation to induce these curvatures in an indeterminate frame must be provided synchronously in the assigned members so that internal loads do not exceed their critical values.

Anderson and Nimmo (1985) investigate, using the finite element method, member strain effects on statically determinate platforms with comparison to analogous, indeterminate platforms having identical size and joint arrangements, thus allowing relative stiffness to be a comparable quantity. The indeterminate frames are formed directly from the determinate frames, themselves tessellations of braced, cubic, skeletal boxes, by the systematic addition of diagonal bracing members. It is found that the indeterminate platforms have a fundamental frequency an order of magnitude greater than their de-

[1] An octet is a space-filling shape comprised of one regular octahedron with two regular tetrahedra adjoining two of its opposing faces. A space frame comprising octet modules is the subject of investigation in Sec. 5.8 and Ch. 7.

terminate analogues. Furthermore, their mode shapes, markedly different from those of the determinate frame platforms, are more akin to those of an equivalent, flat plate. This likeness obviously increases with an increasing overall platform size. Alternative configurations of members in the determinate frames are analysed to show that frequency increases are possible by providing member stiffness in certain directions, but it is apparent that the frequency of the redundant analogue is not attainable. The authors note that it is unlikely that an equivalent determinate frame could compete with the performance of an indeterminate frame. Modifications to statically determinate frames are suggested, without making them redundant, as it is desirable to avoid self-equilibrating, internal forces. These additions include members having controllable stiffness or locking mechanisms.

Alpay and Utku (1973) develop a program, based on the finite element method, to analyse structural response to random excitation of various systems, skeletal and continuum, under the influence prestress. Howson and Williams (1973) explore the natural frequencies of planar frames comprising Timoshenko beam members, both analytically, using the dynamic stiffness matrix method, and experimentally, with each in good agreement. The squares of the first four natural frequencies of a fixed aitch-frame are found to decrease almost linearly with respect to increasing axial load, which is equal in the parallel members, with the fundamental frequency becoming zero at the Euler loads of these members. This suggests that the critical member within a frame still governs the global dynamics, with its Euler load

coincident with the vanishing of the global fundamental frequency.

A comprehensive account of the effects of self-equilibrating forces in two simple, indeterminate frames is given by Mead (2002). Euler-Bernoulli beams are used in two analytical assemblies: two parallel beams joint at their ends and a six beam rectangular, cross-braced, planar frame. The stimulation for this is to give a qualitative account for the analogous effects in thermally stressed rectangular plates, the topic of a later work by Mead (2003). The objective is also to examine the effects of simultaneous tensile and compressive forces on the global frequencies of a frame. As Lord Rayleigh (1877), Shaker (1975), Bokaian (1988) and Bokaian (1990) demonstrate, the frequencies of bars and beams increase with tensile axial force and decrease with compressive axial force, the fundamental frequency vanishing when the Euler buckling load is reached, but the influence of global static force interaction on frame dynamics remains open to enquiry. Although only the symmetric modes of vibration normal to the planes of the frames are considered by Mead, many practical conclusions are made. For both of the frames studied, it is found that the fundamental frequency of the global system, like that of a single beam under compression, vanishes when the Euler buckling load of the most critical frame member is accomplished (this is also found by Ovunc (1980) in a matrix analysis of the effects of axial load on framework dynamics, and, as just mentioned, Howson and Williams). It is the relative buckling loads of the constituent members that dictate whether the global fundamental frequency will initially rise or fall as a particular member is compressed but

ultimately, this will vanish. Further, the variation of the second mode with respect to the axial force in any component member is always complimentary to the first. These comments are indicative of a phenomenon known as locus veering, which is discussed in some depth ahead in Ch. 4. The systems are investigated beyond the fundamental Euler buckling loads (there are two, depending on in which 'direction' the frame is loaded) to give wide ranges of effects on global frequencies. It is thus observed that when buckled, a beam within the frame will oscillate with large amplitude and its affects on neighbouring beams are dependent upon the joint fixity condition: if pinned, the remaining beams will oscillate in rigid body modes, but if fixed they will be rigid over their central portion and flexible towards their ends. Ovunc similarly finds that at buckling, members away from the local buckling will experience rigid body motion without internal strains and stresses.

An earlier study by Przybylski et al. (1996) reports on a two member, parallel beam model, as covered by Mead. Though not as detailed, many effects on the vibration modes are included: variations of external axial load, axial and flexural rigidity distributions and mass distributions between the beams, as well as variations in internal prestress. Experimental data are compared to analytical results, which concern at most the first two natural frequencies. It is found that any change in prestress from a zero state, positive or negative, entails a decrease in the frequencies observed. (N.B. Here, the second mode is asymmetric and its variation is not complimentary to that of the symmetric, fundamental mode.) The variation of the first frequency agrees with Mead,

and, as implied, for a frame comprising members of equal stiffnesses, the frequency is governed by the member in compression and therefore decreases; the frequency of the second, asymmetric mode follows the same pattern as the fundamental mode in the force range investigated. Conclusions are that the parameters investigated can be appropriately attributed to a system of members to passively control its natural frequencies, with greater asymmetry in parameter distribution providing greater variations in frequency.

Baycan et al. (1991) methodically express stiffness changes in indeterminate frames in terms of internal member strains, using a matrix formulation, with the intent of controlling vibration. The object is to manipulate the dynamics of a structure by modifying one of its three governing aspects: mass, stiffness and damping distributions. Although the geometric stiffness of a structure is in value very small compared to its material stiffness below yield, for the transverse modes of a planar truss, where the aforementioned stiffnesses are in different directions, the member forces become significant. It is found that for small member strains, upper bound estimations of the frequencies can be obtained by the application of perturbation theory to the eigenvalue problem (q.v. Eq^{n} 2.5).

Xiaocheng (1999) assesses the coupling effects of static, thermal and dynamic load on a simply supported beam and a continuum structure. The prestress, essentially caused by the static and thermal loads, is successfully accounted for by the finite element method and the effects on modal parameters agree well with analytical solutions. Indeed, the prospect of identifying

force by the methods explored in this thesis rely on the ability of a finite element model to describe the physics of a frame.

Considerable disturbances to modal parameters due to residual stress and prestress in indeterminate structures are investigated by Lieven and Greening (2001). The work includes experimental and finite element investigations of the effects of axial stresses on the transverse modes of a structure identical to the analytical frame of Mead (2002). Stress stiffening effects are included in a finite element model and load identification using Newton's method is performed. As shown by Mead, unlike for a single beam, the global frequencies reallocate in the spectrum by different amounts and in different directions with applied tension or compression. In one instance, the frequencies even exchange locations in the spectrum. This is indicative of a phenomenon known as loci coalescence, discussed in depth ahead in Ch. 4, and is essentially a load-wise crossing of the frequencies. The difficulty in correlating modes is attributed to geometrical variations by the authors, but, as will be shown in this thesis, deterioration in modal correlation can be solely due to the effects of load. A conclusion is made in which the prospect of identifying axial forces by using modal data in a wider range of problems is viewed as a distinct possibility.

In a later work, the previously investigated force identification method is further reviewed by Greening and Lieven (2003). This is an extension of undertakings of Stephens (1936) and Lurie (1951), which explore using dynamic measurement to quantify axial force and the degree of boundary

condition, or joint, fixity in columns — Sundararajan (1992) also contributes to this field with a method, which, although primitive, is analogous to the finite element method application of Greening and Lieven. The rectangular, cross-braced, planar frame is again used for illustration in a finite element model updating process, using Newton's method, that has each of the six member forces as variable parameters. A comparison of the converged axial forces to static strain gauge measurements indicates reasonable success in the method. A detailed account of employing Newton's method to identify static forces in planar frames is given by Greening (1999), which forms the foundation of the work in this thesis.

The effects of prestress on a narrow frequency band of a fifteen times indeterminate frame are investigated by Holnicki-Szulc and Haftka (1992) using a finite element formulation accounting for geometric stiffness. Their intent is to control vibration, not by displacing frequencies from a specific range, as, the authors state, it is unlikely that these can be distanced enough in the spectrum such that their effects become negligible, but to manipulate by prestressing the mode shapes to mitigate amplitudes in specified regions. The aim is to coincide modal nodes with critical regions, but the authors appreciate that this is not possible to achieve with a considerable number of modes. It is felt that the actuators that pre-exist in adaptive structures could be utilised for the above purpose. If enough members were to have actuation, then each force distribution could be investigated to determine the optimal prestress condition, but this is recognised as being unrealistic

and inefficient. The optimisation of the amount of prestress documented in the study is only a proceeding of optimum actuator placement, which is now discussed.

1.4 Frame Actuation

It has been seen that stressing may be used to control the geometry of a space frame. It may be the case that internal forces need to be prescribed to a space frame, perhaps to counter static forces that have naturally arisen or, more relevantly to the present issue, manipulate the frame dynamics. For example, it has been seen that, amongst a number of works, Holnicki-Szulc and Haftka (1992) apply such prestress to suppress modes shapes at designated locations while Baycan et al. (1991) do so to manipulate the frequency spectrum itself. Lu et al. (1999) show that the response of a seismic structure can be mitigated by active members. For these ends, actuators, capable of applying tensile and compressive axial forces, are incorporated into frames transforming them into what are known as adaptive structures. The distribution of actuators within frames has itself formed an important subject of research, recently receiving much attention.

Das et al. (1991) set down explicitly the feasibility of simultaneous displacement and force distribution control in frames of varying determinacy in terms of the number of actuators, the number of independent degrees of freedom at precision locations and the degree of redundancy. Specifically, it is shown that, if n is the degree of structural redundancy with n_ϕ inde-

pendent degrees of freedom requiring geometry control, then the number of actuators required for exact geometry control of these degrees of freedom without inducing stress is

$$n_a = n_\phi + n. \tag{1.17}$$

Exact geometry control is further possible if the following conditions are met, but stress induction will result:

$$n_\phi < n_a < n_\phi + n, \qquad n \geq 1. \tag{1.18}$$

This also directly implies that a space frame may be prestressed without disturbance to precision points. The authors show that n actuators are required to control all member forces, which is a consequence of Axioms 1.2.1 and 1.2.2.

A scheme for placing a limited number of actuators within indeterminate structures is given and is based on assignment of a determinate sub-structure from which the indeterminate structure is developed, if known; the scheme differs depending on whether this substructure is known or not. A suboptimal solution, developed from combining weighted solutions to geometry control and to force distribution control, is also suggested. The concept of including additional redundant members so that prestress is better distributed is explored. This motivates interest in the flow of force through frames of differing degrees of redundancy.

Jalihal et al. (1996) present work that gives algorithms placing additional, actuator-mounted, redundant members in determinate frames to ensure a

completely stressed structure for the overcoming of joint slackness. Without proper placement it is found that increasing the number of actuators is futile in achieving complete stress. Once the optimal prestresses are found, a measure to prevent local and global buckling is suggested.

The intricacy of the problem of placing an increasing number of actuators for vibration control is recognised by Chen et al. (1989) and is surmounted by the use of a developed algorithm that provides approximate solutions to passive and active member location[2]. Analysis of a very large structural system is thus made possible. In the context of this work, optimality is based upon the maximisation of the rate at which energy is dissipated in a structure, since this is indicative of the extent of damping augmentation; the limited approach of striving to attain specific dynamic characteristics is not sought. The addition or removal of actuators results in a discrete change in the structural response and the authors note this entails the optimisation problem being generally more irksome than a continuous optimisation. The proposed methodology includes steps to overcome stagnation in a local optimum, an obstacle that most iterative improvement techniques face. The heuristic technique outlined, which has the capability of discovering the global optimum solution to the placement problem, is named the annealing technique on account of its analogy to the gradual cooling of highly energised atoms in a solid, characterised by overall energy dissipation, with occasional energy upsurges, to a crystalline state; normal iterative techniques

[2]Within a frame, a passive member is one that passively controls vibration and whose properties are fixed, for example a member fitted with a damper; an active member, in the present context, can be force-actuated based on feedback data from a sensor.

are similarly analogised to quenching or rapid cooling to a state lacking order. Non-improving solutions are accepted by the technique according to the Boltzmann probability function in order that the iteration does not settle at a local optimum. Subsequent realisations are created by random perturbations to the current realisation, and again this is in analogy to material cooling; the best solution is always noted. Implementations of the method are included in which a combination of active and passive actuators are optimally placed in a cantilevered boom and in a hundred and fifty member tetrahedral space frame (N.B. the combinatorial problem of placing the ten actuators in the latter frame has in excess of a quadrillion solutions — but the authors state from experience that the algorithm functions better for larger problems).

Haftka (1984) notes the difficulty in anticipating the dynamic disturbances of frames and hence in placing actuators and how for any given actuator configuration there exists some uncontrollable disturbance or disturbances. Thus design against the worst disturbance to be experienced is not always possible. An internally indeterminate, externally determinate frame subject to large wavelength, and hence slowly varying, disturbances is optimally fitted with controls; small wavelength disturbances are neglected on grounds that they are associated with small amplitudes and are therefore of lesser concern.

Other works regarding the optimal placement of active members in space frames include Mackiewicz et al. (1995) and Gao et al. (2003), who concentrate on the placement of sensors for the benefit of actuation; a recent liter-

ature review on mode shape control through actuation is offered by Irschik (2002).

Chapter 2

Problem Formulation

The previous chapter showed that the frequencies of a single beam can be formulated as explicit functions of the axial load it experiences. In this case, the identification of load from a given frequency would be a trivial inverse problem. This is not practical for more complex systems, such as space frames, since the explicit load dependency of the frequencies is by no means easily derived. However, frequencies and mode shapes may be evaluated at discrete load values through modelling the mass and stiffness distributions and solving the resulting eigenvalue problem. Static load effects are included through a geometric stiffness matrix, which modifies the total stiffness by accounting for the changes in flexural stiffness due to axial forces. With the frequencies and mode shapes functions of load, Newton's method provides an iterative means for solving the force identification problem of finding the magnitude of load from a given set of measured frame frequencies. The concept of how overall equilibrium can be described by force distribution superposition is outlined.

2.1 The Eigenproblem

Newton's second law of motion for the time-dependent displacement $\mathbf{u}(t)$ can be expressed for the free vibration of an undamped, axially loaded space frame in terms of its distributions of mass $\mathbf{M}$, structural stiffness $\mathbf{K}$ and geometric stiffness $\mathbf{G}$ as

$$\mathbf{M}\frac{\partial^2 \mathbf{u}}{\partial t^2} + \mathbf{K}\mathbf{u} + \mathbf{G}\mathbf{u} = \mathbf{0}. \tag{2.1}$$

The geometric stiffness is a function of the distribution of axial forces and all of its elements are linear functions of some scalar parameter, P, characterising the extent of loading in an entire force distribution. This differs from the approach investigated by Greening (1999), in which the sought root parameter is a particular member force. Such a formulation necessitates finding all ℓ frame member forces of a distribution independently and makes no use of *a priori* equilibrium knowledge. Although there may be a number of force distributions, n, the number of members, ℓ, is always much larger, and so by imposing equilibrium constraints, the computational cost associated with finding all of the member forces is greatly diminished in the current formulation.

The matrix $\mathbf{G}$ is assembled from ℓ elemental, geometric stiffness matrices, $\mathbf{G}^e$, one corresponding to each of the ℓ members and accounting for the effects of each of the member forces. These member matrices are added to the elements of $\mathbf{G}$ according to the degrees of freedom at the member ends. No thorough account of the well established finite element method is given here,

but details can be found in, for example, Przemieniecki (1968) and Cook (1974). The three-dimensional beam, elemental, geometric stiffness matrix $\mathbf{G}^e$ used is given in Appendix A and accounts for the interaction of axial force with bending in the principal directions, St Venant torsion and flexural shear as the element vibrates. Further, the structural and geometric stiffness matrices are consistent in the sense that for every first order stiffness term in the former, there is a corresponding second order term in the latter. N.B. The factors e_{ij} of each $\mathbf{G}^e$ account for the *relative* values of axial force in a given force distribution, i.e., for a given distribution all ℓ scalars e_{ij} form a normalised set of forces in equilibrium. These are actually the elements of an equilibrium matrix, the concept of which is introduced in Sec. 2.4.

It is convenient to express the geometric stiffness as

$$\mathbf{G} = P\mathbb{G}, \tag{2.2}$$

where, as mentioned, P is some scalar describing the magnitude of load in the entire frame and $\mathbb{G}$ is consequently a geometric stiffness *shell*, independent of the level of load but whose form is dictated by the pattern of load, by virtue of the factors e_{ij} of all the ℓ matrices $\mathbf{G}^e$.

Let the non-dimensional load parameter p be defined as previously in Eq$^{\underline{n}}$ 1.4,

$$p = \frac{Pl^2}{\pi^2 EI}, \tag{2.3}$$

so that

$$\mathbf{G} = pP_E^+\mathbb{G}, \tag{2.4}$$

where $P_E^+ = \frac{\pi^2 EI}{l^2}$ is the fundamental Euler load[1] when the frame is loaded such that the member, of effective length l, to buckle at the lowest value of $|P|$ is in compression. Subsequently, P_E^-, where $\left|P_E^-\right| > \left|P_E^+\right|$, is the fundamental Euler load when the frame is loaded in the opposite direction so that the aforementioned member is in tension at buckling. The parameter p is used in most of the demonstrative, numerical simulations in this thesis; P is used where actual, experimentally determined data are involved.

Assuming the frame oscillates in simple harmonic motion at a particular frequency ω, $\mathbf{u} = \overline{\mathbf{u}} \cos(\omega t + \theta)$, the differential Eq$^{\underline{n}}$ 2.1 leads to

$$\left(\mathbf{K} + pP_E^+ \mathbb{G} - \lambda_r \mathbf{M}\right) \boldsymbol{\phi}_r = \mathbf{0}. \tag{2.5}$$

Eq$^{\underline{n}}$ 2.5 is an eigenvalue problem in which λ_r is the r^{th} eigenvalue and $\boldsymbol{\phi}_r$ its associated eigenvector. Circular frequencies are given by

$$\omega_r = \sqrt{\lambda_r} \tag{2.6}$$

and the eigenvectors describing the vibration mode shapes, $\boldsymbol{\Phi} = [\boldsymbol{\phi}_1 \cdots \boldsymbol{\phi}_N]$, can be made to exhibit mass-orthonormality:

$$\boldsymbol{\Phi}^T \mathbf{M} \boldsymbol{\Phi} = \mathbf{I}. \tag{2.7}$$

The characteristic polynomial of the eigenproblem Eq$^{\underline{n}}$ 2.5 has a zero at its origin of multiplicity D relating to as many rigid body modes. Hence, it

[1]This is of course the Euler load according to the mathematical, dynamic model, and is defined as that which causes the fundamental strain vibration mode frequency to vanish. Consequently, it is assumed that the Euler load is expressible as $P_E^+ = \frac{\pi^2 EI}{l^2}$, with all of the variability attributable to the effective length l, which depends upon the relative stiffnesses of the other members intersecting at the member ends.

happens to be that

$$\lambda_{D+1} \longrightarrow 0^+ \quad \text{as} \quad p \longrightarrow 1 \tag{2.8}$$

and

$$\lambda_{D+1} \longrightarrow 0^+ \quad \text{as} \quad p \longrightarrow \frac{P_E^-}{P_E^+}, \tag{2.9}$$

where λ_{D+1} is the eigenvalue representative of the fundamental, strain mode frequency. In most subsequent circumstances, the rigid body modes are ignored, so that modal designation commences with the fundamental, strain mode.

For a frame with n force distributions, $n > 1$, the associated eigenvalue problem can be expressed as

$$(\mathbf{K} + P_1\mathbb{G}_1 + P_2\mathbb{G}_2 + \cdots + P_n\mathbb{G}_n - \lambda_r\mathbf{M})\,\boldsymbol{\phi}_r = \mathbf{0}. \tag{2.10}$$

For the geometric stiffness matrices to be algebraically added in this way, it has to be assumed that loading in one force distribution does not affect the way in which subsequent distributions load by virtue of changes in axial stiffnesses. This is a very reasonable assumption and the elements of the geometric stiffness matrices relating to axial stiffness are very small in comparison to those relating to flexural terms. That is to say, the axial loading in a force distribution significantly affects the flexural stiffness of the members of a frame, but not their axial stiffness. The loading from multiple force distributions is, therefore, practically uncoupled and Eq$^{\underline{n}}$ 2.10 holds.

2.2 Newton's Method

For generality, identification of force is concerned with a set of n force parameters, $\mathbf{p} = [p_1\ p_2\ \cdots\ p_n]^T$. Newton's method provides an iterative means of finding an approximation $\mathbf{p}^{\mathrm{R}}$ to a sought root $\mathbf{p}^{®}$ such that, for m eigenvalues $\boldsymbol{\lambda} = [\lambda_1\ \lambda_2\ \cdots\ \lambda_m]^T$,

$$\boldsymbol{\lambda}\left(\mathbf{p}^{\mathrm{R}}\right) - \boldsymbol{\lambda}\left(\mathbf{p}^{®}\right) \approx \mathbf{0}; \tag{2.11}$$

roots are classified in Tab. 2.1.

Newton's fundamental theorem of calculus states, for a continuous and differentiable function $\overline{\boldsymbol{\lambda}}$: $\mathbb{R}^n \longrightarrow \mathbb{R}^m$, $m \geq n$,

$$\overline{\boldsymbol{\lambda}}\left(\mathbf{p}^k + \Delta\mathbf{p}\right) = \overline{\boldsymbol{\lambda}}\left(\mathbf{p}^k\right) + \int_{\mathbf{p}^k}^{\mathbf{p}^k+\Delta\mathbf{p}} \mathbf{J}\left(\mathbf{p}\right) d\mathbf{p}. \tag{2.12}$$

The multidimensional case is taken as general, in which $\mathbf{J} \in \mathbb{R}^{m\times n}$ is the Jacobian of eigenvalue derivatives whose order is governed by the n linearly independent force distributions of a space frame upon which the force parameters of the n-tuple $\mathbf{p}$ are factors; $\overline{\boldsymbol{\lambda}}$ is an m-tuple of eigenvalue differences such that

$$\overline{\boldsymbol{\lambda}}\left(\mathbf{p}^k\right) = \boldsymbol{\lambda}\left(\mathbf{p}^k\right) - \boldsymbol{\lambda}\left(\mathbf{p}^{®}\right), \tag{2.13}$$

where $\boldsymbol{\lambda}\left(\mathbf{p}^k\right)$ and $\boldsymbol{\lambda}\left(\mathbf{p}^{®}\right)$ are the eigenvalues, respectively at the current iterate and at the root. Eq$^{\underline{\mathrm{n}}}$ 2.13 is the objective function to be minimised, i.e., brought to 2.11.

If a first order approximation of the indefinite integral is made, then an

affine model[2] $\boldsymbol{\zeta}$ of the eigenvalue functions can be expressed as

$$\boldsymbol{\zeta}\left(\mathbf{p}^k + \Delta\mathbf{p}\right) = \overline{\boldsymbol{\lambda}}\left(\mathbf{p}^k\right) + \mathbf{J}\left(\mathbf{p}^k\right) \cdot \Delta\mathbf{p}. \tag{2.14}$$

Solving for the root of 2.14 leads to the evaluation of the Newton progression

$$\Delta\mathbf{p} = -\mathbf{J}^{+}\left(\mathbf{p}^k\right) \cdot \overline{\boldsymbol{\lambda}}\left(\mathbf{p}^k\right). \tag{2.15}$$

Decomposing $\mathbf{J}$ into its singular values and vectors,

$$\mathbf{J} = \mathbf{U}\boldsymbol{\Sigma}\mathbf{V}^T, \tag{2.16}$$

where $\mathbf{U} \in \mathbb{R}^{m\times m}$ and $\mathbf{V} \in \mathbb{R}^{n\times n}$ are respectively the orthonormal left and right singular vector matrices; $\boldsymbol{\Sigma} = diag\left(\sigma_1, \ldots, \sigma_n\right) \in \mathbb{R}^{m\times n}$ is a diagonal matrix of singular values. The generalised Jacobian inverse in Eq$^{\underline{n}}$ 2.15 is then defined as

$$\mathbf{J}^{+} = \mathbf{V}\boldsymbol{\Sigma}^{+}\mathbf{U}^T; \tag{2.17}$$

$\boldsymbol{\Sigma}^{+} = diag(\sigma_1^{-1}, \ldots, \sigma_n^{-1}) \in \mathbb{R}^{n\times m}$. The Newton progression is in this case a linear least squares solution of the system of equations.

If $rank(\mathbf{J}) = n$, then this generalised inverse is equal to the Moore-Penrose matrix pseudo-inverse

$$\mathbf{J}^{\dagger} = \left(\mathbf{J}^T\mathbf{J}\right)^{-1}\mathbf{J}^T \in \mathbb{R}^{n\times m}. \tag{2.18}$$

If $rank(\mathbf{J}) < n$ the pseudo-inverse is not computable but a non-unique inverse can be determined from Eq$^{\underline{n}}$ 2.17 by zeroing the reciprocals of the zero

[2]An affine model corresponds to an affine subspace, a line not constrained to pass through the origin; a linear subspace is one that necessarily passes through the origin, wherefore the term 'linear' is not used in this context.

singular values such that $\mathbf{\Sigma}^{+} = diag(\sigma_1^{-1}, \ldots, \sigma_n^{-1}, 0, \ldots, 0)$. Such would be the case if the equilibrium of a frame were described by a set of linearly dependent force distributions (q.v. Sec. 3.3).

Following the solution of Eq$^{\underline{n}}$ 2.15, the $(k+1)^{th}$ iterate is

$$\mathbf{p}^{k+1} = \mathbf{p}^{k} + \Delta\mathbf{p}. \tag{2.19}$$

Note that in enforcing equilibrium constraints by formulating the root-finding problem with scalar factors upon each of the n force distributions, $\mathbf{p}$, the dimensionality of Newton's method is many times smaller than if the problem were formulated explicitly with all ℓ member forces, the approach proposed by Greening (1999). This is useful in a number of ways, the most obvious of which is the reduced computational cost. Further, much adversity is avoided by not iterating through an unnecessarily large number of dimensions (which requires more modes to ensure the system of equations 2.15 is at least determined). That is to say, a smaller number of independent parameters is more likely to provide a stable path to convergence. Also, having too many parameters will probably lead to an ill-conditioned set of equations 2.15.

If $\overline{\boldsymbol{\lambda}}$: $\mathbb{R}^n \longrightarrow \mathbb{R}^m$ is overdetermined, i.e., $m \geq n$, then the reasons for formulating Eq$^{\underline{n}}$ 2.12 using eigenvalues and not the eigenvectors are, as noted by Mottershead et al. (1996): considerably greater measurement error is associated with mode shapes and, as discussed ahead in Sec. 4.1, the mode shapes are *comparatively* insensitive to physical parameters. The eigenvalues must of course be sensitive to load and this can be verified by inspecting

their derivatives.

Importantly, the eigenvalue derivatives should be large in the vicinity of a root so that a small error in frequency does not result in a relatively large error in the identified load. The validity of an identified load could be inspected by discarding modes with small gradients at convergence and noting the magnitude of the resulting change in converged value.

2.3 Root Classification

Ahead in the thesis, references will be made to a number of types of root and their associated quantities. It is therefore useful to outline these here.

It is reasonable to assume the true characteristics of the physical frame can never be known. Let, however, the experimentally determined eigenpair be denoted by $\lambda^{®}$ and $\boldsymbol{\phi}^{®}$, and associated load parameters by $\mathbf{p}^{®}$. These load parameters cannot of course solely account for the deviations that the experimentally determined eigenpairs mark from the true values. The values $\mathbf{p}^{®}$ are therefore physically measured, as $\lambda^{®}$ and $\boldsymbol{\phi}^{®}$ are determined from a modal test.

There is further, and potentially greater, loss of accuracy due to any inaptness of the mathematical model representing the physical frame. Assuming convergence is possible, let the analogous quantities in the mathematical model be denoted by λ^{R}, $\boldsymbol{\phi}^{\mathrm{R}}$ and $\mathbf{p}^{\mathrm{R}}$. The eigenpairs are assumedly continuous functions of the load parameter, or parameters, and any other of the frame properties upon which the model is parameterised. Continuity of the

Quantities	Description	Nature of accuracy loss
$\lambda^{®}$, $\phi^{®}$, $\mathbf{p}^{®}$	Experimentally-determined	*Transfer function estimation, data noise, modal parameter extraction method.*
λ^{R}, ϕ^{R}, $\mathbf{p}^{R}$	Analogous mathematical	*Inapt modelling, erroneous parameter values, neglected parameters, insufficient discretisation.*
λ^{*}, ϕ^{*}, $\mathbf{p}^{*}$	Well-converged	*Open-endedness of iterative solution.*

Table 2.1: Root classification and accuracy loss.

eigenpairs is discussed throughout Ch. 3 and Ch. 4.

Newton's method will iteratively converge upon these values — let the well-converged solution quantities be denoted by λ^{*}, ϕ^{*} and $\mathbf{p}^{*}$; accuracy loss here is negligible and greatly decreases with each iteration. Tab. 2.1 summarises the classification of roots and their associated quantities, and shows the accuracy loss at each stage.

2.4 Force Identification

Combining Axioms 1.2.1 and 1.2.2, it is evident that

> **Axiom 2.4.1** 'Any state of equilibrium of a statically indeterminate frame is expressible as the superposition of a number of linearly independent force distributions, equal to the degree of redundancy.'

This concept will be used to determine all ℓ member forces from knowledge of just the n converged force parameters $\mathbf{p}$.

Let $\mathbf{p}^*$ be the well-converged solution approximating the root $\mathbf{p}^{\mathrm{R}}$ to some specified tolerance. Given the number of frame members ℓ, let $\mathbf{E} \in \mathbb{R}^{\ell \times \ell}$ be the square equilibrium matrix such that the general element e_{ij} is the force in the i^{th} frame member corresponding to the distribution induced by strain in the j^{th} member. Owing to frame topology and the number of static redundancies, $\mathbf{E}$ is rank deficient. In fact,

$$rank\,(\mathbf{E}) = n. \tag{2.20}$$

This rank n governs the order of the system of equations 2.15 and hence the number of linearly independent force distributions that need to be sought. By Axiom 1.2.1, n is also equal to the degree of redundancy.

The form of $\mathbf{E}$ is readily known for simple frames; for more complex frameworks, a static finite element analysis may be necessary and one is suggested in Sec. 5.3. Once the rank of the equilibrium matrix is determined, the full rank matrix $\overline{\mathbf{E}} \in \mathbb{R}^{\ell \times n}$ can be established from n suitable columns of $\mathbf{E}$ (in cyclically symmetric frames, there will exist in $\mathbf{E}$ sets of identical columns). This can be done by using the singular values, σ, of $\mathbf{E}$ to inspect its effective rank. If ϵ_e is some empirically determined threshold, then the following conditions should hold:

$$\frac{\sigma_i}{\sigma_1} > \epsilon_e, \qquad i \leq n; \tag{2.21}$$

$$\frac{\sigma_i}{\sigma_1} \leq \epsilon_e, \qquad i > n. \tag{2.22}$$

In practice, the number of significant singular values is typically obvious and $\epsilon_e \approx 0$. If not singular, the condition of $\overline{\mathbf{E}}$ depends upon which columns

are used, but the matrix is generally well conditioned enough for present purposes. The condition of the reduced equilibrium matrix, which completely describes equilibrium in the finite element model, is important because the condition of the Jacobian matrix $\mathbf{J}$ is dependent upon it. Certainly, $rank(\mathbf{J}) = rank(\mathbf{E})$, for $\mathbf{J}$ involving only derivatives with respect to load parameters, and, consequently, if $\overline{\mathbf{E}}$ is rank-deficient, so too to the same degree is $\mathbf{J}$ — a proof of this result is given in Sec. 3.3. In Ch. 7, the force identification problem is actually formulated upon an orthonormal set of force distributions so that the reduced equilibrium matrix is of unit condition number.

It is costly to populate the entire equilibrium matrix $\mathbf{E}$ and determine n according to Eq$^{\underline{n}}$ 2.20. Alternatively, the fact that n satisfies Maxwell's equation can be used:

$$n = \ell - 3b + 6, \tag{2.23}$$

where ℓ is the number of frame members and b the number of joints; it is necessary to include six degrees of freedom to alleviate the externally mechanistic state of the frame. Certainly, Eq$^{\underline{n}}$ 2.23 holds for the frames in this thesis.

Fig. 2.1 shows the construction of the equilibrium matrix for a thrice redundant, regular octahedral space frame, from which the physical interpretation of force distribution superposition can be appreciated.

Upon convergence, the solution to the member forces can then be expressed as

$$\mathbf{f}^* = \overline{\mathbf{E}}\mathbf{p}^*. \tag{2.24}$$

The full rank of this equilibrium matrix means that the solution to the force parameters,

$$\mathbf{p}^* = \overline{\mathbf{E}}^+\mathbf{f}^*, \tag{2.25}$$

is unique for a given state of frame equilibrium.

2.5 Problem Condition

If $\mathbf{p}$ encompasses parameters other than just those relating to load, then there is the potential for the force identification problem to become significantly ill-conditioned. For example, if the problem is parameterised with load parameters in Newtons and member diameter in metres, then the frequencies will be several orders of magnitude more sensitive to diameter than to load. Consequently, the Jacobian $\mathbf{J}$ will be ill-conditioned. However, because the parameters are arbitrarily scaled, the columns of the Jacobian, $\mathbf{j}_1, \mathbf{j}_2, \ldots, \mathbf{j}_n$, can be weighted to alleviate this ill-conditioning — q.v. Golub and Van Loan (1983).

Define

$$\mathbf{H} = \begin{bmatrix} \|\mathbf{j}_1\|_2^{-1} & & \\ & \ddots & \\ & & \|\mathbf{j}_n\|_2^{-1} \end{bmatrix} \tag{2.26}$$

and prescribe, instead of Eq^{n} 2.15, the Newton progression

$$\Delta \mathbf{p} = -\mathbf{H}\left(\mathbf{J}(\mathbf{p}^k)\mathbf{H}\right)^{+} \cdot \overline{\boldsymbol{\lambda}}(\mathbf{p}^k). \tag{2.27}$$

Note that neither the solution nor the path to it are changed by this manipulation.

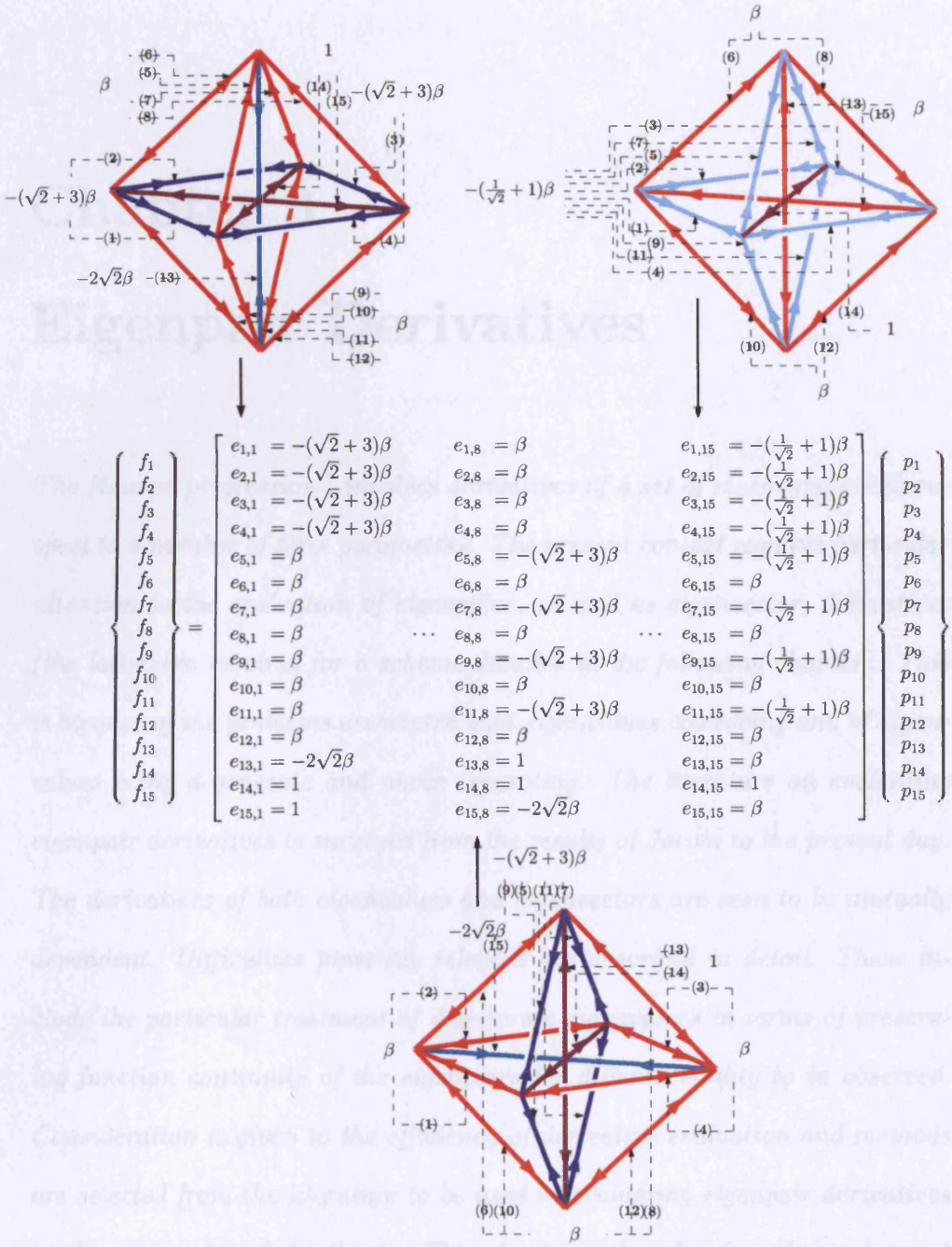

Figure 2.1: Construction of the equilibrium matrix and the physical interpretation of force distribution superposition for a thrice redundant, regular octahedral space frame; $\beta = (2(\sqrt{2}+1))^{-1}$.

Chapter 3

Eigenpair Derivatives

The Newton progression [1] *involves derivatives of a set of eigenvalues with respect to a number of force parameters. The present context requires particular attention to the evaluation of eigenvalue, as well as eigenvector, derivatives (the latter are required for a scheme detailed in the following chapter). This is because of the problems associated with eigenvalues coalescing and of eigenvalues being degenerate and never separating. The literature on evaluating eigenpair derivatives is surveyed from the results of Jacobi to the present day. The derivatives of both eigenvalues and eigenvectors are seen to be mutually dependent. Difficulties presently relevant are described in detail. These include the particular treatment of degenerate eigenvalues in terms of preserving function continuity of the eigenpairs for differentiability to be observed. Consideration is given to the efficiency of derivative evaluation and methods are selected from the literature to be used in evaluating eigenpair derivatives in the remainder of the thesis. This chapter is largely of academic interest and the reader may wish to pass over the material until the closure.*

[1] Eq^{n} 2.15

3.1 Survey of Literature on Eigenpair Derivatives

Jacobi (1846) derives for the symmetric eigenproblem,

$$\mathbf{A}\boldsymbol{\phi} = \lambda\boldsymbol{\phi}, \tag{3.1}$$

expressions for the derivatives of the eigenvalues and eigenvector elements with respect to elements of the real, symmetric matrix $\mathbf{A} \in \mathbb{R}^{N\times N}$. On the condition that the eigenvectors are orthonormal, the eigenvalue derivative may be expressed as

$$\frac{\partial\lambda}{\partial a_{ij}} = \phi_i\phi_j. \tag{3.2}$$

If the differential of the general matrix element is expressible as $\partial a_{ij} = c_{ij}\partial p$, where c_{ij} is some constant and p a factor of the entire matrix $\mathbf{A}$, and noting the total derivative to be the algebraic sum of all derivatives with respect to the respective matrix elements,

$$\frac{\partial\lambda}{\partial p} = \sum_{i=1}^{N}\sum_{j=1}^{N}\phi_i\frac{\partial a_{ij}}{\partial p}\phi_j, \tag{3.3}$$

or, more succinctly,

$$\frac{\partial\lambda}{\partial p} = \boldsymbol{\phi}^T\frac{\partial\mathbf{A}}{\partial p}\boldsymbol{\phi}. \tag{3.4}$$

The latter result is inferred some hundred and twenty years later by Wittrick (1962). In a rigorous treatment, Lancaster (1963, 1964) also shows this result for the distinct eigenvalues of $\mathbf{A}$ and notes the applicability of Newton's method as a numerical approach for solving non-linear matrix problems; the

derivatives of degenerate eigenvalues are separately treated. The particular treatment is later discussed in some depth as there is direct relevance of the association between frame spatial symmetry and eigenvalue multiplicity and also of eigenvalues coalescing as load varies. Garg (1973) arrives at an analogous result to Eq$^{\underline{n}}$ 3.4 for $\mathbf{A}$ complex:

$$\frac{\partial \lambda}{\partial p}\boldsymbol{\phi} = (\mathbf{A} - \lambda \mathbf{I})\frac{\partial \boldsymbol{\phi}}{\partial p} + \frac{\partial \mathbf{A}}{\partial p}\boldsymbol{\phi}, \tag{3.5}$$

which requires a more involved solution, in which complex equations are separated into two sets of real equations. Rudisill and Chu (1975) present numerical methods for evaluating the eigenpair first derivatives and eigenvalue second derivatives of $\mathbf{A}$, which are useful for large eigenproblems in the sense that a complete eigensolution is not necessary for a single sought derivative.

While these results are of academic note, the structural dynamics formulation is seen to lead to a generalised eigenproblem,

$$\mathbf{A}\boldsymbol{\phi} = \lambda \mathbf{B}\boldsymbol{\phi}, \tag{3.6}$$

where $\mathbf{A} \in \mathbb{R}^{N \times N}$ and $\mathbf{B} \in \mathbb{R}^{N \times N}$ are symmetric, sparse and banded. Fox and Kapoor (1968) give expressions for the eigenvalue and eigenvector derivatives, which are derived as follows. Rearrangement of the eigenproblem 3.6 and premultiplication by $\boldsymbol{\phi}^T$ gives

$$\boldsymbol{\phi}^T (\mathbf{A} - \lambda \mathbf{B})\, \boldsymbol{\phi} = 0. \tag{3.7}$$

Partial differentiation with respect to p leads to

$$\frac{\partial \boldsymbol{\phi}^T}{\partial p}(\mathbf{A}-\lambda\mathbf{B})\boldsymbol{\phi}+\boldsymbol{\phi}^T\left(\frac{\partial \mathbf{A}}{\partial p}-\lambda\frac{\partial \mathbf{B}}{\partial p}-\frac{\partial \lambda}{\partial p}\mathbf{B}\right)\boldsymbol{\phi} + \boldsymbol{\phi}^T(\mathbf{A}-\lambda\mathbf{B})\frac{\partial \boldsymbol{\phi}}{\partial p}=0. \tag{3.8}$$

Since $\boldsymbol{\phi}$ is a nullspace of the pencil $\mathbf{A}-\lambda\mathbf{B}$, and since the latter is a symmetric matrix, the outer terms of Eq$^{\underline{n}}$ 3.8 are zero. Noting the $\mathbf{B}$-normality of the eigenvectors, viz.,

$$\boldsymbol{\phi}^T\mathbf{B}\boldsymbol{\phi}=1, \tag{3.9}$$

the eigenvalue derivative is then

$$\frac{\partial \lambda}{\partial p}=\boldsymbol{\phi}^T\left(\frac{\partial \mathbf{A}}{\partial p}-\lambda\frac{\partial \mathbf{B}}{\partial p}\right)\boldsymbol{\phi}. \tag{3.10}$$

With relevance to non-self-adjoint dynamic systems, whose eigenproblems involve unequal left and right eigenvectors, i.e.,

$$\mathbf{A}\boldsymbol{\phi}=\lambda\mathbf{B}\boldsymbol{\phi}, \qquad \boldsymbol{\varphi}^T\mathbf{A}=\lambda\boldsymbol{\varphi}^T\mathbf{B}, \tag{3.11}$$

Rogers (1970) and Stewart (1972) analogously derive the eigenvalue derivative for $\mathbf{A}$ general, not necessarily symmetric, real or Hermitian:

$$\frac{\partial \lambda}{\partial p}=\boldsymbol{\varphi}^T\left(\frac{\partial \mathbf{A}}{\partial p}-\lambda\frac{\partial \mathbf{B}}{\partial p}\right)\boldsymbol{\phi}, \tag{3.12}$$

where $\boldsymbol{\varphi}$ is the left eigenvector, in opposition to and not necessarily equal to the right eigenvector $\boldsymbol{\phi}$. It is seen that in the expression for the eigenvalue derivative, the premultiplying right and left eigenvectors are interchangeable to give results for self-adjoint and non-self-adjoint systems respectively. Plaut

and Huseyin (1973), Rudisill (1974), and Doughty (1982) also derive Eq^{n} 3.12 and go on to obtain expressions for the eigenvalue second derivatives in the general case; one such expression is given ahead in Eq^{n} 3.18.

The results shown hitherto have assumed distinctness of the eigenvalues. Degeneracy of eigenvalues is associated with indeterminacy of their eigenvectors; the eigenvectors of a set of degenerate eigenvalues are arbitrary, non-unique and generally not orthogonal to one another. That is not to say that the degenerate eigenvalue derivative is indeterminate. Indeed, Lancaster (1964) shows that the degenerate eigenvalues of the eigenproblem 3.1 of multiplicity d have first derivatives equal to the eigenvalues of the matrix $\mathbf{Y}^T\mathbf{A}^{(1)}\mathbf{X}$, where $\mathbf{X}$ and $\mathbf{Y}$ are matrices of dimension $N \times d$ satisfying the orthonormality condition $\mathbf{Y}^T\mathbf{X} = \mathbf{I}$; the existence and determination of such matrices is discussed by the author. A similar result for the derivatives of degenerate, general eigenvalues of eigenproblem 3.6 is seen ahead. While the work of Lancaster concerns matrices of simple structure and is only applicable to the first order form of the governing equations, Simpson (1976) proposes a method, based on modal control theory, of determining the eigenpair derivatives, which is applicable to degenerate eigenvalues and has the potential to cope with higher derivatives.

Taylor and Kane (1975) investigate the eigenpair derivatives, including explicitly the eigenvector second derivatives, for the quadratic eigenproblem, as arises in damped dynamic systems:

$$\left(\mathbf{A} + \lambda\mathbf{B} + \lambda^2\mathbf{C}\right)\boldsymbol{\phi} = 0, \tag{3.13}$$

where $\mathbf{C}$ is a damping matrix; the system matrices are taken to be dependent on multiple parameters. For multiparameter eigenproblems, the eigenvectors of degenerate eigenvalues may not necessarily be analytic functions of the parameters, as noted by Taylor and Kane. In this case, evaluation of mixed derivatives is not possible, a problem not encountered by Lancaster, who studied the single parameter case. Andrew (1978, 1979) extends the iterative eigenpair derivative evaluation of Rudisill and Chu (1975) and also finds difficulties near degeneracy of an $\mathbf{A}$ dependent on multiple parameters. Chu (1990) investigates the eigenvalues of matrices dependent on several parameters and analyses degenerate eigenvalues through their weighted mean over the various parameters $\mathbf{p}$. Hou and Kenny (1992) treat the multiparameter eigenproblem in the presence of degenerate eigenvalues by reparameterising in terms of a single parameter in the neighbourhood of degeneracy and thus approximate the eigenpair derivatives.

It is useful at this point to discuss the classification of degeneracy. Degeneracy may be *transitory* or existing only at a particular value of the parameter p; degeneracy may also be *permanent* in the sense that an eigenvalue is degenerate for all values of p. This can happen if the parameter upon which the eigenproblem is dependent varies a space frame in a way that conserves symmetry, and so certain eigenvalues are not able to separate. An example is a symmetric frame dependent upon a symmetric force distribution. There may of course be intermediate cases of *semi-permanent* degeneracy. Further, eigenvalues may be transitorily coalesced in different ways and it is useful to

speak of orders of coalescence. The intersection of eigenvalues in a first order coalescence, which is the type most commonly experienced in structural dynamics problems, is associated with degeneracy of the eigenvalues but distinctness of all of their derivatives. To generalise, a q^{th} order coalescence is defined as one in which only the q^{th} derivative and higher are distinct. Permanent degeneracy is itself an ∞^{th} order coalescence, where the space spanned by the associated eigenvectors is indeterminate. Fig. 3.1 illustrates the various types of degeneracy.

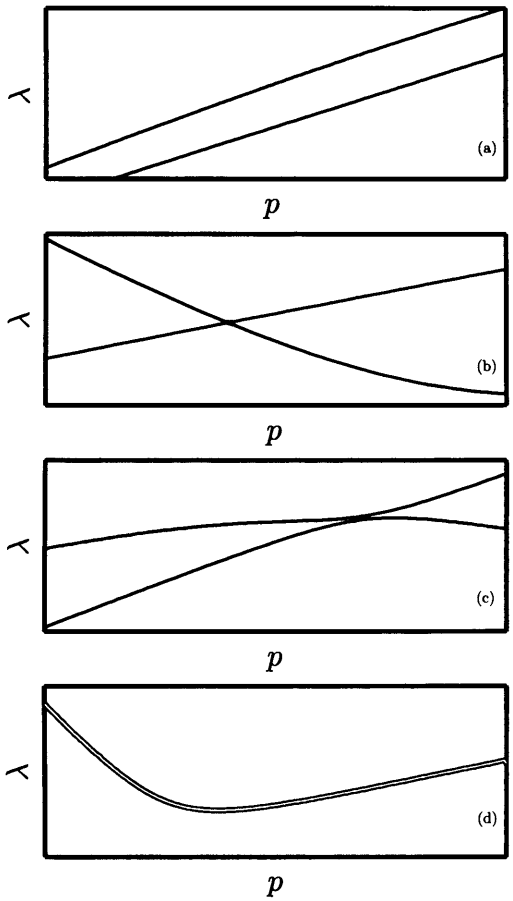

Figure 3.1: Types of eigenvalue degeneracy: (a) distinctness; (b) first order transitory; (c) second order transitory; (d) permanent.

Haug and Rousselet (1980) discuss the differentiability of transitorily coalesced eigenvalues using the order-2 linear operator

$$\mathbf{A}(p_1, p_2) = \begin{pmatrix} p_1 & p_2 \\ p_2 & -p_1 \end{pmatrix}, \tag{3.14}$$

the eigenvalues of which are $\lambda_\pm = \pm\sqrt{p_1^2 + p_2^2}$. Notwithstanding the self-adjointness of $\mathbf{A}$, at $p_1 = p_2 = 0$, where there is a first order coalescence, the eigenvalues are not Fréchet[2] differentiable owing to the arbitrary, numerical ordering and subsequent discontinuity of the defined eigenvalue functions. Each eigenvalue has four Gâteaux[3] derivatives at $p_1 = p_2 = 0$, depending on whether the differential limit is approached from (p_1^+, p_2^+), (p_1^+, p_2^-), (p_1^-, p_2^+) or (p_1^-, p_2^-).

Andrew (1979) notes that the operator

$$\mathbf{A}_1(p) = \begin{pmatrix} \alpha & 1 \\ |p|^{\frac{3}{2}} & \alpha \end{pmatrix}, \tag{3.15}$$

for α constant, clearly has the same eigenvalues at $p = 0$ as

$$\mathbf{A}_2(p) = \begin{pmatrix} \alpha & 1 \\ p^2 & \alpha \end{pmatrix}, \tag{3.16}$$

but, unlike $\mathbf{A}_2$, has eigenvalues that are not Fréchet differentiable at $p = 0$.

While first derivatives are helpful in indicating the results of small perturbations to p, second derivatives offer greater insight when there are considerable perturbations. Brandon (1984) uses a perturbation method similar

[2]For present purposes, the Fréchet derivative is the gradient of a necessarily continuous function. Fréchet differentiability is a strong definition that requires the Jacobian to satisfy $\lim_{\Delta p \to 0} \frac{\|\overline{\lambda}(p^k+\Delta p) - \overline{\lambda}(p^k) - \mathbf{J}(p^k)\Delta p\|}{\|\Delta p\|} = 0$.

[3]The Gâteaux derivative of a locally discontinuous function is directionally dependent; there may be many such derivatives depending upon from which direction the differential limit is approached. Gâteaux differentiability is a weaker definition (cf. definition of Fréchet differentiability) that only requires the Jacobian to satisfy $\lim_{\tau \to 0} \frac{\|\overline{\lambda}(p^k+\tau\Delta p) - \overline{\lambda}(p^k) - \mathbf{J}(p^k)\tau\Delta p\|}{\tau} = 0$.

to that employed by Lancaster (1960) for first derivatives to derive the second eigenpair derivatives where the $\mathbf{A}$ of eigenproblem 3.6 is p-dependent while $\mathbf{B}$ is constant; the reader may be interested in the related references Flax (1985) and Brandon (1985). Brandon (1991) uses the second eigenpair derivatives to assess the suitability of Newton's method, which utilises first order function models, in sensitivity analysis; the conclusions are that while an affine approximation is not always valid, the computational cost of incorporating the second derivatives is considerable and generally prohibitive. Wanxie and Gengdong (1986) derive, noting Rayleigh's principle, an explicit expression for the second fundamental eigenvalue derivative, which is further applicable to twofold degeneracy of the fundamental eigenvalue:

$$\begin{aligned}\frac{\partial^2}{\partial p_1 \partial p_2}(\lambda_{1_2}) = \quad & \boldsymbol{\phi}_{1_2}^T \left(\frac{\partial^2 \mathbf{A}}{\partial p_1 \partial p_2} - \lambda_{1_2} \frac{\partial^2 \mathbf{B}}{\partial p_1 \partial p_2} \right) \boldsymbol{\phi}_{1_2} \\ & - \boldsymbol{\phi}_{1_2}^T \frac{\partial \mathbf{B}}{\partial p_1} \boldsymbol{\phi}_{1_2} \boldsymbol{\phi}_{1_2}^T \left(\frac{\partial \mathbf{A}}{\partial p_2} - \lambda_{1_2} \frac{\partial \mathbf{B}}{\partial p_2} \right) \boldsymbol{\phi}_{1_2} \\ & - \boldsymbol{\phi}_{1_2}^T \frac{\partial \mathbf{B}}{\partial p_2} \boldsymbol{\phi}_{1_2} \boldsymbol{\phi}_{1_2}^T \left(\frac{\partial \mathbf{A}}{\partial p_1} - \lambda_{1_2} \frac{\partial \mathbf{B}}{\partial p_2} \right) \boldsymbol{\phi}_{1_2} \\ + \sum_{r=3}^{N} \Bigg(& \frac{2}{(\lambda_1 - \lambda_r)} \boldsymbol{\phi}_1^T \left(\frac{\partial \mathbf{A}}{\partial p_1} - \lambda_1 \frac{\partial \mathbf{B}}{\partial p_1} \right) \boldsymbol{\phi}_r \boldsymbol{\phi}_r^T \left(\frac{\partial \mathbf{A}}{\partial p_2} - \lambda_1 \frac{\partial \mathbf{B}}{\partial p_2} \right) \boldsymbol{\phi}_1 \\ & + \boldsymbol{\phi}_2^T \left(\frac{\partial \mathbf{A}}{\partial p_1} - \lambda_1 \frac{\partial \mathbf{B}}{\partial p_1} \right) \boldsymbol{\phi}_r \boldsymbol{\phi}_r^T \left(\frac{\partial \mathbf{A}}{\partial p_2} - \lambda_1 \frac{\partial \mathbf{B}}{\partial p_2} \right) \boldsymbol{\phi}_2 \Bigg). \end{aligned} \tag{3.17}$$

It is worth comparing this result to that of Plaut and Huseyin (1973), in Eq$^{\underline{n}}$ 3.18, for a general, non-defective, non-self-adjoint system. The similarity of the two equations is immediately apparent, with the non-summation terms completely analogous. There is of course the stipulation that the eigenvalue be distinct since the modal summation term involves a denominator that is

undefined for degenerate eigenvalues, $\lambda_r = \lambda_s$:

$$\begin{aligned}
\frac{\partial^2}{\partial p_1 \partial p_2}(\lambda_s) = {} & \boldsymbol{\varphi}_s^T \left(\frac{\partial^2 \mathbf{A}}{\partial p_1 \partial p_2} - \lambda_s \frac{\partial^2 \mathbf{B}}{\partial p_1 \partial p_2} \right) \boldsymbol{\phi}_s \\
& - \boldsymbol{\varphi}_s^T \frac{\partial \mathbf{B}}{\partial p_1} \boldsymbol{\phi}_s \boldsymbol{\varphi}_s^T \left(\frac{\partial \mathbf{A}}{\partial p_2} - \lambda_s \frac{\partial \mathbf{B}}{\partial p_2} \right) \boldsymbol{\phi}_s \\
& - \boldsymbol{\varphi}_s^T \frac{\partial \mathbf{B}}{\partial p_2} \boldsymbol{\phi}_s \boldsymbol{\varphi}_s^T \left(\frac{\partial \mathbf{A}}{\partial p_1} - \lambda_s \frac{\partial \mathbf{B}}{\partial p_1} \right) \boldsymbol{\phi}_s \\
+ \sum_{\substack{r=1 \\ r \neq s}}^{N} \Bigg(& \frac{1}{(\lambda_s - \lambda_r)} \boldsymbol{\varphi}_s^T \left(\frac{\partial \mathbf{A}}{\partial p_1} - \lambda_s \frac{\partial \mathbf{B}}{\partial p_1} \right) \boldsymbol{\phi}_r \boldsymbol{\varphi}_r^T \left(\frac{\partial \mathbf{A}}{\partial p_2} - \lambda_s \frac{\partial \mathbf{B}}{\partial p_2} \right) \boldsymbol{\phi}_s \\
& + \frac{1}{(\lambda_s - \lambda_r)} \boldsymbol{\varphi}_r^T \left(\frac{\partial \mathbf{A}}{\partial p_1} - \lambda_s \frac{\partial \mathbf{B}}{\partial p_1} \right) \boldsymbol{\phi}_s \boldsymbol{\varphi}_s^T \left(\frac{\partial \mathbf{A}}{\partial p_2} - \lambda_s \frac{\partial \mathbf{B}}{\partial p_2} \right) \boldsymbol{\phi}_r \Bigg),
\end{aligned} \tag{3.18}$$

in which there are different left and right eigenvectors, $\boldsymbol{\varphi}$ and $\boldsymbol{\phi}$, respectively.

* * *

Jacobi (1846) is the first to study the subject of eigenvector derivatives, giving expressions for the derivative of an h^{th} general eigenvector element of the s^{th} eigenvector, ϕ_{hs}, with respect to a general element of the matrix $\mathbf{A}$ in 3.1:

$$\frac{\partial \phi_{hs}}{\partial a_{ij}} = \phi_{js} \sum_{\substack{r=1 \\ r \neq s}}^{N} \frac{\phi_{hr} \phi_{ir}}{\lambda_s - \lambda_r}. \tag{3.19}$$

If the differential of the general matrix element is expressible as $\partial a_{ij} = c_{ij} \partial p$, where c_{ij} is some constant and p a factor of the entire matrix $\mathbf{A}$, and noting the total derivative to be the algebraic sum of all derivatives with respect to the respective matrix elements,

$$\frac{\partial \phi_{hs}}{\partial p} = \sum_{i=1}^{N} \sum_{j=1}^{N} \phi_{js} \frac{\partial a_{ij}}{\partial p} \sum_{\substack{r=1 \\ r \neq s}}^{N} \frac{\phi_{hr} \phi_{ir}}{\lambda_s - \lambda_r}. \tag{3.20}$$

Kollo and Neudecker (1997), using an alternate method, also give the eigenvector derivatives related to a real, symmetric $\mathbf{A}$, assuming there is no degeneracy of the eigenvalues and the eigenvectors form an orthogonal set.

Fox and Kapoor (1968) give two formulations for the derivatives of eigenvectors of the general eigenproblem 3.6; one of these involves a series expansion of the derivative and relates to the result of Jacobi; the derivation proceeds as follows. Since the eigenvectors form a complete vector set, any vector can be expressed as some linear combination of the eigenvectors. Thus

$$\frac{\partial \boldsymbol{\phi}_s}{\partial p} = \sum_{r=1}^{N} c_r \boldsymbol{\phi}_r. \tag{3.21}$$

Substitution of Eq$^{\underline{n}}$ 3.21 into the eigenproblem 3.6 differentiated, viz.,

$$(\mathbf{A} - \lambda_s \mathbf{B}) \frac{\partial \boldsymbol{\phi}_s}{\partial p} = -\left(\frac{\partial \mathbf{A}}{\partial p} - \lambda_s \frac{\partial \mathbf{B}}{\partial p} - \frac{\partial \lambda_s}{\partial p} \mathbf{B} \right) \boldsymbol{\phi}_s, \tag{3.22}$$

gives

$$(\mathbf{A} - \lambda_s \mathbf{B}) \sum_{r=1}^{N} c_r \boldsymbol{\phi}_r = -\left(\frac{\partial \mathbf{A}}{\partial p} - \lambda_s \frac{\partial \mathbf{B}}{\partial p} - \frac{\partial \lambda_s}{\partial p} \mathbf{B} \right) \boldsymbol{\phi}_s. \tag{3.23}$$

In premultiplying by some eigenvector, $\boldsymbol{\phi}_r^T$, $r \neq s$, the general r^{th} term gives the coefficient

$$c_r = \frac{\boldsymbol{\phi}_r^T \left(\frac{\partial \mathbf{A}}{\partial p} - \lambda_s \frac{\partial \mathbf{B}}{\partial p} \right) \boldsymbol{\phi}_s}{(\lambda_s - \lambda_r)}, \tag{3.24}$$

noting **B**-orthonormality and **A**-orthogonality. Now, substitution of Eq$^{\underline{n}}$ 3.21 into Eq$^{\underline{n}}$ 3.9 differentiated, viz.,

$$2\boldsymbol{\phi}_s^T \mathbf{B} \frac{\partial \boldsymbol{\phi}_s}{\partial p} = -\boldsymbol{\phi}_s^T \frac{\partial \mathbf{B}}{\partial p} \boldsymbol{\phi}_s, \tag{3.25}$$

gives

$$c_s = -\frac{1}{2} \boldsymbol{\phi}_s^T \frac{\partial \mathbf{B}}{\partial p} \boldsymbol{\phi}_s. \tag{3.26}$$

The result may be summarised as

$$\frac{\partial \phi_s}{\partial p} = \sum_{\substack{r=1 \\ r \neq s}}^{N} \frac{\phi_r^T \left(\frac{\partial \mathbf{A}}{\partial p} - \lambda_s \frac{\partial \mathbf{B}}{\partial p} \right) \phi_s}{\lambda_s - \lambda_r} \phi_r - \frac{1}{2} \left(\phi_s^T \frac{\partial \mathbf{B}}{\partial p} \phi_s \right) \phi_s. \tag{3.27}$$

Lim et al. (1987) derive an analogous result for a general, non-self-adjoint system, noting that previous derivations mistakenly ignore the eigenvector in question in the expansion of its derivative, since, for non-self-adjoint systems, the eigenvectors are generally not orthogonal. Wang (1991) investigates methods that approximate the eigenvector derivative through a truncated partial sum and suggests ways in which to improve the approximation. Liu et al. (1994) inspect the contribution of the truncated eigenvectors to the eigenvector derivative and assess to what extent these may be neglected; further, it is shown that the contribution can be accounted for by a convergent series independent of the truncated eigenvectors. Zhao et al. (1999), in a parallel effort, produce results applicable to damped dynamic systems, as defined by the eigenproblem 3.13. Bernard and Bronowicki (1994) extend the truncated modal expansion method to account for second order eigenvalue coalescence.

If the matrix $\mathbf{A}$ is singular, as would be the case for a free-free structural system, then the characteristic polynomial of eigenproblem 3.6 has a zero at its origin of multiplicity equal to the number of rigid body modes. For a free-free, unbuckled frame, there would be six such zero-eigenvalue modes. In a separate paper, Liu et al. (1994) present a truncated modal summation method that takes into account the contribution from the rigid body modes: the eigenproblem is recast to another eigenproblem in which the equivalent

matrix to $\mathbf{A}$ is non-singular (a requirement of the method owing to Wang (1991), which involves an inversion of $\mathbf{A}$) and which possesses the same eigenpair derivatives as the original. Akgün (1994) proposes a family of modal summation methods that have the capability of handling non-self-adjoint systems with zero eigenvalues.

The other formulation owing to Fox and Kapoor (1968) is algebraic and follows from the derivation of the eigenvalue derivative. Note that even in the absence of eigenvalue degeneracy, the pencil $\mathbf{A} - \lambda\mathbf{B}$ is singular since λ is one of its eigenvalues. Hence, it is not possible to obtain an expression for the eigenvector derivative from Eq$^{\underline{n}}$ 3.22 through direct algebraic division. Instead, it is necessary to use the constraint of the orthonormality condition, which is valid since Eq$^{\underline{n}}$ 3.25 is a scalar equation, linearly independent of Eq$^{\underline{n}}$ 3.22. Premultiplication of Eq$^{\underline{n}}$ 3.22 by $(\mathbf{A} - \lambda\mathbf{B})^T$, Eq$^{\underline{n}}$ 3.25 by $\left(\boldsymbol{\phi}^T\mathbf{B}\right)^T$ and addition of the resulting terms gives

$$\frac{\partial\boldsymbol{\phi}}{\partial p} = -\left((\mathbf{A} - \lambda\mathbf{B})^2 + 2\mathbf{B}\boldsymbol{\phi}\boldsymbol{\phi}^T\mathbf{B}\right)^{-1} \cdot$$
$$\cdot \left((\mathbf{A} - \lambda\mathbf{B})^T \left(\frac{\partial\mathbf{A}}{\partial p} - \lambda\frac{\partial\mathbf{B}}{\partial p} - \frac{\partial\lambda}{\partial p}\mathbf{B}\right) + \mathbf{B}\boldsymbol{\phi}\boldsymbol{\phi}^T\frac{\partial\mathbf{B}}{\partial p}\right)\boldsymbol{\phi}. \qquad (3.28)$$

Evaluation of the derivative by this equation is inefficient since the algebraic manipulation that is required to circumvent the singularity of the pencil destroys the banded nature of the system matrices. An alternative, algebraic method that preserves matrix bandedness owes to Nelson (1976) and is as follows — the derivation therein pertains to the eigenproblem 3.1, but shall be given here as for the general eigenproblem 3.6.

With reference to Eq$^{\underline{n}}$ 3.22, let

$$\begin{aligned} \boldsymbol{\xi} &= (\mathbf{A} - \lambda\mathbf{B})\frac{\partial \boldsymbol{\phi}}{\partial p} \\ &= -\left(\frac{\partial \mathbf{A}}{\partial p} - \lambda_s \frac{\partial \mathbf{B}}{\partial p} - \frac{\partial \lambda_s}{\partial p}\mathbf{B}\right)\boldsymbol{\phi}_s. \end{aligned} \tag{3.29}$$

Since $\boldsymbol{\phi}$ is a nullspace of the matrix pencil, if $\boldsymbol{\xi} = (\mathbf{A} - \lambda\mathbf{B})\,\mathbf{v}$ is satisfied by any $\mathbf{v}$, then for any constant c it is also satisfied by $\mathbf{v} + c\boldsymbol{\phi}$. The eigenvector derivative may thus be separated respectively into a particular solution and a constraint function, which are to be sought in turn:

$$\frac{\partial \boldsymbol{\phi}}{\partial p} = \mathbf{v} + c\boldsymbol{\phi}. \tag{3.30}$$

The particular solution can be found by forcing an element of $\mathbf{v}$ to zero and solving for the remaining elements, which is valid for $\boldsymbol{\xi}$ in the range of the pencil so long as the corresponding element of $\boldsymbol{\phi}$ is non-zero. Therefore, let

$$\mathcal{P} = \mathbf{A} - \lambda\mathbf{B}; \tag{3.31}$$

for $|\phi_\kappa| = \|\boldsymbol{\phi}\|_\infty$, let

$$\overline{\xi}_\kappa = 0, \tag{3.32}$$

$$\overline{\mathcal{P}}_{i\kappa} = \delta_{i\kappa}, \qquad i = 1, 2, \ldots n, \tag{3.33}$$

$$\overline{\mathcal{P}}_{\kappa j} = \delta_{\kappa j}, \qquad j = 1, 2, \ldots n, \tag{3.34}$$

where δ is the Kronecker delta and, other than for the elements defined in Eq$^{\underline{n}}$ 3.32-3.34, $\overline{\boldsymbol{\xi}}$ is the same as $\boldsymbol{\xi}$ and $\overline{\mathcal{P}}$ is the same as $\mathcal{P}$. Since $\boldsymbol{\xi}$ is in the range of $\mathcal{P}$, any $\mathbf{v}$ that is the solution to the manipulated and now invertible set of linear equations

$$\overline{\mathcal{P}}\mathbf{v} = \overline{\boldsymbol{\xi}}, \tag{3.35}$$

i.e.,

$$\mathbf{v} = \overline{\mathcal{P}}^{-1}\overline{\boldsymbol{\xi}}, \tag{3.36}$$

is the particular solution and it remains only to find the scalar c. Substitution of Eq$^{\underline{n}}$ 3.30 into Eq$^{\underline{n}}$ 3.25 gives

$$c = -\left(\mathbf{v}^T\mathbf{B} + \frac{1}{2}\boldsymbol{\phi}^T\frac{\partial \mathbf{B}}{\partial p}\right)\boldsymbol{\phi}, \tag{3.37}$$

and the solution to the eigenvector derivative is now given by Eq$^{\underline{n}}$ 3.30. The similarity, term for term, of the direct method just shown and the modal summation method, as expressed by Eq$^{\underline{n}}$ 3.27, is immediately apparent. Tang and Wang (1999) expose this intrinsic relation and therefrom arrive at a general, unified method, which can be shown to be an asymptotic expansion of a special, direct method with biorthogonal decomposition.

Lim et al. (1987) utilise the method owing to Nelson for a general non-self-adjoint system. Liu et al. (1995) perform a QR decomposition of the pencil $\mathcal{P}$ to evaluate the eigenvector derivatives and thus alleviate the necessity of finding a pivotal κ^{th} element as above and solution is in an automated sense. This approach is applicable also to viscously damped systems.

The foregoing method has assumed distinctness of eigenvalues. Ojalvo (1988) presents a modification to Nelson's method to overcome this, but is in fact restricted to solving for the permanently degenerate case. The method is as follows. It was earlier stated that the eigenvectors associated with degenerate eigenvalues are arbitrary, non-unique and generally not orthogonal to one another. Assuming that there exists some $\mathbf{B}$-orthonormal

basis for the d eigenvectors associated with the d-fold degenerate eigenvalues, $\boldsymbol{\Psi} = \left[\boldsymbol{\psi}_r \cdots \boldsymbol{\psi}_{r+(d-1)}\right]$, i.e.,

$$\boldsymbol{\Psi}^T \mathbf{B} \boldsymbol{\Psi} = \mathbf{I} \tag{3.38}$$

(obtaining such a basis is discussed in Sec. 3.2), the eigenproblem for the subset of eigenpairs at degeneracy may be expressed as

$$\mathbf{A} \boldsymbol{\Psi} = \mathbf{B} \boldsymbol{\Psi} \boldsymbol{\Lambda}, \tag{3.39}$$

where $\boldsymbol{\Lambda} = diag(\lambda_r, \ldots, \lambda_{r+(d-1)}) = diag(\lambda_r, \ldots, \lambda_r)$. Note that even if Eq$^{\underline{n}}$ 3.38 is satisfied, Eq$^{\underline{n}}$ 3.10, i.e., the expression $\boldsymbol{\Psi}^T \left(\frac{\partial \mathbf{A}}{\partial p} - \lambda \frac{\partial \mathbf{B}}{\partial p} \right) \boldsymbol{\Psi}$, will generally not give the correct eigenvalue derivatives.

If the d eigenvalues separate upon parameter perturbation, then the associated eigenvectors will become unique. In order for differentiability of the eigenvectors to be defined, those eigenvectors at degeneracy, $\boldsymbol{\Psi}(p)$, must be oriented as the adjacent eigenvectors, $\boldsymbol{\Psi}(p + \delta p)$, $\delta p \longrightarrow 0$. In a first order eigenvalue coalescence, use may be made of the distinctness of the eigenvalue first derivatives to anticipate the adjacent eigenvectors and thus define a transformation $\boldsymbol{\Gamma}$ such that the correctly oriented vectors $\boldsymbol{\Phi} = \left[\boldsymbol{\phi}_r \cdots \boldsymbol{\phi}_{r+(d-1)}\right]$ are determined through

$$\boldsymbol{\Phi} = \boldsymbol{\Psi} \boldsymbol{\Gamma}. \tag{3.40}$$

N.B. $\boldsymbol{\Gamma}$ is an orthonormal transformation since

$$\boldsymbol{\Phi}^T \mathbf{M} \boldsymbol{\Phi} = \boldsymbol{\Gamma}^T \boldsymbol{\Psi}^T \mathbf{M} \boldsymbol{\Psi} \boldsymbol{\Gamma} = \boldsymbol{\Gamma}^T \boldsymbol{\Gamma} = \mathbf{I}. \tag{3.41}$$

Let the eigenproblem at degeneracy be defined for the vectors $\mathbf{\Phi}$:

$$\mathbf{A\Phi} = \mathbf{B\Phi\Lambda}. \tag{3.42}$$

Premultiplication of eigenproblem 3.42 by $\mathbf{\Psi}^T$, differentiation and substitution of Eq$^{\underline{n}}$ 3.40 leads to the auxiliary eigenproblem

$$\left[\mathbf{\Psi}^T\left(\frac{\partial \mathbf{A}}{\partial p} - \lambda\frac{\partial \mathbf{B}}{\partial p}\right)\mathbf{\Psi}\right]\mathbf{\Gamma} = \mathbf{\Gamma}\frac{\partial \mathbf{\Lambda}}{\partial p}, \tag{3.43}$$

whence $\mathbf{\Gamma}$ is found as the auxiliary eigenvector matrix; further, the eigenvalue derivatives are now correctly obtained as the auxiliary eigenvalues.

Analogously to Nelson's method, let

$$\mathbf{\Xi} = -\left(\frac{\partial \mathbf{A}}{\partial p} - \lambda\frac{\partial \mathbf{B}}{\partial p}\right)\mathbf{\Phi} + \mathbf{B\Phi}\frac{\partial \mathbf{\Lambda}}{\partial p}, \tag{3.44}$$

and let the pencil $\mathcal{P}$ be defined as in Eq$^{\underline{n}}$ 3.31. The latter has rank $N - d$, and a nullspace spanned by the eigenvectors $\mathbf{\Phi}$. Therefore, if it is given that $\mathbf{V}$ is a solution to the set of linear equations $\mathcal{P}\mathbf{V} = \mathbf{\Xi}$, then $\mathbf{V} + \mathbf{\Phi C}$ is also a solution, where $\mathbf{C} \in \mathbb{R}^{d\times d}$ is an arbitrary matrix.

The approach to reducing equations to allow for the inversion of $\mathcal{P}$ is as before, q.v. Eq$^{\underline{n}}$ 3.32-3.34, but needs to be performed d times for each of the eigenvectors associated with the d-fold degenerate eigenvalues, without repetition of κ (this may mean that κ relates to a successive maximum). The particular solution is then obtained as

$$\mathbf{V} = \overline{\mathcal{P}}^{-1}\mathbf{\Xi}. \tag{3.45}$$

It remains to find the constraint completing the solution to the eigenvector

derivative. Substitution of the general solution

$$\frac{\partial \mathbf{\Phi}}{\partial p} = \mathbf{V} + \mathbf{\Phi C} \tag{3.46}$$

into the **B**-orthonormality condition, viz.,

$$\mathbf{\Phi}^T \mathbf{B} \mathbf{\Phi} = \mathbf{I}, \tag{3.47}$$

differentiated leads to

$$\mathbf{C} + \mathbf{C}^T = -\mathbf{V}^T \mathbf{B} \mathbf{\Phi} - \mathbf{\Phi}^T \mathbf{B} \mathbf{V} - \mathbf{\Phi}^T \frac{\partial \mathbf{B}}{\partial p} \mathbf{\Phi}. \tag{3.48}$$

Ojalvo assumes the matrix **C** to be diagonal such that

$$\mathbf{C} = \frac{1}{2} \mathbf{\Phi}^T \frac{\partial \mathbf{B}}{\partial p} \mathbf{\Phi} - \mathbf{\Phi}^T \mathbf{B} \mathbf{V}. \tag{3.49}$$

The solution defined by Eq$^{\underline{n}}$ 3.45, Eq$^{\underline{n}}$ 3.46 and Eq$^{\underline{n}}$ 3.49 is valid for the following reasons. In the permanently degenerate case, a pair of degenerate eigenvalues remain equal over all p, so that as p varies, the associated d-dimensional eigenvector space does not separate into distinct 1-dimensional spaces, as would be the case with transitory eigenvalue coalescence. The derivatives of the eigenvectors cannot therefore be unique and any of a continuum of derivatives will take $\mathbf{\Phi} = \left[\boldsymbol{\phi}_r \cdots \boldsymbol{\phi}_{r+(d-1)}\right]$ into the perturbed eigenspace as p varies. The matrix **C** is then arbitrary to the extent that if Eq$^{\underline{n}}$ 3.48 is fulfilled, the resulting derivative is permissible although non-unique. It is interesting to note that the non-unique eigenvector derivatives associated with degenerate eigenvalue derivatives are analogous to the non-unique eigenvectors that are associated with degenerate eigenvalues.

Mills-Curran (1988) and Dailey (1989) find $\mathbf{C}$ non-symmetric so as to treat the case of first order transitory eigenvalue coalescence; twice differentiation of the eigenproblem 3.39, premultiplication by $\mathbf{\Phi}^T$ and substitution of Eq$^{\underline{n}}$ 3.46 leads to

$$\begin{aligned}\mathbf{\Upsilon} &\equiv \left(\mathbf{C}\frac{\partial \mathbf{\Lambda}}{\partial p} - \frac{\partial \mathbf{\Lambda}}{\partial p}\mathbf{C}\right) + \frac{1}{2}\frac{\partial^2 \mathbf{\Lambda}}{\partial p^2} \\ &= \mathbf{\Phi}^T\left(\left(\frac{\partial \mathbf{A}}{\partial p} - \lambda\frac{\partial \mathbf{B}}{\partial p}\right)\mathbf{V} + \frac{1}{2}\left(\frac{\partial^2 \mathbf{A}}{\partial p^2} - \lambda\frac{\partial^2 \mathbf{B}}{\partial p^2}\right)\mathbf{\Phi}\right. \\ &\qquad \left. - \left(\frac{\partial \mathbf{B}}{\partial p}\mathbf{\Phi} + \mathbf{B}\mathbf{V}\right)\frac{\partial \mathbf{\Lambda}}{\partial p}\right). \end{aligned} \tag{3.50}$$

Note that the first term will have a diagonal of zeros, while the matrix of eigenvalue second derivatives is diagonal. The construction of $\mathbf{C}$ is then according to

$$c_{ij} = \frac{v_{ij}}{\left(\frac{\partial \lambda_j}{\partial p} - \frac{\partial \lambda_i}{\partial p}\right)}, \qquad i \neq j; \tag{3.51}$$

the diagonal is defined by Eq$^{\underline{n}}$ 3.49, as proposed by Ojalvo. If desired, the eigenvalue second derivatives are obtainable as

$$\frac{\partial^2 \lambda_{ij}}{\partial p^2} = \frac{1}{2}v_{ij}, \qquad i = j. \tag{3.52}$$

The approach here given to reduce the set of linear equations, to allow for the inversion of Eq$^{\underline{n}}$ 3.45, owes to Nelson (1976) is also employed by Ojalvo (1988) and Dailey (1989). Under certain circumstances, this can fail to alleviate the singularity of $\mathcal{P}$ and the approach proposed by Mills-Curran (1988) needs to be employed; an example of such a circumstance is given by Mills-Curran (1989).

Shaw and Jayasuriya (1991) and Friswell (1996) treat the case of second order eigenvalue coalescence in a progression of the work of Ojalvo (1988), Mills-Curran (1988) and Dailey (1989) and expectedly obtain the eigenvector second derivatives and eigenvalue third derivatives. This is simply an employment of the foregoing philosophy that the distinct q^{th} eigenvalue derivatives in a q^{th} order coalescence can be used to anticipate how the eigenvalues will separate and hence how the associated d-dimensional eigenspace will separate into distinct 1-dimensional spaces.

Kim and Wallerstein (1987) use a linear perturbation method to evaluate eigenpair derivatives, which is effectively the same as that of Dailey and Mills-Curran. Song et al. (1995) circumvent completely the need to invert a set of linear equations and present a method that evaluates eigenvector derivatives, in the presence of degeneracy, through a generalised Schmidt orthogonalisation that orthogonalises a set of basis vectors, the linear combination of which provides the particular solution $\mathbf{V}$. Lee and Jung (1997) partition $\underline{\text{Eq}}^{\underline{\text{n}}}$ 3.22 and $\underline{\text{Eq}}^{\underline{\text{n}}}$ 3.25 to form a set of determined equations, which upon inversion yield both the eigenvector and eigenvalue derivatives; the equivalent constraint is provided by the eigenvectors immediately adjacent to coalescence, used as side conditions. This approach is more easily extended to treat damped dynamic systems as is shown by Lee et al. (1999).

For the first order transitory coalescence case, a number of other approaches to evaluating eigenpair derivatives in the presence of degenerate eigenvalues exist. Lim and Juang (1989) use singular value decomposition

to determine the basis of the degenerate eigenspace in order to define the eigenvector derivatives. (A similar approach for a degenerate 'equilibrium space' is given in Sec. 7.2.) Irwanto et al. (2003) utilise the spatial symmetry of cyclic structures to increase the efficiency of eigenpair derivative computation through employment of Fourier matrices.

In an effort to encapsulate the many studies on eigenpair derivatives, Jankovic (1994) derives expressions giving any q^{th} derivative of an eigenpair of a non-linear or linear eigenproblem, although these are only valid in the absence of degeneracy. Friswell (1994) extends Nelson's method to compute any q^{th} eigenpair derivative. Choi et al. (2004) employ an algebraic approach to give expressions for general q^{th} derivatives of eigenvalues and eigenvectors in the presence of degeneracy for damped systems. Andrew (1998) proposes a unified approach of calculating eigenvalue derivatives and provides an elementary proof that the familiar formulae hold under weaker hypotheses than are commonly applied, e.g., the derivative of an eigenvalue can be unique even when that of its associated eigenvector is not.

There exist a number of iterative methods for evaluating eigenpair derivatives further to that owing to Rudisill and Chu (1975). For eigenvector derivatives, Eldred et al. (1992) develop eigenvector normalisation methods that improve iterative convergence in terms of controlling oscillation and aiding stability. Andrew and Tan (1996) suggest a modification to a simultaneous iterative method for evaluating eigenvalue and eigenvector derivatives, which has the capability of treating the case of second order eigenvalue coalescence.

Lee and Lee (1996) develop an iterative method for computing eigenvector derivatives, which is almost parallel to the method of Mills-Curran (1988), but uses a shift applied to the eigenvalues, thus alleviating the matrix singularity and avoiding computation of the particular solution $\mathbf{V}$ and coefficient matrix $\mathbf{C}$. Lin et al. (1996) adopt an iterative scheme involving singular value decomposition to obtain the eigenvector derivatives.

A couple of survey papers covering some of the aforementioned references exist: Adelman and Haftka (1986) review eigenpair derivatives as used in a number of fields; Murthy and Haftka (1988) provide a survey for the eigenpair derivatives of a general, complex matrix. Several methods for computing eigenvector derivatives are assessed for their computational efficiency amongst Sutter et al. (1988) and Yu et al. (1997). Results indicate that the type of method owing to Nelson (1976) is most appealing since it is efficient, especially in multiparameter cases, and because it provides exact derivatives. Indeed, the approach to evaluating eigenvector derivatives in this thesis is that of Nelson and the subsequent, modified methods of Ojalvo, Mills-Curran and Dailey in the case of degenerate eigenvalues. The latter methods are also necessary to obtain the correct eigenvalue derivatives in certain circumstances of degeneracy of the corresponding eigenvalues; when the eigenvalues are distinct, Eq$^{\underline{n}}$ 3.10 is valid.

3.2 B-Orthonormal Bases for Eigenvectors at Degeneracy

It has been assumed that there exists an orthonormal basis for the eigenvectors at degeneracy. If the set of these vectors is not rank-deficient, then an orthogonal set can be obtained through Gram-Schmidt orthogonalisation. Let $\boldsymbol{\Psi} = \left[\boldsymbol{\psi}_r \cdots \boldsymbol{\psi}_{r+(d-1)}\right]$ be the set of eigenvectors at degeneracy, not **B**-orthogonal; a **B**-orthonormal set may be defined by

$$f : \boldsymbol{\psi}_i \longrightarrow \frac{\mathbf{g}_i}{\mathbf{g}_i^T \mathbf{B} \mathbf{g}_i}, \qquad i = r+1, \ldots, r+d-1, \tag{3.53}$$

where,

$$\mathbf{g}_i = \boldsymbol{\psi}_i - \sum_{j=1}^{i-1} \frac{f\left(\boldsymbol{\psi}_j\right)^T \mathbf{B} \boldsymbol{\psi}_i}{f\left(\boldsymbol{\psi}_j\right)^T \mathbf{B} f\left(\boldsymbol{\psi}_j\right)} f\left(\boldsymbol{\psi}_j\right). \tag{3.54}$$

In fact, in permanent degeneracy or in the event that all eigenvalues separate after coalescence, an orthonormal basis for the eigenvectors can be obtained through the transformation of Ojalvo (1988):

$$\boldsymbol{\Psi} \longrightarrow \boldsymbol{\Psi}\boldsymbol{\Gamma} \begin{bmatrix} w_{11}^{-\frac{1}{2}} & & \\ & \ddots & \\ & & w_{dd}^{-\frac{1}{2}} \end{bmatrix}, \tag{3.55}$$

where the modal mass matrix is defined as

$$\mathbf{W} = \boldsymbol{\Gamma}^T \boldsymbol{\Psi}^T \mathbf{B} \boldsymbol{\Psi} \boldsymbol{\Gamma}, \tag{3.56}$$

and is required to enforce **B**-normality; $\boldsymbol{\Gamma}$ is given by Eq$^{\underline{n}}$ 3.43.

3.3 $rank(\mathbf{J}) = rank(\mathbf{E})$

The rank of all Jacobian matrices associated with a finite element model formulated on a general equilibrium matrix, **E**, is equal to the rank of that

equilibrium matrix, independent of the values of the force parameters P.

Proof Assume a finite element model is solely parameterised with all distributions of force of the equilibrium matrix $\mathbf{E}$, so that there are ℓ global geometric stiffness matrices. From Eq$^{\underline{n}}$ 3.10, the corresponding Jacobian at any point $\mathbf{P}$ and for any m modes, $\mathbf{J}$, is

$$\begin{bmatrix} \frac{1}{P_1}\boldsymbol{\phi}_1^T\mathbf{G}_1\boldsymbol{\phi}_1 & \frac{1}{P_2}\boldsymbol{\phi}_1^T\mathbf{G}_2\boldsymbol{\phi}_1 & \cdots & \frac{1}{P_n}\boldsymbol{\phi}_1^T\mathbf{G}_n\boldsymbol{\phi}_1 & \cdots & \frac{1}{P_\ell}\boldsymbol{\phi}_1^T\mathbf{G}_\ell\boldsymbol{\phi}_1 \\ \frac{1}{P_1}\boldsymbol{\phi}_2^T\mathbf{G}_1\boldsymbol{\phi}_2 & \frac{1}{P_2}\boldsymbol{\phi}_2^T\mathbf{G}_2\boldsymbol{\phi}_2 & & & & \\ \vdots & & \ddots & & & \\ \frac{1}{P_1}\boldsymbol{\phi}_m^T\mathbf{G}_1\boldsymbol{\phi}_m & & & & & \frac{1}{P_\ell}\boldsymbol{\phi}_m^T\mathbf{G}_\ell\boldsymbol{\phi}_m \end{bmatrix}, \quad (3.57)$$

where a general element is the quadratic form

$$\frac{1}{P}\boldsymbol{\phi}^T\mathbf{G}\boldsymbol{\phi} = \frac{1}{P}\begin{pmatrix} g_{11}\phi_1^2 & + & g_{12}\phi_1\phi_2 & + & \cdots & + & g_{1N}\phi_1\phi_N \\ g_{21}\phi_2\phi_1 & + & g_{22}\phi_2^2 & + & \cdots & + & g_{2N}\phi_2\phi_N \\ & & & & \cdots & & \\ g_{N1}\phi_N\phi_1 & + & g_{N2}\phi_N\phi_2 & + & \cdots & + & g_{NN}\phi_N^2 \end{pmatrix}. \quad (3.58)$$

Any global stiffness matrix $\mathbf{G}$ is particular to a force distribution and is assembled with elemental stiffness matrices of the form $\mathbf{G}^e = e_{ij}\mathbb{G}^e$ (q.v. Appendix A), where e_{ij} is a general element of the equilibrium matrix $\mathbf{E}$.

If $\mathbf{E}$ is rank deficient, then a general column can be expressed as a linear combination of all other columns, e.g.,

$$\mathbf{e}_\ell = c_1\mathbf{e}_1 + c_2\mathbf{e}_2 + \cdots + c_n\mathbf{e}_n + \cdots + c_{\ell-1}\mathbf{e}_{\ell-1}, \quad (3.59)$$

and it follows that

$$g_{ij,\ell} = c_1 g_{ij,1} + c_2 g_{ij,2} + \cdots + c_n g_{ij,n} + \cdots + c_{\ell-1} g_{ij,\ell-1} \quad (3.60)$$

and

$$\mathbf{G}_\ell = c_1\mathbf{G}_1 + c_2\mathbf{G}_2 + \cdots + c_n\mathbf{G}_n + \cdots + c_{\ell-1}\mathbf{G}_{\ell-1}. \quad (3.61)$$

A general element of the ℓ^{th} column of $\mathbf{J}$ is

$$\frac{1}{P_\ell}\boldsymbol{\phi}^T\mathbf{G}_\ell\boldsymbol{\phi} = \frac{1}{P_\ell}\boldsymbol{\phi}^T\left(c_1\mathbf{G}_1 + c_2\mathbf{G}_2 + \cdots + c_n\mathbf{G}_n + \cdots + c_{\ell-1}\mathbf{G}_{\ell-1}\right)\boldsymbol{\phi}. \quad (3.62)$$

Since the elements g_{ij} form the coefficients of the second order polynomial 3.58,

$$\frac{1}{P_\ell}\boldsymbol{\phi}^T\mathbf{G}_\ell\boldsymbol{\phi} =$$
$$\frac{1}{P_\ell}\left(c_1\boldsymbol{\phi}^T\mathbf{G}_1\boldsymbol{\phi} + c_2\boldsymbol{\phi}^T\mathbf{G}_2\boldsymbol{\phi} + \cdots + c_n\boldsymbol{\phi}^T\mathbf{G}_n\boldsymbol{\phi} + \cdots + c_{\ell-1}\boldsymbol{\phi}^T\mathbf{G}_{\ell-1}\boldsymbol{\phi}\right) \quad (3.63)$$

and

$$\mathbf{j}_\ell = \frac{1}{P_\ell}\left(c_1\mathbf{j}_1 + c_2\mathbf{j}_2 + \cdots + c_n\mathbf{j}_n + \cdots + c_{\ell-1}\mathbf{j}_{\ell-1}\right). \quad (3.64)$$

Evidently, from Eq$^{\underline{n}}$ 3.59 and Eq$^{\underline{n}}$ 3.64,

$$rank\left(\mathbf{E}\right) = n \Rightarrow rank\left(\mathbf{J}\right) = n; \quad (3.65)$$

$$rank\left(\mathbf{J}\right) = rank\left(\mathbf{E}\right) \quad \square \quad (3.66)$$

It is always prudent to formulate a finite element model on a full rank equilibrium matrix $\overline{\mathbf{E}}$ to avoid singularity of the Jacobian and consequent non-uniqueness of the problem root.

3.4 Closure

Although a very small asymmetric perturbation to the mathematical model would alleviate degeneracy, the evaluation of eigenpair derivatives in the presence of eigenvalue degeneracy has been surveyed to be of academic interest. As such, it is not necessary to apply asymmetric perturbations and

the results that have been presented can be used to address the degeneracy issues.

The aspects of this chapter relevant to the remainder of the thesis are as follows. When the eigenvalues are distinct, the expression of Fox and Kapoor (1968), Eq^{n} 3.10, suffices to give the eigenvalue derivatives. The corresponding eigenvector derivatives are computed by the method devised by Nelson (1976), which offers efficiency of solution; this is defined over Eq^{n} 3.29-3.37.

When the eigenvalues are permanently degenerate, the modification given by Ojalvo (1988), extending Nelson's method, is used to evaluate derivatives of both the eigenvalues and their eigenvectors; this is defined over Eq^{n} 3.38-3.49. The eigenvector derivatives are, in this case, non-unique but valid, because for permanent degeneracy of the eigenvalues, the associated d-dimensional eigenvector space never separates into distinct 1-dimensional spaces.

In the event of simple eigenvalue coalescence, in which the eigenvalues are only transitorily degenerate, the associated d-dimensional eigenvector space does separate (with the eigenvalues). The methods of Mills-Curran (1988) and Dailey (1989), whose supplementation to the method of Ojalvo is shown in Eq^{n} 3.50-3.52, are used in this circumstance. Incidentally, the eigenvalue second derivatives are obtained.

In this way, the cases of permanent and first order transitory coalescence are addressed. A further, special case is the coalescence involving distinct

and permanently degenerate loci. In this type of degeneracy, Eq$^{\underline{n}}$ 3.10 will not return the correct eigenvalue derivatives. Assuming the eigenvectors at degeneracy form a **B**-orthonormal set, the correct eigenvalue derivatives have to be obtained as the auxiliary eigenvalues of Eq$^{\underline{n}}$ 3.43. The auxiliary eigenvectors form a transformation matrix to separate any eigenvectors at degeneracy whose eigenvalues separate after transitory coalescence, i.e., whose adjacent eigenvectors occupy distinct 1-dimensional spaces. Such eigenvectors can be used as the pivotal vectors when reinstating **B**-orthonormality through the Gram-Schmidt method. The eigenvectors whose eigenvalues remain permanently degenerate away from transitory coalescence remain arbitrarily oriented.

The following chapter shows how such eigenvectors associated with permanent degeneracy can be numerically aligned to their adjacent eigenvectors, or indeed other eigenvectors at subsequent parameter values.

It is interesting to note that for derivatives with respect to force parameters, the expression $\frac{\partial \mathbf{A}}{\partial p} - \lambda \frac{\partial \mathbf{B}}{\partial p}$, which occurs in Eq$^{\underline{n}}$ 3.10 and Eq$^{\underline{n}}$ 3.43, by Eq$^{\underline{n}}$ 2.4 reduces to $P_E^+ \mathbb{G}$ since $\mathbf{A} \equiv \mathbf{K}+\mathbf{G}$, $\mathbf{B} \equiv \mathbf{M}$ and $\mathbf{K}$ and $\mathbf{M}$ are independent of p. The eigenvalue derivative according to Eq$^{\underline{n}}$ 3.10, for example, is simply

$$\frac{\partial \lambda}{\partial p} = P_E^+ \boldsymbol{\phi}^T \mathbb{G} \boldsymbol{\phi}, \tag{3.67}$$

which does not explicitly include p; since $\mathbb{G}$ is a constant matrix for a particular distribution of force, there is no computational cost associated with having to re-evaluate $\frac{\partial \mathbf{A}}{\partial p} - \lambda \frac{\partial \mathbf{B}}{\partial p}$. N.B. Although $\mathbb{G}$ is independent of p, its form *is* dictated by the pattern of loading in a given force distribution, since

the ℓ elemental matrices $\mathbb{G}^e$ from which it is constructed are factored by the elements of $\mathbf{E}$, e_{ij}.

Chapter 4

Behaviour of Eigenvalue Loci

Much consideration needs to be given to the manner in which the eigenvalues behave with respect to parameters and the potential effect this has upon iteration. Mechanisms by which iteration might fail are identified and solutions are suggested. The main problem is of frequencies exchanging places in the spectrum. This is problematic because the eigenvalues that relate to the frequencies are numerically ordered and, due to this exchanging phenomenon, form non-smooth functions of the parameters. Measures for iterates to trace an eigenvalue locus passed coalescence points, where eigenvalues intersect, are found, the desire being to preserve function continuity. These mode tracing strategies make use of eigenvector consistencies across coalescence points to identify the true, smooth eigenvalue functions. However, these are seen to break down if there are abrupt changes in mode shapes, such as are associated with strong veering of the eigenvalues. A new routine is suggested to overcome this shortfall, which involves modelling the eigenvectors as first order functions to approximate what they are at the adjacent iterate.

4.1 Adversity to Newton's Method Imposed by Locus Behaviour and the Mode Tracing Solution

The definition of a mode is somewhat more superficial than might first be thought. When dependent upon physical parameters, both the frequencies and mode shapes, the properties that characterise these modes, may be subject to significant changes. Frequencies are known to coalesce and mode shapes to couple. There are then problems in describing a *mode*, both physically and mathematically. Much of the work in this thesis serves to expose the difficulties associated with the volatile nature of eigenpairs dependent upon load and the consequent predicament of defining a mode.

The ordering of eigenpairs is arbitrary. Typically, eigenpairs are ordered according to the magnitudes of the eigenvalues. If this is done, then transitory eigenvalue coalescence with respect to some independent variable defines non-smooth eigenvalue functions of that variable. This is detrimental to Newton's method in terms of abrupt changes in function gradient sign and the increased likelihood of iteration failing, as indicated by Fig. 4.1. This issue is encountered, but not resolved, by Greening (1999) and Greening and Lieven (2003), in work upon which present methods of force identification in this thesis are founded. It is in fact a great concern, making the success of convergence a great improbability, and indeed much of the investigation in the present and subsequent chapters is involved in detail with overcoming the adverse effects of eigenvalue coalescence.

While the eigenvalues exhibit considerable variation with respect to a parameter, the eigenvectors can experience *relatively* little change over particular ranges of parameter. Mead (2002) notes that the mode shapes of a six member, planar, fixed-jointed frame subject to self-equilibrating forces change little if at all with respect to loading. Previous work has exploited the steadfastness of eigenvectors in correlating modes, preceding and proceeding parameter perturbation. Ting et al. (1995) have used the Modal Assurance Criterion (*mac*), an eigenvector consistency measure formulated by Allemang and Brown (1982), to develop a binary, permutation operator, operating upon the nominated subset of eigenvectors of a current iterate and permuting them to concur in a physical sense with those at another iterate. Kim and Kim (2000) have utilised the *mac* similarly in structural topology optimisation. Analogously, cross-mass-orthogonality (*xor*) has been implemented to the same end with good effect by Gibson (1992), Eldred et al. (1995a) and Eldred et al. (1995b). Other methods of pairing modes include those that deal with perturbation expansions of the eigenproblem, q.v. Eldred et al. (1992), but these are deemed computationally expensive and not as suitable for the present task of mode tracing in frame force identification (cf. Sec. 4.6, which describes a first order expansion of the eigenvectors).

Mode tracing in load identification must use the root as a reference, so that not only are the frequencies to be determined from the investigated, physical frame, but also the mode shapes. It is desirable that the detail to which a mode shape has to be defined be minimal. Experience has shown

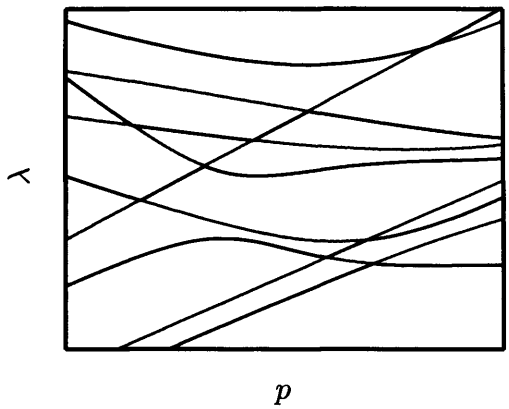

Figure 4.1: Non-smooth functions defined by eigenvalue coalescence.

that good consistency holds between mathematical eigenvectors and simulated mode shapes defined at a very limited number of degrees of freedom. Presently, *mac* is the consistency measure used for tracing modes and is implemented as outlined shortly. Note that since the mass matrix is stationary with respect to the force parameters, *xor*, which by definition involves the mass matrix **M**, could also be used as an efficient mode tracer, if, hypothetically, all responses at all degrees of freedom were measured. Cross orthogonality is analysed in this chapter alongside *mac* as a comparison and, as a more mathematically sound consistency measure, serves to highlight problems with *mac* in the studies that follow.

Let there be s modes in the root subset S, which are those modes observed in the physical structure, and let there be t modes in a subset T at the current iterate, k. Generally, t should be greater than s in order that T encompasses all of the modes in S. However, t cannot be too large for reasons of computational cost and spatial aliasing, which is discussed ahead.

Further, let

$$mac_{ij}\left(\boldsymbol{\phi}_i^{\circledR}, \boldsymbol{\phi}_j^k\right) = \frac{\left|\left(\boldsymbol{\phi}_i^{\circledR}\right)^T \boldsymbol{\phi}_j^k\right|^2}{\left\|\boldsymbol{\phi}_i^{\circledR}\right\|_2^2 \left\|\boldsymbol{\phi}_j^k\right\|_2^2} \in [0,1], \tag{4.1}$$

$i = 1, 2, \ldots, s$, $j = 1, 2, \ldots, t$, be the elements of the **MAC** matrix of dimension $s \times t$ relating the vector consistency between the i^{th} eigenvector in S and the j^{th} eigenvector in T.

The cross-mass-orthogonality matrix **XOR** is defined by the elements

$$xor_{ij}\left(\boldsymbol{\phi}_i^{\circledR}, \boldsymbol{\phi}_j^k\right) = \left(\boldsymbol{\phi}_i^{\circledR}\right)^T \mathbf{M}\left(\boldsymbol{\phi}_j^k\right) \in [0,1], \tag{4.2}$$

$i = 1, 2, \ldots, s$, $j = 1, 2, \ldots, t$, which signify the deviation from **M**-orthonormality as parameters, and hence eigenvectors, vary.

The permutation of modes in T may be expressed as

$$\rho_1 : \left[\boldsymbol{\phi}_1^k \cdots \boldsymbol{\phi}_t^k\right] \longrightarrow \left[\boldsymbol{\phi}_1^k \cdots \boldsymbol{\phi}_t^k\right] \boldsymbol{\Theta}^T, \tag{4.3}$$

and, consistently,

$$\rho_2 : \{\lambda_1^k \cdots \lambda_t^k\} \longrightarrow \{\lambda_1^k \cdots \lambda_t^k\} \boldsymbol{\Theta}^T, \tag{4.4}$$

where the $s \times t$ operator $\boldsymbol{\Theta}$ is a binary permutation matrix whose rows contain exclusive units corresponding to the row maxima of the matrix **MAC**, or, for that matter, **XOR**. By permutations ρ_1 and ρ_2, with the assumption that there is no ambiguity in vector correlation, there are always s modes with physically consistent permutations in consideration at iterate k.

Choosing the size of the subset of modes at the current iterate, T, is not simple and no robust means exists for doing so. If the number of modes t

is too small, then T will not contain the eigenvectors with which the eigenvectors in S are truly consistent. The incompleteness of the resulting permutation matrix serves to annihilate or zero the absent eigenvectors and eigenvalues when operations 4.3 and 4.4 are performed. On the other hand, if t is too large, erroneous pairings can occur because of a spatial aliasing problem. That is to say, extra to the correct pairings of modes, there may exist secondary pairings with higher order modes in T because the level of discretisation of the finite element model and the degrees of freedom where the root mode shapes are defined. As far as the scrutiny of the consistency measure, *mac* or *xor*, is concerned, two different mode shapes may appear similar in such a circumstance. Due to the aliasing issue, and also for reasons of computational cost, t should be upper-bounded, and this can be done by using aliasing arguments. Fig. 4.2 illustrates the spatial aliasing problem; if, as in this example, $s = 100$ (the initial 100 modes), in order to avoid ambiguity with the higher order mode cluster, T could encompass the first $t = 200$ modes at each iterate. While not entirely robust, such a strategy could be adopted at $k = 0$ to choose t for all subsequent iterates. If all of the N modes are used, then there is the risk that experimental error, for example, causes low consistency with the correct mode in T, but a higher consistency with a higher order mode, thus causing iteration to fail.

In order to assess the applicability of the mode tracing scheme outlined, it is necessary to appreciate the behaviour of the eigenvalue loci and to what extent the eigenvector consistency can be deemed a reliable foundation for

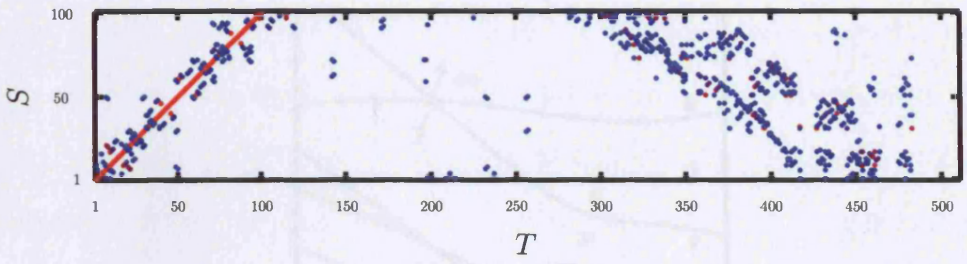

Figure 4.2: The spatial aliasing problem demonstrated in the *mac* consistency between the first hundred modes and all N modes of a finite element model; all eigenvectors are defined at 28.2 per cent of the total number N of degrees of freedom; 0 1 *mac* consistency scale.

defining locus smoothness. Two examples are here given: the first is an order-2 linear operator, used by Kato (1976) to demonstrate the analytic perturbation of eigenvalues and by Haug and Rousselet (1980) to show that numerically ordered, degenerate eigenvalues are only Gâteaux, or directionally, differentiable (because of the coalescence-induced non-smoothness); the second is a simple, bi-tetrahedral space frame model.

N.B. In all of the examples in this chapter, the *entire* eigenvectors are used in computing consistency values. In this way, problems in tracing modes even when complete data is available are highlighted. The issues that arise despite possessing perfect, errorless root data, are most exemplified in the final example of the octet frame. Mode tracing with the additional problem of having a limited number of eigenvector degrees of freedom is deferred to the experimental chapters, Ch. 6 and Ch. 7. Involving all of the degrees of freedom also allows *xor*, which requires in its evaluation the entire mass matrix, to be employed as a comparative consistency measure to *mac*.

Before presenting the examples, it is first necessary to discuss another

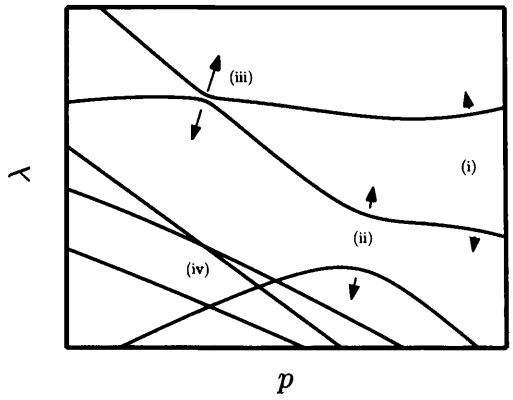

Figure 4.3: Eigenvalue locus veering: (i) weak veering; (ii) intermediate veering; (iii) strong veering; (iv) various coalescences.

phenomenon exhibited by eigenvalue loci which affects the tracing of modes. Eigenvalue coalescence can be thought of as a limiting case of a more general phenomenon known as locus veering, examples of which are seen in Fig. 4.3. Here, the eigenvalue loci veer away from one another by a degree that is dependent upon the closeness of the eigenvalues at the veering point. Eigenvalue coalescence involves two or more loci passing through each other without interaction or any coupling of the respective eigenvectors, except at the coalescence point itself. In veering, analogously, it is the pair of diagonally opposing branches that demonstrate mutual consistency of their eigenvectors; consequently, the veering point marks a rapid transition of the coupling eigenvectors from one pair to the other, so that they can become 'unrecognisable'.

While veering can be an actual phenomenon of a physical frame and manifest itself in the mathematical model, it can also be induced by low model discretisation and unsuitable modelling in closed-form solutions, as noted by

Leissa (1974). The effects of discretisation on veering, as well as geometric symmetry and non-adjointness of the system matrices, is demonstrated by Perkins and Mote (1986). Low discretisation is found to bring about veering, although increasing the finite number of terms in the discrete formulation by one can change a veering into a coalescence; symmetry-breaking is seen to change coalescences to veerings. This is a transformation that also holds in reality, where the physical structure can never be perfectly symmetric, and therefore some of its frequencies may veer with respect to some parameter rather than coalesce, as might be indicated mathematically. The general veering problem is further discussed in some depth by Petyt and Fleischer (1971), Kuttler and Sigillito (1981), Pierre and Dowell (1987), Pierre (1988), Pierre and Cha (1989), and Natsiavas (1993), amongst others.

4.2 Loci of an Order-2 Linear Operator

The eigenpairs of an order-2 linear operator,

$$\mathbf{A}\left(p_1, p_2\right) = \begin{pmatrix} p_1 & p_2 \\ p_2 & -p_1 \end{pmatrix}, \tag{4.5}$$

are investigated as functions of the independent variables p_1 and p_2 and used to explore the behaviour of *mac*,

$$mac_{ij}\left(\boldsymbol{\phi}_i\left(p_1^o, p_2^o\right), \boldsymbol{\phi}_j\left(p_1, p_2\right)\right) = \frac{\left|\boldsymbol{\phi}_i\left(p_1^o, p_2^o\right)^T \boldsymbol{\phi}_j\left(p_1, p_2\right)\right|^2}{\left\|\boldsymbol{\phi}_i\left(p_1^o, p_2^o\right)\right\|_2^2 \left\|\boldsymbol{\phi}_j\left(p_1, p_2\right)\right\|_2^2}, \tag{4.6}$$

and cross-orthogonality,

$$xor_{ij}\left(\boldsymbol{\phi}_i\left(p_1^o, p_2^o\right), \boldsymbol{\phi}_j\left(p_1, p_2\right)\right) = \boldsymbol{\phi}_i\left(p_1^o, p_2^o\right)^T \boldsymbol{\phi}_j\left(p_1, p_2\right); \tag{4.7}$$

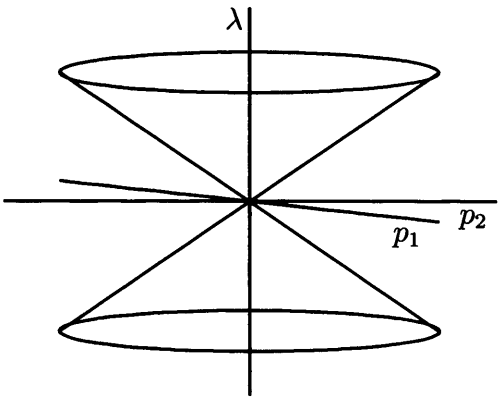

Figure 4.4: Eigenvalues of **A** as functions of its parameters p_1 and p_2.

(p_1^o, p_2^o) are fixed points of (p_1, p_2), so that $\boldsymbol{\phi}\,(p_1^o, p_2^o)$ is a stationary eigenvector. Note that in this special case, because the value of all eigenvector norms is unity, the denominator of Eq$^{\underline{n}}$ 4.6 is unity and $mac_{ij} = xor_{ij}^2$.

The nature of **A** is useful as its eigenvalues are conical functions of p_1 and p_2 — q.v. Fig. 4.4 — and so for constant p_2, say, varying degrees of veering can be simulated in the λ-p_1 plane according to the value of p_2 with $p_2 = 0$ corresponding to the case of eigenvalue coalescence.

Fig. 4.5 shows the variations of the eigenvalues with respect to p_1 at various values of constant p_2. Deviation from the coalescence case, $p_2 = 0$, is easily appreciable as p_2 increases and the eigenvalues exhibit veering with diminishing strength. Veering is indeed dependent upon the closeness of the eigenvalues at the veering event, a point noted by Liu (2002), who proposes it as a key measure of the degree of the phenomenon and further notes that the eigenvector derivative and the eigenvalue second derivative can anticipate the onset of veering[1]. Perkins and Mote (1986) also propose quantities to

[1]Recall Ch. 3 showing that the eigenvector derivative and the eigenvalue second deriva-

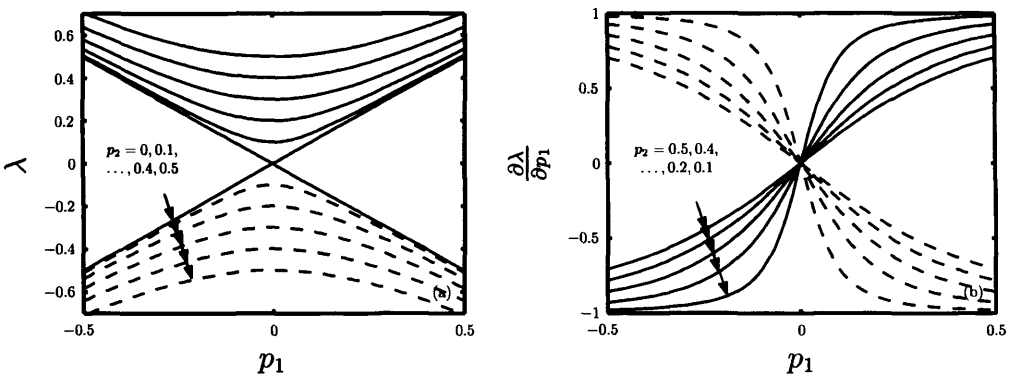

Figure 4.5: (a) Eigenvalues of **A** as functions of p_1 at various values of constant p_2; (b) eigenvalue derivatives as functions of p_1 at various values of constant p_2; ———— upper loci; – – – – lower loci.

distinguish eigenvalue locus veering from eigenvalue coalescence.

Since the eigenvalue loci of Fig. 4.5 are effectively a series of conic sections, the paths of the eigenvalues trace out sets of hyperbola as p_1 varies. Increasing p_2 is exactly analogous to focussing on the veering event. When evaluating consistency, the stationary eigenvector $\boldsymbol{\phi}(p_1^o, p_2^o)$ will arbitrarily be taken as the eigenvector at $p_1 = -0.5$ or $p_1 = 0$, while $\boldsymbol{\phi}(p_1, p_2)$ will be the eigenvector varying with respect to p_1, noting p_2 is constant.

Fig. 4.5 further shows the corresponding eigenvalue partial derivatives as functions of p_1 at various values of constant p_2. It is clear that at the eigenvalue coalescence case, not shown here, the eigenvalue derivatives are discontinuous step functions. Consequently, although the linear operator **A** is self-adjoint, the partial derivatives of its eigenvalues in the case of coalescence, $p_2 = 0$, are not Fréchet differentiable at $p_1 = 0$; as was discussed in

tive are inherently dependent upon one another. This was seen in the method of evaluating the eigenvector derivative owing to Nelson (1976) producing the eigenvalue second derivative as a by-product to the solution.

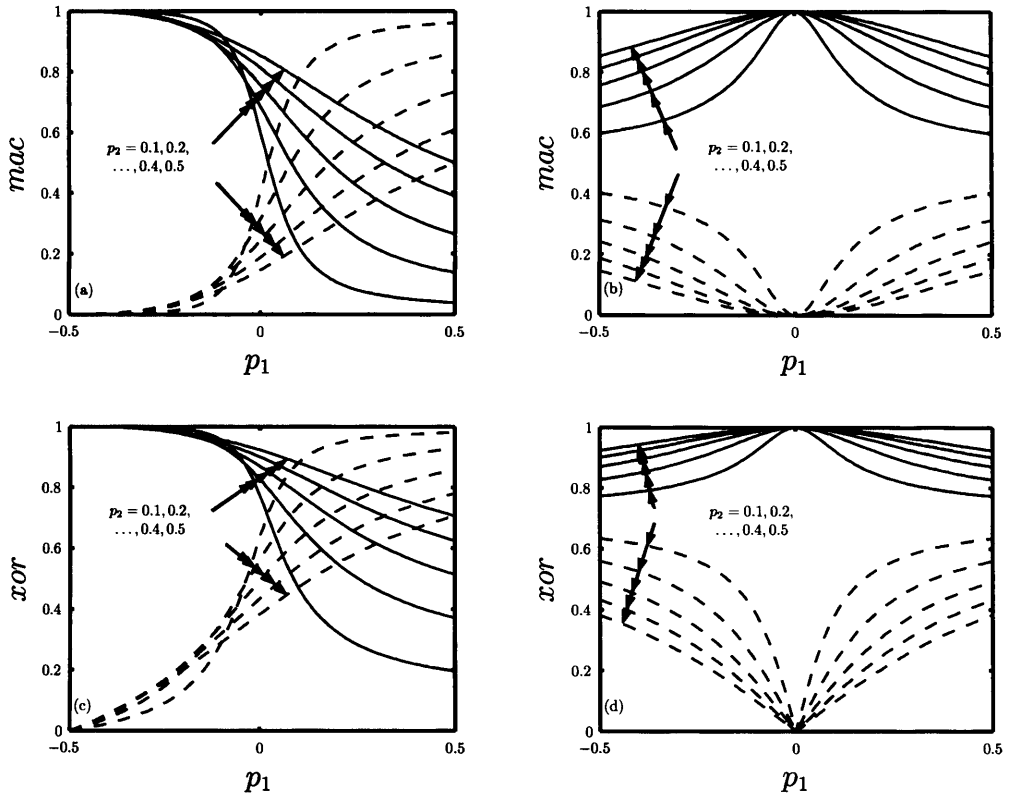

Figure 4.6: (a) *mac* as a function of p_1 at various values of constant p_2 with $p_1^o = -0.5$; (b) *mac* as a function of p_1 at various values of constant p_2 with $p_1^o = 0$; (c) *xor* as a function of p_1 at various values of constant p_2 with $p_1^o = -0.5$; (d) *xor* as a function of p_1 at various values of constant p_2 with $p_1^o = 0$; (q.v. Fig. 4.5), ———— consistency within upper locus, – – – – corruption with lower locus.

Ch. 3, there exist two Gâteaux derivatives depending on whether the limit is approached from p_1^- or p_1^+.

Fig. 4.6(a) shows the *mac* of the upper loci as a function of p_1 at various values of constant p_2, for $\phi(p_1^o, p_2^o)$ taken as the eigenvector at $p_1 = -0.5$; Fig. 4.6(b) shows the same with $\phi(p_1^o, p_2^o)$ taken as the eigenvector at $p_1 = 0$; Fig. 4.6(c) and Fig. 4.6(d) show analogous *xor* variations. From Fig. 4.6(a) and Fig. 4.6(c), it is evident that as the stationary, datum eigenvector tends away from the veering event, both *mac* and *xor* tend to a linear relationship

with the eigenvalue derivative — cf. Fig. 4.5(b). This reiterates the strong relationship between the eigenvector derivative and the eigenvalue second derivative as mentioned earlier and noted by Liu (2002).

While *xor* shows greater overall consistency, it also demonstrates greater overall corruption — consistency with the lower locus — with consistency and corruption functions always crossing at a value of $\frac{1}{\sqrt{2}}$; as a consequence of $mac_{ij} = xor_{ij}^2$, *mac* has consistency and corruption functions symmetrical about and crossing at a value $\frac{1}{2}$. It follows that for certain values of p_1, *xor* and *mac* are completely ambiguous in this example, having equal consistency and corruption terms. Mode tracing requires not so much high consistency, although this is desirable, but a minimum ambiguity so that there is confidence in tracing modes. Ultimately, smooth traces should be established.

Fig. 4.6(b) and Fig. 4.6(d) show the consistency and corruption between the point where the eigenvectors undergo their maximum rate of change and the range $-0.5 \leq p_1 \leq 0.5$. Here, the graphs at increasing values of p_2 are simply increasing magnifications of the original curve. For *mac* and *xor*, the consistency and corruption curves are respectively asymptotic to $\frac{1}{2}$ and $\frac{1}{\sqrt{2}}$, the values at which they intersect in Fig. 4.6(a) and Fig. 4.6(c).

N.B. The asymptotic property demonstrated in Fig. 4.6(b) and Fig. 4.6(d) indicates an important attribute of eigenvalue loci to acknowledge in general: consistency and corruption approaching a constant value means that the eigenvectors away from veering, where the eigenvalue loci become straighter,

are quasi-constant. Further, the relationship between the eigenvectors, or eigenvector consistency, and the eigenvalue derivative can be appreciated from a physical argument that has manifested itself in the veering phenomenon. Isolated dynamic systems that exhibit linear, or quasi-linear, eigenvalue loci with respect to some parameter, with constant, or quasi-constant, associated eigenvectors, when coupled into a global system exhibit loci veering corresponding to rapid transformations of the eigenvectors. One example is the linear eigenvalue loci and constant eigenvectors of axially loaded, simply supported beams, which, when assembled in a framework, couple to exhibit veering events joining two otherwise straight loci. This suggests that simple loci veering experienced in dynamic systems forms, as in the present example, hyperbolic eigenvalue loci. However, as will be seen in Sec. 4.4, the loci veering demonstrated by more complicated, coupled dynamic systems are not always simple and can have high degrees of curvature and behave erratically.

4.3 Mode Traces in Permanently Degenerate Eigensystems

Ch. 3 discussed the eigenvectors of permanently degenerate eigenvalues and their arbitrariness. Any linear combination of these eigenvectors is a nullspace of the pencil $\mathbf{A}-\lambda\mathbf{B}$. While an orthonormal basis for the eigenvectors can be found, it is not unique. Consequently, there arises a problem in tracing the modes of permanently degenerate eigensystems since the eigenvectors may

at each value of p be at various different spatial orientations. It is proposed, therefore, that the eigenvectors be aligned by minimising the squares of their discrepancies. That is to say, the eigenvectors at a general iterate k, which will occur in pairs spanning two-dimensional subspaces, are to be aligned to an eigenvector at the root $\boldsymbol{\phi}^{®}$ — one physically observed. It is assumed that all eigenvectors are forced to exhibit **B**-orthonormality (q.v. Sec. 3.2).

For the **B**-orthonormal set of eigenvectors $\boldsymbol{\Phi} = \left[\boldsymbol{\phi}_r \cdots \boldsymbol{\phi}_{r+(d-1)}\right]$ associated with d-fold permanently degenerate eigenvalues at iterate k, let the transformation matrix $\overline{\boldsymbol{\Gamma}}$ be defined as

$$\overline{\boldsymbol{\Gamma}} = \left(\left(\boldsymbol{\Phi}^k\right)^T \boldsymbol{\Phi}^k\right)^{-1} \left(\left(\boldsymbol{\Phi}^k\right)^T \boldsymbol{\phi}^{®}\right) \begin{bmatrix} w_{11}^{-\frac{1}{2}} & & \\ & \ddots & \\ & & w_{dd}^{-\frac{1}{2}} \end{bmatrix}, \tag{4.8}$$

where the matrix preserving **B**-normality is

$$\mathbf{W} = \left(\left(\left(\boldsymbol{\Phi}^k\right)^T \boldsymbol{\Phi}^k\right)^{-1} \left(\left(\boldsymbol{\Phi}^k\right)^T \boldsymbol{\phi}^{®}\right)\right)^T \left(\boldsymbol{\Phi}^k\right)^T \mathbf{B} \cdot \boldsymbol{\Phi}^k \left(\left(\boldsymbol{\Phi}^k\right)^T \boldsymbol{\Phi}^k\right)^{-1} \left(\left(\boldsymbol{\Phi}^k\right)^T \boldsymbol{\phi}^{®}\right). \tag{4.9}$$

Eq^{n} 4.8 serves to perform the least squares minimisation

$$\min\left(trace\left(\left(\boldsymbol{\Phi}^k\overline{\boldsymbol{\Gamma}} - \boldsymbol{\phi}^{®}\right)^T \left(\boldsymbol{\Phi}^k\overline{\boldsymbol{\Gamma}} - \boldsymbol{\phi}^{®}\right)\right)\right). \tag{4.10}$$

The multiplicity d is, in all permanently degenerate cases observed in this thesis, two. Walther et al. (2004) recognise that if the physical mode shapes are well defined in terms of the degrees of freedom measured, and the mathematical eigenvectors are reduced accordingly, then

$$\left(\boldsymbol{\Phi}^k\right)^T \boldsymbol{\Phi}^k \approx \mathbf{I} \tag{4.11}$$

and, consequently, Eq$^{\underline{n}}$ 4.8 approximates to

$$\overline{\mathbf{\Gamma}} \approx \left(\left(\mathbf{\Phi}^k \right)^T \boldsymbol{\phi}^{\circledR} \right) \begin{bmatrix} w_{11}^{-\frac{1}{2}} & & \\ & \ddots & \\ & & w_{dd}^{-\frac{1}{2}} \end{bmatrix}. \tag{4.12}$$

The aligned eigenvectors are given by

$$\overline{\boldsymbol{\phi}} = \mathbf{\Phi} \overline{\mathbf{\Gamma}}, \tag{4.13}$$

so that *mac* consistency is evaluated as

$$mac\left(\boldsymbol{\phi}^{\circledR}, \overline{\boldsymbol{\phi}} \right) = \frac{\left| \left(\boldsymbol{\phi}^{\circledR} \right)^T \overline{\boldsymbol{\phi}} \right|^2}{\left\| \boldsymbol{\phi}^{\circledR} \right\|_2^2 \left\| \overline{\boldsymbol{\phi}} \right\|_2^2} \in [0, 1]. \tag{4.14}$$

Note that the eigenvector $\overline{\boldsymbol{\phi}}$ is **B**-orthonormal since it is a linear sum of the **B**-orthonormal eigenvectors $\mathbf{\Phi}$ and that $\overline{\mathbf{\Gamma}}$ is defined as an orthonormal transformation. Such vector alignment has been used in the reconciliation of mathematical and observed eigenvectors in the presence of repeated frequencies by Lallement and Kosanek (1993) and Peŝek (1995). Presently, it is used in ensuring continuity of the eigenvector degrees of freedom for the purposes of mode tracing.

D'Ambrogio and Fregolent (2003) inspect the case where a root mode can be correlated with a two-dimensional subspace spanned by mathematical eigenvectors, i.e., one that may be expressible as a linear sum of two theoretical eigenvectors, and derive an explicit consistency expression, equal to Eq$^{\underline{n}}$ 4.14, that is independent of the transformation $\overline{\mathbf{\Gamma}} = [\overline{\gamma_1}\ \overline{\gamma_2}]^T$:

$$mac\left([\overline{\gamma_1} \boldsymbol{\phi}_r + \overline{\gamma_2} \boldsymbol{\phi}_{r+1}], \boldsymbol{\phi}^{\circledR} \right) \equiv \tag{4.15}$$

$$\frac{\left(\hat{\mathbf{x}}^T \hat{\mathbf{y}}_1 \right)^2 - 2 \left(\hat{\mathbf{x}}^T \hat{\mathbf{y}}_1 \right) \left(\hat{\mathbf{y}}_1^T \hat{\mathbf{y}}_2 \right) \left(\hat{\mathbf{x}}^T \hat{\mathbf{y}}_2 \right) + \left(\hat{\mathbf{x}}^T \hat{\mathbf{y}}_2 \right)^2}{1 - \left(\hat{\mathbf{y}}_1^T \hat{\mathbf{y}}_2 \right)^2}, \tag{4.16}$$

where,

$$\hat{\mathbf{x}} = \frac{\boldsymbol{\phi}^{®}}{\|\boldsymbol{\phi}^{®}\|_2}; \quad \hat{\mathbf{y}}_1 = \frac{\boldsymbol{\phi}_r}{\|\boldsymbol{\phi}_r\|_2}; \quad \hat{\mathbf{y}}_2 = \frac{\boldsymbol{\phi}_{r+1}}{\|\boldsymbol{\phi}_{r+1}\|_2}. \tag{4.17}$$

It is the hypothesis that the root eigenvector to which the d mathematical eigenvectors are aligned can be represented by their linear combination. It may be the case that in reality, both of the repeated modes exist but that it is difficult to determine both experimentally by virtue of their closeness; also, they may be coupled so that the physical mode is a superposition of the d mode shapes. In either case, Eq$^{\underline{n}}$ 4.14 is amenable to the task of discerning the maximum possible consistency values. Walther et al. (2004) speculate that a physical mode may also be two or more qualitatively different modes coupled and use Eq$^{\underline{n}}$ 4.8 (Eq$^{\underline{n}}$ 4.12 would not approximate $\overline{\mathbf{\Gamma}}$ well in this case) to align several (distinct space) mathematical eigenvectors, in various combinations, to a physical mode to determine the optimum consistency value. However, one should be weary of this proposal since any single mode is expressible as a linear combination of all eigenvectors, and therefore continual addition of mathematical eigenvectors to the description of a physical mode shape can only ever be improving. A better notion may be to quantitatively assess the improvement attained with each mathematical eigenvector and use this to speculate which modes are present in the mode observed. This is a subject for further study. An important question that arises from this is whether the finite element loci would resemble the actual loci of a physical frame, to the detail of coalescences, veerings and hence the ways in which the mode shapes couple.

Since it is not known which degenerate mode at the root should be the reference to which the degenerate modes at iterate k are aligned, all the possible consistency matrices, equal to the number of modes in set S, and corresponding to all possible alignments, need to be evaluated. The row units of the permutation matrix $\boldsymbol{\Theta}$ in this instance are positioned in correspondence to the locations of the global row maxima of the set of s consistency matrices.

4.4 Loci of an Axially Loaded, Bi-Tetrahedral Space Frame

The finite element formulation of the dynamics of an axially loaded space frame provides an eigenproblem representative of a more realistic problem than that of the idealised, linear operator of Sec. 4.2. The bi-tetrahedral frame is depicted in Fig. 4.7 and its material properties are given in Tab. 4.1. The frame is modelled with two beam finite elements per member, resulting in an order-90 eigenproblem: $(\mathbf{K} + pP_E^+\mathbb{G})\boldsymbol{\phi} = \lambda\mathbf{M}\boldsymbol{\phi}$.

A pair of distinct, veering modes arising in the frame model — the ninth and seventeenth strain modes — are now investigated for their consistency characteristics. The veering event is shown in Fig. 4.8(a), with the varia-

Young's Modulus	2.10×10^{11}
Density	7.85×10^{3}
(Cylindrical) member diameter	1.00×10^{-2}
Sectional area	$\frac{\pi}{4} \times 10^{-4}$

Table 4.1: Bi-tetrahedral frame material and geometrical properties, SI units.

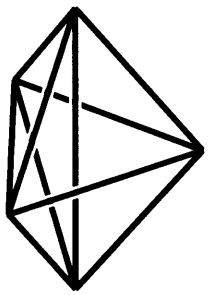

Figure 4.7: Bi-tetrahedral space frame.

tions in eigenvalue derivatives given in Fig. 4.8(b). Of note is the fact that the veering is different from that experienced by the loci of the order-2 linear operator, but not wholly dissimilar. The hyperbola of Fig. 4.8(a) are effectively the conic sections of a cone tipped at some angle from the vertical axis, which leads to asymmetry of the eigenvalue derivative loci. Further, an event not evident from the figure, the upper eigenvalue locus experiences another veering with a further mode after $p = 1.0$.

The Modal Assurance Criterion is here defined as

$$mac_{ij}(\boldsymbol{\phi}_i(p_E^-), \boldsymbol{\phi}_j(p)) = \frac{\left|\boldsymbol{\phi}_i(p_E^-)^T \boldsymbol{\phi}_j(p)\right|^2}{\|\boldsymbol{\phi}_i(p_E^-)\|_2^2 \, \|\boldsymbol{\phi}_j(p)\|_2^2}. \tag{4.18}$$

Since the eigenvectors are forced to obey the condition of **M**-orthonormality, *xor* is defined as the cross-*mass*-orthogonality,

$$xor_{ij}(\boldsymbol{\phi}_i(p_E^-), \boldsymbol{\phi}_j(p)) = \boldsymbol{\phi}_i(p_E^-)^T \mathbf{M} \boldsymbol{\phi}_j(p), \tag{4.19}$$

where p_E^- is the normalised, negative Euler buckling load (where the fundamental, strain mode frequency is zero) and is used as a fixed point so that $\boldsymbol{\phi}_i(p_E^-)$ is a stationary eigenvector.

Investigating the consistency functions, *xor*, shown in Fig. 4.8(d), is seen

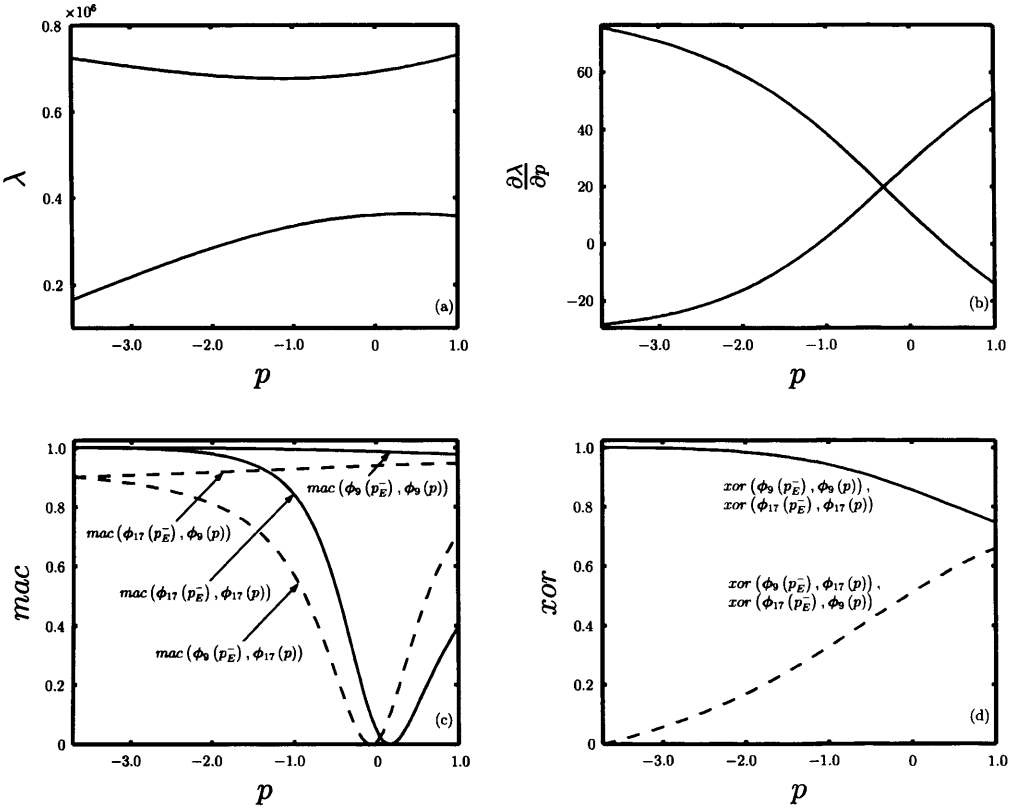

Figure 4.8: Eigenvalue locus veering of the bi-tetrahedral frame modes: (a) eigenvalue locus veering, modes 9 and 17; (b) corresponding eigenvalue derivative loci; (c) *mac* consistency and corruption as functions of p; (d) *xor* consistency and corruption as functions of p.

to concur to a high degree with the behaviour of the idealised loci of the order-2 linear operator — cf. Fig. 4.6(c). Of further note is the characteristic that *xor* deteriorates within mode 9 exactly as it does within mode 17, the two graphs being superimposed in Fig. 4.8(d); the cross-mode *xor* corruptions are also superimposed, meaning that both the confidence of tracing and the ambiguity are identical from the standpoint of either of the two modes.

In Fig. 4.8(c), it is seen that all variations of *mac* for which the floating eigenvector $\phi(p)$ relates to mode 9 follow the behaviour of the loci of the

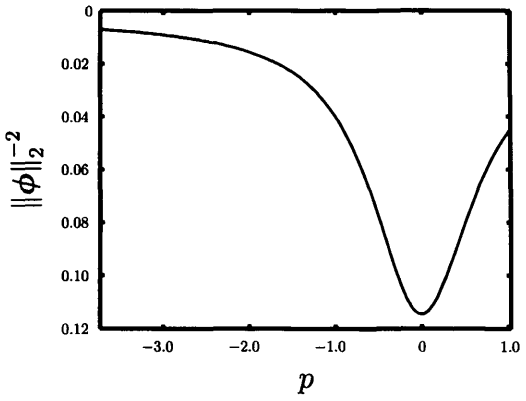

Figure 4.9: Reciprocal of the inner eigenvector product of bi-tetrahedral mode 17, as a function of p.

order-2 linear operator, Fig. 4.6(a). However, all the variations of *mac* for which the floating eigenvector $\phi(p)$ relates to mode 17 show a somewhat unanticipated behaviour, with consistency within and corruption with mode 17 deteriorating to zero as p tends to zero, only to begin increasing again thereafter. This is essentially due to the aforementioned, second veering after $p = 1$. Fig. 4.9 shows the variation of the reciprocal of the inner eigenvector product of mode 17, and an analogous behaviour to that just described. It is this coefficient of expression 4.18, upon which *mac* is dependent by definition, that appears to govern its peculiar behaviour. The discrepancy between *mac* and *xor*, insomuch as the latter behaves in a manner that can be anticipated while the former does not, owes to *xor* being an inherent property of the M-orthonormalised eigenvectors and *mac* being somewhat synthetic to the mode tracing task. It is the necessary but artificial normalising denominator of expression 4.18 that here forfeits the predictability of *mac*.

Ma and Ng (2004) investigate the criteria for which the dot product of M-

orthonormal eigenvectors indicates orthogonality in the normal sense (that is to say, given that certain conditions on the mass and stiffness matrices are fulfilled, the matrices $\mathbf{\Phi}^T\mathbf{M}\mathbf{\Phi}$ and $\mathbf{\Phi}^T\mathbf{\Phi}$ are mutually diagonal). This may be the key in ascertaining when *mac* will behave in a controlled manner as does *xor*, since it essentially evaluates cross orthogonality without using knowledge of **M**-orthonormality, and then forces a scaling with respect to unity.

As has been said, in mathematical models of real structures, coupling is intricate and can occur between more than two modes. While the example of Sec. 4.2 helped in appreciating the characteristics of simple veering, in reality this only occurs under special circumstances. The bi-tetrahedral space frame of the present example offers an example of an intricate event in which four degenerate mode pairs interact with one another, within the buckling limits of the frame. Being degenerate, it is necessary to first align all eigenvectors to appropriate datum vectors, as is outlined in Sec. 4.3. In the illustration that follows, when depicting the consistency with a datum eigenvector in a particular mode, all degenerate mode eigenvectors of all modes are aligned to that one datum eigenvector. This demonstrates that the least squares, eigenvector basis-aligning transformation matrix defined by Eq$^{\underline{n}}$ 4.8 does not introduce numerical alignments resulting in misleading corruptions. As discussed by Bahra and Greening (2005a), in practice, mode tracing would need to perform this alignment of all modes a number of times, in turn to all of the modes at the root, and then assess the greatest consistency with consid-

eration to all of these evaluations — q.v. Sec. 4.3.

Being such an involved interaction of modes, for clarity consistency is indicated on the eigenvalue loci in a colour dimension. The graphs of Fig. 4.10 illustrate the heightened ambiguity of assessing *xor* in a system coupling four modes. It is also apparent that the simple type of veering encountered hitherto is not resembled here. In Fig. 4.10(a) and Fig. 4.10(d), consistency appears to vaguely follow as close as it can a straight trend and involves only two of the four modes. Fig. 4.10(b) and Fig. 4.10(c), however, show all of the four mode pairs involved, with corruption considerable in each. Such a circumstance would be problematic in mode tracing in that the ambiguity does not allow modes to be traced with a desirable degree of confidence. If, on the other hand, the datum eigenvector is thought of as some root mode to be sought by Newton's method, then it does not matter so much which of the modes are traced at some arbitrarily chosen starting point so much as tracing conserves smoothness of the eigenvalue loci.

One final illustration concerning tracing in highly coupled modes is the difference between how *mac* and *xor* measure consistency. For comparison, Fig. 4.10(a) is reproduced in Fig. 4.11 using *mac* as the consistency measure in place of *xor*. Again, it can be appreciated that the synthetic nature of *mac* leads to greater corruption. Not only is considerable corruption introduced between the two degenerate modes traced by *xor*, but some corruption is brought about in the other two degenerate modes.

What would be useful, considering the more robust nature of *xor* as a

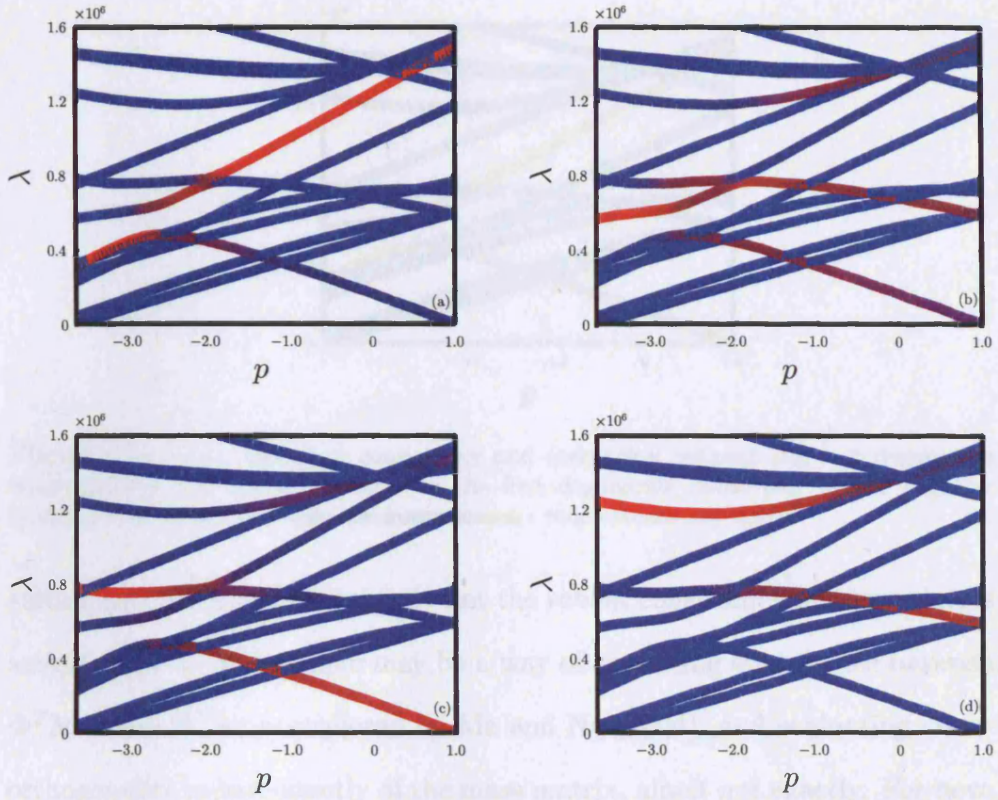

Figure 4.10: Load-wise *xor* consistency and corruption between the four degenerate mode pairs of a coupling system, with datum modes at the negative buckling load: (a) first degenerate mode pair as datum; (b) second degenerate mode pair as datum, *&c.*; 0 1 *xor* consistency scale.

consistency measure, would be to develop a *xor* analogue employable when the degrees of freedom are limited to those measured in an experiment; the mass matrix would in that instance need to be suitably reduced, if at all possible. A measure known as the pseudo-orthogonality check, *poc*, evaluates cross orthogonality with either some reduction of the finite element model or expansion of the experimental mode shapes. This artificial change in dimensions is known to have detrimental effects on the consistency value and, although some reduction schemes have been developed to minimise the re-

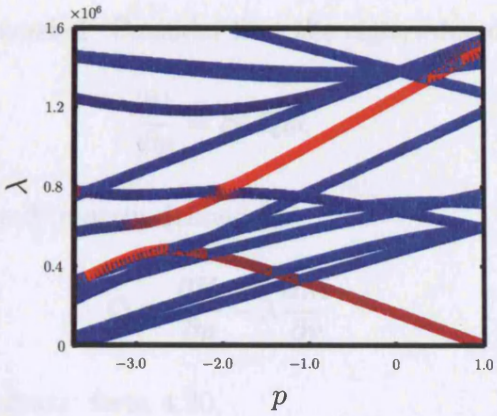

Figure 4.11: Load-wise *mac* consistency and corruption between the four degenerate mode pairs of a coupling system with the first degenerate mode pair at the negative buckling load as datum; 0 1 *mac* consistency scale.

sulting distortion, *poc* is certainly not the robust consistency measure that is sought. Alternatively, there may be a way of exploiting equivalence between $\mathbf{\Phi}^T\mathbf{M}\mathbf{\Phi}$ and $\mathbf{\Phi}^T\mathbf{\Phi}$, as explored by Ma and Ng (2004), and evaluating cross-orthogonality independently of the mass matrix, albeit not exactly. For now, outside this investigatory chapter, *mac* is the chosen consistency measure, in numerical simulations and experimental chapters, because it can involve any number of degrees of freedom. However, its unpredictability, as exposed in this section, is not left unheeded.

4.5 The Eigenvalue Derivative, *mac* and *xor*

Although not a cogent relationship, it is interesting to note the similarities between *mac*, *xor* and the eigenvalue derivative, as functions of some independent variable, p. Later, in Sec. 5.8 and Ch. 7, a predictor such as, possibly, the eigenvalue derivative, of fluctuations in consistency is seen as

something greatly needed. Consider first the eigenvalue derivative:

$$\frac{\partial \lambda}{\partial p} = \boldsymbol{\phi}^T \mathbf{Q} \boldsymbol{\phi}, \tag{4.20}$$

where $\mathbf{Q}$ is the $N \times N$ matrix defined by

$$\mathbf{Q} \equiv \frac{\partial \mathbf{K}}{\partial p} - \lambda \frac{\partial \mathbf{M}}{\partial p}. \tag{4.21}$$

Expanding the quadratic form 4.20,

$$\frac{\partial \lambda}{\partial p} = \begin{array}{ccccccc} q_{11}\phi_1^2 & + & q_{12}\phi_1\phi_2 & + & \cdots & + & q_{1N}\phi_1\phi_N \\ +q_{21}\phi_2\phi_1 & + & q_{22}\phi_2^2 & + & \cdots & + & q_{2N}\phi_2\phi_N \\ & & & & \cdots & & \\ +q_{N1}\phi_N\phi_1 & + & q_{N2}\phi_N\phi_2 & + & \cdots & + & q_{NN}\phi_N^2 \end{array}. \tag{4.22}$$

More succinctly,

$$\frac{\partial \lambda}{\partial p} = \begin{array}{ccccccc} q_{11}\phi_1^2 & + & 2q_{12}\phi_1\phi_2 & + & \cdots & + & 2q_{1N}\phi_1\phi_N \\ & + & q_{22}\phi_2^2 & + & \cdots & + & 2q_{2N}\phi_2\phi_N \\ & & & & \cdots & & \\ & & & & & & q_{NN}\phi_N^2 \end{array}, \tag{4.23}$$

or

$$\frac{\partial \lambda}{\partial p} = \begin{array}{ccccccc} \phi_1(q_{11}\phi_1 & + & q_{12}\phi_2 & + & \cdots & + & q_{1N}\phi_N) \\ +\phi_2(q_{21}\phi_2 & + & q_{22}\phi_2 & + & \cdots & + & q_{2N}\phi_N) \\ & & & & \cdots & & \\ +\phi_N(q_{N1}\phi_1 & + & q_{N2}\phi_2 & + & \cdots & + & q_{NN}\phi_N) \end{array}. \tag{4.24}$$

Expansions of *mac* and *xor* are given in Eq$^{\underline{n}}$ 4.25-4.27. It is apparent from expressions 4.24 and 4.27 that *xor* and the eigenvalue derivative are series in the same variables with different, but respectively constant, coefficients. The linearity of the relationship between the expressions depends upon the proportionality of the matrices $\mathbf{Q}$ and $\mathbf{M}$, and the similarity of the datum and floating eigenvectors, $\boldsymbol{\phi}(p^o)$ and $\boldsymbol{\phi}(p)$ respectively. The former requirement is likely to hold, albeit loosely, if mass and stiffness are distributed similarly

Expanding the numerator of the Modal Assurance Criterion leads to:

$$mac\left(\boldsymbol{\phi}\left(p^o\right),\boldsymbol{\phi}\left(p\right)\right)=\left\|\boldsymbol{\phi}\left(p^o\right)\right\|_2^{-2}\left\|\boldsymbol{\phi}\left(p\right)\right\|_2^{-2}\cdot$$
$$\cdot\begin{pmatrix}\phi_1\left(p^o\right)^2\phi_1\left(p\right)^2 & + & 2\phi_1\left(p^o\right)\phi_2\left(p^o\right)\phi_1\left(p\right)\phi_2\left(p\right) & + & \cdots & + & 2\phi_1\left(p^o\right)\phi_N\left(p^o\right)\phi_1\left(p\right)\phi_N\left(p\right)\\ & + & \phi_2\left(p^o\right)^2\phi_2\left(p\right)^2 & + & \cdots & + & 2\phi_2\left(p^o\right)\phi_N\left(p^o\right)\phi_2\left(p\right)\phi_N\left(p\right)\\ & & & & \cdots & & \\ & & & & & + & \phi_N\left(p^o\right)^2\phi_N\left(p\right)^2\end{pmatrix}. \tag{4.25}$$

Cross-mass-orthogonality is essentially a symmetric, bilinear form and can be expressed as

$$\begin{aligned}xor\left(\boldsymbol{\phi}\left(p^o\right),\boldsymbol{\phi}\left(p\right)\right)=&\ \mathbf{M}_{11}\phi_1\left(p^o\right)\phi_1\left(p\right) + \mathbf{M}_{12}\phi_1\left(p^o\right)\phi_2\left(p\right) + \cdots + \mathbf{M}_{1N}\phi_1\left(p^o\right)\phi_N\left(p\right)\\ +&\ \mathbf{M}_{21}\phi_2\left(p^o\right)\phi_1\left(p\right) + \mathbf{M}_{22}\phi_2\left(p^o\right)\phi_2\left(p\right) + \cdots + \mathbf{M}_{2N}\phi_2\left(p^o\right)\phi_N\left(p\right)\\ &\ \cdots\\ +&\ \mathbf{M}_{N1}\phi_N\left(p^o\right)\phi_1\left(p\right) + \mathbf{M}_{N2}\phi_N\left(p^o\right)\phi_2\left(p\right) + \cdots + \mathbf{M}_{NN}\phi_N\left(p^o\right)\phi_N\left(p\right),\end{aligned} \tag{4.26}$$

or, factorising the row expansions by noting constant coefficients,

$$\begin{aligned}xor\left(\boldsymbol{\phi}\left(p^o\right),\boldsymbol{\phi}\left(p\right)\right)=&\ \phi_1\left(p^o\right)\left(\mathbf{M}_{11}\phi_1\left(p\right) + \mathbf{M}_{12}\phi_2\left(p\right) + \cdots + \mathbf{M}_{1N}\phi_N\left(p\right)\right)\\ +&\ \phi_2\left(p^o\right)\left(\mathbf{M}_{21}\phi_1\left(p\right) + \mathbf{M}_{22}\phi_2\left(p\right) + \cdots + \mathbf{M}_{2N}\phi_N\left(p\right)\right)\\ &\ \cdots\\ +&\ \phi_N\left(p^o\right)\left(\mathbf{M}_{N1}\phi_1\left(p\right) + \mathbf{M}_{N2}\phi_2\left(p\right) + \cdots + \mathbf{M}_{NN}\phi_N\left(p\right)\right).\end{aligned} \tag{4.27}$$

within a structure and if the independent variable p governing the variations in the eigenvalues is a factor upon either the mass or the stiffness.

Likewise, expressions 4.23 and 4.25 indicate that the numerator of *mac* and the eigenvalue derivative are also series in the same variables with respectively constant but different coefficients. However, the denominator of *mac* involves the inner product of the floating eigenvector and hence dependency upon it. It is likely that this is the cause for *mac* tending to follow variations in $\|\phi(p)\|_2^{-2}$ in certain circumstances of simple veering as opposed to the eigenvalue derivative, such as was noted and demonstrated in Sec. 4.4.

This somewhat heuristic investigation supports sections of this chapter by showing that, under the correct conditions, consistency can be quasi-linearly related to the eigenvalue derivative. These conditions include the relative location of the datum eigenvector and of course the simplicity of the veering characteristic. In suitable circumstances, rapid decreases in the eigenvalue derivative can afford mode tracing the insight to the amount of consistency and corruption that can be anticipated when pairing modes across parameter intervals. It can also indicate when mode tracing is likely to force iterates to transcend eigenvalue loci, i.e., undergo a 'consistency jump'.

4.6 An Augmented Modal Assurance Routine

Occasionally, the degree of consistency can be undesirably low, with accompanying corruption. Consequently, the exclusive row units of Θ in 4.3 and

4.4 cannot be designated with confidence due to ambiguity in the consistency matrices. Such would be the case if an iterate found itself in the midst of a veering event, a point noted by Ting et al. (1995) who propose suspension of tracing of the particular, affected mode or modes and reinstating them at the proceeding iterate. However, generally, this will not be a successful strategy in the event of multiple ambiguities because the determinacy of Newton's method might be threatened. In such circumstances, it is worth gaining further insight into the problem. An augmented modal assurance routine is here proposed, which potentially augments the assurance of tracing. It may alleviate the aforementioned predicament and also increase the maximum permissible parameter perturbation dictated by Newton's method. The notion of the routine is to forward and backward cast the eigenvector elements by utilising the knowledge of their derivatives in an affine function model.

Of course, mode traces are typically made between the root, ®, and current, k, iterates. However, it is very conceivable that while eigenvector consistency can be near unity between ® and $k = 0$, it can be greatly diminished between ® and certain subsequent iterates, $k > 0$, if they settle in the midst of veering events. It may be possible to utilise iterates adjacent to the consistency loss, in the augmented assurance strategy, to strengthen consistency, i.e., if consistency is weak, the ambiguous eigenvectors at $k+1$, for example, might be strengthened according to those at k, or vice versa. To this end, the following additions to the vector consistency evaluation are

proposed to potentially alleviate ambiguity:

$$\overrightarrow{mac}_{ij}\left(\mathbf{a}_i\left(\mathbf{a}_i^T\mathbf{M}\mathbf{a}_i\right)^{-\frac{1}{2}},\boldsymbol{\phi}_j^{\mathrm{k}+1}\right)=\frac{\left|\left(\mathbf{a}_i\left(\mathbf{a}_i^T\mathbf{M}\mathbf{a}_i\right)^{-\frac{1}{2}}\right)^T\boldsymbol{\phi}_j^{\mathrm{k}+1}\right|^2}{\left\|\mathbf{a}_i\left(\mathbf{a}_i^T\mathbf{M}\mathbf{a}_i\right)^{-\frac{1}{2}}\right\|_2^2\left\|\boldsymbol{\phi}_j^{\mathrm{k}+1}\right\|_2^2}\in[0,1],\quad(4.28)$$

$$\overrightarrow{xor}_{ij}\left(\mathbf{a}_i\left(\mathbf{a}_i^T\mathbf{M}\mathbf{a}_i\right)^{-\frac{1}{2}},\boldsymbol{\phi}_j^{\mathrm{k}+1}\right)=\left|\left(\mathbf{a}_i\left(\mathbf{a}_i^T\mathbf{M}\mathbf{a}_i\right)^{-\frac{1}{2}}\right)^T\mathbf{M}\boldsymbol{\phi}_j^{\mathrm{k}+1}\right|\in[0,1],\quad(4.29)$$

$$\mathbf{a}_i=\left(\boldsymbol{\phi}_i^k+\frac{\partial\boldsymbol{\phi}_i^k}{\partial p}\left(p^{\mathrm{k}+1}-p^k\right)\right);\quad(4.30)$$

$$\overleftarrow{mac}_{ij}\left(\boldsymbol{\phi}_i^k,\mathbf{a}_j\left(\mathbf{a}_j^T\mathbf{M}\mathbf{a}_j\right)^{-\frac{1}{2}}\right)=\frac{\left|\left(\boldsymbol{\phi}_i^k\right)^T\mathbf{a}_j\left(\mathbf{a}_j^T\mathbf{M}\mathbf{a}_j\right)^{-\frac{1}{2}}\right|^2}{\left\|\boldsymbol{\phi}_i^k\right\|_2^2\left\|\mathbf{a}_j\left(\mathbf{a}_j^T\mathbf{M}\mathbf{a}_j\right)^{-\frac{1}{2}}\right\|_2^2}\in[0,1],\quad(4.31)$$

$$\overleftarrow{xor}_{ij}\left(\boldsymbol{\phi}_i^k,\mathbf{a}_j\left(\mathbf{a}_j^T\mathbf{M}\mathbf{a}_j\right)^{-\frac{1}{2}}\right)=\left|\left(\boldsymbol{\phi}_i^k\right)^T\mathbf{M}\mathbf{a}_j\left(\mathbf{a}_j^T\mathbf{M}\mathbf{a}_j\right)^{-\frac{1}{2}}\right|\in[0,1],\quad(4.32)$$

$$\mathbf{a}_j=\left(\boldsymbol{\phi}_j^{\mathrm{k}+1}+\frac{\partial\boldsymbol{\phi}_j^{\mathrm{k}+1}}{\partial p}\left(p^k-p^{\mathrm{k}+1}\right)\right).\quad(4.33)$$

Note the M-normalisation employed here is really only necessary for the *xor* expressions since *mac* is independent of vector scaling, having its own normalising denominator. Expressions 4.28-4.29 and 4.31-4.32 supplement 4.1 and 4.2 by making affine models of the eigenvector elements at either the general k^{th} or $(k+1)^{th}$ iterate from the knowledge of their derivatives and the parameter perturbation $\left|p^{\mathrm{k}+1}-p^k\right|$ dictated by Newton's method — q.v. Eq$^{\underline{\mathrm{n}}}$ 2.15. Thus, amongst *mac* and *xor*, insight into eigenvector consistency is augmented threefold. Attention must be paid to the eigenvectors associated with degenerate eigenvalues in terms of alignment of the eigenvector bases across iterates; a full discussion of this can be found in Sec. 4.3. An example is now given of the employment of consistency expressions 4.28 and 4.29.

4.7 The Augmented Modal Assurance Routine Employed

The following example serves to demonstrate mode traces in degenerate eigensystems and the augmentation of the assurance with which tracing can be performed. Fig. 4.12 depicts a cyclic plane frame formed by a pentagon of unit circumradius accommodating a pentalpha in its interior. At the intersection of the members are two translational degrees of freedom, so that the entire structure is associated with ten freedoms. Tab. 4.2 gives the geometric and material properties nominated for the members. Although a problem not physically realisable, by virtue of the inevitable onset of buckling (here ignored), the present example serves to demonstrate the concepts outlined hitherto, such as achieving orthonormal bases in a coalescence involving a permanently degenerate and a distinct mode, employment of the modal permutation described by mappings 4.3 and 4.4, the care needed in tracing permanently degenerate eigenvalue loci and the utility of the proposed augmented assurance.

In accordance with the present theme, perturbation to the eigenpairs is chosen to be induced by the cyclically symmetric distribution of axial forces

Young's Modulus	2.10×10^{11}
Density	7.85×10^{3}
(Cylindrical) member diameter	1.00×10^{-2}
Sectional area	$\frac{\pi}{4} \times 10^{-4}$

Table 4.2: Pentagonal frame material and geometrical properties, SI units.

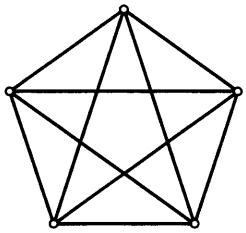

Figure 4.12: Pentagonal frame structure.

within the frame. The resulting conservation of symmetry with respect to variations in p entails permanent degeneracy of most of the eigenvalues. The statically admissible force distribution, the magnitude of which is described by p, is such that the forces in the general pentagonal and general pentalpha members are in the ratio $1 : -\frac{1}{2}\sec(\frac{\pi}{5})$.

The elemental, total stiffness and mass matrices of the members are taken to be respectively

$$\mathbf{A}^e = \mathbf{K}^e + \mathbf{G}^e = \mathbf{T}_1^T \frac{1}{L} \begin{bmatrix} EA & 0 & -EA & 0 \\ 0 & p & 0 & -p \\ -EA & 0 & EA & 0 \\ 0 & -p & 0 & p \end{bmatrix} \mathbf{T}_1 \tag{4.34}$$

and

$$\mathbf{B}^e = \mathbf{M}^e = \mathbf{T}_2^T \frac{\rho AL}{2} \begin{bmatrix} 1 & 0 \\ 0 & 1 \end{bmatrix} \mathbf{T}_2, \tag{4.35}$$

where the coordinate transformation matrices are

$$\mathbf{T}_1 = \begin{bmatrix} \alpha & \beta & 0 & 0 \\ \beta & \alpha & 0 & 0 \\ 0 & 0 & \alpha & \beta \\ 0 & 0 & \beta & \alpha \end{bmatrix} \tag{4.36}$$

and

$$\mathbf{T}_2 = \begin{bmatrix} \alpha & \beta & 0 & 0 \\ 0 & 0 & \alpha & \beta \end{bmatrix}; \tag{4.37}$$

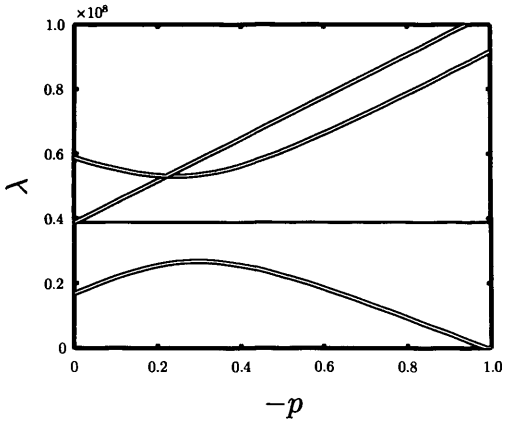

Figure 4.13: Eigenvalue loci of the pentagonal frame.

α and β are the direction cosines in nominated orthogonal directions for the members and L is the member length.

The mass matrix is of course stationary with respect to variations in the axial forces and its derivative is a zero matrix. The elemental mass and stiffness matrices are assembled into global matrices to form an eigenproblem of order ten. The zero eigenvalue, rigid body modes, amounting to three, are excluded in the investigation to follow and the initial modal designation relates to the first strain mode.

The eigenvalue loci are given in Fig. 4.13. Amongst these is a mode completely unaffected by the onset of load, a permanently degenerate mode whose eigenvectors remain constant by virtue of its linear eigenvalue locus and a pair of permanently degenerate, veering modes. In order to show the utility of the proposed augmented assurance routine, modes shall be traced between $p = 0$ and $p = -0.3$, which falls in the midst of the veering pair of modes, where the eigenvectors are rapidly transforming between the loci.

Firstly, orthonormal bases for the degenerate eigenvectors at $p = 0$ are achieved by Gram-Schmidt orthonormalisation, described in Sec. 3.2; for the thrice degenerate set, involving the coalescence of a permanently degenerate and a distinct locus, the following series of procedures is applied.

1. The three eigenvectors are **M**-orthonormalised through Gram-Schmidt orthonormalisation.

2. The sundering of one of the eigenvectors is anticipated through post-multiplication of the transformation matrix of the auxiliary eigenproblem 3.43; the first eigenvector then becomes its adjacent eigenvector.

3. Gram-Schmidt orthonormalisation is re-applied, noting that one of the eigenvectors is its adjacent eigenvector, i.e., this is used as the pivotal eigenvector.

Following this, the permanently degenerate eigenvectors at $p = -0.3$ are **M**-orthonormalised and aligned to those of the same loci at $p = 0$ through the transformation matrix defined by Eq$^{\underline{n}}$ 4.8. The consistency evaluations arising thereafter are given in Eq$^{\underline{n}}$ 4.38 and Eq$^{\underline{n}}$ 4.39.

There are a few features of the consistency matrices worth noting. The straight loci, whose eigenvectors are consequently stationary with respect to p, expectedly return unit consistencies. With *mac*, the remaining modes are correlated with undesirably low assurance. While this assurance is greater with *xor*, there exists in both considerable corruption terms as arise in veering events.

$$\mathbf{MAC} = \begin{bmatrix} 0.616 & 0 & 0 & 0 & 0.088 & 0 & 0 \\ 0 & 0.616 & 0 & 0.088 & 0 & 0 & 0 \\ 0 & 0 & 1 & 0 & 0 & 0 & 0 \\ 0 & 0 & 0 & 0 & 0 & 1 & 0 \\ 0 & 0 & 0 & 0 & 0 & 0 & 1 \\ 0 & 0.449 & 0 & 0.870 & 0 & 0 & 0 \\ 0.449 & 0 & 0 & 0 & 0.870 & 0 & 0 \end{bmatrix} ; \qquad (4.38)$$

$$\mathbf{XOR} = \begin{bmatrix} 0.872 & 0 & 0 & 0.007 & 0.490 & 0 & 0 \\ 0 & 0.872 & 0 & 0.490 & 0.007 & 0 & 0 \\ 0 & 0 & 1 & 0 & 0 & 0 & 0 \\ 0 & 0 & 0 & 0 & 0 & 1 & 0 \\ 0 & 0 & 0 & 0 & 0 & 0 & 1 \\ 0.007 & 0.490 & 0 & 0.872 & 0 & 0 & 0 \\ 0.490 & 0.007 & 0 & 0 & 0.872 & 0 & 0 \end{bmatrix} . \qquad (4.39)$$

The consistency evaluations 4.28 and 4.29 are now employed on the inadequately traced modes. The eigenvectors at $p = 0$ are forward cast, that they might augment the assurance of tracing these modes. The eigenvector derivatives are therefore required and these are computed by the method owing to Ojalvo (1988), as described in Ch. 3, and are given in Tab. 4.3 along with the corresponding eigenvalues and their derivatives.

The forward cast eigenvectors are shown in comparison to their original forms at $p = 0$ and to those at $p = -0.3$ in Tab. 4.4-4.6. The anticipation was that the resemblance between the forward cast eigenvectors and the eigenvectors at $p = -0.3$ would be greater than that between the eigenvectors at $p = 0$ and $p = -0.3$, and such is the indication. Note that not all of the elements in Tab. 4.6 approximate those in Tab. 4.5. This owes to the shortfall of the affine modelling of the degrees of freedom. However, if the assumption of affineness holds for enough degrees of freedom, as is likely, then the forward

	mode 1	mode 2	mode 6	mode 7
λ	1.68×10^7	1.68×10^7	5.89×10^7	5.89×10^7
$\frac{\partial \lambda}{\partial P}$	0.546	0.546	-0.393	-0.393
$\frac{\partial \phi}{\partial P} \times 10^{-8}$	0.003	-0.385	-0.015	0.075
	0.014	-0.105	-0.044	-0.251
	0.117	0.185	-0.089	0.202
	-0.197	-0.269	-0.088	0.120
	0.239	0.071	0.194	-0.078
	0.291	0.109	-0.138	0.092
	-0.358	0.105	0.094	-0.010
	0.131	-0.053	0.244	0.051
	-0.001	0.023	-0.185	-0.190
	-0.240	0.318	0.026	-0.012

Table 4.3: Eigenpair derivatives of the pentagonal frame at $p = 0$; q.v. Fig. 4.13 for locus numbering.

cast vectors will lead to greater consistency and lesser corruption:

$$\overrightarrow{mac}_{ij} = \begin{bmatrix} 0.899 & 0.012 & 0.002 & 0.005 \\ 0.012 & 0.899 & 0.005 & 0.002 \\ 0.003 & 0.273 & 0.962 & 0.004 \\ 0.273 & 0.003 & 0.004 & 0.962 \end{bmatrix} \quad \begin{cases} i = 1, 2, 6, 7 \\ j = 1, 2, 4, 5 \end{cases} ; \quad (4.40)$$

$$\overrightarrow{xor}_{ij} = \begin{bmatrix} 0.959 & 0.127 & 0.075 & 0.240 \\ 0.127 & 0.959 & 0.240 & 0.075 \\ 0.034 & 0.243 & 0.968 & 0.055 \\ 0.243 & 0.034 & 0.055 & 0.968 \end{bmatrix} \quad \begin{cases} i = 1, 2, 6, 7 \\ j = 1, 2, 4, 5 \end{cases} . \quad (4.41)$$

The $\overrightarrow{mac}$ and $\overrightarrow{xor}$ consistencies between the eigenvectors at $p = -0.3$ and the forward cast vectors are shown above (note that for the evaluation of the latter, the forward cast vectors are necessarily forced to be mass-orthonormal). Overall, consistency is increased by the proposed routine and corruption is diminished, as shown in Eq$^{\underline{n}}$ 4.40 and Eq$^{\underline{n}}$ 4.41. The proposed augmented assurance scheme is herein utilised as a supplement to consistency evaluation in terms of increasing the insight into how to trace modes. It must

be noted that this is only possible in single parameter problems since the eigenvectors may not be analytic functions of multiple parameters. That is not to say that mode tracing assurance cannot be augmented in the manner here shown when there is more than one parameter, but that further research is needed.

ϕ_1	ϕ_2	ϕ_6	ϕ_7
0.163	-0.015	0.333	-0.016
-0.221	-0.036	0.239	-0.040
0.152	-0.062	-0.292	-0.160
0.179	-0.134	0.198	0.140
-0.090	0.246	-0.030	-0.125
0.062	-0.067	-0.160	-0.357
-0.032	0.008	-0.093	0.401
0.065	0.267	0.022	0.005
-0.193	-0.770	0.082	-0.100
-0.086	-0.031	-0.300	0.252

Table 4.4: Eigenvectors of the pentagonal frame at $p = 0$.

ϕ_1	ϕ_2	ϕ_4	ϕ_5
0.148	-0.176	0.284	0.066
-0.175	-0.149	0.189	-0.142
0.213	0.088	-0.284	-0.065
0.086	-0.213	0.108	0.211
-0.017	0.229	0.094	-0.155
0.230	0.018	-0.172	-0.281
-0.224	0.055	-0.077	0.334
0.054	0.222	0.150	0.035
-0.120	-0.195	-0.017	-0.180
-0.196	0.122	-0.277	0.178

Table 4.5: Eigenvectors of the pentagonal frame at $p = -0.3$.

mode 1	mode 2	mode 6	mode 7
0.164	-0.130	0.328	0.006
-0.216	-0.068	0.226	-0.115
0.187	-0.006	-0.319	-0.099
0.120	-0.215	0.172	0.176
-0.018	0.268	0.028	-0.149
0.149	-0.034	-0.201	-0.330
-0.140	0.039	-0.064	0.398
0.105	0.252	0.095	0.020
-0.193	-0.170	0.026	-0.157
-0.158	0.065	-0.292	0.248

Table 4.6: Forward cast eigenvectors for the pentagonal frame from $p = 0$.

Chapter 5

Numerical Simulation

Five numerical simulations showing success of the title method are given and exemplify the issues raised in previous, theoretical chapters. General concepts, such as mode tracing and overdetermination, are demonstrated in the case of a frame with one distribution of axial force, and hence one force parameter. Frames of regular and irregular geometries are then used to illustrate force determination in cases where there are multiple distributions of force. Symmetry in frames is seen to pose problems of root ambiguity. It is shown that load can be updated alongside other physical parameters. The nominated frames offer bases from which concepts for more general space frames can be extrapolated. Use is made of the finite element models to anticipate factors that might affect the determination of force in real frames. Effects of noise are included to indicate the bounds upon errors that can be expected. The chapter ends with an example of a large order frame resembling a practical structure and serves to show that the more complicated a frame is, the more difficult it is to arrive at a solution to the force identification problem.

5.1 General

The numerical simulations are intended for demonstrating issues highlighted in previous, theoretical chapters and how they affect Newton's method. Iteration progresses according to Eq^{n} 2.19, with the Newton progression defined in Eq^{n} 2.15. The necessity of overdetermining this set of linear equations is shown in the examples that follow; treating their condition is also explored. The way in which mode tracing overcomes the eigenvalue coalescence issue, and how it behaves in the presence of locus veering, is also made evident. Mode tracing is further seen to alleviate the ambiguous root problems of symmetric frames, as anticipated in Sec. 5.2. Where necessary, the disoriented, permanently degenerate modes at each iterate have had to be aligned to the root modes in order to see how modes should be traced, as discussed in Sec. 4.3.

Other concerns investigated are whether load can be identified alongside other parameters and the effects of having errors in the root, or simulated experimental frequencies. The chapter ends with an example of a large, complicated frame, the nature of whose dynamic characteristics greatly tests the means of identifying force proposed in this thesis.

All member discretisation for dynamic modelling is six elements, except for the final example of the octet frame, for which the size of the problem has demanded only four elements per member for practical purposes. Modal designation is stated according to the ordering at the root and irrespective of the ordering at any other loaded state, so that mode r is not necessarily

the r^{th} mode at a particular value of p. All member material properties are as follows: Young's modulus, 2.1×10^{11} Nm^{-2}; density, 7.85×10^{3} kgm^{-3}. Without being stated, mode tracing, as outlined in Eq$^{\underline{n}}$ 4.3-4.4, is in all places used by default.

Note that there is an assumption of constant geometry with respect to frame loading. Of course, in practice, deviations in geometry would accompany the approach to buckling, and this second order effect may need to be taken into account in the mathematical modelling. A useful reference that deals with this is Greening (1999).

Before the numerical simulation examples are given, the following two sections raise issues that need to be acknowledged regarding frame symmetry.

5.2 Geometries Exhibiting Cyclic Symmetry

If the eigenproblem is not formulated on n linearly independent force distributions, the Jacobian matrix of eigenvalue derivatives will be singular and its inverse will not exist. The inverse of the Jacobian of Eq$^{\underline{n}}$ 2.15 could be taken with truncation of the zero singular values of the Jacobian, that is to say force their reciprocals to zero in the matrix $\mathbf{\Sigma}^{+}$ of Eq$^{\underline{n}}$ 2.17, in order for the Newton progression to be determined. However, there would then exist an infinite number of solutions to the force parameters, a cluster of which would exist within the pre-buckled region of the iteration space. There would be no guarantee of discovering the true root, although beneficially any of such a family of roots would lead to the correct solution to the member forces.

However, the dimensionality of the iteration space would be unnecessarily large, encumbering iteration on more counts than just iterative adversity, as discussed at the end of the current section. It is therefore advisable to always seek a full rank equilibrium matrix $\overline{\mathbf{E}}$.

In the case of symmetric space frames with multiple axes of spatial periodicity, the hypersurfaces representing the eigenvalue functions of the n force parameters $\mathbf{p}$ have an n-dimensional focus of symmetry, defined as the hyperplane where all of the parameters are equal. This owes to the spatial ambiguity; certain force distributions will be identical in every sense but orientation and will therefore be interchangeable independent variables with respect to the eigenvalue functions. At the symmetry focus, the eigenvalue functions are transitorily coalesced. The coalescence is not simple and may involve combinations of distinct and twofold degenerate eigenvalue curves intersecting. The equation computing the Fréchet eigenvalue derivative 3.10 no longer holds here. Gâteaux (directional) derivatives could be approximated by finite difference schemes, but would pose computational expense. It is an easy matter and simpler to avoid this focus by ensuring that the vector $\mathbf{p}^0$ at which iteration commences has non-repeated values p_i^0, $i = 1, 2, \ldots, n$; the event of encountering it subsequently is immensely improbable. Alternatively, the eigenvectors of the set of degenerate eigenvalues at the symmetry focus can be treated through a combination of Gram-Schmidt orthonormalisation and a transformation matrix that anticipates any potential sundering of the eigenvalues — q.v. Sec. 3.2 and Sec. 4.7.

Further for frames possessing more than one axis of spatial periodicity — for example, those based on platonic solids — there exist roots to the set of non-linear eigenvalue functions which, although not leading to the correct solution to the member forces, give a solution that describes the actual sought force distribution at some different spatial orientation. This owes to the spatial ambiguity of the geometries of such frames in that they are identical from multiple spatial aspects. There are then a number of roots $\mathbf{p}^{\text{Я}}$ at which the eigenvalue constraints are exactly satisfied, i.e., $\boldsymbol{\lambda}\left(\mathbf{p}^{\text{R}}\right) - \boldsymbol{\lambda}\left(\mathbf{p}^{\text{Я}}\right) = \mathbf{0}$. These ambiguous roots are informative in that they identify the member forces, but it is the designation of the each member force remains uncertain. One would not be able to confidently ascribe the found member forces. This issue would jeopardise the uniqueness of the solution $\mathbf{p}^{\text{R}}$ were it not for mode tracing discerning the eigenvalue functions upon which the unique solution lies. If mode tracing is not employed, then the roots $\mathbf{p}^{\text{R}}$ and $\mathbf{p}^{\text{Я}}$, which conform to the same hyperplane — since they give rise to the same frame eigenvalues and are symmetric through the symmetry focus — lie on the same non-smooth eigenvalue function as defined by numerical ordering, introducing ambiguity. The above is diagrammatically described in Fig. 5.1, where, for a frame whose eigenvalues are dependent upon two force parameters, modes 1 and 4 (numerical designations) are chosen at the root for the iteration. Since the starting surfaces are nominated according to the consistency of their eigenvectors with the root eigenvectors, stagnation at the $\mathbf{p}^{\text{Я}}$ root is avoided and convergence to $\mathbf{p}^{\text{R}}$ ensues. Thus the modes at the point at

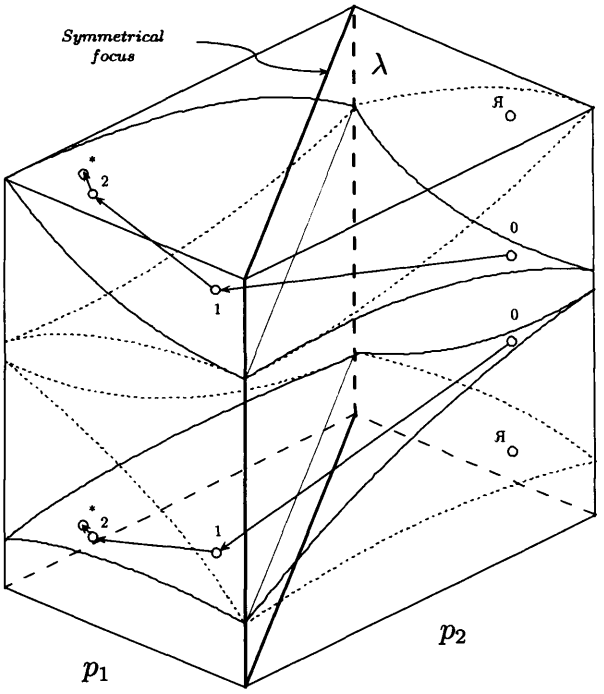

Figure 5.1: Mode tracing overcoming root ambiguity in the force identification of a cyclically symmetric frame possessing two axes of spatial periodicity.

which iteration commences are 2 and 3 (numerical designations), respectively, corresponding to those at the root. The physical interpretation of why mode tracing overcomes this ambiguity is that, although the force distributions are spatially ambiguous, the eigenvector-force distribution relationships are unique, and so the eigenvector-based mode tracing is afforded discernment of the unique root.

Note that if the dimensionality of the iteration space is unnecessarily large because of incomplete reduction of the equilibrium matrix, as just discussed, then even mode tracing cannot prevent convergence to an erroneous root. This is because of the possibility of discovering a $\mathbf{p}^{\text{Я}}$ root, which, because

of their abundance and locations on the eigenvalue hypersurfaces, would not allow the type of discernment depicted in Fig. 5.1. This is the main incentive for reducing the dimensionality of Newton's method when identifying load in cyclically symmetric frames.

5.3 Geometries Deviating from Cyclic Symmetry

If the geometry of a space frame is such that it marks a deviation from some regular, cyclic form to generate an irregular frame, then particularities of symmetric frames do not hold (for example, the symmetrical focus wanders into less readily defined space) — however, they are not wholly alleviated. Although the force distribution matrix $\mathbf{E}$ will have developed distinct columns, it will still be rank-deficient and therefore, again, a full rank matrix $\overline{\mathbf{E}}$ needs to be developed. That is to say, particular force distributions will be expressible as linear combinations of other distributions, and therefore present surplus force parameters, for which reason they should be disregarded. The number of linearly independent force distributions in an irregular frame will be equal to that for its regular counterpart due to topology conservation, since the degree of redundancy is a function of topology and not geometry — q.v. Axiom 1.2.1. However, the degree of orthogonality of the set of force distributions *is* a function of geometry. N.B. Some orthogonal basis for $\overline{\mathbf{E}}$ will exist.

The geometries of such frames may mean that the force distributions are

not immediately apparent. In this case, a static analysis can be employed in which successive members are removed, one end restrained in six degrees of freedom to alleviate singularity of the stiffness matrix, **K**, and a force parallel to the removed member applied at the other end. The global solution vector of displacements is simply the inverse of the constant stiffness matrix multiplied by the applied force vector. This allows evaluation of member forces resulting from a particular member strain, which are then normalised accordingly to establish **E**.

5.4 Once Redundant, Bi-Tetrahedral Frame

The bi-tetrahedral frame comprises two skeletal, regular tetrahedra having three mutual members; an internal spar joins the opposing apices to introduce static indeterminacy. The redundancy entails frame loading following member strain — a statically determinate frame would not be loaded but would instead deform geometrically. The frame can be seen in Fig. 5.2. According to Eq$^{\underline{n}}$ 2.23, the degree of redundancy is $10-3\times5+6 = 1$. The length of the external frame member is nominated as 0.5 m and the members are of circular section and diameter 0.01 m. The member centre-lines are concurrent at the joints so that the transfer of axial force alone is possible, in the static sense.

The variations of the frame eigenvalues are shown in Fig. 5.3 between the buckling limits at which the fundamental frequency — whatever mode that may be in that load vicinity — vanishes. The curves are seen to be non-

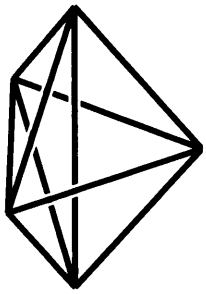

Figure 5.2: Bi-tetrahedral space frame.

linear, with the eigenvalue coalescence and loci veering phenomena clearly visible. As acknowledged in Ch. 4, Newton's method can be encumbered if the functions are non-smooth.

For the once redundant, bi-tetrahedral frame, the eigenvector-force distribution relative orientation is conserved at all loads. In the mathematical model therefore, certain pairs of eigenvalues are permanently degenerate in that they will not separate upon parameter perturbation. Indeed, many of the eigenvalue loci in Fig. 5.3 are two loci, one superimposing the other. The existence of multiple force distributions in the frames of subsequent examples means that the frame eigenvalues are generally distinct, and so it is only really in the once redundant, symmetric case that the special treatment of vector bases is required. This is achieved for the bi-tetrahedral numerical simulations by the methods outlined in Ch. 3 and Ch. 4.

Convergence will be very rapid if the eigenvalue locus nominated for use in the iteration is near straight between the root and the point at which iteration commences. This is simply a result of the apt affine modelling of the indefinite integral in Eq^{n} 2.12 in Newton's method. If such modes are

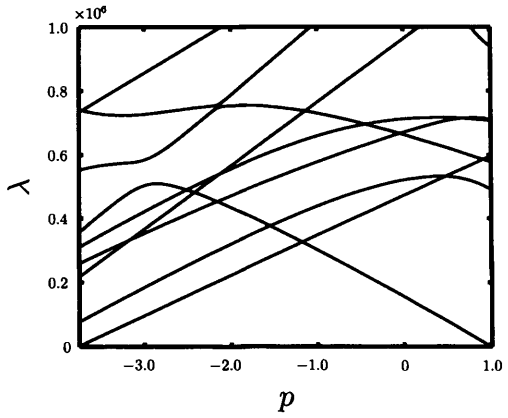

Figure 5.3: Pre-buckled eigenvalue loci of the bi-tetrahedral frame.

utilised, then convergence even across the extreme buckling limits can be achieved practically after a single iteration. It is of course a matter of chance whether a straight eigenvalue function is nominated for the identification or not and is not a matter of choice unless second and higher derivatives are inspected.

The curvatures of the coupled loci in Fig. 5.3 potentially give rise to root multiplicity, since for a given eigenvalue there can be two roots on a given, veered curve. This is important to know since convergence upon an erroneous root is misleading, and in fact worse than the iteration diverging. The advantage of the present context of structural dynamics is that, within reason, there are many modes available as functions of the force parameter, and hence the system of equations 2.15 can be overdetermined, as is common practice, to alleviate the ambiguity of multiple roots.

Fig. 5.4 shows convergence upon the positive buckling load, and as a rigorous test, iteration is chosen to commence at the negative buckling load.

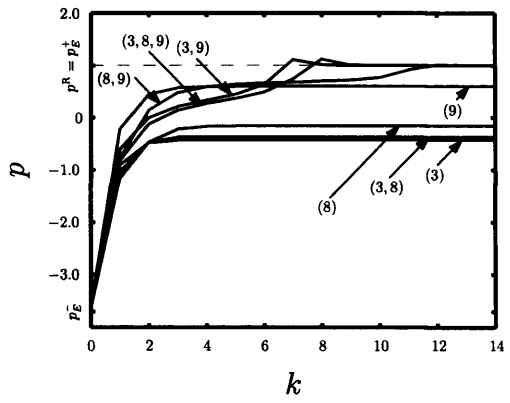

Figure 5.4: Buckling-to-buckling convergences resulting from all combinations of three ambiguous bi-tetrahedral frame eigenvalue loci.

For this task, all combinations of the three modes 3, 8 and 9 are used. For reference, these are represented by the three loci in Fig. 5.3 whose stationarity is in the vicinity of $p = 0.5$. Respectively, each of these modes used independently is seen to converge to its erroneous root since the true root is in each instance 'over hill' of the former. In combination, correct convergence is seen to result since mutuality between the modes must be fulfilled in convergence. One exception is the combination of modes 3 and 8 — here, the Newton progression at the erroneous root is near zero, and hence the iteration stagnates there. This is a rare occurrence and, nevertheless, a good degree of overdetermination is a robust means for overcoming root ambiguity. Note that from Fig. 5.4, iteration is seen to depart slightly from the pre-buckled region, but in doing so does not impede the eventual convergence. This should, however, in general, be avoided as the validity of the finite element model post-buckling is questionable, i.e., the eigenvalue loci and their derivatives may become numerically unstable and erratic.

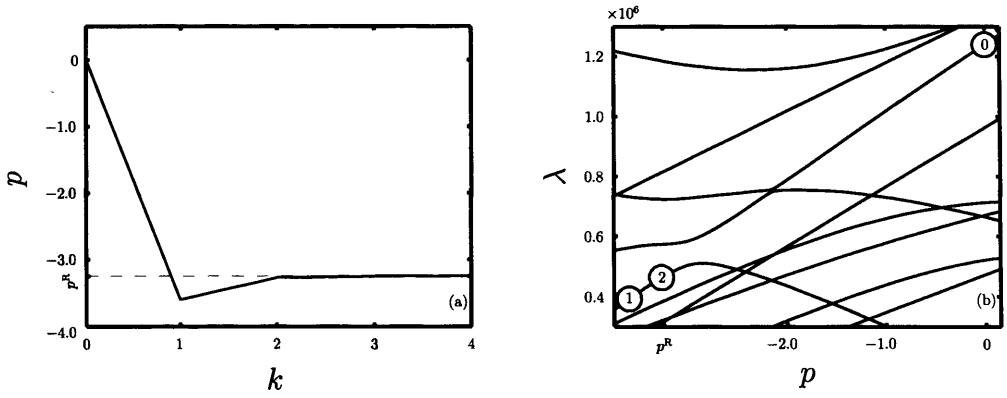

Figure 5.5: Iteration transcending bi-tetrahedral frame eigenvalue loci past a veering event; (a) progression with respect to iteration number; (b) progression along loci.

With locus veering, it is possible for iterates to transcend curves (perform 'consistency jumps') when mode tracing is employed, as has been observed in Ch. 4. Fig. 5.5 shows how iteration transcends curves at the veering around $p = -3.0$; the root is just past the veering point and iteration commences from $p = 0$. Correct convergence ensues using mode 8, illustrating that the purpose of employing mode tracing is to conserve function smoothness for the benefit of the iteration; the definition of the functions between the initial parameter value and root is otherwise not of importance. Note that this is completely analogous to what happens in the limiting case of mode tracing passed an eigenvalue coalescence point.

5.5 Once Redundant, Regular, Octahedral Frame

Analogously to the tetrahedral frame, a redundant member can be accommodated by an octahedral, skeletal frame, as depicted in Fig. 5.6. According

to Eq$^{\underline{n}}$ 2.23, the degree of redundancy is $13-3\times6+6=1$. This example will be used to demonstrate the identification of load simultaneously with that of other parameters. As well as load then, the density of the material forming the frame members, ρ, and the diameter of the members, d, are sought and it is assumed that they are initially known to nominal values: $\rho^1 = 7850$ kgm^{-3} and $d^1 = 0.01$ m. It is also assumed that the frame is completely unloaded at the beginning of iteration. Density governs the mass of the frame and it is obvious that the frequencies will decrease with increasing ρ; diameter will of course increase the frame stiffness and the frequencies will increase with respect to d. The length of the external frame member is nominated as 0.5 m.

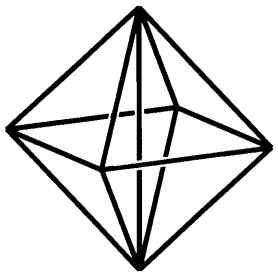

Figure 5.6: Once redundant, octahedral frame.

This example will also be used to demonstrate the importance of aligning the eigenvectors of permanently degenerate modes during iteration (q.v. Sec. 4.3). This is an issue for the once redundant, octahedral frame because, although the problem is parameterised with parameters other than just load, the variation of these parameters does not break the symmetry of the model. Some of the eigenvalues are therefore permanently degenerate. Iteration will

progress with mode tracing but without the alignment of eigenvectors in order to expose the potentially detrimental effects of such neglect.

The root is chosen as

$$\left\{ \begin{array}{c} P^{\mathrm{R}} \\ d^{\mathrm{R}} \\ \rho^{\mathrm{R}} \end{array} \right\} = \left\{ \begin{array}{c} 4000.0 \\ 0.0109 \\ 7864.2 \end{array} \right\}, \tag{5.1}$$

where the seven modes selected for iteration have frequencies in Hz of 105.18, 109.56, 112.84, 119.38, 152.94, 153.66 and 165.67, some of which are repeated. The modes are selected from the lower end of the spectrum, with the mode at 105.18 Hz the fundamental mode.

Normally, for demonstrative purposes in numerical simulations, the load factor p is used to intimate the relation of the loads during iteration to the buckling load. However, for the present example, as the finite element model is parameterised with member diameter, the buckling load itself is variable and so the load factor P is used instead.

Making use of Eq$^{\underline{\mathrm{n}}}$ 3.10, the eigenvalue derivatives with respect to the three independent variables are computed as follows:

$$\frac{\partial \lambda}{\partial P} = \boldsymbol{\phi}^T \mathbb{G} \boldsymbol{\phi}; \tag{5.2}$$

$$\frac{\partial \lambda}{\partial d} = \boldsymbol{\phi}^T \left(\frac{\partial \mathbf{K}}{\partial d} - \lambda \frac{\partial \mathbf{M}}{\partial d} \right) \boldsymbol{\phi}; \tag{5.3}$$

$$\frac{\partial \lambda}{\partial \rho} = -\boldsymbol{\phi}^T \left(\lambda \frac{\partial \mathbf{M}}{\partial \rho} \right) \boldsymbol{\phi}. \tag{5.4}$$

All elemental mass and stiffness matrix derivatives are given explicitly in Appendix 1.

The progress of iteration is given in Fig. 5.7, which shows how the initial eigenvalues are brought to the root eigenvalues and also the convergence of

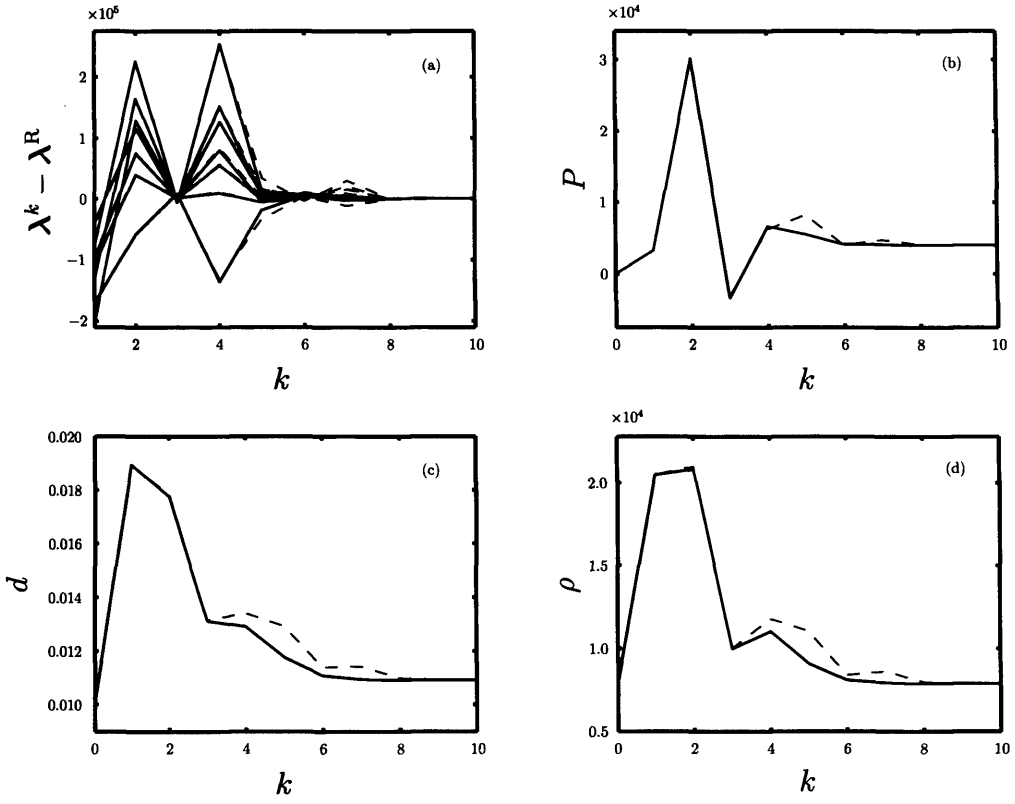

Figure 5.7: Progression of quantities with respect to iteration number for the once redundant, octahedral frame: (a) current and root eigenvalue difference; (b) load, P; (c) diameter, d; (d) density, ρ; ———— without Jacobian column weighting; – – – – with Jacobian column weighting.

the three independent variables upon the root values. It is seen that, for the present example, load can be updated alongside other physical parameters.

Inspection of the Jacobian near the root,

$$\mathbf{J}^* = \begin{bmatrix} 29.3 & 3.70 \times 10^7 & -55.5 \\ -11.3 & 1.03 \times 10^8 & -60.3 \\ 8.01 & 8.03 \times 10^7 & -63.9 \\ 1.61 & 1.01 \times 10^8 & -71.5 \\ -19.6 & 1.98 \times 10^8 & -117 \\ -6.44 & 1.80 \times 10^8 & -119 \\ 5.34 & 1.91 \times 10^8 & -138 \end{bmatrix}, \tag{5.5}$$

demonstrates that, because of the arbitrary way the problem has been para-

meterised, the second column of the matrix, that pertaining to d, is several orders of magnitude greater than the other two. Consequently, the Jacobian is ill-conditioned, with singular values of $\sigma_1 = 3.70 \times 10^8$, $\sigma_2 = 53.9$ and $\sigma_3 = 0.0528$.

Although convergence is observed, the condition of $\mathbf{J}$ is treated, as described in Sec. 2.5. This is seen to take the condition number of the Jacobian at the root, or the ratio of the greatest singular value to the smallest, from 7.00×10^9 to 6.82×10^3. The iteration is re-observed with this conditioning and the results are also given in Fig. 5.7. Note that such conditioning does not change the values of the Newton progressions $\Delta\mathbf{p}$, and so both the solution and the path to it are not expected to be different between Eq$^{\underline{n}}$ 2.15 and Eq$^{\underline{n}}$ 2.27. Fig. 5.7, however, shows otherwise. This can be explained as follows.

Although by conditioning the Jacobian the Newton progressions do not change in theory, there are very small discrepancies brought about by the inevitable rounding errors associated with numerical computation. Normally, such discrepancies are so minute that they are utterly insignificant; presently, they seem to have been significant enough to have changed the orientations of the degenerate mode eigenvectors at each iterate (such eigenvectors are arbitrarily oriented at all values of the parameters). If a mode trace is naturally ambiguous because of low consistency and high corruption, the further lowering of consistency that arises due to not aligning degenerate mode eigenvectors can be enough to change the trace path. This of course only has to

happen to one mode once during iteration to completely alter the path Newton's method takes. Fortunately in Fig. 5.7 the correct solution is reached in both iteration schemes (N.B. in the philosophy of mode tracing, there is no correct path to the solution but a smooth path should be found), but there is always the possibility that divergence could ensue. The conclusion is that the alignment of the eigenvectors of permanently degenerate mode eigenvectors must be performed to minimise ambiguity in mode tracing.

5.6 Thrice Redundant, Regular, Octahedral Frame

The opposing apices of the bi-tetrahedral frame made is possible to insert an internal redundancy; the octahedral frame has the potential to accommodate three internal members. According to Eq^{n} 2.23, the degree of redundancy is $15 - 3 \times 6 + 6 = 3$. Again, the length of the external frame member is nominated as 0.5 m and the members are of circular section and diameter 0.01 m. The octahedral frame is depicted in Fig. 5.8.

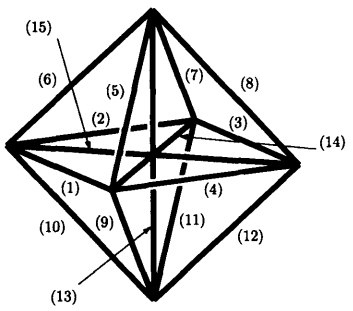

Figure 5.8: Thrice redundant, octahedral space frame.

From a simple compatibility analysis, it is found that about any single

axis of the frame, there exist two classes of force distribution. These classes may be distinguished by the type of member that needs to be strained to induce them: external (class I) or internal (class II). However, since the frame possesses three axes of spatial periodicity and is identical from the aspect of each, the total number of distinct force distribution types is six. These are given in Fig. 2.1, with member numbers corresponding to Fig. 5.8. The first column shown in the matrix given therein is fourfold multiple because of the symmetry of the regular octahedral frame — this can be appreciated by seeing that the external frame is formed of three orthogonal, square, planar frames and that straining of any one member of these is the same as straining any other. Further, since the frame is identical from three orthogonal aspects, two more sets of fourfold identical columns follow, with all these sets permutations of one another. The last three, distinct vectors of the equilibrium matrix relate to straining of an internal frame member, and therefore represent class II distributions. As seen, the three distributions of the respective classes amongst themselves represent the same force distribution orientated according to the three different axes of spatial periodicity, so that variations of eigenvalues with respect to each of them are identical.

With p_1, p_2 and p_3 relating to class I distributions, and p_4, p_5 and p_6 to class II distributions, Fig. 5.9 shows how the frame eigenvalues vary with respect to loading between the buckling limits. The two plots are not wholly disparate and each parameter set affects the eigenvalues in a similar way.

It is found that the equilibrium matrix has rank three, and further that

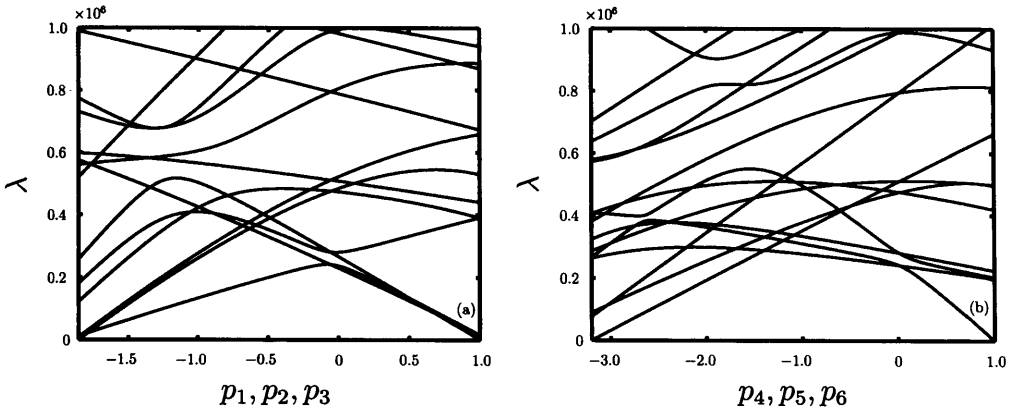

Figure 5.9: Pre-buckled eigenvalue loci of the thrice redundant, octahedral space frame.

a reduced, full rank matrix can be established with the three distributions of class I alone, for example, i.e., $\overline{\mathbf{E}} = [\mathbf{e}_1\ \mathbf{e}_5\ \mathbf{e}_6]$. The physical interpretation is that the any possible state of equilibrium of the octahedral frame can be expressed as a linear combination of these three linearly independent force distributions. Therefore, let the force parameters governing the iteration space be factors upon the first three types of force distribution, p_1, p_2 and p_3.

The point made in Sec. 5.2 regarding root uniqueness is well demonstrated by seeking a root

$$\mathbf{p}^{\mathrm{R}} = -\left\{ \begin{array}{c} 0.1634 \\ 0.4902 \\ 0.8170 \end{array} \right\} \tag{5.6}$$

and initiating iteration at a permuted set of values

$$\mathbf{p}^{\mathrm{Я}} = -\left\{ \begin{array}{c} 0.8170 \\ 0.1634 \\ 0.4902 \end{array} \right\}, \tag{5.7}$$

at which there exists an ambiguous root. This coordinate simply represents the distribution of force in the frame as at the true root but at a different

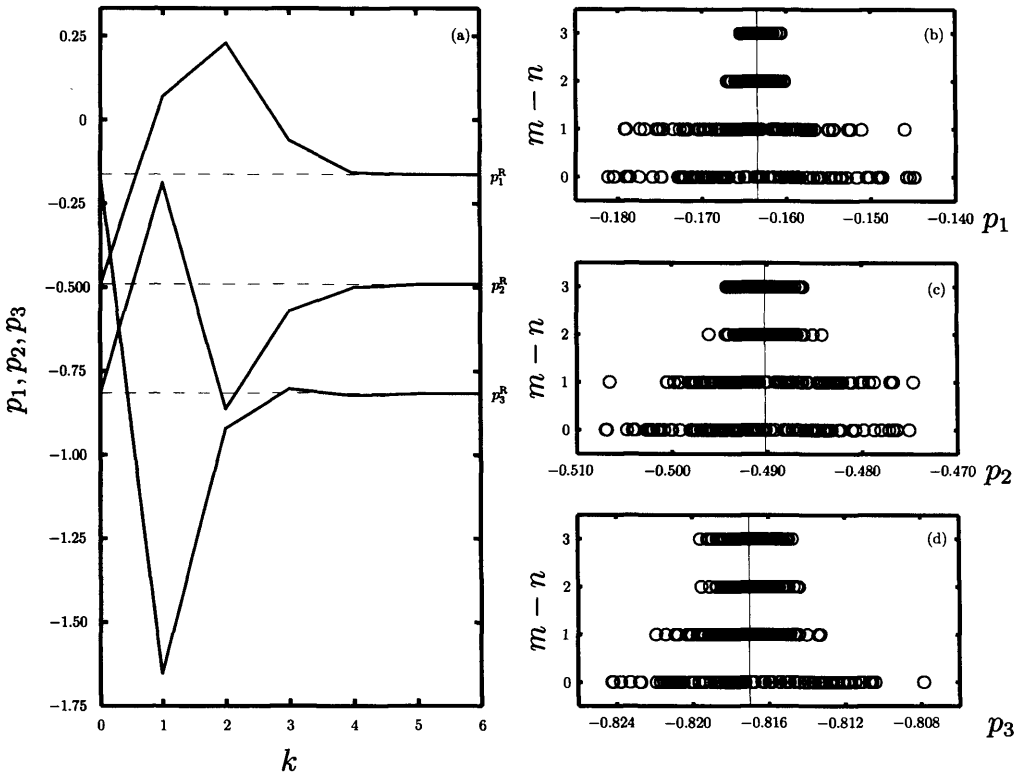

Figure 5.10: Mode tracing overcoming root ambiguity in the force identification of the thrice redundant, octahedral space frame: (a) iterative progression of load parameters; Monte Carlo noise simulations with varying degrees of overdeterminacy for (b) p_1, (c) p_2 and (d) p_3; O converged solution.

spatial orientation. Without mode tracing, the iteration would not make a progression from this starting value since the eigenvalue hypersurface upon which the false root lies is a reflection through the 3-dimensional focus of symmetry of the hypersurface upon which the true root lies, and therefore the eigenvalue constraint would automatically be satisfied. Fig. 5.10 shows that with mode tracing employed on the first three root modes, the correct eigenvalue curve is discerned so that the true root is discovered. (N.B. The iterative progression of all three force parameters can be shown on the same

set of axes since they represent distributions with the same P_E^+.) The reason that the curve of the $\mathbf{p}^{\mathfrak{R}}$ root is not traced with the curve of the true root $\mathbf{p}^{\mathrm{R}}$, and that curve consistency is maintained, can be appreciated from seeing that the eigenvectors of these respective roots used in the mode tracing have a unique relation to their force distributions, which are further spatially orthogonal and therefore on a global level mode tracing does not pair them. That is to say, the ambiguity arising from the non-uniqueness of the eigenvectors is overcome by utilising the uniqueness of the eigenvector-force distribution relation.

Noise is simulated by Monte Carlo runs in which the nominated random noise is at most ± 5 % of the root fundamental frequency, for any given frequency used in the identification. Although the noise model is unrealistic, with all levels of noise having equal probability and relative noise greater for lower frequencies, it is felt that it is a conservative one. For each degree of overdeterminacy, the solution spreads resulting from one hundred runs can be seen in Fig. 5.10(b)-(d). Expectedly, overdetermination helps to improve the precision of identification.

5.7 Thrice Redundant, Irregular, Octahedral Frame

A topologically identical but geometrically different frame is now considered. If the spatial locations of the five apices of the regular, octahedral frame are

described by the matrix

$$\mathbf{D} = \begin{bmatrix} \frac{1}{2} & -\frac{1}{2} & -\frac{1}{2} & \frac{1}{2} & 0 & 0 \\ -\frac{1}{2} & -\frac{1}{2} & \frac{1}{2} & \frac{1}{2} & 0 & 0 \\ 0 & 0 & 0 & 0 & \frac{1}{\sqrt{2}} & -\frac{1}{\sqrt{2}} \end{bmatrix}, \tag{5.8}$$

then the geometry of the irregular frame is described by $\mathbf{D} + [\ \mathbf{I}\ \ \mathbf{I}\ ]$. All other properties are conserved in the transformation from the regular frame. Owing to the more complex geometry, force distributions are determined from the static matrix analysis outlined in Sec. 5.3. The irregular, octahedral frame is shown in Fig. 5.11 with member numbering consistent with that in Fig. 5.8.

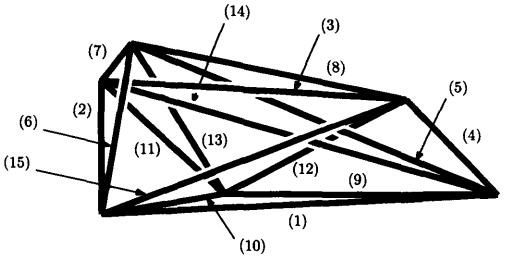

Figure 5.11: Thrice redundant, irregular, octahedral space frame.

Establishment of the reduced matrix $\overline{\mathbf{E}}$ is possible after observing the number of non-zero singular values of the equilibrium matrix $\mathbf{E}$, which equals three. From this, it is found that the number of linearly independent force distributions — that is to say, the minimum number whose linear superposition suffices in describing any possible equilibrium state — is conserved following the breaking of symmetry. In other words, the irregular frame has the same number of force distributions as the regular frame from which it is deformed. This must hold since the topology is conserved. Physically,

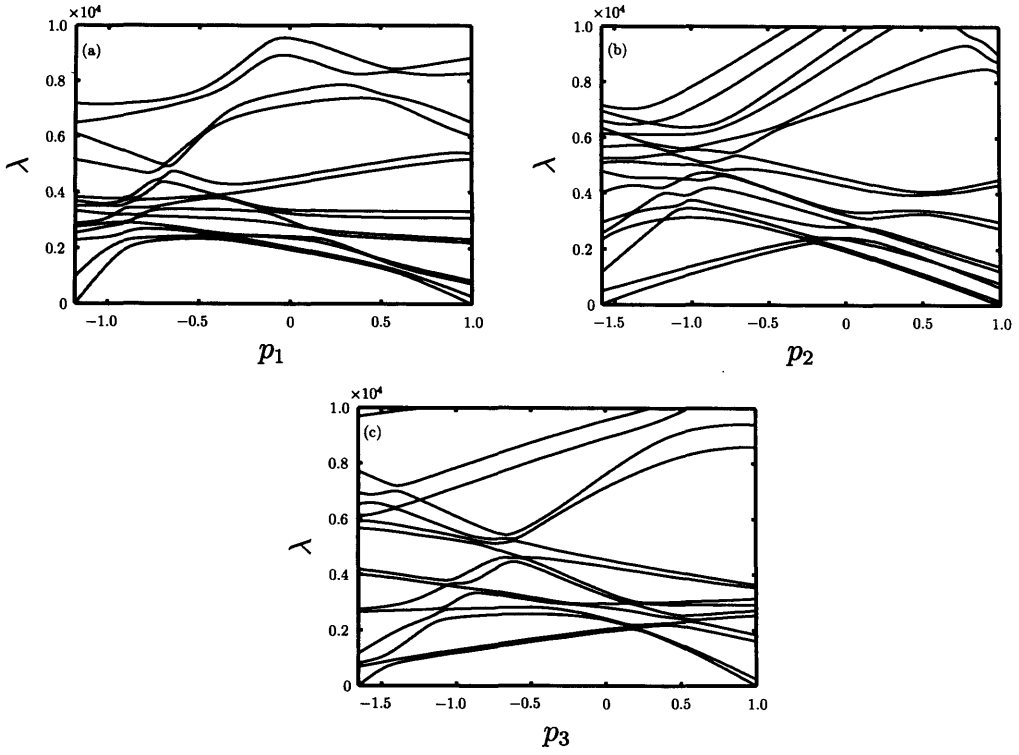

Figure 5.12: Pre-buckled eigenvalue loci of the thrice redundant, irregular, octahedral frame.

the member-joint relations remain identical and therefore the irregular frame cannot possess any further linearly independent force distributions in comparison to the regular frame.

The eigenvalue-force parameter loci for three particular distributions are given in Fig. 5.12. These distributions are those that arise from the straining of members 1, 2 and 3 — q.v. Fig. 5.11. Of immediate note is the increased erratic characteristic of the loci, potentially posing difficulty for the iteration. Supportive of the suggestion by Perkins and Mote (1986), as discussed in Sec. 4.1, is the fact that, upon closer observation, the breaking of symmetry is seen to have turned all coalescences into veerings.

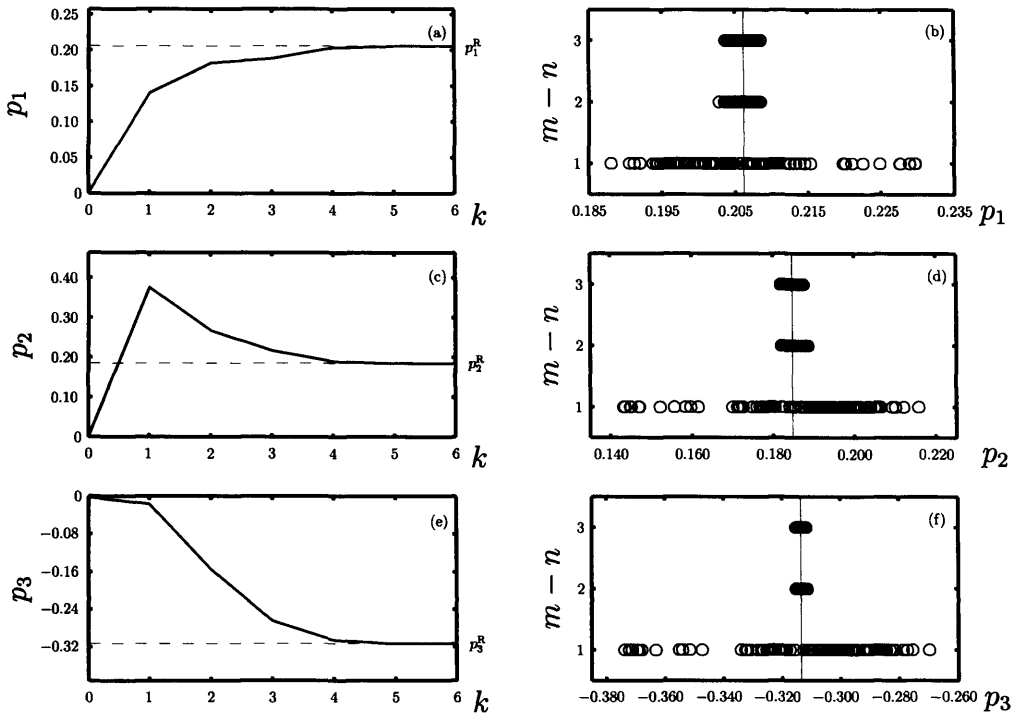

Figure 5.13: Force identification of the thrice redundant, irregular, octahedral frame: iterative progression of load parameters and Monte Carlo noise simulations with varying degrees of overdeterminacy for (a)-(b) p_1, (c)-(d) p_2 and (e)-(f) p_3; O converged solution.

Owing to the increased slenderness of some of the members of the irregular frame, the frequencies are in general lower. Consequently, the irregular frame cannot withstand as much loading as its regular analogue.

A target root of

$$\mathbf{p}^{\mathrm{R}} = \left\{ \begin{array}{c} 0.2062 \\ 0.1848 \\ -0.3135 \end{array} \right\} \tag{5.9}$$

is nominated and convergence using the initial four root modes from an unloaded state is shown in Fig. 5.13. Four modes are used since a degree of overdeterminacy one is the minimum required for convergence to result at all. Again, simulated noise is included in the manner previously described and is

found to behave similarly with respect to increasing overdetermination, but with overdetermination providing more constraint to the solution than in the previous example.

5.8 Thrice Redundant Octet Frame

So far, the numerical simulations have involved structures that have been simple in form with few members; real space frames typically comprise many times more members, joined together to form complicated shapes. In order to introduce physical relevance, this next simulation is therefore concerned with a spatial beam structure comprising octet sub-frames. An octet is a regular, octahedral frame, with two regular tetrahedral frames adjoining two of its opposing faces, and with the capability of space-filling — the three dimensional analogue of tessellation. Being formed of sub-frames already studied in this chapter, and also representing a physically practical structure, the octet frame is a useful bridge between the problems that have been dealt with hitherto and how they might manifest themselves in actual space frames. It also follows the natural progression that began with single beams and went on to investigate the behaviour of these beams coupled within elementary space frames; it is these elementary frames that are now coupled within a bigger structure.

The octet frame is shown in Fig. 5.14. The frame is slightly modified in that the two most central, internal members have been removed and replaced with a longer member in the very centre of the structure, member 55. The

reason for this is to lower the buckling limit and hence decrease the magnitude of force in the frame required to cause the fundamental vibration mode to vanish. In this way, the effects of force on the dynamics of the system will be more significant. The rank of the equilibrium matrix, **E**, is three, indicating that there are three redundancies and as many linearly independent force distributions. This is also shown by Eq$^{\underline{n}}$ 2.23: $63-3\times 22+6=3$. The order of the problem is therefore the same as for the previous two space frames.

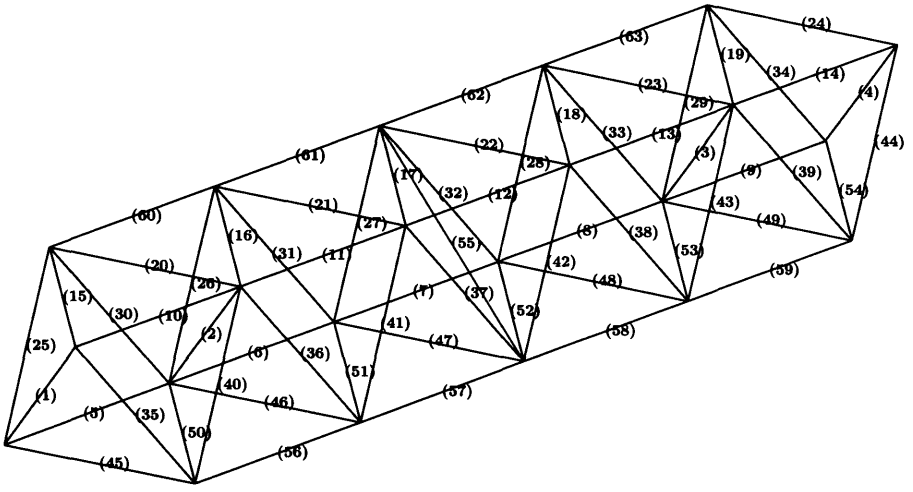

Figure 5.14: Octet frame.

What is of particular note is the intricacy of the example eigenvalue-force parameter loci, shown for the distribution arising from the straining of member 1 in Fig. 5.15. Up until now, observation of how the eigenvalues vary with respect to load for each of the frames investigated has supported the point discussed in Ch. 1 that the dynamics of space frames can be thought of as the coupled dynamics of all the constituent members. An example of this is that the vanishing of the fundamental frequency has been seen to

coincide with the buckling of the most susceptible member. A consequence of the local beam systems coupling into the global structural system is that the more members there are forming the structure, the more dense will be the eigenvalue loci. This has been observed across the eigenvalue loci plots, from those of the bi-tetrahedral frame through to the once and then thrice redundant octahedral frames, and is now made very apparent with the sixty three member octet frame. The implications of having such a high modal density, in terms of the effects of on mode tracing, and, indeed, on the ability to define what a mode is in an inconstant landscape of varying frequencies *and* mode shapes, are discussed later. What is apparent is that the usual characteristics all feature in Fig. 5.15. The fundamental frequency vanishes at two values of p, positive and negative, corresponding to opposite directions of loading for the frame. Both eigenvalue coalescence and locus veering abound, although there is no permanent degeneracy of the eigenvalues. A strange feature at zero load and around $\lambda = 1.35 \times 10^6$ indicates an explosion in which a family of modes diverges as the frame is loaded in either direction.

Of great concern is the fact that, in comparison to the pre-buckled loci of the previously investigated frames, those of the octet frame are shallow. That is to say, generally, their gradients are small, indicating that in regions the eigenvalues are fairly insensitive to load. This can be appreciated as a problem by inspecting Eq$^{\underline{n}}$ 2.15. For a given difference between current and root eigenvalues, the smaller the eigenvalue derivative in the Jacobian, the greater will be the Newton progression $\Delta\mathbf{p}$. With a frame for which

mode shapes are rapidly changing with respect to load, this is extremely detrimental as the progression could send the next iterate far enough from the root that the current and root eigenvectors bear little, if any, resemblance to one another. The prospect of tracing modes in this event, and therefore employing Newton's method for load identification at all, does not exist. In extreme cases, iteration may be sent far from the pre-buckled region of the finite element model where the frequencies, mode shapes and their numerical stability are questionable.

Complicated space frames will be seen to present demands on the iterative schemes that have, until now, proved to be fairly robust, nearly always identifying the numerically ascribed root. Certainly for the octet frame, convergence upon a root is rather the exception, not the rule. One successful convergence is now shown.

The properties of the octet frame model are as follows. The length of the regular frame member is nominated as 0.5 m and all members are of circular section and diameter 0.01 m. The finite element model is formulated on columns 51, 53 and 55 of the equilibrium matrix $\mathbf{E}$, which relate to the force distributions that would arise if, respectively, these frame members were strained (q.v. Fig. 5.14). With the standard normalisation of the force distributions, i.e., where the force in the member most susceptible to buckling is unity, the condition number of $\overline{\mathbf{E}} = [\mathbf{e}_{51}\ \mathbf{e}_{53}\ \mathbf{e}_{55}]$ is 725. It is assumed that $\overline{\mathbf{E}}$, whose range is capable of describing any state of equilibrium in the octet frame, is well conditioned enough for numerical purposes.

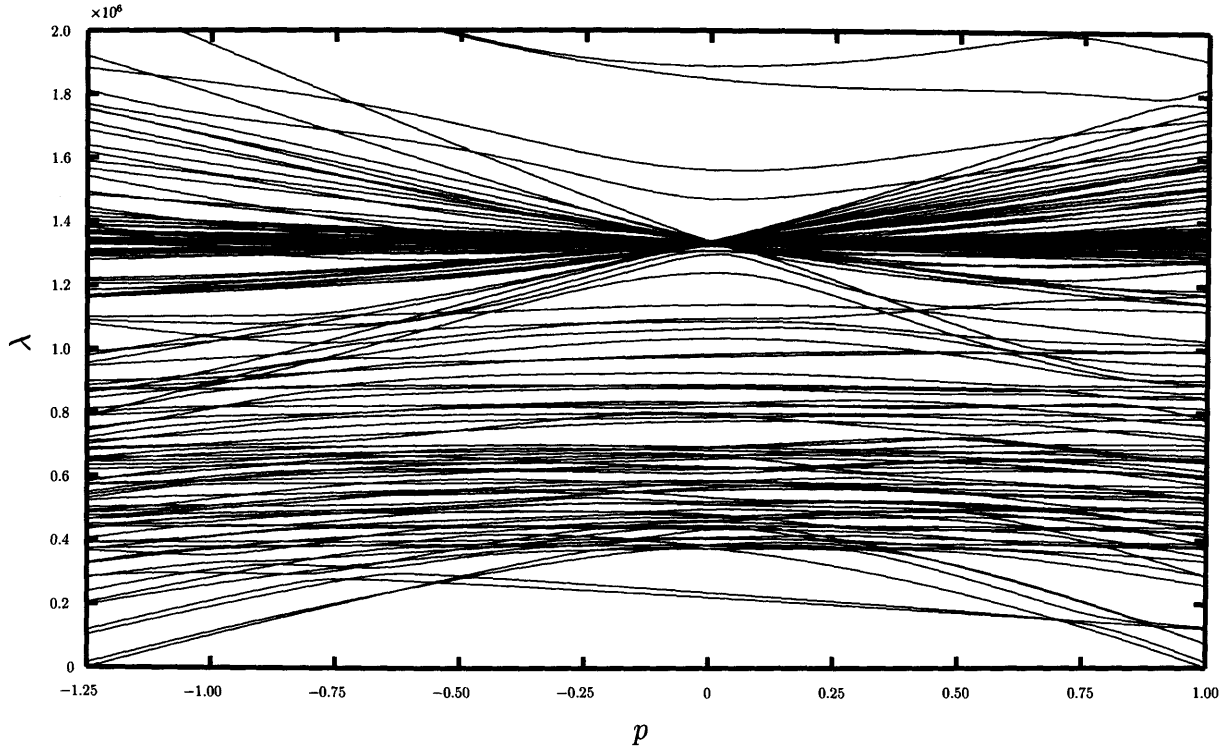

Figure 5.15: Eigenvalue loci of the octet frame with p a factor upon the normalised force set arising from the straining of member 1 (q.v. Fig. 5.14).

The root is chosen as

$$\mathbf{p}^{\mathrm{R}} = \left\{ \begin{array}{c} 0.1 \\ 0.2 \\ 0.3 \end{array} \right\}, \tag{5.10}$$

with iteration commencing from

$$\mathbf{p}^{0} = -\left\{ \begin{array}{c} 0.1 \\ 0.2 \\ 0.3 \end{array} \right\}. \tag{5.11}$$

At the root, the twenty modes selected for iteration have frequencies in Hz of: 48.8, 93.4, 99.0, 100.8, 105.1, 107.24, 112.1, 114.4, 119.3, 122.6, 125.2, 127.8, 130.1, 134.3, 140.7, 144.5, 148.3, 152.5, 160.3 and 168.1. This is in fact the first twenty of every third mode beginning with, and inclusive of, the fundamental mode.

Iterative progression is seen in Fig. 5.16, which depicts how the initial eigenvalues are brought to the root eigenvalues. Also shown is identification of each of the three force parameters, with p_1 and p_2 coincidentally taking very similar paths to the solution, and the corresponding member forces with respect to iteration number. Although the force parameters are many times greater than their initial and root values, the member forces indicate that iteration remains entirely within the pre-buckled iteration space, which is partially bounded by $P_E^+ = 7210$ N. The member forces are, of course, seen to change sign but conserve magnitude due to the values of the initial and root force parameters. The final plot in the figure shows how a particular eigenvector consistency measure varies with iteration. The measure is the mean of the *mac* values between each of the root eigenvectors and the eigenvectors with which they are most consistent at each iterate. The value

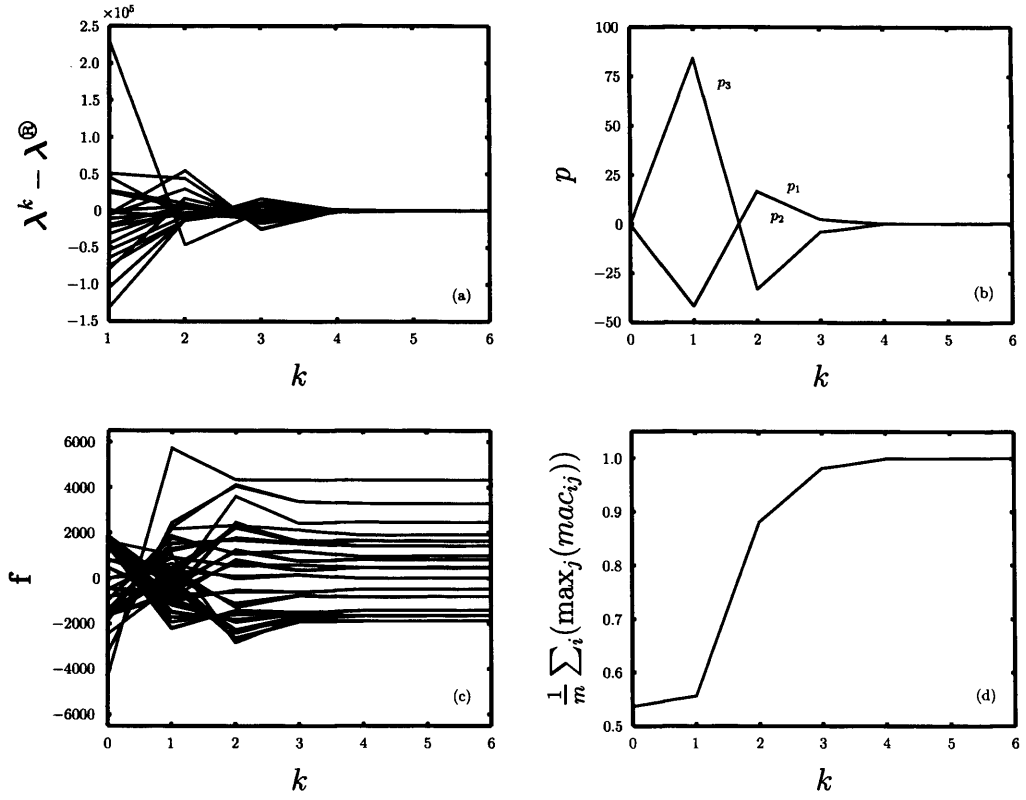

Figure 5.16: Progression of quantities with respect to iteration number for the octet frame: (a) current and root eigenvalue difference; (b) force parameters; (c) member forces; (d) mean of the maximum consistencies attained by each root eigenvector with the current iterate eigenvectors.

naturally converges to unity but is seen to be almost half this at the start of iteration. This serves to show that the eigenvectors at $\mathbf{p}^0$ and those at $\mathbf{p}^R$ are markedly different. It must be emphasised that because of rapidly changing eigenvectors and generally small eigenvalue gradients, roots can prove to be rather elusive.

This point is worth investigating further. Fig. 5.17 shows the *mac* values the root eigenvectors achieve with the eigenvectors of a subset of the initial sixty-five modes at each iterate. At iterates four and five, almost unit

consistency, with practically zero corruption, is observed; this is where the solution is well converged. Iterates two and three show that modes can be clearly paired and that coalescence has taken place since some consistency values are 'off diagonal'. Going back to the first iterate, few modes are strongly paired and consistency is generally very weak. At $k = 0$, where the initial basis for tracing modes is performed, the values of *mac* are seriously small with accompanying corruption terms. In light of this, it is remarkable that iteration started well at all.

Note that no ambiguity is introduced by the inclusion of the six rigid body modes; if this is of concern, it is an easy matter to exclude the rigid body modes from the subset of modes T at the current iterate used to pair the root modes in S (q.v. Sec. 4.1).

In order to assess the degree by which consistency of eigenvectors deteriorates, the frame is loaded at four magnitudes in the distribution of force relating to the straining of member 51: $p_1 = 0$, $p_1 = \frac{1}{3}$, $p_1 = \frac{2}{3}$ and $p_1 = 1$. The weakening of consistency of the first third of all of the modes in the finite element model from the unloaded state to the buckled state is shown in Fig. 5.18. Fig. 5.19 is a similar plot with the same magnitude of force at each stage in member 55, except in this instance loading progresses simultaneously in all three of the force distributions: $\mathbf{p} = [0\ 0\ 0]^T$, $\mathbf{p} = \left[\frac{1}{9}\ \frac{1}{9}\ \frac{1}{9}\right]^T$, $\mathbf{p} = \left[\frac{2}{9}\ \frac{2}{9}\ \frac{2}{9}\right]^T$ and $\mathbf{p} = \left[\frac{1}{3}\ \frac{1}{3}\ \frac{1}{3}\right]^T$. In all of these plots, the entire eigenvectors have been used to compute *mac* values so that none of the deterioration can be attributed to shortage of data.

From the *automac* plots, which should indicate the degree of corruption present at the unloaded state of the octet frame (the diagonal terms are, of course, all unity), it is observed that as well as the usual, small amounts of corruption, there also exists strong 'off diagonal' correlation. A family of modes at around designation 100 are seen to have a secondary consistency with another family of modes at around designation 350. This is due to the spatial aliasing problem with the mode shapes and is a shortfall of the level of member discretisation. While the modes in each family are in reality different, the inability of the discretisation level to describe the higher modes to sufficient detail has made all of these modes look very similar as far as the scrutiny of *mac* is concerned. As discussed in Sec. 4.1, spatial aliasing arguments should be used to upper-bound the modes in the subset T at the current iterate used to pair the root modes in S. In this way, the possibility of an erroneous mode pairing with a higher order mode is allayed.

The first *crossmac* plots show that the modes that lend themselves to the spatial aliasing problem are also susceptible to a phenomenon in which their eigenvector consistencies are drastically diminished, both amongst themselves and with the ambiguous higher order modes. Further, the correlation of the ambiguous higher order modes amongst themselves is also seen to deteriorate, suggesting that there is a more fundamental, underlying property of all of these modes that makes them prone to this variation in eigenvectors. Stranger still is that another patch of disruption has formed in the 'diagonal' terms at around designation 225, which is at the centre of the 'square'

formed by this phenomenon. It is not known what precisely is giving rise to this disturbance of the eigenvectors, but evidently it is the family of modes associated with the explosive characteristic observed in Fig. 5.15, in which an entire group of modes diverges as load is applied in either direction of sign. Clearly, some means of identifying which are the prone modes needs to be found so that the relatively immutable modes can be used in iteration.

The weakening of eigenvectors increases in the subsequent *crossmac* evaluations with eigenvectors at greater loaded states, with even the modes immune to the aliasing becoming significantly inconsistent. Note that Fig. 5.19, which involves loading in all three force distributions simultaneously is similar to Fig. 5.18, which involves loading in just the first force distribution. The loading in the former, like the latter, is still linear, but in a hybrid force distribution that is not realisable with the straining of just one member. This does not seem to display a significantly lesser or greater manifestation of the phenomenon.

Promisingly, there *are* relatively immutable modes that could pass as candidates for updating a finite element model. Even so, the selection of a starting point for iteration is crucial for a solution to succeed. Eigenvectors, as well as the eigenvalues used in Newton's method, have been shown to change rapidly with respect to load, ultimately undermining the crucial mode tracing strategy required to ensure steady convergence. It is no longer a sufficient condition to begin iteration in the neighbourhood of the root in terms of the eigenvalue functions, as the classic requirement for Newton's

method demands, but also now in terms of the consistency of the eigenvector function with the root eigenvectors. It is already known that constancy of an eigenvector is dependent upon the derivative of its eigenvalue locus. The straighter the locus, or the more constant the eigenvalue derivative, the more constant will be the eigenvector. Sec. 4.4 illustrated that when there is intricate coupling of modes such that the eigenvalue loci exhibit high degrees of curvature, the eigenvector consistency is smeared across the coupled system so that the confidence of tracing modes is greatly diminished. The octet frame is a more severe example of this modal coupling, with closer modes erratically veering in confined regions of the spectrum, and it is a natural consequence that the prospect of tracing modes is generally less likely.

In order to appreciate the mechanism by which eigenvector consistency is lost, Fig. 5.20-5.23 depict the loss of *mac* consistency for the initial four modes from p_E^- to p_E^+; the datum eigenvectors are those at p_E^-. For all of these four plots, the consistency is, as expected, strong in the relatively straighter portion of the eigenvalue function. As the locus enters the intricate host of coupling, veering modes, consistency abruptly diminishes to almost zero. After $p = 0$, all of the modes, as are defined at p_E^-, are, for all purposes, non-existent. It is difficult to define what a mode is in such a landscape of varying frequencies *and* mode shapes. It is more sensible to speak of modes dying and being born as parameters vary. Indeed, they may even be resurrected — the modes of Fig. 5.20-5.23 could very well come back into existence as p increases.

5.9 Conclusions

Demonstrative numerical simulations have been given to illustrate foregoing issues. It was intended that certain issues be made evident, so that if such a method were to be employed in reality, these would be anticipated and treated and the models used in the numerical simulations suffice to do so. Indeed, the methodology of force determination here presented relies upon good model-to-structure correlation, and minimal noise in the modal data. It is hoped that both of these are achievable with the simple structural nature of skeletal, space frames.

Since Newton's method extends readily and in a natural way to multiple dimensions, the one-dimensional problem has been used to illustrate the utility of overdetermination and mode tracing. The former is helpful in distinguishing between ambiguous roots and for reducing the error range due to noise; the latter helps to overcome the phenomena of eigenvalue coalescence and locus veering by defining smooth eigenvalue functions for the benefit of Newton's method. In fact, both eigenvalue coalescence and locus veering are overcome in the same manner, so that at veering iterates transcend loci (perform 'consistency jumps'). In all of the simulations, including one- and three-dimensional Newton's methods, absence of mode tracing, and therefore the definition of non-smooth eigenvalue functions, is known to have potentially detrimental consequences, such as divergence and, worse, convergence to erroneous roots. It is therefore found to be an imperative measure. Erroneous convergence can also occur with traced modes if the eigenvalue function

curvature is such that root ambiguity is introduced. Overdetermination is here an aid to establishing root uniqueness, and so the two strategies should necessarily be used in conjunction.

Mode tracing is seen to overcome a special problem of root ambiguity in the case of frames with multiple axes of spatial periodicity. Here, the unique root is isolated by virtue of the uniqueness of the eigenvector-force distribution relative orientation, and so the eigenvector-based mode tracing is afforded discernment of the true solution.

Emphasis has been placed upon minimising the number of force distributions needed to account for any state of frame equilibrium, and hence the dimensionality of Newton's method. The bases for doing so are arguments of equilibrium constraints. This advancement from previous schemes of force identification is necessary in terms of easing the progression of iteration. Further, in cases of frames with multiple axes of spatial periodicity, this prevents a solution that, while discerning the correct forces, would imply incorrect member designations.

The example of the once redundant, octahedral frame has served to indicate that load can be identified in the case when other variables are parameterised alongside it in the finite element model. It has been shown that the alignment of eigenvectors associated with permanently degenerate eigenvalues across iterates is crucial. If this is not done, the ambiguity that already exists when tracing modes will be worsened.

As seen from the irregular octahedral frame, the slenderness of frame

members governs the magnitudes of the frame frequencies. The low frequencies of slender frames may be of concern in terms of noise-dependent errors in modal measurement.

The octet frame serves to show that great demands can be placed on Newton's method and mode tracing schemes, due to shallow eigenvalue gradients, high degrees of coupling leading to eigenvector, and therefore consistency, deterioration and peculiar phenomena exhibited by the model. Success of iteration is in this case the exception rather than the rule. The emphasis must be to select thoughtfully and prudently the starting point for iteration and also the modes used at the root.

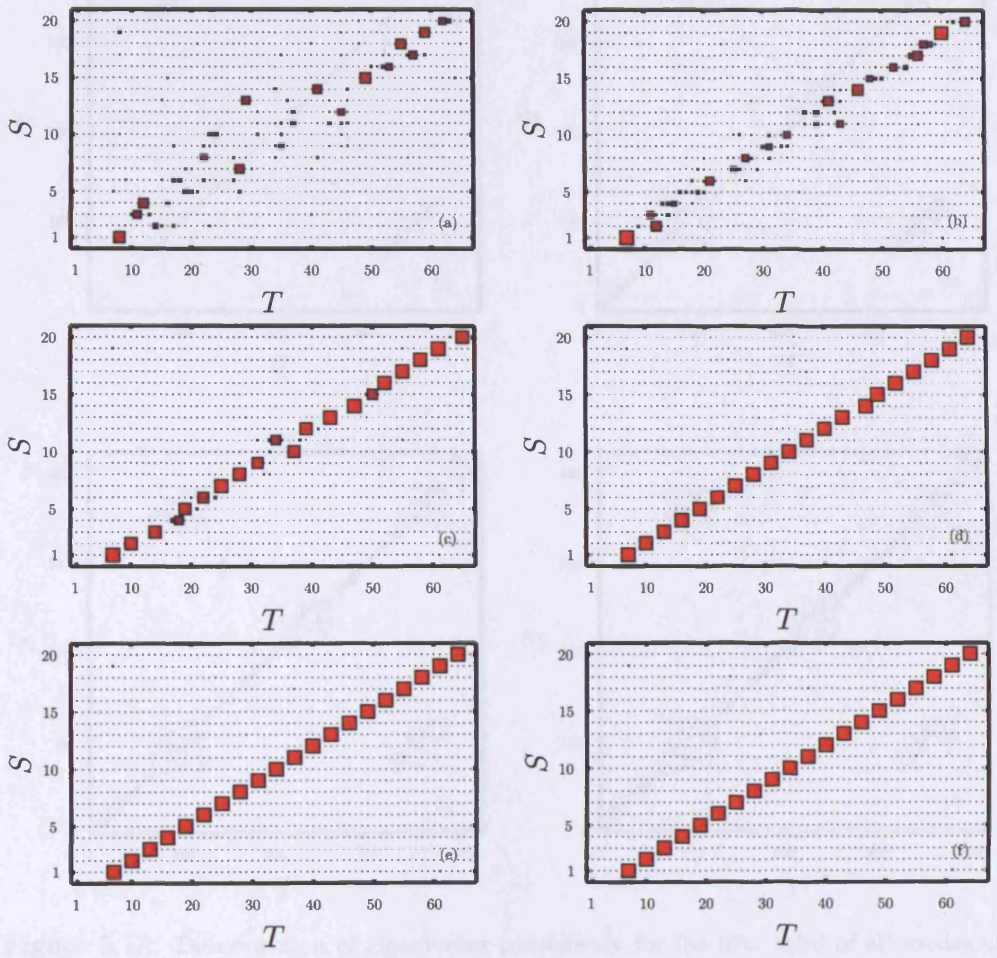

Figure 5.17: Values of *mac* between root modes and the initial sixty-five modes at each iterate for the octet force identification; (a)-(f), iterates $k = 0, 1, \ldots, 5$ respectively; 0 1 *mac* consistency scale.

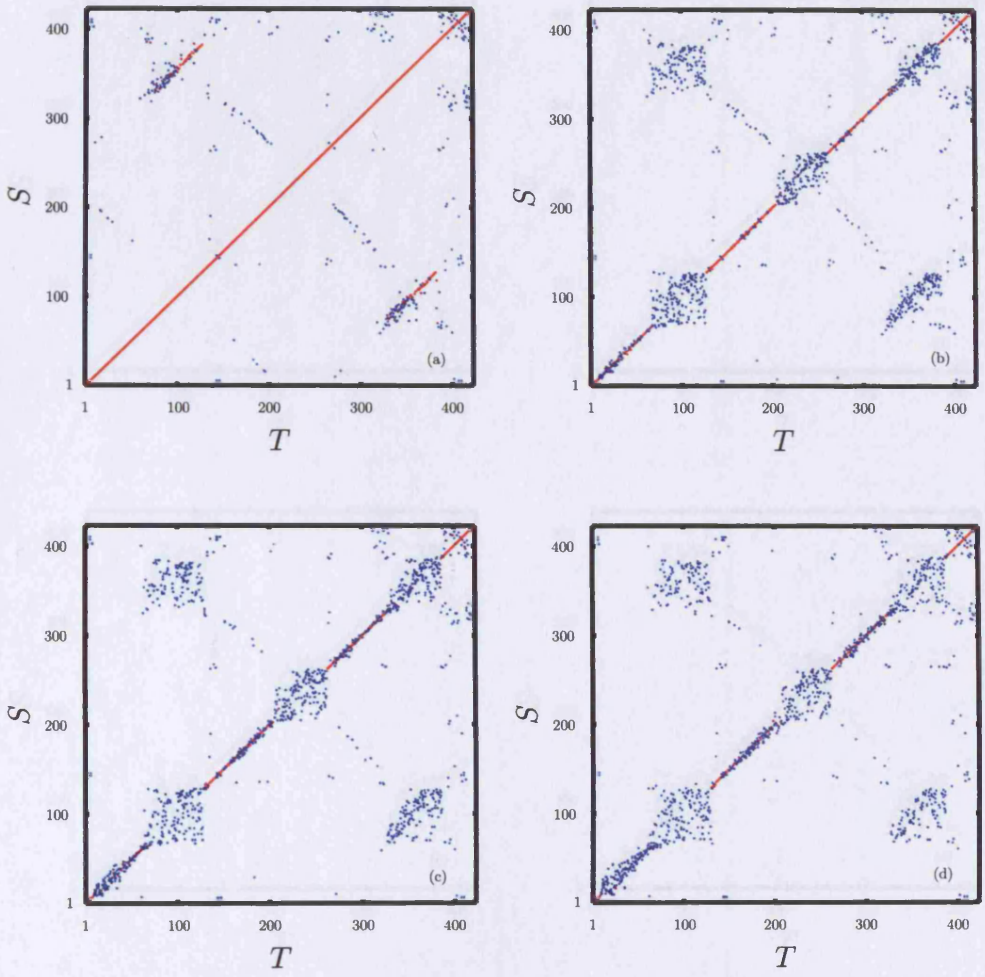

Figure 5.18: Deterioration of eigenvector consistency for the first third of all modes of the octet frame model with respect to loading in a single force distribution (S is the subset of eigenvectors at the unloaded state and T is the subset of eigenvectors at subsequent loaded states): (a) *automac* of eigenvectors at $p_1 = 0$; (b) *mac* between eigenvectors at $p_1 = 0$ and those at $p_1 = \frac{1}{3}$; (c) *mac* between eigenvectors at $p_1 = 0$ and those at $p_1 = \frac{2}{3}$; (d) *mac* between eigenvectors at $p_1 = 0$ and those at $p_1 = 1$; consistencies below 0.1 are omitted; 0 1 *mac* consistency scale.

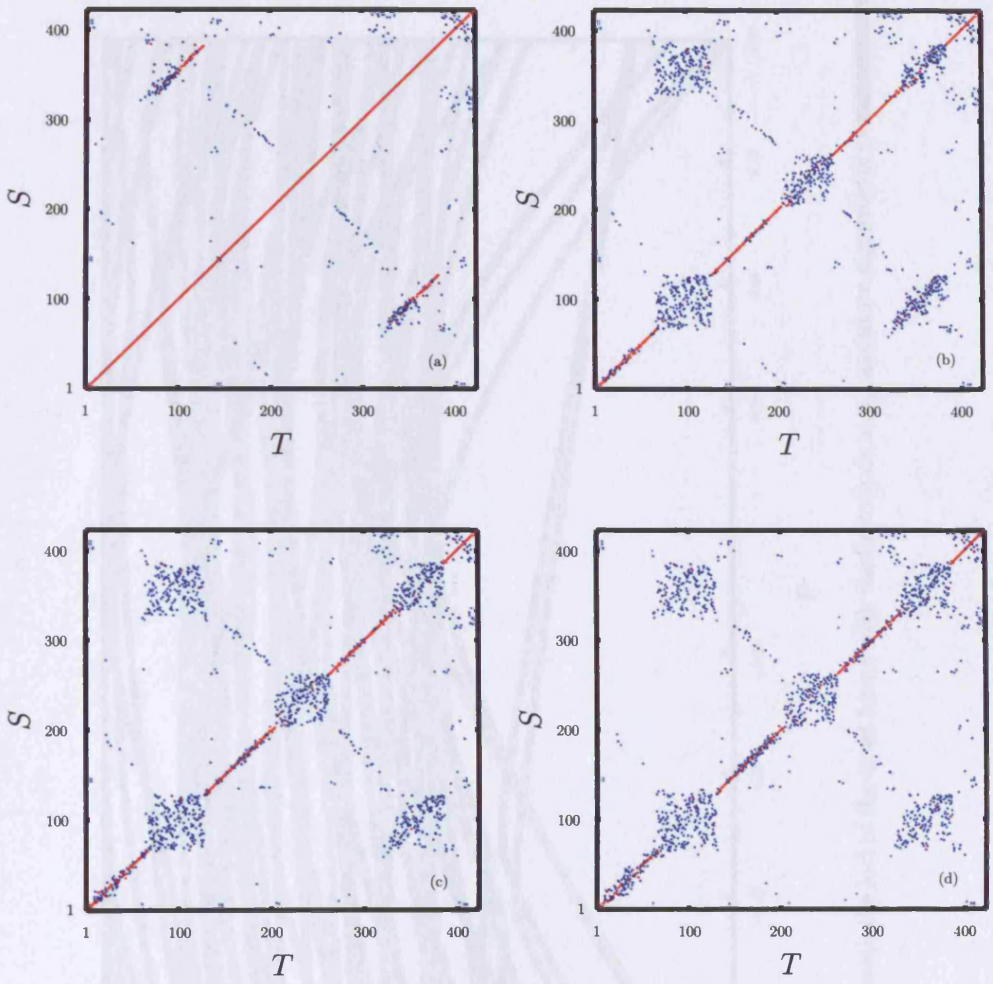

Figure 5.19: Deterioration of eigenvector consistency for the first third of all modes of the octet frame model with respect to simultaneous loading in three force distributions (S is the subset of eigenvectors at the unloaded state and T is the subset of eigenvectors at subsequent loaded states): (a) *automac* at $\mathbf{p} = [0\ 0\ 0]^T$; (b) *mac* between eigenvectors at $\mathbf{p} = [0\ 0\ 0]^T$ and those at $\mathbf{p} = [\frac{1}{9}\ \frac{1}{9}\ \frac{1}{9}]^T$; (c) *mac* between eigenvectors at $\mathbf{p} = [0\ 0\ 0]^T$ and those at $\mathbf{p} = [\frac{2}{9}\ \frac{2}{9}\ \frac{2}{9}]^T$; (d) *mac* between eigenvectors at $\mathbf{p} = [0\ 0\ 0]^T$ and those at $\mathbf{p} = [\frac{1}{3}\ \frac{1}{3}\ \frac{1}{3}]^T$; consistencies below 0.1 are omitted; 0 1 *mac* consistency scale.

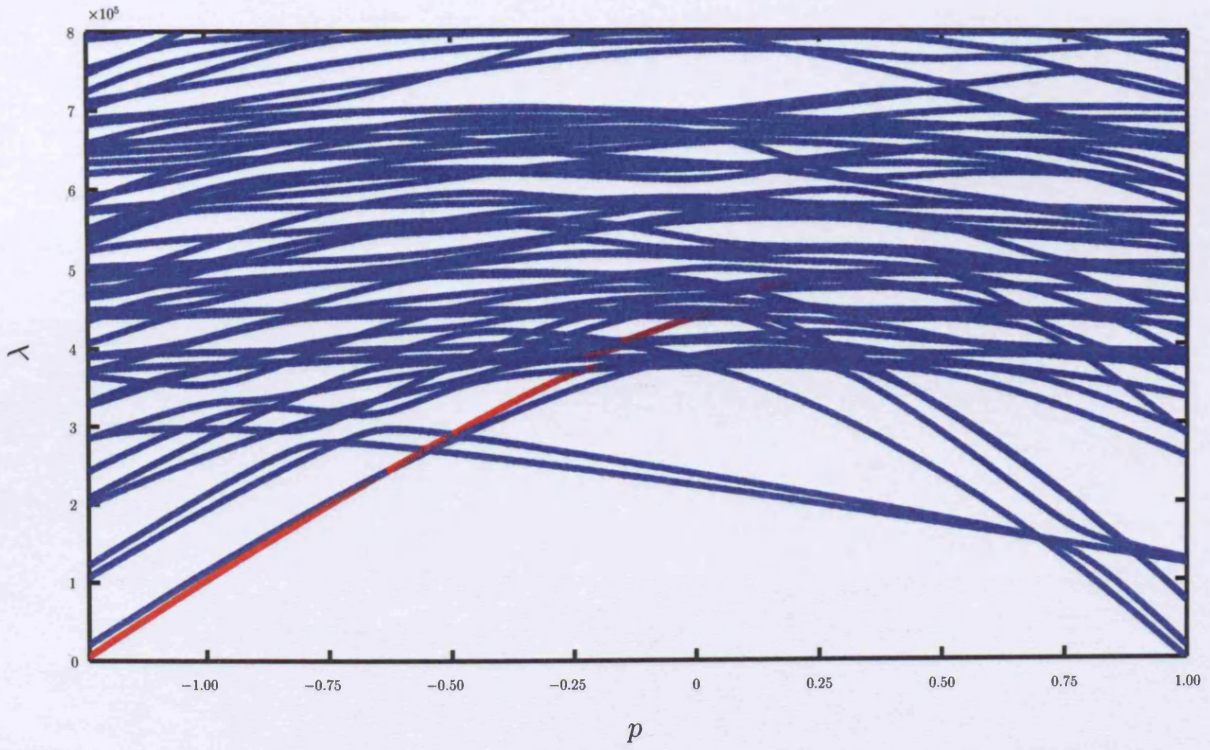

Figure 5.20: *mac* consistency through the loci of the octet frame with the first mode at $p_{\bar{E}}$ as datum eigenvector; 0 1 *mac* consistency scale.

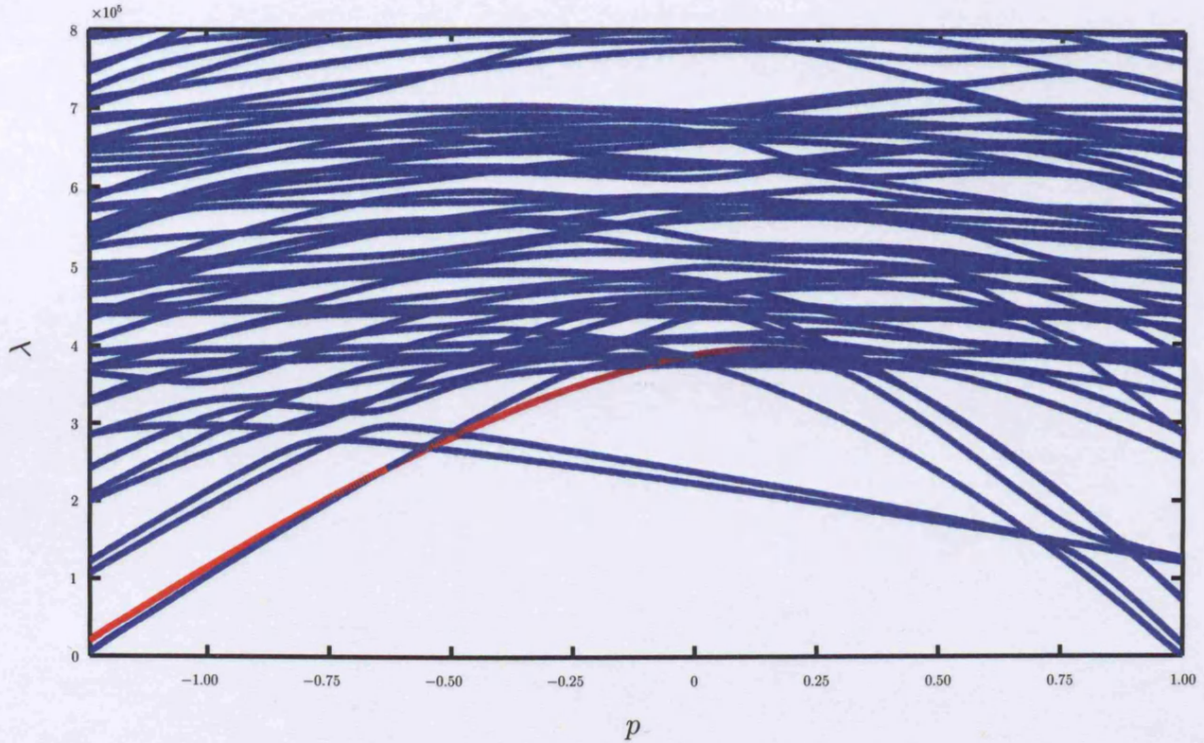

Figure 5.21: *mac* consistency through the loci of the octet frame with the second mode at p_E^- as datum eigenvector; 0 1 *mac* consistency scale.

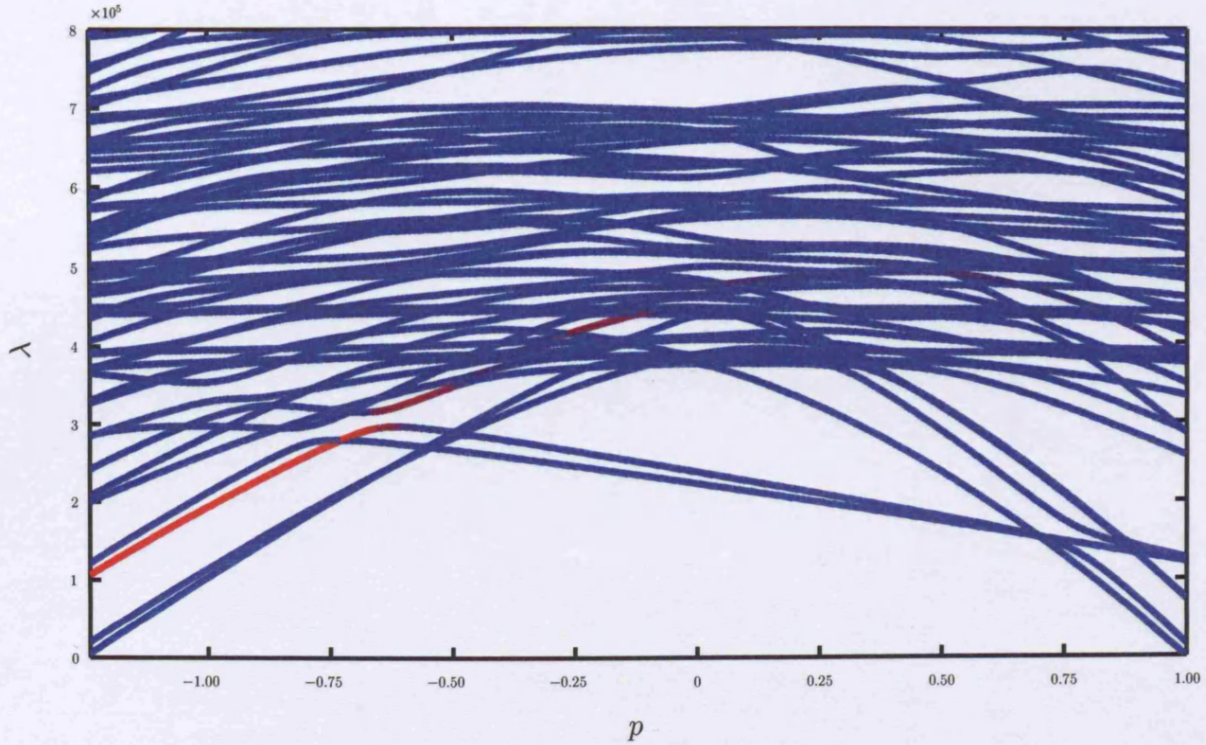

Figure 5.22: *mac* consistency through the loci of the octet frame with the third mode at p_E^- as datum eigenvector; 0 1 *mac* consistency scale.

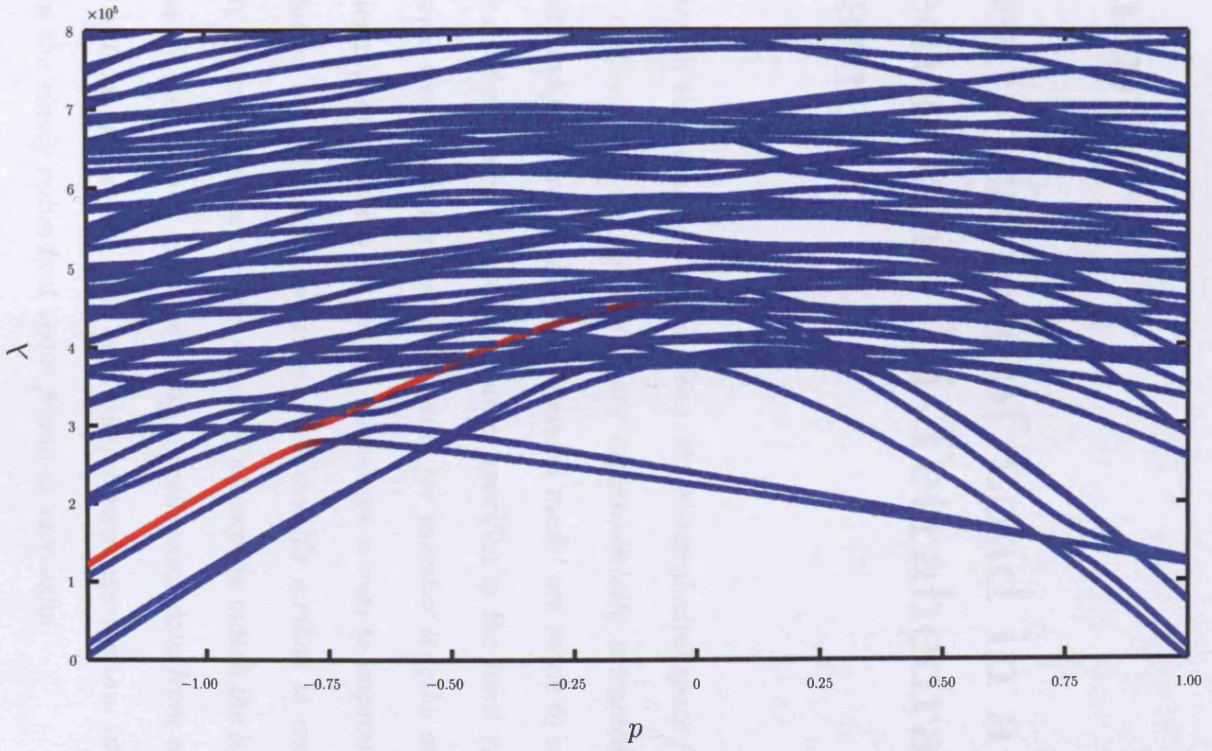

Figure 5.23: *mac* consistency through the loci of the octet frame with the fourth mode at $p_{\bar{E}}$ as datum eigenvector; 0 1 *mac* consistency scale.

Chapter 6

Identification of Load in a Once Redundant, Bi-Tetrahedral Frame

The first of the numerical simulations, the bi-tetrahedral space frame, is physically realised and its dynamic data experimentally extracted once loaded. Several modifications to the finite element model are made to account for the less-than-ideal properties of the frame, specifically the joint characteristics. 'Effective length parameters' accounting for member lengths and offsets (the rigid lengths of members within the joints) are shown to improve the accuracy of solution and stabilise convergence. Newton's method is employed with a variety of parameter combinations in an attempt to match the loads physically measured. Iteration is repeated using experimental data from a total of three levels of load, and shows that, with careful parameterisation, identification of load in the singly redundant space frame is successful.

6.1 Frame Realisation

The validity of the proposed method of force identification was tested on a real, singly redundant space frame. The nominated structure is a physical realisation of the bi-tetrahedral frame of the previous chapter, Fig. 5.2; the actual frame can be seen in Fig. B.2. The three members that are mutual to the two tetrahedra of the frame are referred to as equatorial members, the internal member is referred to as the polar member and the remaining members are referred to as hemispherical members, all for obvious reasons. Significant alterations to the finite element model were made to account for the less-than-ideal physical properties. A description of the physical frame is first given.

The bi-tetrahedral frame comprises cylindrical, steel members and aluminium joints of such a nature as to allow both assembly of the frame and its loading. The members have at one end a regular, right-handed thread and at the opposing end a left-handed thread. The joints are accordingly threaded, so that rotating a member about its longitudinal axis causes it to pull the joints at its ends inwards or push them outwards, depending on the direction of turn. As discussed in Sec. 1.2, this freedom of movement, that is to say, geometric alteration, is realistically only applicable to statically determinate space frames. The presence of a redundant member acts to restrain the freedom of movement necessary to assemble a frame (although movement is not impossible). Essentially, by threading the members into the joints during assembly the effect is to reduce all member lengths by some factor. The

frame is therefore assembled without the internal spar in order to reduce it to a determinate structure. Once all measured external member lengths are equal, the remaining, redundant member is added as follows. Both ends of the redundant member are fitted with right-hand threaded jackets of a larger diameter than the member itself. With corresponding, larger threads in the joints, the final member is fed in from one end of the frame to the other. It may be necessary to turn the regular members of the frame by small amounts so that the geometry is such that the threads align between the redundant member and the joints.

The member-joint intersection inevitably involves some slackness. Experience shows that this leads to slight non-linearity in both the excitation and response of the frame. For example, response to a sinusoidal driving force has been seen to contain harmonics of the resonance frequency. In order to overcome this, the members are provided with nuts and washers that can be tightened to alleviate slackness (the actual joint system used can be seen in Fig. B.1). This itself modifies the magnitude of load within the frame, but all loading is accounted for by the use of strain gauges, as is now described.

6.2 Axial Strain Measurement

The aim of applying strain gauges to the structure is to measure the axial load that develops in the space frame and thus provide a means of verifying the results of frequency-based load identification. Due to inevitable, initial, geometric imperfections in the beams, secondary bending develops in com-

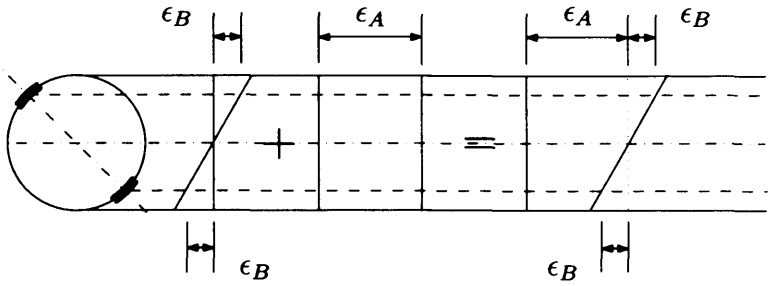

Figure 6.1: Axial strain measurement with elimination of secondary bending strain for a beam of circular cross-section.

pressed members. This is most significant in the internal spar owing to it having the largest magnitude of force and greatest effective length. A sort of negative, secondary bending also develops in tensed members for the same reason of initial imperfection. It is the assumption that all bending, the geometrical displacement associated with it and the ensuing non-linearity of the lengthwise axial force distribution are small enough not to affect significantly and further the dynamic characteristics. That is to say, the disturbances to the eigenvalues and eigenvectors are assumed to be accounted for *predominantly* by the axial force distribution. Further, it can sensibly be assumed that the magnitudes of force in a given force distribution remain in proportion to one another since the members are relatively fixed at the joints and therefore the relative member angles, and consequently the relative force flow at the joints, remain unchanged. The possibility that parameters accounting for boundary conditions alleviate the need to capture the secondary, geometric displacement effects, should they actually become significant, is discussed ahead in Sec. 6.3.

The scheme for measuring axial strain whilst eliminating any bending

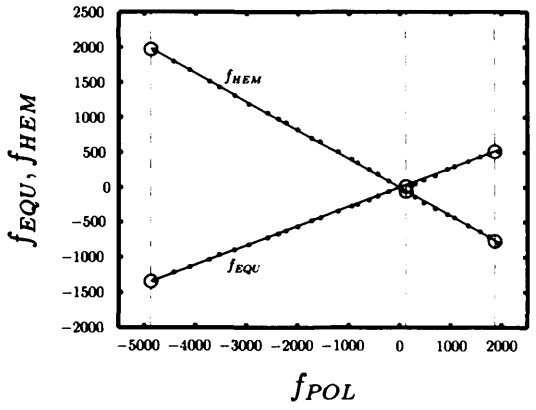

Figure 6.2: Measured equatorial and hemispherical bi-tetrahedral frame member forces in relation to the polar member force; ———— least squares regression line; O equilibrium states at which the three modal tests were performed.

strain is depicted in Fig. 6.1. Two strain gauges are adhered, opposite one another, to the member in which strain is to be measured. As can be appreciated from the figure, regardless of the axis about which secondary bending occurs relative to the axis of the gauges, the axial component of strain is always the mean of the two measured strains. For confidence, two pairs of gauges are applied at two different orientations and lengthwise locations; the gauge applications are at the internal polar member, at a hemispherical member and at an equatorial member. The equilibrium of forces upon loading is illustrated in Fig. 6.2, which shows loading at a number of discrete data points within the buckling and elastic limits of the structure. Least squares regression lines are fitted to the graphs with R-squared values of 0.999. These allow comparison of the theoretical and physical distributions of static force, as summarised in Tab. 6.1. The similarity across the theoretical and experimental values suggests that the physical frame geometry was close to ideal when the forces were measured.

	$f_{EQU} : f_{POL}$	$f_{HEM} : f_{POL}$
Theoretical	0.272	-0.408
Experimental	0.276	-0.407

Table 6.1: Theoretical and experimentally determined member force relations for the bi-tetrahedral frame.

Once assembled, it is possible to prestress the frame without significant change in geometry, by virtue of its redundant nature, by rotating the external members. A zero load state is always apparent by the inability of the unloaded joints to transfer vibratory energy from beam to beam. Thus, it is possible to identify an unloaded datum for the strain gauges, from which to initiate load, by striking the frame and ensuring that no lengthy resonance results. This highlights the problems related to direct strain measurement with gauges in that a load datum needs always to be known.

6.3 Parameterisation of the Finite Element Model

As mentioned, significant alterations to the finite element model were made to account for the less-than-ideal physical properties. Firstly, following indications from a discretisation analysis, each member was divided into nine elements. The frame was assumed to be pin-jointed as far as the static equilibrium was concerned. This holds as long as there is concurrence of all member centre lines at the joints. Certainly, it is acceptable to assume this is true for the physical frame as it was specifically designed to have this

concurrence property.

To quote Greening (1999),

> Recent methods which update geometric parameters appear to offer a more versatile method of changing finite element models, particularly in specific regions such as joints. This versatility comes at the expense of considerable engineering judgement being required to assess the number, location and type of updating parameters to use on a case-by-case basis.

Not only the versatility, but the physical significance of geometric parameters, plays a crucial role in parameterising the bi-tetrahedral frame finite element model. As far as the engineering judgement is concerned, a variety of combinations of parameters have to be applied in a number of updating schemes to assess their applicability. The knowledge gained thus is taken to the force identification of a more complicated frame in Ch. 7.

In a dynamic context, the joints of the frame are assumed to be such that the members are fully fixed with respect to one another so as to provide continuity of the flexural modes. Such a property can never be achieved in reality due to the slackness between a member and a joint, even if the interface is tightened with a nut and washer. Further to this, a finite length of member within the joint is incapable of the flexure experienced by the length of member outside the joint. The effective length of a frame member is not then solely dependent upon the overall length and the relative fixity at the joints, but is also a function of the joint size, member-joint interface

and the tightness of the fixing nuts. Since these effects are not directly measurable, it has been deemed necessary to parameterise the finite element model with a set of parameters accounting for the indeterminate effective lengths. With the eigenvalue loci and Euler buckling loads being intrinsically linked, it would seem sensible to parameterise the finite element model with both load and effective length parameters.

Although Greening (1999) finds success in parameterising planar frame models with force and deformation, the latter is not included here. One of the implications in the aforementioned study is that structural deformation in an example plate only significantly affects the fundamental frequency (generally, deformation is seen to affect the lower frequencies more) in the presence of a constraining boundary condition and not when the plate is free-free. It is felt that the inclusion of parameters describing effective length, and therefore, indirectly, boundary conditions, may suffice in accounting for the secondary effects to the frequencies, without having to consider deformation. In other words, casting the boundary conditions as variables rather than the member deformations, may capture the frequency changes brought about by the mutual presence of deformation and constraining boundaries. Since one of the achievements of the present study has been to minimise the number of force parameters, it would be regrettable to have to include a multitude of parameters describing the deformation of each member. Since, by topological arguments, a space frame will have significantly less joints than members, updating boundary conditions, if successful, may prove to be more efficient

than updating deformation. A description of how the finite element model is parameterised with effective length parameters follows.

It is possible to modify the Euler-Bernoulli beam finite elements to account for a finite length of the element statically displacing or, with relevance to the present context, vibrating, as a rigid body. The assumption is that the length of beam embedded in the joint, the offset parameter, cannot flex. Presently these modified beam elements — q.v. Appendix A — are used as those adjacent to joints, in conjunction with the overall member lengths, to account for the effective member lengths. The validity and physical relevance of this choice of parameters are later discussed. It is necessary to group certain beam end elements to avoid setting up an over-parameterised problem. The effect of this is also qualified ahead.

The uncertainty associated with joint modelling has attracted much attention in recent times, but still presents difficulty in mathematically describing the member-joint interface. Mottershead et al. (1996) investigate the use of physically significant, geometric properties to bring an initial finite element model to better agreement with a set of experimental data. The structure in question therein is a cantilever plate clamped between two bolted steel blocks. Modelling of the boundary conditions is attempted by parameterising the problem with the lengths of the finite elements adjacent to the boundary. The derivatives of the first six eigenvalues with respect to this length parameter, the plate thickness and the rotational stiffness of a pinned boundary serve to show that the dynamic system is as sensitive to length as

it is to thickness and several magnitudes more sensitive to length than the rotational parameter (with parameter values normalised to an initial value of unity). In this sense, boundary element length seems a good candidate parameter to improve eigenvalue consistency between model and experiment. Indeed, in the aforementioned study, for four different bolt torques (tightnesses), the theoretical and experimental eigenvalues are brought into very close agreement. As can be appreciated, the higher the applied bolt torque, and hence the boundary stiffness, the higher the eigenvalues become upon convergence and the associated boundary element length becomes smaller to reflect the increased stiffness. The fact that a single length parameter can be used to update a joint model with such success is a motivation for updating the element lengths of the bi-tetrahedral frame.

Mottershead et al. also achieve the successful update of a welded joint between two beams utilising two offset parameters affecting the structural stiffness matrices, as the assumption is that very stiff welds are rigid bodies in a dynamic sense.

In subsequent papers, Mottershead and James (1998) and Mottershead et al. (2000) update offset parameters, which modify the stiffness and mass matrices, for an aluminium space frame in comparison to, and in conjunction with, other parameters. The frame studied by the authors is in concept similar to the bi-tetrahedral frame in that it is comprised of aluminium beams, in this case of hollow section, which thread into joints to form a structure resembling a three-story building. All threads are regular so that the members are

in this case tightened by means of a compression fitting between a member and joint. The base nodes are clamped to a heavy table. The finite element model discretises each member into four elements and the base boundary is modelled by four further beam elements. In the second of the two papers, five iteration schemes are performed, including two in which offset parameters are updated with beam wall thickness. It is found that the use of these updated parameters, including the offsets, in models of subsequent frame reconfigurations, gives the best agreement between test and theory. The offset parameters, when updated with beam wall thickness, are also seen to compete very well with other sets of parameters such as substructure multipliers and generic element matrices. The authors consider the offset parameters as providing an improvement to the modelling in a physical sense, as opposed to some converged parameters not being justifiable physically.

Offset parameters modifying the elemental stiffness and mass matrices are therefore included in the present study along with elemental length. A number of combinations of offsets and length have been considered, as facilitating parameters to load, in order to evaluate their validities.

Point masses are added to the appropriate degrees of freedom of the mass matrix to account for presence of the joints. These are based on physical measurements of the actual joint masses, including the nuts and washers, and are 0.0995 kg for the polar joints and 0.0795 kg for the equatorial joints. Other constant properties of the frame were taken as follows: $E = 2.1 \times 10^{11}$ Nm^{-2}, based on supply data; $\rho = 7591.9$ kgm^{-3} and $d = 0.00785$ m,

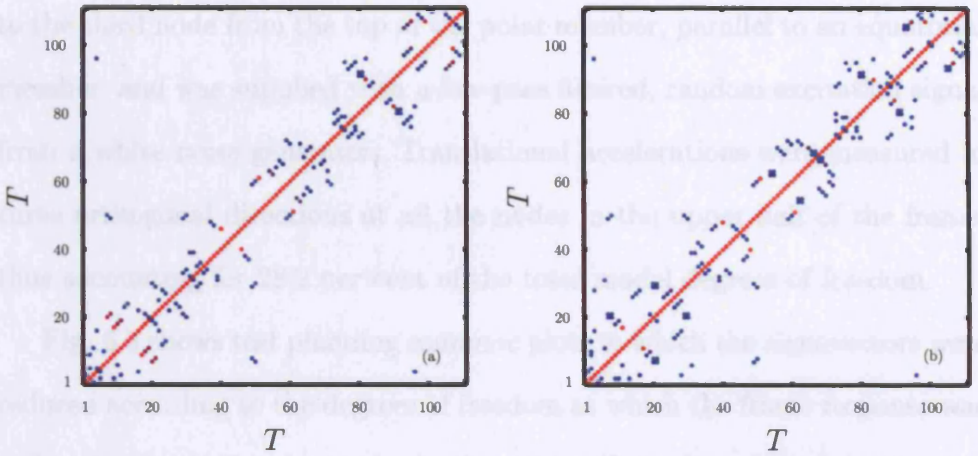

Figure 6.3: Bi-tetrahedral frame test planning *automac* plots, with eigenvectors defined at 28.2 per cent of the total number of model degrees of freedom: (a) $P = 0$, $L = 0.41$, $d = 0.00785$, no offset parameters; (b) $P = 1000$, $L = 0.41$, $d = 0.00785$, no offset parameters; 0 1 *mac* consistency scale.

based on indirect and direct measurements, respectively.

6.4 Modal Testing of the Frame

The dynamic characteristics were extracted at three magnitudes of load as measured by the strain gauges and as depicted in Fig. 6.2: near zero ($P^{®} = +127$ N), high tension in the polar member ($P^{®} = -4866$ N) and high compression in the polar member ($P^{®} = +1870$ N). At these loads, modal tests were run using a single, suspended shaker fitted with a force transducer of sensitivity 11.24 mVN^{-1} and an accelerometer of sensitivity 1.02 $\text{mV}(\text{ms}^{-2})^{-1}$ to measure response at a number of locations. In order to measure acceleration in the nominated, global coordinate system, where necessary the accelerometer was mounted on lightweight, aluminium, angled studs with wax before being adhered to the structure. The shaker was applied

to the third node from the top of the polar member, parallel to an equatorial member, and was supplied with a low-pass filtered, random excitation signal from a white noise generator. Translational accelerations were measured in three orthogonal directions at all the nodes in the upper half of the frame, thus accounting for 28.2 per cent of the total model degrees of freedom.

Fig. 6.3 shows test planning *automac* plots in which the eigenvectors were reduced according to the degrees of freedom at which the frame response was to be measured. For the modes in the subset T shown, which were the first $t = 110$ modes of the finite element model considered at each iteration for mode tracing purposes, a little corruption exists but overall the nominated measurement locations seem to suffice in unambiguously describing the structural response.

With the finite element model suggesting an abundance of modes below 2000 Hz, a sampling frequency of 5208 Hz and a discrete Fourier transform size of 1024 were chosen; the random excitation was filtered with a low pass cut-off frequency of 1730 Hz (approximately two thirds of the Nyquist frequency) before it reached the shaker. The excitation force and response acceleration signals were then amplified and sent back to a computer via a data acquisition unit. A schematic is given in Fig. 6.4.

Transfer function estimates were performed within a Visual Basic code, which itself calls the function spectrum.m in the Matlab signal processing toolbox. The results from this system have previously been validated against transfer function estimates from a spectrum analyser (Data Transla-

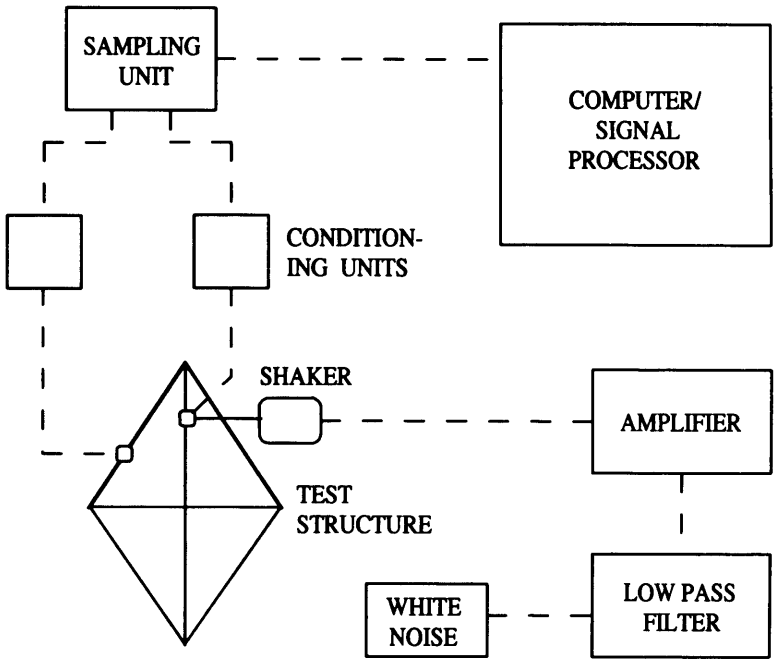

Figure 6.4: Experimental test configuration.

tion PL2000). Each frequency response function was averaged over a number of estimates.

6.5 Newton's Method Applied to Force Identification

Four iteration schemes were run for each of the three load magnitudes with a number of different parameters: (i) P; (ii) P and L; the remaining two schemes involved offset parameters. The offsets were put into the following sets: equatorial member in equatorial joint (η_{ee}), polar member in polar joint (η_{pp}), hemispherical member in equatorial joint (η_{eh}) and hemispherical member in polar joint (η_{ph}). The two other iterations involved four and six parameters respectively: (iii) P, L, $\eta_{eh} = \eta_{ee}$ and $\eta_{ph} = \eta_{pp}$; (iv) P, L,

η_{ee}, η_{pp}, η_{eh} and η_{ph}. The results for iteration schemes (iii) and (iv) are first shown in Fig. 6.5-6.10, which demonstrate the minimisation of the theoretical and experimental frequency discrepancy and the iterative progressions of all of the updating parameters. In all instances, iteration commenced from a completely unloaded state, with all offset parameters used at zero and the regular member length at 0.41 m. For iteration, a total of nine measured, root modes were used for iteration.

While parameters further to load were included, they were of such a nature not to destroy the symmetry of the structure. The permanent degeneracy of the eigenvalues of the bi-tetrahedral frame was therefore conserved and mode tracing had to account for the disorientation of the finite element model eigenvectors, as outlined in Sec. 4.3.

While for iteration (iii), targeting $P^{®} = +127$ N (Fig. 6.5), the eigenvalue difference $\boldsymbol{\lambda}^{k} - \boldsymbol{\lambda}^{®}$ was well minimised, with length and offset parameters converging to sensible values, the converged load was far from what was sought. Iteration (iii) targeting $P^{®} = +1870$ N (Fig. 6.6) failed to converge and instead found a stable oscillation about the theoretical buckling load. This highlights an important point: some means must be found for preventing iterates leaving the pre-buckled region of the iteration space, where the model can become extremely erratic and unstable. One possible solution may be to monitor the fundamental eigenvalue, which, if it should become zero, would indicate that a shortening of the Newton progression is required until iteration returns to the pre-buckled region. Of course, having an overdeter-

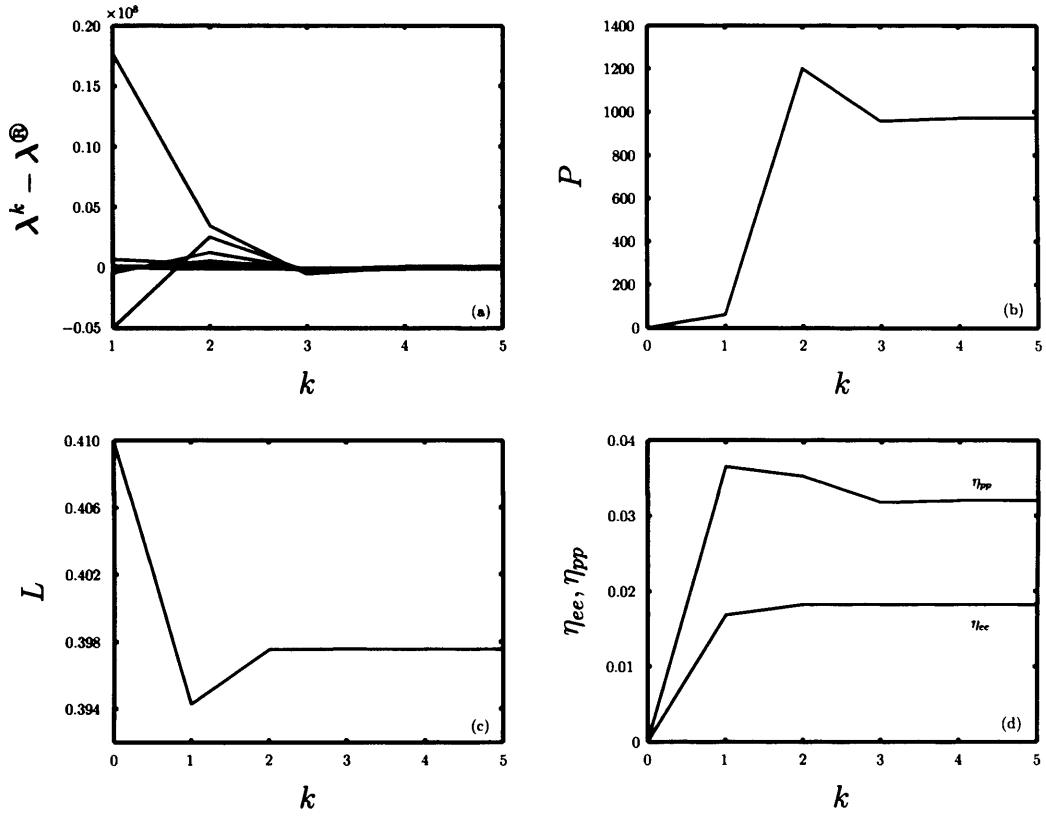

Figure 6.5: Iteration towards $P^{®} = +127$ N involving the four parameters P, L, $\eta_{eh} = \eta_{ee}$ and $\eta_{ph} = \eta_{pp}$: (a) minimisation of the eigenvalue difference; (b) iterative progression of the load parameter; (c) iterative progression of the length parameter; (d) iterative progression of the offset parameters.

mined system of equations and a well-posed problem are helpful restraints against such a circumstance.

Iteration (iii) targeting $P^{®} = -4866$ N (Fig. 6.7) had both the length and offset parameters converging upon realistic values and load converging to a value only 1.04 times that measured in the experiment, but failed to minimise satisfactorily the eigenvalue difference, thus placing doubt upon the updated parameters.

When the offset parameters were described in more detail in iteration

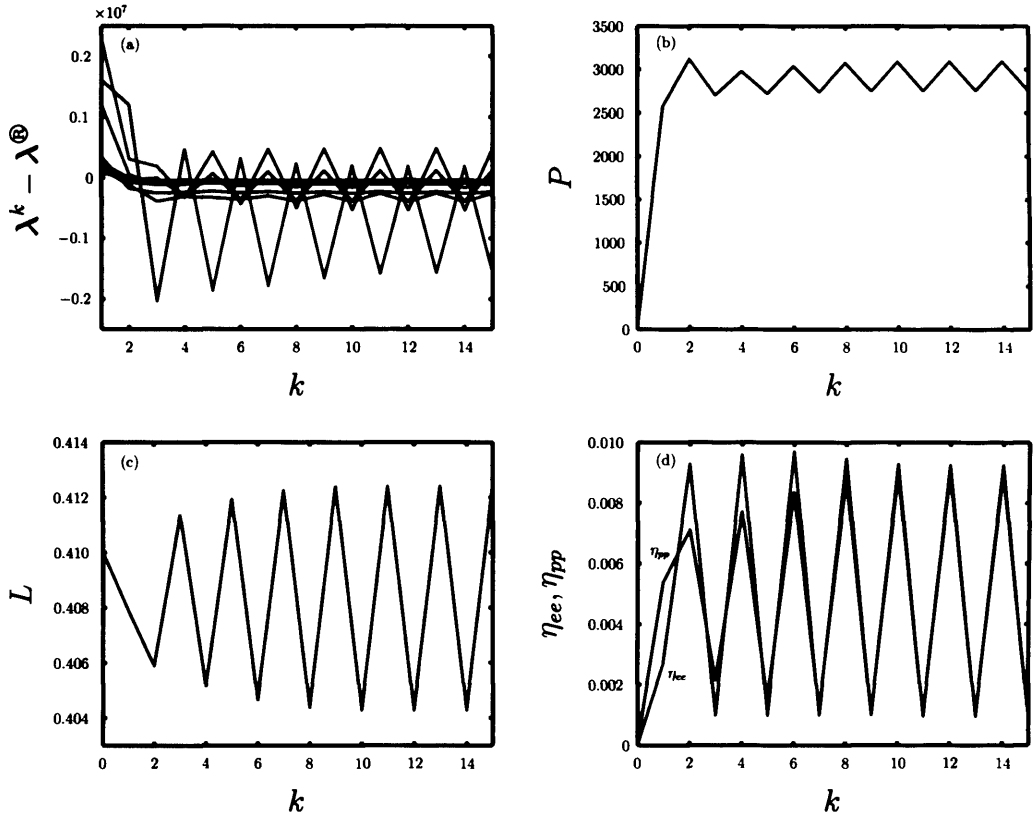

Figure 6.6: Iteration towards $P^{®} = +1870$ N involving the four parameters P, L, $\eta_{eh} = \eta_{ee}$ and $\eta_{ph} = \eta_{pp}$: (a) minimisation of the eigenvalue difference; (b) iterative progression of the load parameter; (c) iterative progression of the length parameter; (d) iterative progression of the offset parameters.

scheme (iv), a general improvement in iteration was seen in that the eigenvalue difference was consistently well minimised for all three load convergences. Further, the converged loads were in each case consistent in sign with the values measured by the strain gauges. Iteration (iv) targeting $P^{®} = +127$ N (Fig. 6.8) converged to $P^{*} = 177.9$ N, indicating a successful identification of force. For the higher load magnitudes, viz., $P^{®} = +1870$ N (Fig. 6.9) and $P^{®} = -4866$ N (Fig. 6.10), iteration (iv) underestimated the loading in the frame by similar amounts: the converged to experimentally-

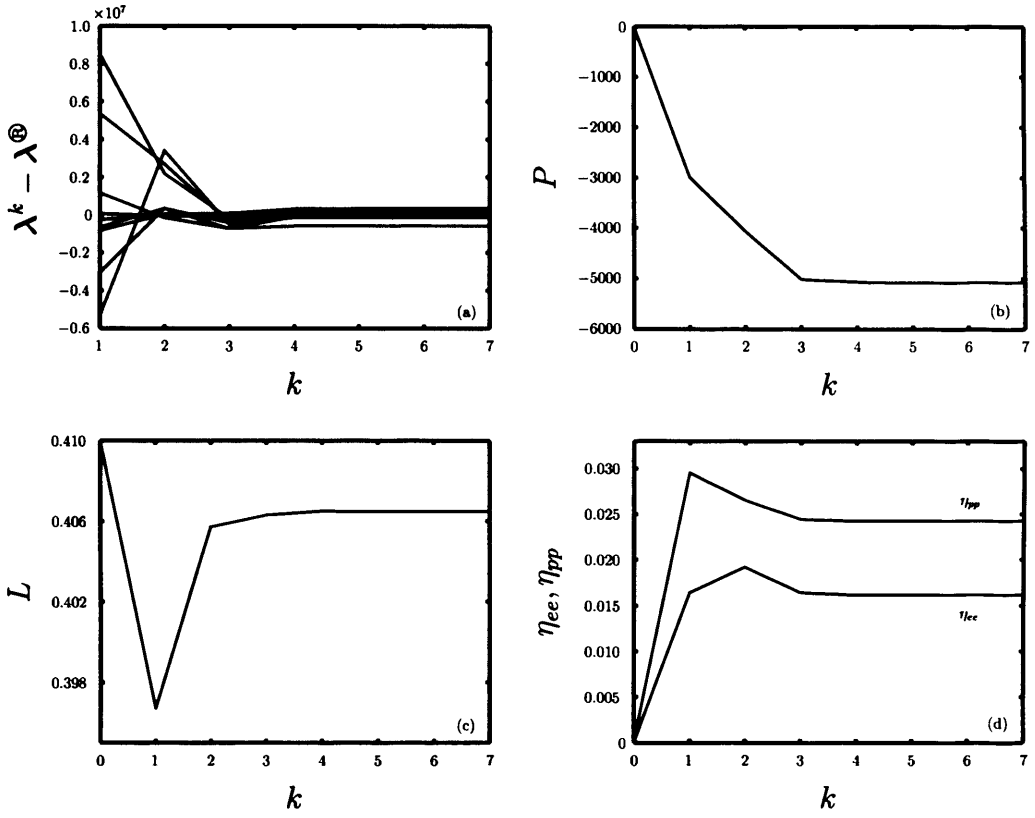

Figure 6.7: Iteration towards $P^{®} = -4866$ N involving the four parameters P, L, $\eta_{eh} = \eta_{ee}$ and $\eta_{ph} = \eta_{pp}$: (a) minimisation of the eigenvalue difference; (b) iterative progression of the load parameter; (c) iterative progression of the length parameter; (d) iterative progression of the offset parameters.

determined ratios are 0.78 and 0.72, respectively. This shortfall is discussed ahead. All results are summarised in Tab. 6.2-6.4.

Although force identification was successful when using iteration scheme (iv), with the length parameter converging to approximately the same value each time, the converged values for the offset parameters were not consistent across the iterations to the three magnitudes of load. In some instances, these even became negative. Of course, this may relate to the different load signs and magnitudes affecting the conditions at the joints differently; the nuts may

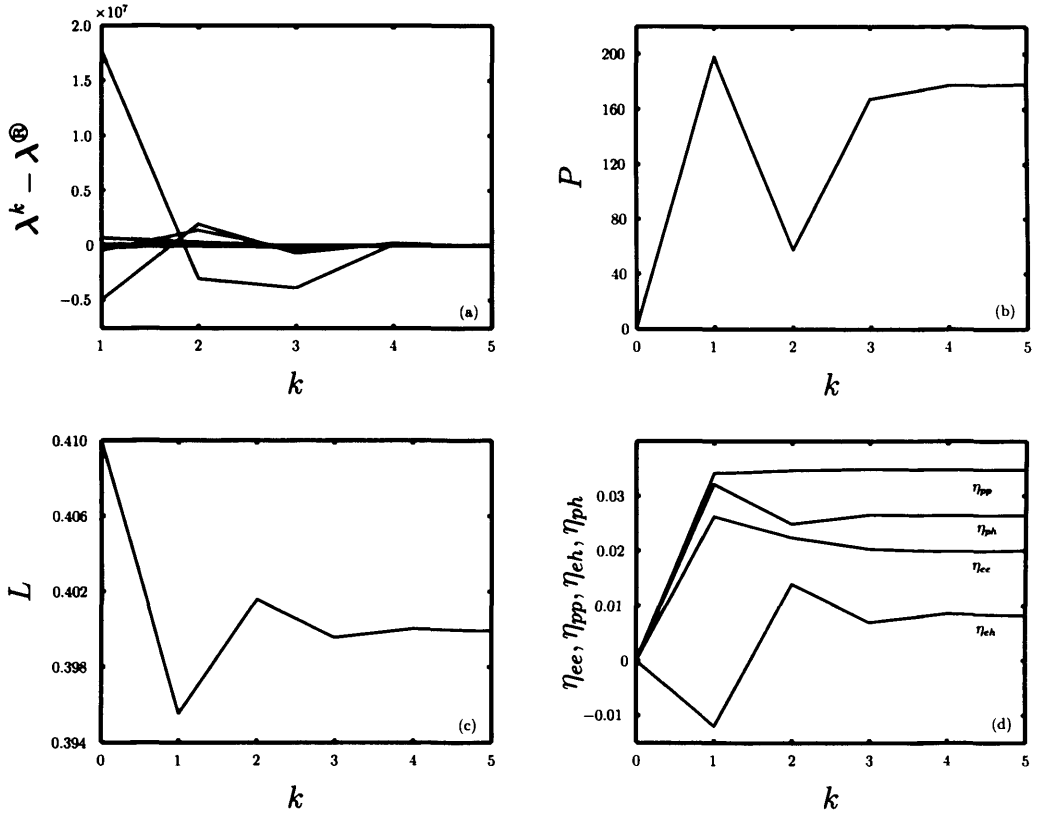

Figure 6.8: Iteration towards $P^{®} = +127$ N involving the six parameters P, L, η_{ee}, η_{pp}, η_{eh} and η_{ph}: (a) minimisation of the eigenvalue difference; (b) iterative progression of the load parameter; (c) iterative progression of the length parameter; (d) iterative progression of the offset parameters.

also have helped to alter joint fixity in each instance. It would have been useful if the near zero magnitude of load identified offset parameter values to be used as constant, model characteristics when attempting to identify non-zero magnitudes of load. With this pre-load identification, future iterations could have been performed in a reduced number of dimensions. However, this was certainly not anticipated from the outset and the great inconsistency of the offset parameters across the different load levels has indicated that this is not realistic. An attempt to use the identified offset parameters at the

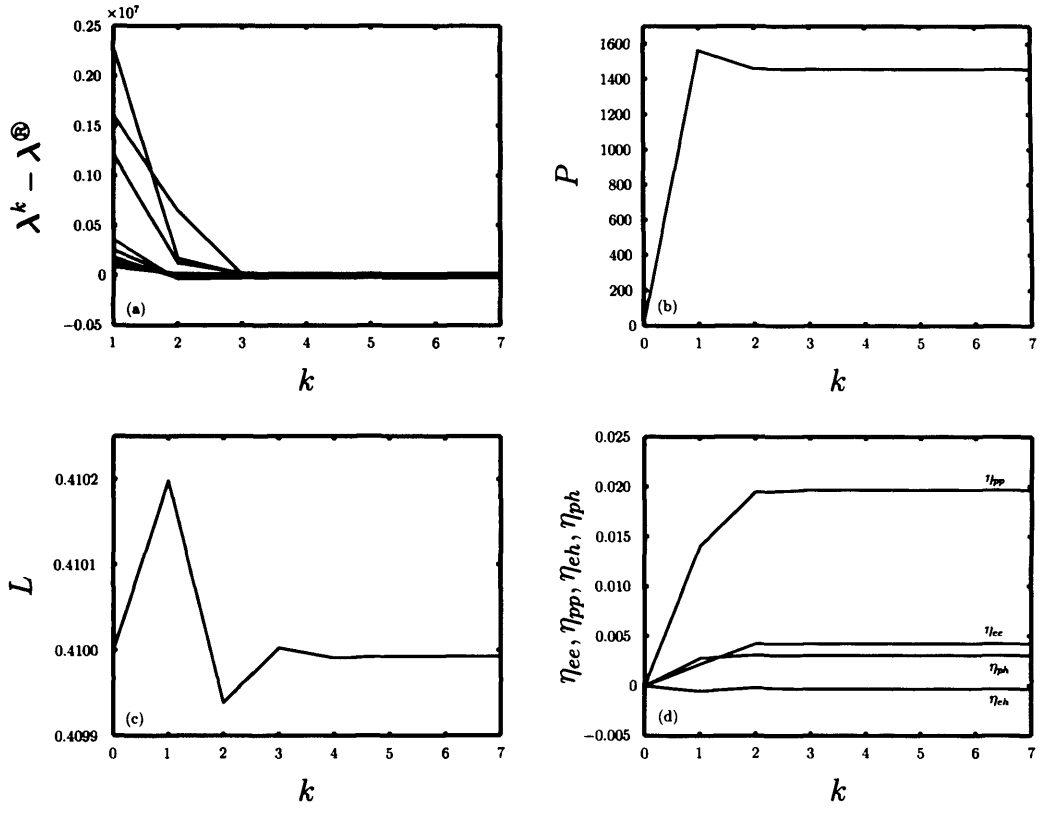

Figure 6.9: Iteration towards $P^{®} = +1870$ N involving the six parameters P, L, η_{ee}, η_{pp}, η_{eh} and η_{ph}: (a) minimisation of the eigenvalue difference; (b) iterative progression of the load parameter; (c) iterative progression of the length parameter; (d) iterative progression of the offset parameters.

near zero load *was* made, but identification of load for the remaining two load levels was unsuccessful. Although a way in which to quantify the joint uncertainty is not presently conceivable, what is known is the fact that load, along with the length parameter and a fairly detailed description of the offset parameters, has encouragingly led to well minimised differences between the theoretical and experimental eigenvalues.

It may very well be the case that the values of the parameters describing effective length, viz., length and offsets, are necessarily different at each load

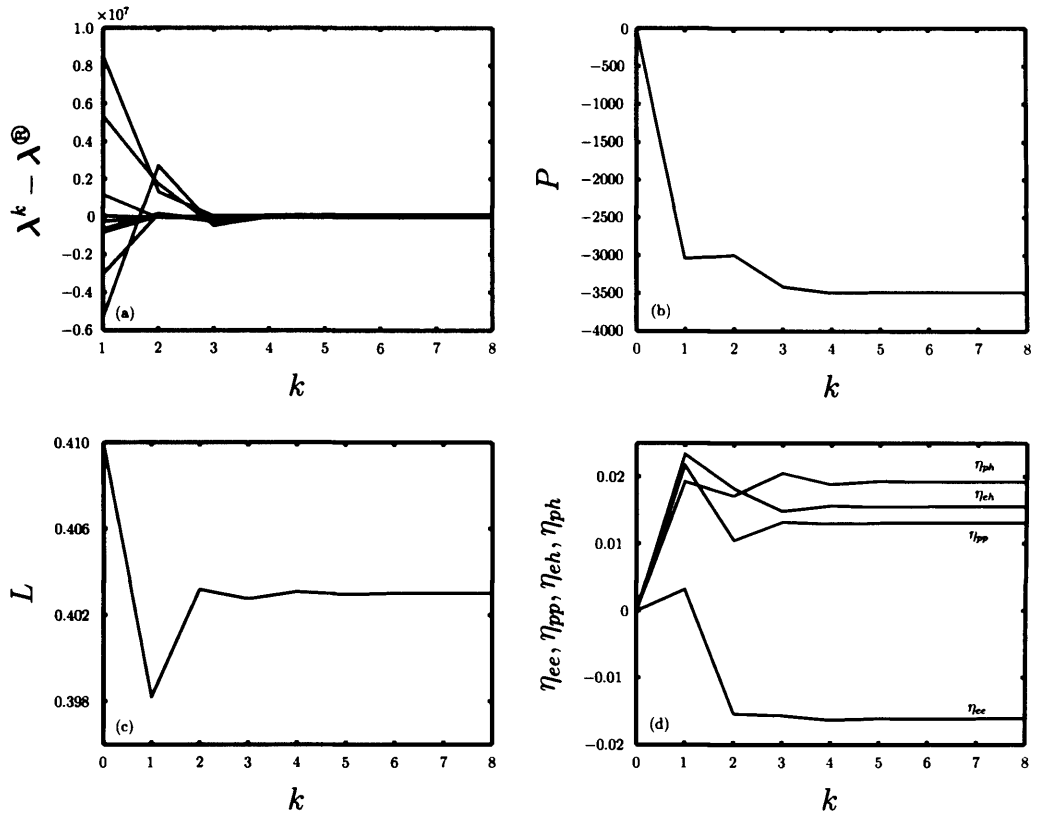

Figure 6.10: Iteration towards $P^{®} = -4866$ N involving the six parameters P, L, η_{ee}, η_{pp}, η_{eh} and η_{ph}: (a) minimisation of the eigenvalue difference; (b) iterative progression of the load parameter; (c) iterative progression of the length parameter; (d) iterative progression of the offset parameters.

level because they are providing alternative parameters to deformation — with which Greening (1999) had success in minimising the eigenvalue difference, and which would be different depending on the direction of load — in accounting for secondary effects to the frequencies. Certainly, the finite element model has indicated that boundary conditions are load-dependent variables and should therefore be included with load in model parameterisation.

Fig. 6.11, summarises the iteration schemes (iii) and (iv) and further

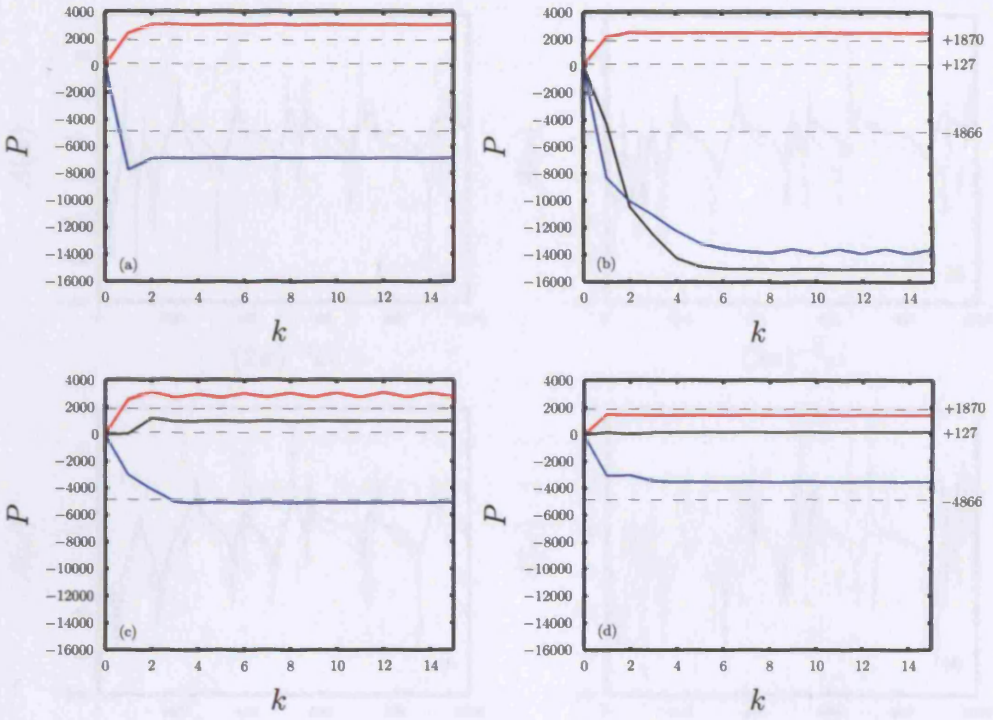

Figure 6.11: Load parameter convergences for the three levels of load using various combinations of parameters: (a) P; (b) P and L; (c) P, L, $\eta_{eh} = \eta_{ee}$ and $\eta_{ph} = \eta_{pp}$; (d) P, L, η_{ee}, η_{pp}, η_{eh} and η_{ph}; ——— iteration targeting $P^{®} = +127$ N; ——— iteration targeting $P^{®} = +1870$ N ; ———. iteration targeting $P^{®} = -4866$ N.

shows schemes (i) and (ii), in which P and P with L were used respectively to improve the finite element model.

The question arises as to what factor causes the theoretical and experimental eigenvalues to converge, whilst maintaining a marked discrepancy between the converged load and the load measured in experiment. Certainly, progressively taking away modes associated with the largest discrepancies in $\overline{\boldsymbol{\lambda}}$ of Eq$^{\underline{n}}$ 2.13 to achieve a more minimised solution did not result in P^{R} moving significantly closer to $P^{®}$.

Fig. 6.12 shows the converged, theoretical frequency response functions

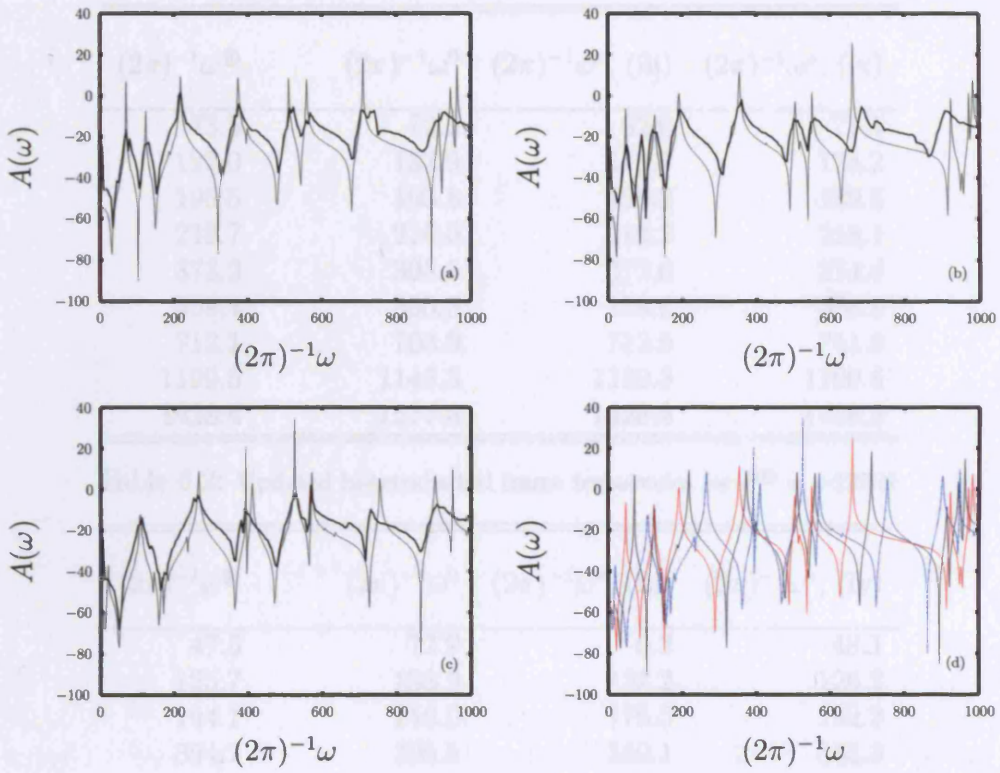

Figure 6.12: Converged, theoretical and scaled, experimental frequency response functions at each magnitude of load tested: (a) +127 N; (b) +1870 N; (c) -4866 N; ——— theoretical frequency response function; ——— experimental frequency response function; (d) overlaid theoretical functions; ——— $P^{®}$ = +127 N; ——— $P^{®}$ = +1870 N; ——— $P^{®} = -4866$ N.

at each of the load magnitudes considered. The averaged, experimentally-determined estimates of the accelerances are also shown[1]. Good agreement was found between theory and experiment, further raising the query into what factor accounts for the failure to identify load more accurately given that the converged finite element model represents the frame well. It is

[1]These were scaled based on a calibration test in which a known mass was excited by a sinusoidal force, measured by a force transducer, and the response was measured by an accelerometer; the scaling factor was then determined knowing that, from Newton's second law of motion, the transducer to accelerometer voltage amplitude ratio needed to equal the vibrated mass.

$(2\pi)^{-1}\omega^{®}$	$(2\pi)^{-1}\omega^{0}$	$(2\pi)^{-1}\omega^{*}$, (iii)	$(2\pi)^{-1}\omega^{*}$, (iv)
73.5	72.9	62.0	71.1
122.0	133.9	119.7	124.2
195.5	193.8	188.2	189.5
219.7	216.0	210.2	218.1
373.2	395.5	372.6	374.6
559.4	555.3	559.6	558.9
712.1	703.9	713.6	711.8
1199.5	1145.5	1199.3	1199.6
1428.4	1577.6	1428.4	1428.4

Table 6.2: Updated bi-tetrahedral frame frequencies for $P^{®} = +127$ N.

$(2\pi)^{-1}\omega^{®}$	$(2\pi)^{-1}\omega^{0}$	$(2\pi)^{-1}\omega^{*}$, (iii)	$(2\pi)^{-1}\omega^{*}$, (iv)
47.5	72.9	6.2	48.1
125.7	133.9	122.2	126.2
194.1	216.0	176.5	192.2
354.7	395.5	349.1	355.3
504.9	508.8	495.1	505.2
551.2	555.3	542.2	551.3
661.4	703.9	651.2	661.3
954.7	975.8	957.4	954.7
1022.2	1025.3	1021.9	1022.2

Table 6.3: Updated bi-tetrahedral frame frequencies for $P^{®} = +1870$ N.

evident that a significant, albeit very small, degree of damping exists within the physical frame, most probably attributable to energy loss at the joints. Fig. 6.12(d) depicts the variations in converged frequencies across the three magnitudes of load. The several thousand Newton change in load in the polar member sees great shifts in frequencies, in one instance nearly as much as 100 Hz. As anticipated by early plots of eigenvalue loci for this frame, in which coalescence and veering were abundant, and the findings of Mead

$(2\pi)^{-1}\omega^{®}$	$(2\pi)^{-1}\omega^{0}$	$(2\pi)^{-1}\omega^{*}$, (iii)	$(2\pi)^{-1}\omega^{*}$, (iv)
108.1	72.9	115.8	108.1
143.7	148.1	131.5	143.2
261.0	216.0	276.6	266.2
396.1	432.1	376.5	394.2
524.9	508.8	521.5	526.4
757.1	703.9	755.8	756.2
805.9	930.0	807.0	806.7
904.7	976.9	906.8	904.1
1202.9	1145.5	1202.5	1203.0

Table 6.4: Updated bi-tetrahedral frame frequencies for $P^{®} = -4866$ N.

(2002), the spectrum demonstrates that while most frequencies decrease with respect to compression in the polar member, some also increase.

Of interest is the appearance of a new peak at the lower end of the spectrum in the high tension frequency response function, Fig. 6.12(c). The apparent mode in the finite element model is in fact comprised of one degenerate and one distinct mode, both of which have been brought into existence by loading. While these modes could not be extracted from the modal analysis of test data, the experimentally determined transfer function estimate shows a peak corresponding to the theoretical one. Upon investigation of the finite element model, it was found that the degree of loading forced the three rotational rigid body modes to become strain modes with non-zero frequencies 19.5 Hz and 24.9 Hz. Of relevance is the finding of Liu et al. (1996), as mentioned in Ch. 2, who report that high tension in a free-free beam transforms one of the rigid body modes — the pitching mode — to one exhibiting flexure. This previously overlooked result is confirmed by the authors both

analytically and through a finite element formulation. The analogy of high tension in the polar spar bringing about new modes, together with the characteristic of the fundamental eigenvalue vanishing at its buckling, serves to demonstrate that although a space frame comprises many coupled, single beams, it is still governed to a great extent by a single constituent member. The tension-transformed modes of the bi-tetrahedral frame are given in Fig. 6.13. In essence, the mode shapes are little changed, which is expected as the frequencies are relatively small. There is however slight curvature introduced in the members, with the joints vibrating as rigid bodies by virtue of the offset elements.

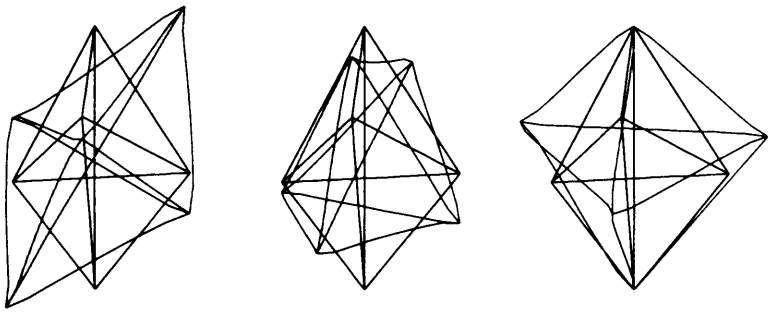

$\frac{1}{2\pi}\sqrt{\lambda} = 19.5$ Hz $\frac{1}{2\pi}\sqrt{\lambda} = 19.5$ Hz $\frac{1}{2\pi}\sqrt{\lambda} = 24.9$ Hz

Figure 6.13: The three rotational rigid body modes of the bi-tetrahedral frame transformed to strain modes by the high tension level of load.

The mode shapes for the structure at each of the three levels of load are shown in relation to the theoretical eigenvectors in Fig. 6.14-6.16. For the degenerate modes, which accounted for nearly all of those used for iteration due to their abundance, the eigenvectors shown have been numerically aligned to those measured, by Eq^{n} 4.13. Before alignment, *mac* values were

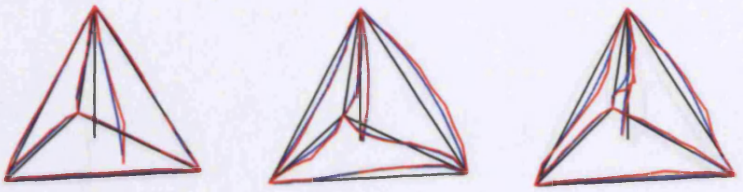

$\frac{1}{2\pi}\omega^{®} = 73.5$ Hz
$\frac{1}{2\pi}\sqrt{\lambda^{*}} = 71.1$ Hz
$mac(\phi^{*}, \phi^{®}) = 0.985$
$\xi = 0.0342$

$\frac{1}{2\pi}\omega^{®} = 122.0$ Hz
$\frac{1}{2\pi}\sqrt{\lambda^{*}} = 124.2$ Hz
$mac(\phi^{*}, \phi^{®}) = 0.952$
$\xi = 0.0190$

$\frac{1}{2\pi}\omega^{®} = 195.5$ Hz
$\frac{1}{2\pi}\sqrt{\lambda^{*}} = 189.5$ Hz
$mac(\phi^{*}, \phi^{®}) = 0.902$
$\xi = 0.0243$

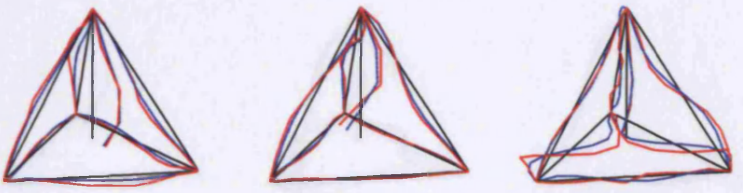

$\frac{1}{2\pi}\omega^{®} = 219.7$ Hz
$\frac{1}{2\pi}\sqrt{\lambda^{*}} = 218.1$ Hz
$mac(\phi^{*}, \phi^{®}) = 0.898$
$\xi = 0.0196$

$\frac{1}{2\pi}\omega^{®} = 373.2$ Hz
$\frac{1}{2\pi}\sqrt{\lambda^{*}} = 374.6$ Hz
$mac(\phi^{*}, \phi^{®}) = 0.963$
$\xi = 0.0084$

$\frac{1}{2\pi}\omega^{®} = 559.4$ Hz
$\frac{1}{2\pi}\sqrt{\lambda^{*}} = 558.9$ Hz
$mac(\phi^{*}, \phi^{®}) = 0.727$
$\xi = 0.0104$

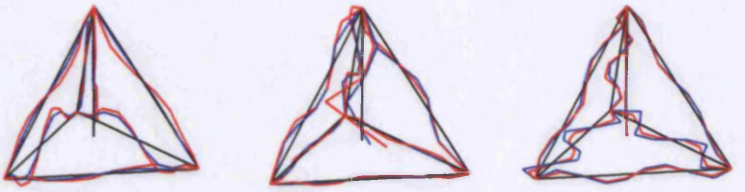

$\frac{1}{2\pi}\omega^{®} = 712.1$ Hz
$\frac{1}{2\pi}\sqrt{\lambda^{*}} = 711.8$ Hz
$mac(\phi^{*}, \phi^{®}) = 0.930$
$\xi = 0.0040$

$\frac{1}{2\pi}\omega^{®} = 1199.5$ Hz
$\frac{1}{2\pi}\sqrt{\lambda^{*}} = 1199.6$ Hz
$mac(\phi^{*}, \phi^{®}) = 0.819$
$\xi = 0.0254$

$\frac{1}{2\pi}\omega^{®} = 1428.4$ Hz
$\frac{1}{2\pi}\sqrt{\lambda^{*}} = 1428.4$ Hz
$mac(\phi^{*}, \phi^{®}) = 0.891$
$\xi = 0.0057$

Figure 6.14: Theoretical and experimental mode shapes of the modes used in iteration towards $P^{®} = +127$ N; ———— undisplaced frame; ———— theoretical mode shape, mathematically aligned to the experimental mode shape; ———— experimental mode shape.

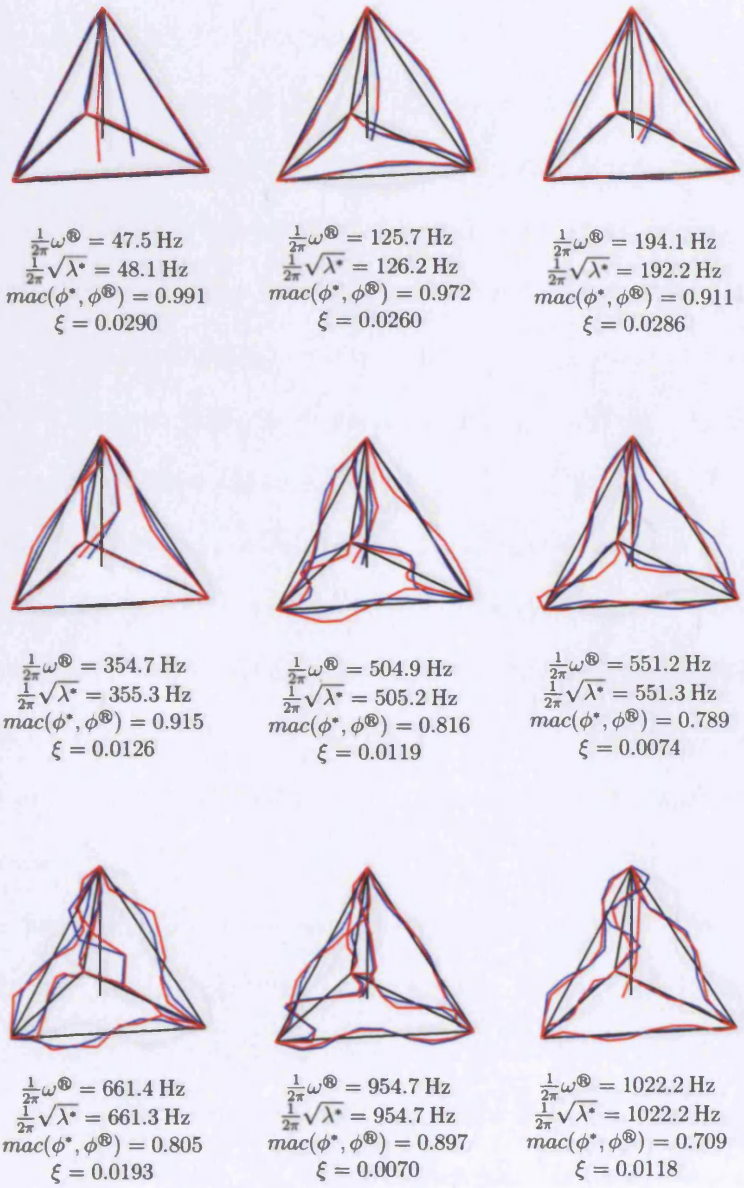

Figure 6.15: Theoretical and experimental mode shapes of the modes used in iteration towards $P^{®} = +1870$ N; ———— undisplaced frame; ———— theoretical mode shape, mathematically aligned to the experimental mode shape; ———— experimental mode shape.

$\frac{1}{2\pi}\omega^{®} = 108.1$ Hz
$\frac{1}{2\pi}\sqrt{\lambda^*} = 108.1$ Hz
$mac(\phi^*, \phi^{®}) = 0.865$
$\xi = 0.0176$

$\frac{1}{2\pi}\omega^{®} = 143.7$ Hz
$\frac{1}{2\pi}\sqrt{\lambda^*} = 143.2$ Hz
$mac(\phi^*, \phi^{®}) = 0.867$
$\xi = 0.0016$

$\frac{1}{2\pi}\omega^{®} = 261.0$ Hz
$\frac{1}{2\pi}\sqrt{\lambda^*} = 266.2$ Hz
$mac(\phi^*, \phi^{®}) = 0.944$
$\xi = 0.0260$

$\frac{1}{2\pi}\omega^{®} = 396.1$ Hz
$\frac{1}{2\pi}\sqrt{\lambda^*} = 394.1$ Hz
$mac(\phi^*, \phi^{®}) = 0.682$
$\xi = 0.0170$

$\frac{1}{2\pi}\omega^{®} = 524.9$ Hz
$\frac{1}{2\pi}\sqrt{\lambda^*} = 526.4$ Hz
$mac(\phi^*, \phi^{®}) = 0.731$
$\xi = 0.0082$

$\frac{1}{2\pi}\omega^{®} = 757.1$ Hz
$\frac{1}{2\pi}\sqrt{\lambda^*} = 756.2$ Hz
$mac(\phi^*, \phi^{®}) = 0.909$
$\xi = 0.0127$

$\frac{1}{2\pi}\omega^{®} = 805.9$ Hz
$\frac{1}{2\pi}\sqrt{\lambda^*} = 806.7$ Hz
$mac(\phi^*, \phi^{®}) = 0.835$
$\xi = 0.0093$

$\frac{1}{2\pi}\omega^{®} = 904.7$ Hz
$\frac{1}{2\pi}\sqrt{\lambda^*} = 904.1$ Hz
$mac(\phi^*, \phi^{®}) = 0.730$
$\xi = 0.0302$

$\frac{1}{2\pi}\omega^{®} = 1202.9$ Hz
$\frac{1}{2\pi}\sqrt{\lambda^*} = 1203.0$ Hz
$mac(\phi^*, \phi^{®}) = 0.667$
$\xi = 0.0157$

Figure 6.16: Theoretical and experimental mode shapes of the modes used in iteration towards $P^{®} = -4866$ N; ———— undisplaced frame; ———— theoretical mode shape, mathematically aligned to the experimental mode shape; ———— experimental mode shape.

in certain instances below 0.1, giving no indication that potentially modes could be paired with consistencies greater than 0.9. Some computational cost was therefore involved in aligning all of the subset of theoretical eigenvectors to each of the measured mode shapes in turn before establishing the binary operator of Eq^{n} 4.3 and Eq^{n} 4.4. Although this worked very well, presently no alternative way has been conceived to match degenerate modes more efficiently. Consistency was also seen to significantly increase from iterate $k = 0$ to convergence, as expected, since the loci are non-linear, and shown in previous numerical simulations.

Note that the distinct modes of the finite element model can be identified as those that involve zero displacement of the internal spar. This is because the distinct modes must uphold rotational symmetry in their mode shapes; movement from the internal spar is particular to the degenerate mode pair eigenvectors, whose linear combination can account for this spar vibrating in any direction.

Visual inspection indicates that at convergence, mode shapes are well correlated. For the near zero load level — Fig. 6.14 — generally high *mac* values are achieved, with the lowest value being 0.727; graphically however, it is seen that this mode was also correctly correlated. For the case in which the polar spar was compressed, Fig. 6.15, *mac* values were again above 0.7. The fundamental mode was traced with almost unit consistency notwithstanding that, upon inspection, the positions of the polar member according to theory and the measurement to which this has been aligned were seen to be not

coincident. The same can be said of the case in which the polar member was tensed, Fig. 6.16, although here, deformation has leaked into the measurement lowering the consistency value. Further, here the *mac* values were generally lower. Note that low consistency may be largely attributable to veering-induced deterioration in the model.

Damping factors for all of the extracted modes were generally low, which supports the absence of damping in the finite element model. The frame was further known to resonate for lengthy periods following impact excitation. Fig. 6.12 shows that damping *is* present in the frame, but the peaks are still well defined enough for damping not to become significant to the mathematical description.

The plots of the modes across the three loads allow certain mode shapes to be visually traced from figure to figure. Fig. 6.17-6.18 indicate the measured frequencies at each load and how these trace load-wise. Also shown are the corresponding converged frequencies of the finite element model. The loci shown connecting these are artificially generated by linearly varying the load, offset and length parameters between the converged values since these were of course different at each converged load. That is to say, the theoretical loci were computed as best as could be based on the limited data and that they serve to demonstrate the general variations of the theoretical frequencies. Indeed, this is seen to agree well with the variations in the measured frequencies. The discrepancies between converged and measured load are evident in these figures, and it is obvious that were it not for this, the similarity

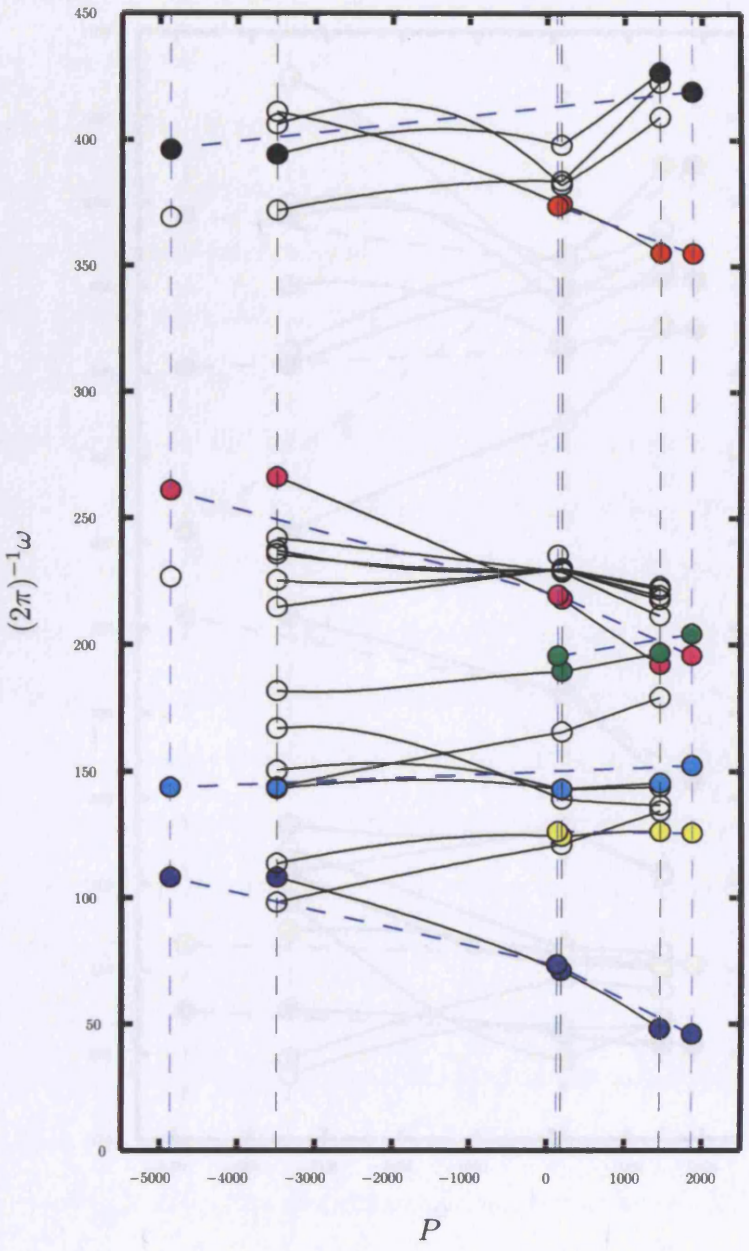

Figure 6.17: Load-wise comparison of converged, theoretical eigenvalues and experimental frequencies (lower range of frequencies); – – – – loads converged upon; – – – – loads measured; ● modes matched between the theoretical model and experiment; ○ modes unmatched between the theoretical model and experiment; ——— theoretical interpolation; – – – – experimental interpolation.

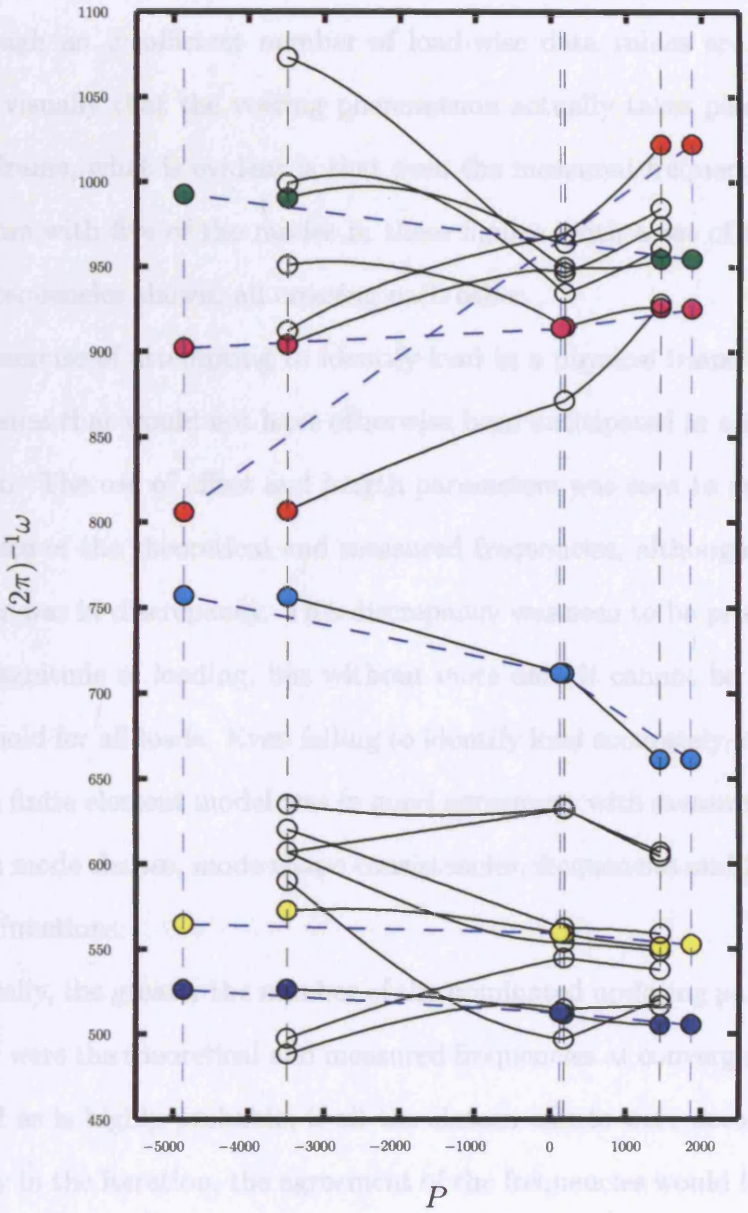

Figure 6.18: Load-wise comparison of converged, theoretical eigenvalues and experimental frequencies (upper range of frequencies); – – – – loads converged upon; – – – – loads measured; ● modes matched between the theoretical model and experiment; ○ modes unmatched between the theoretical model and experiment; ———— theoretical interpolation; – – – – experimental interpolation.

of the finite element and physical frequency loci would be even greater.

Although an insufficient number of load-wise data values are available to verify visually that the veering phenomenon actually takes place for the physical frame, what is evident is that even the measured frequencies cross. This occurs with five of the modes in these figures, with a set of three, the highest frequencies shown, all crossing each other.

The exercise of attempting to identify load in a physical frame has highlighted issues that would not have otherwise been anticipated in a numerical simulation. The use of offset and length parameters was seen to greatly aid convergence of the theoretical and measured frequencies, although the load parameter was in discrepancy. This discrepancy was seen to be proportional to the magnitude of loading, but without more data it cannot be said that this will hold for all loads. Even failing to identify load accurately, at convergence the finite element model was in good agreement with measurement, as seen from mode shapes, mode shape consistencies, frequencies and frequency response functions.

Generally, the greater the number of the nominated updating parameters, the closer were the theoretical and measured frequencies at convergence. Perhaps, and as is highly probable, if all the sixteen offsets were accounted for separately in the iteration, the agreement of the frequencies would have been better. Load may also have been identified more accurately. Conversely, it may not because of the danger that load and effective length may not be close enough to orthogonality as far as how they affect the frequencies is

concerned.

Consider the eigenvalues as functions of load and effective length, some parameter accounting for offsets and length together, taking the forms as seen in this thesis with values of zero coinciding with Euler buckling loads. The effect of varying effective length would be, to describe it coarsely, to augment or diminish the loci load-wise. This stretching of the loci may help to explain why the results indicate that the eigenvalue constraints have been met whilst the load has not been identified as accurately. Fig. 6.17-6.18 in particular suggest that both the frequencies and load could have converged well if in the theoretical frequency-load plane the loci had been stretched.

What is needed is a balance such that the finite element model is not under or over parameterised. Even so, the results have served to show that the identification method achieved significant success and may be a useful indicator to the extent of loading in a space frame. That an *unconstrained* Newton's method has resulted in convergence to physically determined data to identify load is most encouraging.

Chapter 7

Identification of Load in a Thrice Redundant Octet Frame

With the success of identifying load in the bi-tetrahedral frame, the last of the numerical simulations, the octet frame, is physically realised and its dynamic data experimentally extracted at loaded states. The finite element model is modified based on experience previously gained; both length and offset quantities are used to supplement load in parameterising the model. Heeding the particular difficulties associated with this more complicated structure to strengthen convergence, Newton's method is employed in an attempt to match physically measured loads. Updating is repeated for two states of load, both of which are generated by random member straining, and indicates that identification is not only successful, but also its accuracy is not affected by the existence of more than one force distribution. What is an issue is beginning iteration in the neighbourhood and 'eigenvector neighbourhood' of the root, a minimum condition for convergence to result at all. Strategies useful to iteration are suggested, including one increasing mode tracing confidence.

7.1 General

The numerical simulation of the octet frame in Ch. 5 demonstrated that the chances of converging upon the root of the problem are small. For there to be hope of convergence, two things certainly must hold. Firstly, iteration must start in the neighbourhood of the root; this is a classic criterion for Newton's method. Secondly, and mutually, the consistency of the eigenvectors at each iterate and the eigenvectors at the root must be strong enough for there to be a smooth trace of the eigenvalue functions to the solution. Away from the root, it is possible, as seen in Sec. 5.8, for the eigenvectors to bear little or no resemblance to the root eigenvectors.

In approaching the application of the method of force identification to a such demanding and real structure, for which further difficulties of experimental error and lack of data exist, some helpful modifications are now first explored. These involve formulating a better conditioned problem and strengthening the consistency during iteration.

7.2 Formulating upon an Orthonormal Basis for the Distributions of Force

Until now, the models of multiply redundant frames have been formulated on distributions of force such as to attain a reduced equilibrium matrix $\overline{\mathbf{E}}$ of full rank, but not necessarily of unit condition number. Although in this case a small amount of dependency exists between the columns of $\overline{\mathbf{E}}$, even when the optimum columns are selected from $\mathbf{E}$, its condition is sufficient to

deliver a numerically stable solution.

Whether formulating the finite element model on an orthonormal basis for the distributions of force significantly improves the quality of iteration is unknown, but for good practice it should be done. Certainly, one question to be answered is whether the condition of the Jacobian is largely dependent upon the condition of the force distributions. It *is* known that a problem formulated on a singular equilibrium matrix will lead to a singular Jacobian and non-unique roots, which is a consequence of $rank(\mathbf{J}) = rank(\mathbf{E})$, for $\mathbf{J}$ involving only derivatives with respect to load parameters — q.v. Sec. 3.3. There must therefore be some relation between the conditions of the reduced equilibrium and Jacobian matrices.

Decomposing $\overline{\mathbf{E}} \in \mathbb{R}^{\ell \times n}$ into its singular values and vectors,

$$\overline{\mathbf{E}} = \mathbf{U}\boldsymbol{\Sigma}\mathbf{V}^T, \tag{7.1}$$

where $\mathbf{U} \in \mathbb{R}^{\ell \times \ell}$ and $\mathbf{V} \in \mathbb{R}^{n \times n}$ are respectively the orthonormal left and right singular vector matrices; $\boldsymbol{\Sigma} = diag\,(\sigma_1, \ldots, \sigma_n) \in \mathbb{R}^{\ell \times n}$ is a diagonal matrix of singular values. It follows that

$$\overline{\mathbf{E}} = \sum_{i=1}^{n} \sigma_i \mathbf{u}_i \mathbf{v}_i^T. \tag{7.2}$$

All force vectors that lie in $range(\overline{\mathbf{E}})$,

$$\mathbf{f} = \overline{\mathbf{E}}\mathbf{p}, \tag{7.3}$$

$\mathbf{p} \in \mathbb{R}^{n \times 1}$, lie in the span of the first n columns of $\mathbf{U}$, which is an orthonormal matrix,

$$\mathbf{U}^T\mathbf{U} = \mathbf{I}. \tag{7.4}$$

In turn, the first n columns of $\mathbf{U}$ lie in $range(\overline{\mathbf{E}})$ since, from Eq$^{\underline{n}}$ 7.2,

$$\mathbf{u}_i = \frac{1}{\sigma_i}\overline{\mathbf{E}}\mathbf{v}_i, \qquad i = 1, 2, \ldots, n. \tag{7.5}$$

Thus $[\mathbf{u}_1 \cdots \mathbf{u}_n]$ form an orthonormal basis of $range(\overline{\mathbf{E}})$. It is then factors upon these left singular vectors that will form the parameters of the finite element model relating to load, so that the member forces are expressible as

$$\mathbf{f} = \overline{\mathbf{U}}\mathbf{p}_u, \tag{7.6}$$

or

$$\mathbf{f} = [\mathbf{u}_1 \cdots \mathbf{u}_n]\,\mathbf{p}_u. \tag{7.7}$$

What is lost in the physical meaningness of the force parameters is gained in being able to describe the statics of a frame in terms of entirely uncoupled, orthogonal force distributions. For convention, let the columns of the reduced equilibrium matrix be normalised such that

$$\|\overline{\mathbf{e}}_i\|_\infty = 1, \qquad i = 1, \ldots, n, \tag{7.8}$$

before singular value decomposition is performed.

7.3 Modal Tagging

Typically, at the start of iteration, the root mode shapes of subset S are compared to a subset of eigenvectors, T, at $k = 0$. Due to practical limitations, the root mode shapes will generally not be fully described and, further, may have significant experimental error associated with them. If the start

of iteration is sufficiently close to the root and unambiguous pairings exist between the eigenvectors there and the root mode shapes, an opportunity exists for consistency to be potentially strengthened during iteration. The notion is to tag the experimentally extracted frequencies with the eigenvectors with which their associated mode shapes are consistent at $k = 0$. That is to say, $\boldsymbol{\phi}^{®}$ are replaced with their paired $\boldsymbol{\phi}^{k=0}$. This obviously requires initially strong consistencies between experimental and model mode shapes, but may alleviate any potential iterative decline in *mac* arising from experimental error or, more likely, the mode shapes being described at only a limited number of degrees of freedom. It must be emphasised that modal tagging is an artificial approach. It *may* recover an otherwise ill-fated iteration or it may not, although the hope is that the former is the more frequent circumstance. This is investigated later. The intention is that, even though the initial consistencies must by stipulation be strong, tagged modes will fare better than untagged modes should an iterate subsequently land far from the root.

Formally, the unmodified mode tracing philosophy seeks to pair all modes $\boldsymbol{\phi}^{®}$ in the root subset S with some in a subset T at a general iterate k by computing between all the modes in each subset the consistency

$$mac\left(\boldsymbol{\phi}^{®}, \boldsymbol{\phi}^{k}\right) = \frac{\left|\left(\boldsymbol{\phi}^{®}\right)^{T} \boldsymbol{\phi}^{k}\right|^{2}}{\left\|\boldsymbol{\phi}^{®}\right\|_{2}^{2} \left\|\boldsymbol{\phi}^{k}\right\|_{2}^{2}} \in [0,1]\,, \tag{7.9}$$

and acknowledging the maximum *mac* as indicating the smoothest trace of

eigenvalues. Modal tagging uses as its basis the consistency

$$mac\left(\boldsymbol{\phi}^{\circledR}, \boldsymbol{\phi}^{k=0}\right) = \frac{\left|\left(\boldsymbol{\phi}^{\circledR}\right)^T \boldsymbol{\phi}^{k=0}\right|^2}{\|\boldsymbol{\phi}^{\circledR}\|_2^2 \, \|\boldsymbol{\phi}^{k=0}\|_2^2} \in [0,1]\,, \tag{7.10}$$

to tag the experimental frequencies and use, instead of 7.9, the consistency

$$mac\left(\boldsymbol{\phi}^{k=0}, \boldsymbol{\phi}^{k}\right) = \frac{\left|\left(\boldsymbol{\phi}^{k=0}\right)^T \boldsymbol{\phi}^{k}\right|^2}{\|\boldsymbol{\phi}^{k=0}\|_2^2 \, \|\boldsymbol{\phi}^{k}\|_2^2} \in [0,1] \tag{7.11}$$

to trace modes. From Eq$^{\underline{n}}$ 7.11, it is obvious that, in a modal tagging scheme, at the start of iteration consistency is unity. Note that the eigenvectors of Eq$^{\underline{n}}$ 7.11 are of dimension equal to the order of the finite element model, N (which means the mode shapes are now described in their fullest detail), whereas those of Eq$^{\underline{n}}$ 7.9 are limited to being only of an order governed by the number of degrees of freedom at which mode shapes are experimentally measured. This is not indicated in the notation, as the limiting number of degrees of freedom is obvious from the types of eigenvector used to compute *mac*. If, however, the number of degrees of freedom used to compute *mac* is less than the total available, this *is* indicated.

7.4 Frame Realisation

The frame investigated is a physical realisation of the octet space frame of Ch. 5, Fig. 5.14; the actual frame can be seen in Fig. B.3. The octet frame is formed in the same way and of the same steel member and aluminium joint system as the bi-tetrahedral frame (q.v. Ch. 6), so as to allow self-equilibrating forces to develop throughout the frame. Similarly, the frame is first assembled as the statically determinate outer frame in the absence of

the three internal members 2, 3 and 55, which later provide the three redundancies, and, hence, force distributions. As before, the reason for this is to allow freedom of movement that is not easy once the structure is redundant. In this way, it is ensured that all member lengths are equal so as to form a regular frame before the internal redundancies are inserted. Before a modal test is performed, the joint non-linearity is alleviated by the application of nuts and washers at the member-joint interfaces.

7.5 Axial Strain Measurement

Any state of equilibrium of the octet frame lies in, at most, the range of three linearly independent distributions of force. Because of the success of the axial strain measuring system depicted in Fig. 6.1, it is again employed here. Use can be made of the reduced equilibrium matrix, which is now the set of orthonormal left singular vectors $\overline{\mathbf{U}} = [\mathbf{u}_1\ \mathbf{u}_2\ \mathbf{u}_3]$, so that measuring all member forces is not necessary — this is made apparent shortly. In fact, as the order of the linear system of equilibrium equations is three, only three member force measurements are required to know all member forces, in theory. However, it is prudent to measure more than just three member forces in order to have an overdetermined set of equations. Axial strain is therefore observed in ten of the frame members: 9, 10, 18, 24, 27, 42, 51, 55, 56 and 63 — q.v. Fig. 5.14. Determining all member forces from measuring just these ten is performed as follows.

For m measured axial forces and i the designations of their members,

assume the overdetermined subset of linear equilibrium equations can be expressed as follows with the measured forces in the range of the subset of the equilibrium matrix:

$$\begin{Bmatrix} f_{i_1} \\ \vdots \\ f_{i_m} \end{Bmatrix}^{\circledR} = \begin{bmatrix} u_{i_1,1} & \cdots & u_{i_1,n} \\ \vdots & \ddots & \\ u_{i_m,1} & & u_{i_m,n} \end{bmatrix} \begin{Bmatrix} p_{u_1} \\ \vdots \\ p_{u_n} \end{Bmatrix}^{\circledR}. \tag{7.12}$$

The force parameters are then

$$\begin{Bmatrix} p_{u_1} \\ \vdots \\ p_{u_n} \end{Bmatrix}^{\circledR} = \begin{bmatrix} u_{i_1,1} & \cdots & u_{i_1,n} \\ \vdots & \ddots & \\ u_{i_m,1} & & u_{i_m,n} \end{bmatrix}^{+} \begin{Bmatrix} f_{i_1} \\ \vdots \\ f_{i_m} \end{Bmatrix}^{\circledR}, \tag{7.13}$$

and the entire set of forces can be calculated through reconstruction as

$$\mathbf{f}^{\circledR} = \overline{\mathbf{U}}\mathbf{p}_u^{\circledR}, \tag{7.14}$$

where $\overline{\mathbf{U}} = [\mathbf{u}_1 \cdots \mathbf{u}_n]$.

Precisely how much overdeterminacy, $m - n$, is required to attain an accurate, stable solution to the member forces is unknown. However, for $i = [9\ 10\ 18\ 24\ 27\ 42\ 51\ 55\ 56\ 63]$, $m = 10$, the entire member force set $\mathbf{f}^{\circledR}$ is seen to be little changed as m is decreased to 5 or 6, indicating forces are correctly determined.

7.6 Parameterisation of the Finite Element Model

Experience from identifying load in the bi-tetrahedral frame was used in modifying the finite element model of the octet to better represent the physical frame.

Due to the size of the model, member discretisation for the octet frame is only four. However, Mottershead and James (1998) and Mottershead et al. (2000) find success in updating the frequencies of an aluminium frame finite element model, to converge well to physically observed frequencies, and use a member discretisation of only four for the three storey structure. This suggests that a discretisation of four for the octet frame may be sufficient; the global beam modes would certainly not require a very detailed description.

Based on the study for the bi-tetrahedral frame in the previous chapter regarding the inclusion of parameters accounting for member effective lengths, both member length and offset parameters are included in the modified octet model. Since all of the octet joints are identical, rhombic dodecahedra, all members other than member 55 are of the same length and have similar lengths embedded in the joints. Only two offset parameters, therefore, are considered: the regular member offset and the member 55 offset.

Point masses are added to the appropriate degrees of freedom of the mass matrix to account for presence of the joints. These are a mean value of 0.095 kg based on physical measurements of the actual joint masses, nuts and washers. Other constant properties of the frame were taken as follows: $E = 2.1 \times 10^{11}$ Nm^{-2}, based on supply data; $\rho = 7591.9$ kgm^{-3} and $d = 0.00785$ m, based on indirect and direct measurements, respectively.

7.7 Modal Testing of the Frame

The experimental set-up for the octet frame was identical to that schematised in Fig. 6.4 for the bi-tetrahedral frame. The dynamic characteristics were extracted at two states of load, each induced by the random straining of a number of frame members and measured as outlined in Sec. 7.5. Modal tests were run using a single, suspended shaker fitted with a force transducer of sensitivity 11.24 mVN^{-1} and an accelerometer of sensitivity 1.02 $\text{mV}(\text{ms}^{-2})^{-1}$ to measure response at a number of locations. Angled aluminium studs were used to mount the accelerometer in each of the orthogonal directions of the global coordinate system. The position of the shaker was at the first node down from the top of member 2 and excitation was applied parallel to the plane of members 16, 20 and 60 and perpendicular to the longitudinal axis of the frame. Filtered, random excitation was provided from a white noise generator. Accelerations were measured in three orthogonal directions at a select number of nodes in one half of the frame; only 7.98 percent of the total degrees of freedom were measured but measurement locations were chosen so as to minimise ambiguity of mode shapes. Fig. 7.1 shows test planning *automac* plots in which the eigenvectors were reduced according to the degrees of freedom at which the frame response was to be measured. For the modes in the subset T shown, which were the first $t = 400$ modes of the finite element model considered at each iteration for mode tracing purposes, much corruption is present, but this is deemed inevitable and measuring at a greater number of locations is impractical. What inspecting *automac* plots

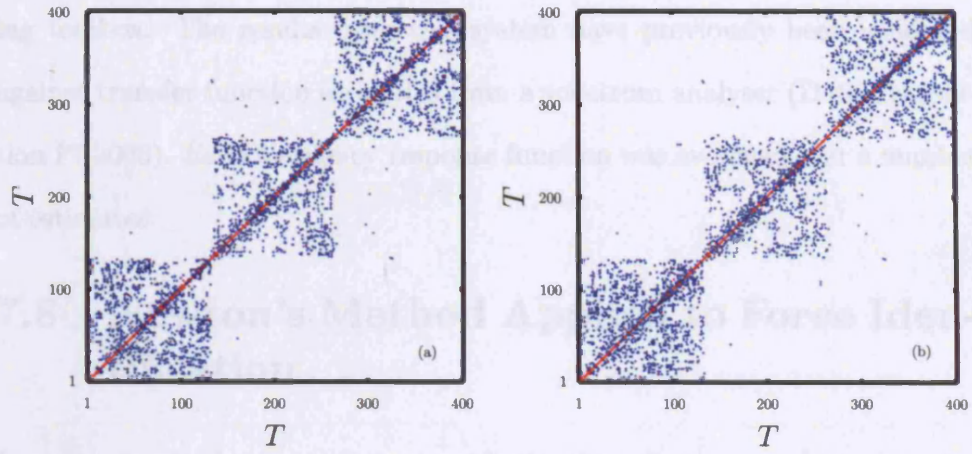

Figure 7.1: Octet frame test planning *automac* plots, with eigenvectors defined at 7.98 per cent of the total number of model degrees of freedom: (a) $p_{u_1} = p_{u_2} = p_{u_3} = 0$, $L = 0.42$, $d = 0.00785$, no offset parameters; (b) $p_{u_1} = p_{u_2} = p_{u_3} = 1000$, $L = 0.42$, $d = 0.00785$, no offset parameters; 0 1 *mac* consistency scale.

of reduced eigenvectors further exposes is that the modes travel in massive families, revealed in their square patches, among which they bear similarities to, and can only be subtly different from, one another.

As the octet finite element model revealed a higher modal density than that of the bi-tetrahedral frame, a smaller sampling frequency of 2604 Hz was nominated, whilst keeping a discrete Fourier transform size of 1024, in the hope of extracting in more detail the abundant lower frequencies and their mode shapes. The low pass cut-off frequency of the filter was then accordingly set at approximately two thirds of the Nyquist frequency, 860 Hz. Amplified excitation force and response acceleration signals were then sent back to a computer via a data acquisition unit.

Transfer function estimates were performed within a Visual Basic code, which itself calls the function spectrum.m in the Matlab signal process-

ing toolbox. The results from this system have previously been validated against transfer function estimates from a spectrum analyser (Data Translation PL2000). Each frequency response function was averaged over a number of estimates.

7.8 Newton's Method Applied to Force Identification

Iteration involved six parameters, with the three force parameters, p_{u_1}, p_{u_2} and p_{u_3}, supplemented by member length, L, and the two offset parameters, η_1 and η_2, respectively relating to the regular and member 55 offsets. Iteration was performed using, in each case, ten modes to identify two physically measured states of load, State 1 and State 2, each of which was generated by the random straining of a number of frame members.

The geometry of the frame and the existence of multiple force parameters meant that there was no permanent degeneracy of the eigenvalues and therefore mode tracing was simpler to perform than in the case of the bi-tetrahedral frame in that sense.

Finding a starting point for iteration that led to convergence posed significant difficulty. The issues raised by the numerical simulation for the octet frame suggest that the starting point must be close to the root in terms of both the magnitudes of the eigenvalues and the consistencies of the eigenvectors. Since no methodical global method for establishing a starting point for Newton's method is known for the present type of problem, an ad hoc

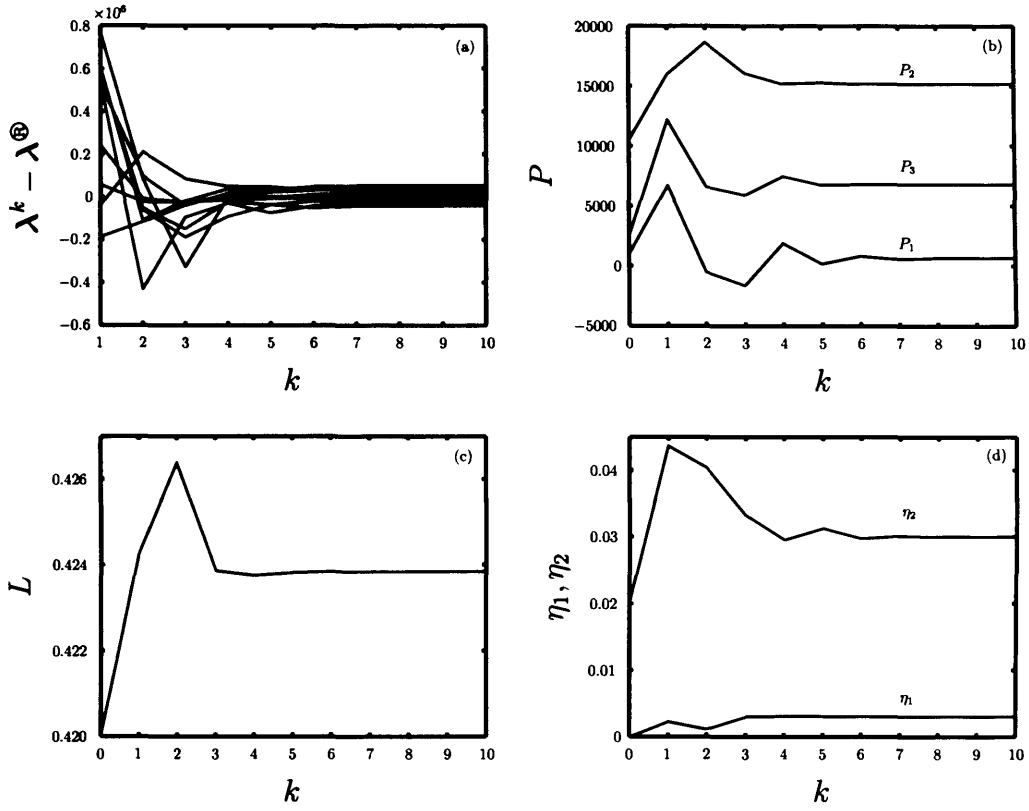

Figure 7.2: Iteration for the octet frame loaded in State 1: (a) minimisation of the eigenvalue difference; (b) iterative progression of the load parameters; (c) iterative progression of the length parameter; (d) iterative progression of the offset parameters.

approach was adopted. (No advantage was taken of the knowledge of the measured forces, as this would have been an unfair aid to the success of force identification.) Starting points were established through randomly varying the parameters and beginning a damped Newton's method, where a sufficient number of strong mode shape consistencies were found, with constrained progressions $\alpha\Delta p$, $0 < \alpha < 1$ — q.v. Eq$^{\underline{n}}$ 2.15. Once it was felt that a close enough starting point was established, the unmodified Newton's method was initiated with modal tagging. This is by no means a robust approach, as it does not guarantee success of convergence, and the issue of finding some

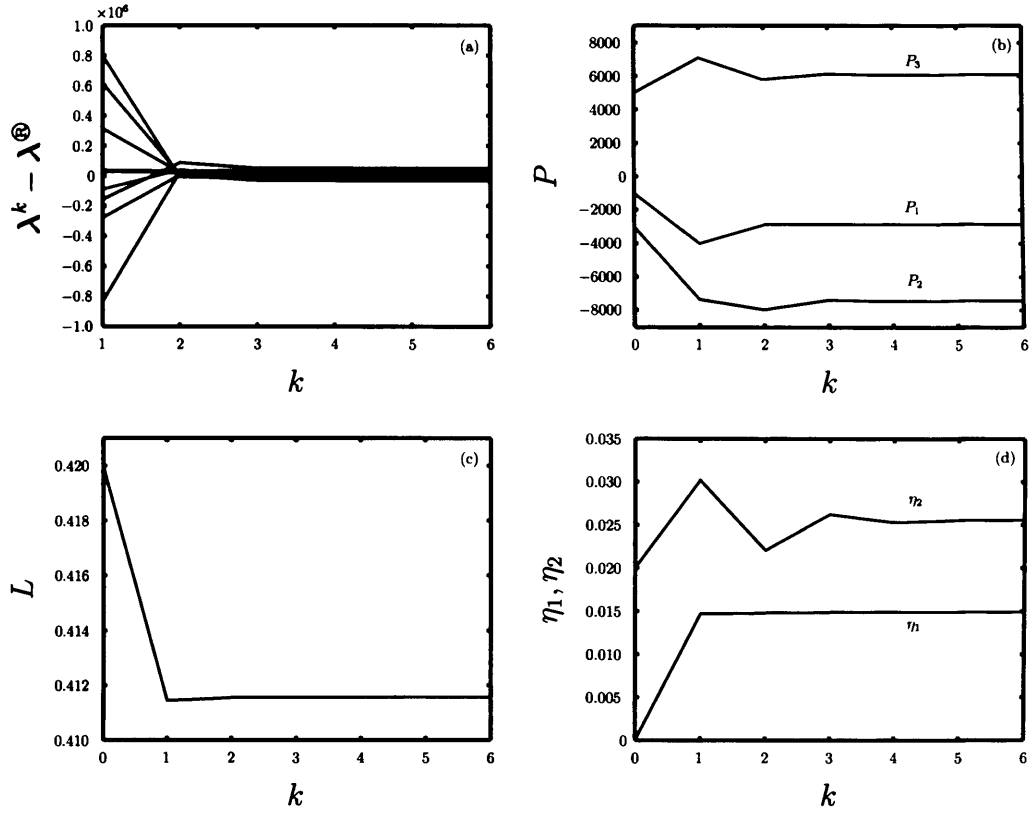

Figure 7.3: Iteration for the octet frame loaded in State 2: (a) minimisation of the eigenvalue difference; (b) iterative progression of the load parameters; (c) iterative progression of the length parameter; (d) iterative progression of the offset parameters.

global strategy for establishing a starting point for Newton's method needs to be addressed. Line search algorithms, which meaningfully control the value of α, based on current function information, to ensure function minimisation at each iteration, are not capable of addressing the eigenvector deterioration problem that hinders mode tracing. This is still open to investigation.

Eventually, starting points were found that led to successful convergence. For State 1, the start of iteration was at $p_{u_1} = 1000$, $p_{u_2} = 10500$, $p_{u_3} = 2500$, $\eta_1 = 0$, $\eta_2 = 0.02$ and $L = 0.42$; for State 2, it was at $p_{u_1} = -1000$, $p_{u_2} =$

$(2\pi)^{-1}\omega^{®}$	$(2\pi)^{-1}\omega^{0}$	$(2\pi)^{-1}\omega^{*}$
138.1	143.3	137.5
247.7	245.7	249.3
294.6	286.5	294.2
316.6	326.2	316.8
343.1	365.0	345.0
366.1	384.1	367.3
377.4	394.9	376.0
410.5	428.4	409.8
430.2	447.1	428.9
519.9	538.4	520.3

Table 7.1: Updated octet frame frequencies for State 1.

-3000, $p_{u_3} = 5000$, $\eta_1 = 0$, $\eta_2 = 0.02$ and $L = 0.42$. Fig. 7.2-7.3 show the minimisation of the theoretical and experimental frequency discrepancy and the iterative progressions of all of the updating parameters for, respectively, loaded State 1 and State 2. For both load states, the eigenvalue difference was well minimised and the updating parameters converged upon what appear to be physically reasonable values. What is noteworthy is the fact that across the convergences, as previously with the bi-tetrahedral frame, all of the 'effective length' parameters, L, η_1 and η_2, are different. Again, this suggests that these parameters are not constant, but load-dependent, and it is therefore wise to include them when updating load. A summary of the root, initial and converged frequencies is given in Tab. 7.1-7.2.

A comparison of the converged load parameters, in relation to those measured, are summarised in Fig. 7.4. The similarity between model and observation is promising. Further, the discrepancy associated with each force

$(2\pi)^{-1}\omega^{®}$	$(2\pi)^{-1}\omega^{0}$	$(2\pi)^{-1}\omega^{*}$
81.9	85.9	82.9
138.2	141.7	139.8
176.4	178.8	179.0
245.3	237.2	247.9
247.6	233.0	245.9
266.1	261.9	265.8
313.4	325.9	314.1
358.7	385.9	358.2
433.7	451.3	433.6
660.9	644.7	660.8

Table 7.2: Updated octet frame frequencies for State 2.

parameter seems to be of an order similar to that exhibited by the single force parameter of the bi-tetrahedral frame (cf. Fig. 6.11). This suggests that shortfalls of the model in identifying the actual load in a frame are not accumulative across the force parameters, but that discrepancies between model and observation are, in a sense, constrained by the suitability of the model and are not dependent upon the number of force distributions required to describe frame equilibrium. That is to say, constraint is provided by the state of equilibrium, irrespective of how many linearly independent distributions of force are needed in describing it. This is encouraging, even though loads have not been identified accurately. The idea is supported further by inspecting the converged member forces in relation to those measured.

Fig. 7.5-7.6 show that iteration had indeed attempted to converge to the measured force distributions. Generally, the member forces are identified as greater than what has been measured, unlike identification for the bi-

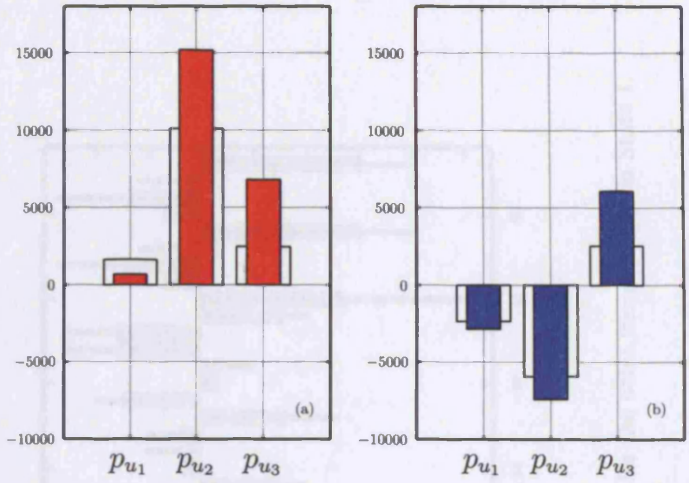

Figure 7.4: Converged octet frame force parameters (colour) in relation to measured force parameters (white): (a) State 1; (b) State 2.

tetrahedral frame, which underestimated the member forces. Error is not then consistent in this sense.

The question of whether just ten modes, for each of the two tests, were sufficient in characterising the dynamic characteristics of the frame fully needs to be asked. In order to explore this, the scaled, averaged, point frequency response functions are shown in Fig. 7.7 for each load state and in relation to the frequency response functions of the converged model. The similarity of the experimental accelerance estimates and the theoretical frequency response functions reveals that the modifications to the finite element model owing to the updating of the six parameters using ten modes *has* reasonably accounted for the dynamic characteristics of the octet frame, at least within the frequency bandwidth shown.

With the octet frame also, it is evident that a small degree of damping exists within the physical frame and is most probably attributable to energy

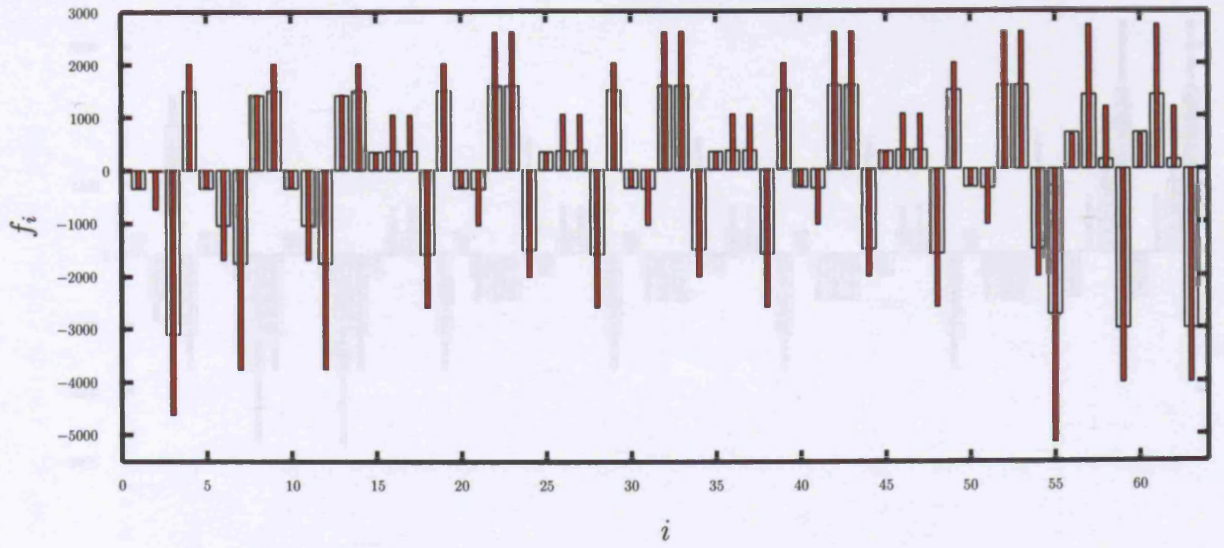

Figure 7.5: Converged frame forces (colour) in relation to measured forces (white) for the octet frame loaded in State 1.

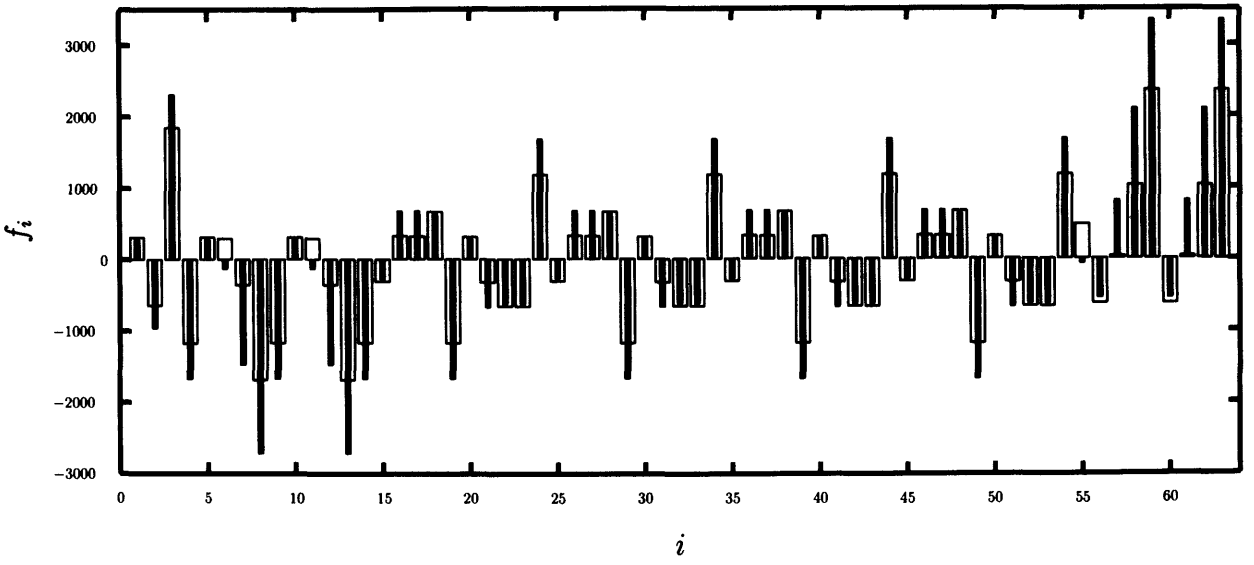

Figure 7.6: Converged frame forces (colour) in relation to measured forces (white) for the octet frame loaded in State 2.

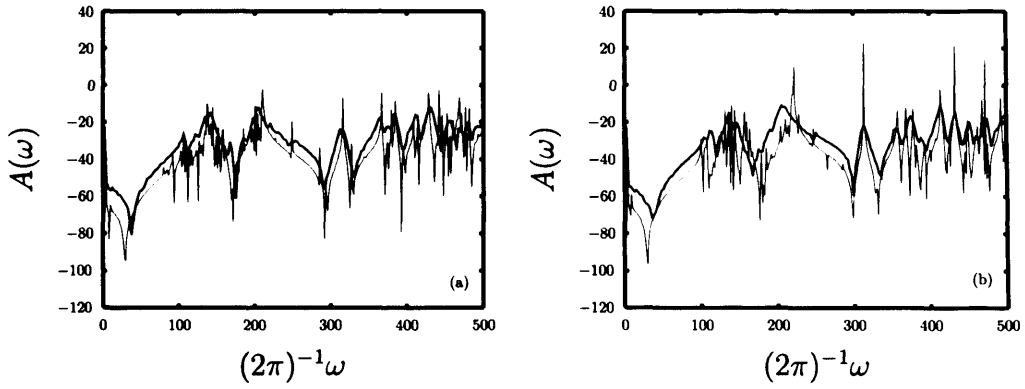

Figure 7.7: Converged, theoretical and scaled, experimental frequency response functions at each octet load state: (a) State 1; (b) State 2; ———— theoretical frequency response function; ———— experimental frequency response function.

loss at the joints.

The ten mode shapes for each of State 1 and State 2 are shown in relation to the theoretical eigenvectors in Fig. 7.8-7.17. There is generally good agreement between model and experimental mode shapes, although in some instances for certain experimental mode shapes, a few of the members oscillate π radians out of phase with what the model predicts. In a moment, this will be seen to be extremely detrimental.

Accompanying the mode shapes plots are, as well as experimental and converged frequencies, and damping factors, the following consistency values:

- $mac(\phi^{\circledR}, \phi^{*})$, the maximum consistency between the experimentally extracted mode shape and a model eigenvector at convergence;

- $mac(\phi^{\circledR}, \phi^{k=0})$, the maximum consistency between the experimentally extracted mode shape and a model eigenvector at the start of iteration, i.e., the basis for modal tagging, with $\phi^{k=0}$ the tagging eigenvector;

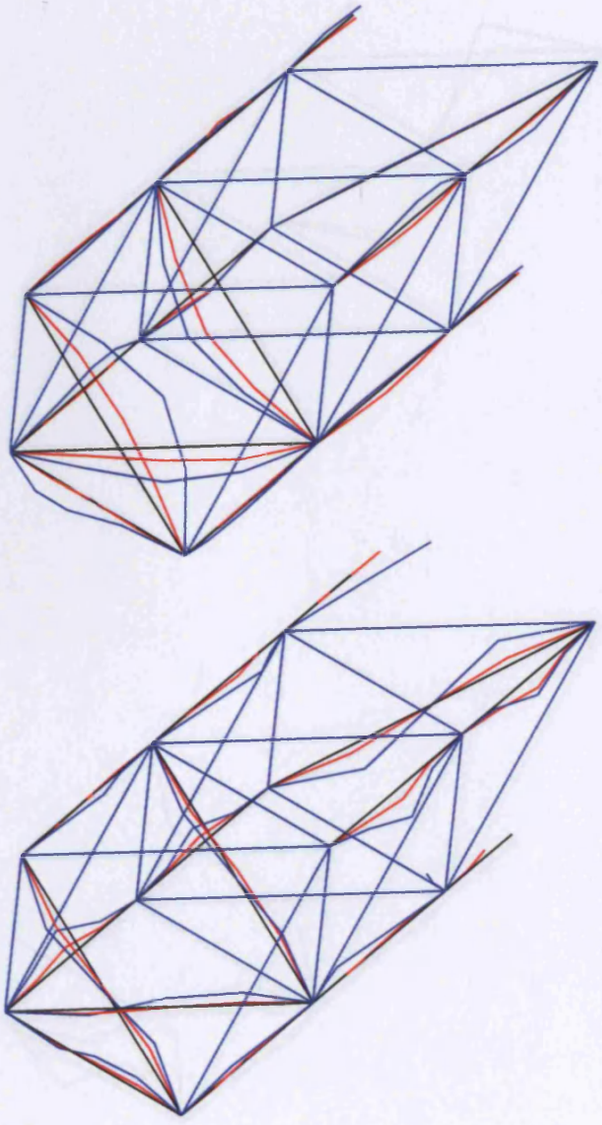

$\frac{1}{2\pi}\omega^{\circledR} = 138.1$ Hz
$\frac{1}{2\pi}\sqrt{\lambda^*} = 137.5$ Hz
$mac(\phi^{\circledR}, \phi^*) = 0.704$
$mac(\phi^{\circledR}, \phi^{k=0}) = 0.741$
$mac(\phi^{k=0}, \phi^*) = 0.775$
$mac(\phi^{k=0}_{101\times1}, \phi^*_{101\times1}) = 0.905$
$\xi = 0.0176$

$\frac{1}{2\pi}\omega^{\circledR} = 247.7$ Hz
$\frac{1}{2\pi}\sqrt{\lambda^*} = 249.3$ Hz
$mac(\phi^{\circledR}, \phi^*) = 0.911$
$mac(\phi^{\circledR}, \phi^{k=0}) = 0.854$
$mac(\phi^{k=0}, \phi^*) = 0.951$
$mac(\phi^{k=0}_{101\times1}, \phi^*_{101\times1}) = 0.909$
$\xi = 0.0088$

Figure 7.8: Theoretical and experimental mode shapes of the octet modes used in iteration towards State 1; modes 1 and 2; ———— undisplaced frame; ———— theoretical mode shape; ———— experimental mode shape; note that convergence is achieved with the inclusion of the modal tagging strategy.

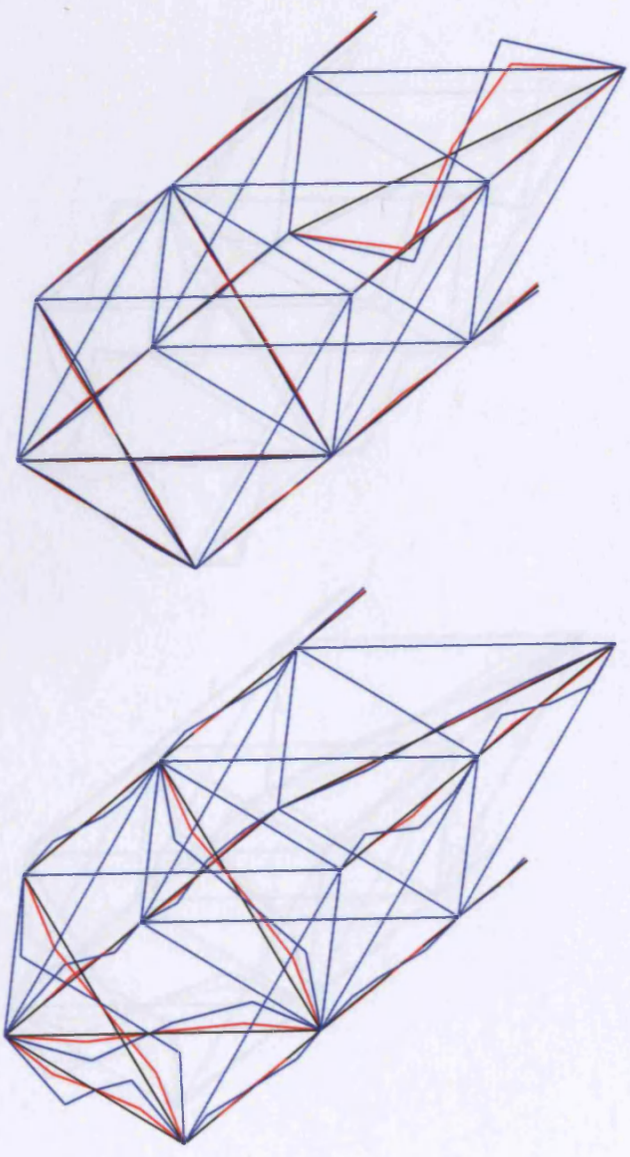

$\frac{1}{2\pi}\omega^{\circledR} = 294.6$ Hz
$\frac{1}{2\pi}\sqrt{\lambda^*} = 294.2$ Hz
$mac(\phi^{\circledR}, \phi^*) = 0.901$
$mac(\phi^{\circledR}, \phi^{k=0}) = 0.918$
$mac(\phi^{k=0}, \phi^*) = 0.971$
$mac(\phi^{k=0}_{101\times1}, \phi^*_{101\times1}) = 0.997$
$\xi = 0.0139$

$\frac{1}{2\pi}\omega^{\circledR} = 316.6$ Hz
$\frac{1}{2\pi}\sqrt{\lambda^*} = 316.8$ Hz
$mac(\phi^{\circledR}, \phi^*) = 0.835$
$mac(\phi^{\circledR}, \phi^{k=0}) = 0.815$
$mac(\phi^{k=0}, \phi^*) = 0.992$
$mac(\phi^{k=0}_{101\times1}, \phi^*_{101\times1}) = 0.995$
$\xi = 0.0071$

Figure 7.9: Theoretical and experimental mode shapes of the octet modes used in iteration towards State 1; modes 3 and 4; ———— undisplaced frame; ———— theoretical mode shape; ———— experimental mode shape; note that convergence is achieved with the inclusion of the modal tagging strategy.

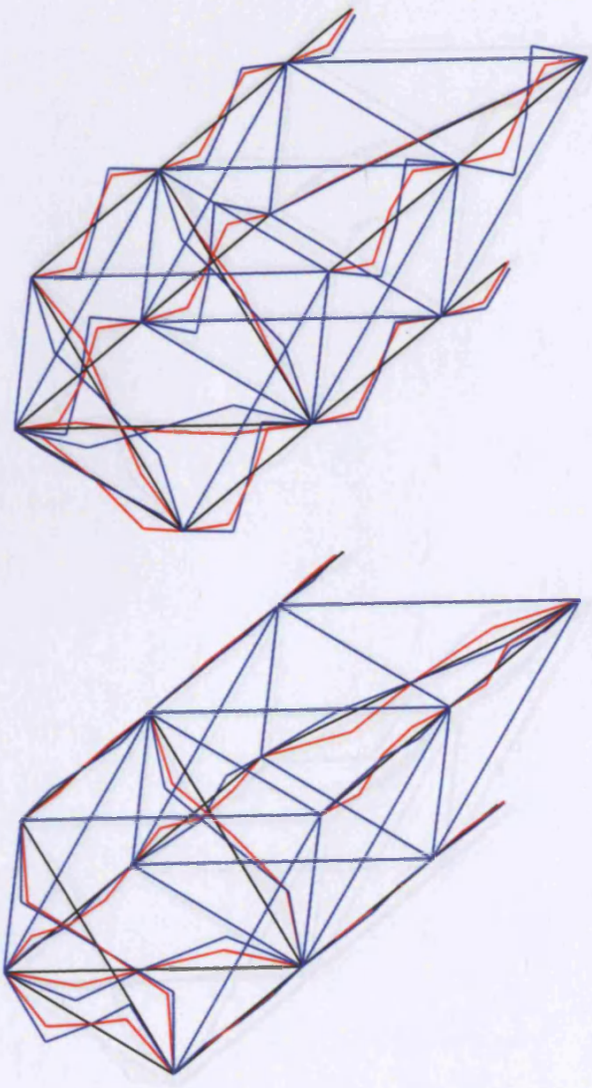

$\frac{1}{2\pi}\omega^{\circledR} = 343.1$ Hz
$\frac{1}{2\pi}\sqrt{\lambda^*} = 345.0$ Hz
$mac(\phi^{\circledR}, \phi^*) = 0.626$
$mac(\phi^{\circledR}, \phi^{k=0}) = 0.655$
$mac(\phi^{k=0}, \phi^*) = 0.983$
$mac(\phi^{k=0}_{101\times1}, \phi^*_{101\times1}) = 0.967$
$\xi = 0.0083$

$\frac{1}{2\pi}\omega^{\circledR} = 366.1$ Hz
$\frac{1}{2\pi}\sqrt{\lambda^*} = 367.3$ Hz
$mac(\phi^{\circledR}, \phi^*) = 0.730$
$mac(\phi^{\circledR}, \phi^{k=0}) = 0.787$
$mac(\phi^{k=0}, \phi^*) = 0.579$
$mac(\phi^{k=0}_{101\times1}, \phi^*_{101\times1}) = 0.887$
$\xi = 0.0122$

Figure 7.10: Theoretical and experimental mode shapes of the octet modes used in iteration towards State 1; modes 5 and 6; ———— undisplaced frame; ———— theoretical mode shape; ———— experimental mode shape; note that convergence is achieved with the inclusion of the modal tagging strategy.

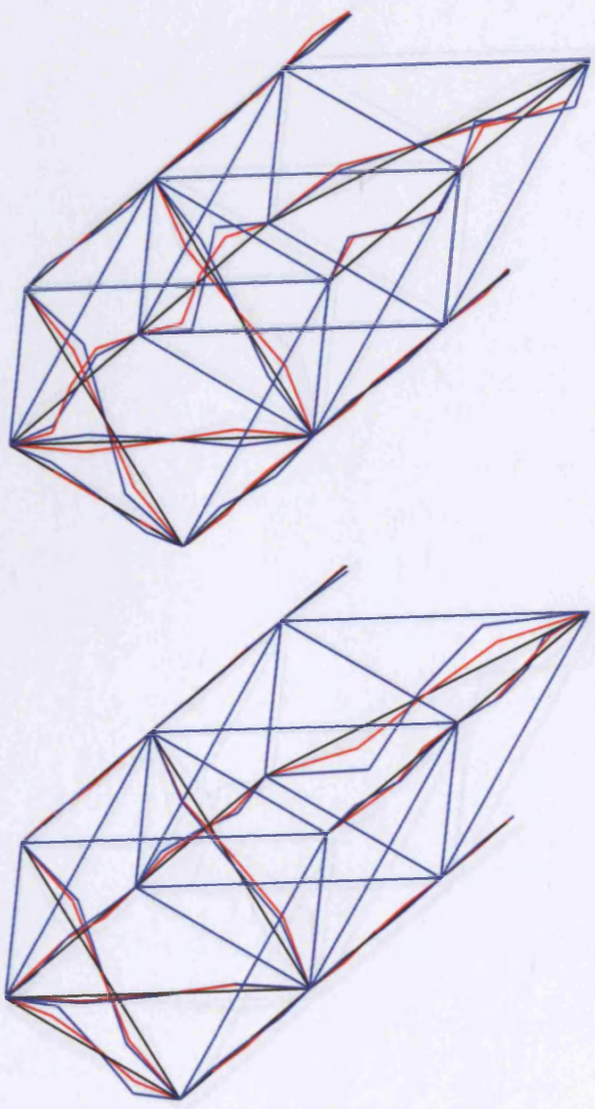

$\frac{1}{2\pi}\omega^{\circledR} = 377.4$ Hz
$\frac{1}{2\pi}\sqrt{\lambda^*} = 376.0$ Hz
$mac(\phi^{\circledR}, \phi^*) = 0.575$
$mac(\phi^{\circledR}, \phi^{k=0}) = 0.551$
$mac(\phi^{k=0}, \phi^*) = 0.691$
$mac(\phi^{k=0}_{101\times1}, \phi^*_{101\times1}) = 0.844$
$\xi = 0.0144$

$\frac{1}{2\pi}\omega^{\circledR} = 410.5$ Hz
$\frac{1}{2\pi}\sqrt{\lambda^*} = 409.8$ Hz
$mac(\phi^{\circledR}, \phi^*) = 0.701$
$mac(\phi^{\circledR}, \phi^{k=0}) = 0.749$
$mac(\phi^{k=0}, \phi^*) = 0.816$
$mac(\phi^{k=0}_{101\times1}, \phi^*_{101\times1}) = 0.651$
$\xi = 0.0089$

Figure 7.11: Theoretical and experimental mode shapes of the octet modes used in iteration towards State 1; modes 7 and 8; ———— undisplaced frame; ———— theoretical mode shape; ———— experimental mode shape; note that convergence is achieved with the inclusion of the modal tagging strategy.

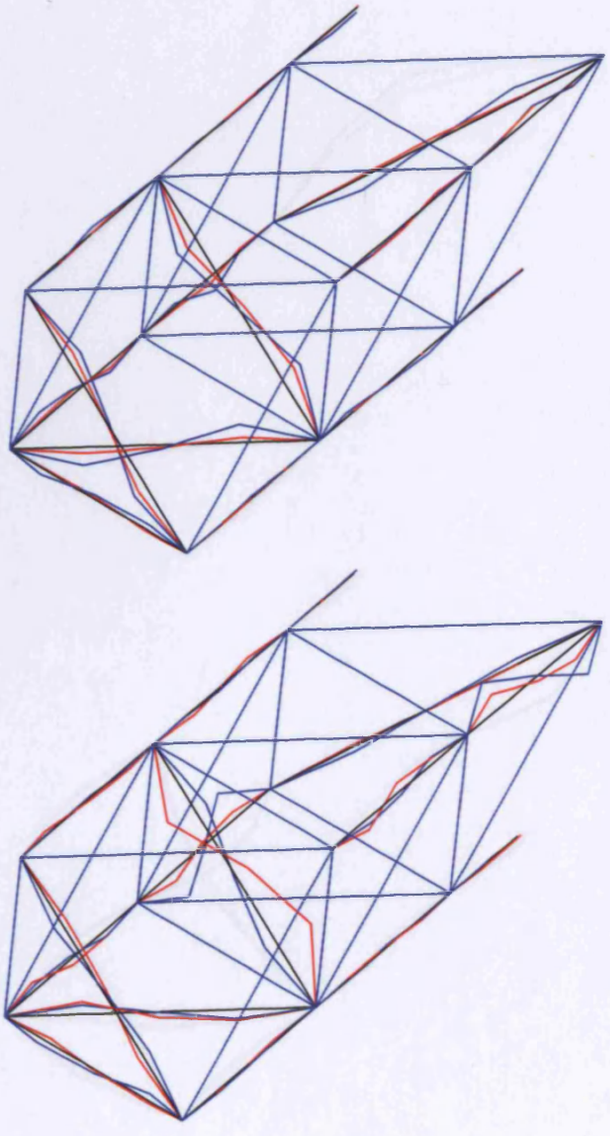

$\frac{1}{2\pi}\omega^{\circledR} = 430.2$ Hz
$\frac{1}{2\pi}\sqrt{\lambda^*} = 428.9$ Hz
$mac(\phi^{\circledR}, \phi^*) = 0.576$
$mac(\phi^{\circledR}, \phi^{k=0}) = 0.471$
$mac(\phi^{k=0}, \phi^*) = 0.595$
$mac(\phi^{k=0}_{101\times1}, \phi^*_{101\times1}) = 0.531$
$\xi = 0.0067$

$\frac{1}{2\pi}\omega^{\circledR} = 519.9$ Hz
$\frac{1}{2\pi}\sqrt{\lambda^*} = 520.3$ Hz
$mac(\phi^{\circledR}, \phi^*) = 0.000$
$mac(\phi^{\circledR}, \phi^{k=0}) = 0.528$
$mac(\phi^{k=0}, \phi^*) = 0.668$
$mac(\phi^{k=0}_{101\times1}, \phi^*_{101\times1}) = 0.178$
$\xi = 0.0125$

Figure 7.12: Theoretical and experimental mode shapes of the octet modes used in iteration towards State 1; modes 9 and 10; ———— undisplaced frame; ———— theoretical mode shape; ———— experimental mode shape; note that convergence is achieved with the inclusion of the modal tagging strategy.

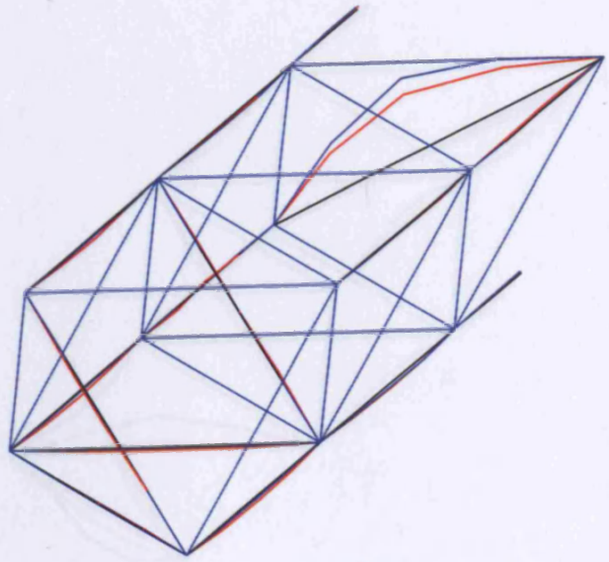

$\frac{1}{2\pi}\omega^{®} = 81.9\,\text{Hz}$
$\frac{1}{2\pi}\sqrt{\lambda^*} = 82.9\,\text{Hz}$
$mac(\phi^{®}, \phi^*) = 0.938$
$mac(\phi^{®}, \phi^{k=0}) = 0.938$
$mac(\phi^{k=0}, \phi^*) = 0.971$
$mac(\phi^{k=0}_{101\times1}, \phi^*_{101\times1}) = 0.999$
$\xi = 0.0397$

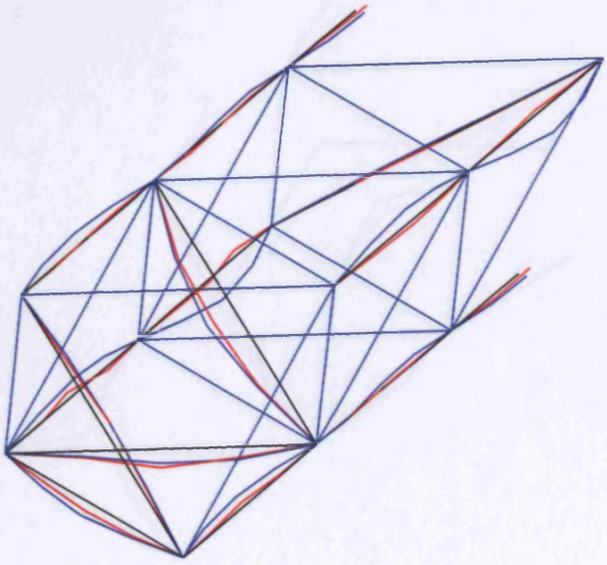

$\frac{1}{2\pi}\omega^{®} = 138.2\,\text{Hz}$
$\frac{1}{2\pi}\sqrt{\lambda^*} = 139.8\,\text{Hz}$
$mac(\phi^{®}, \phi^*) = 0.446$
$mac(\phi^{®}, \phi^{k=0}) = 0.489$
$mac(\phi^{k=0}, \phi^*) = 0.790$
$mac(\phi^{k=0}_{101\times1}, \phi^*_{101\times1}) = 0.723$
$\xi = 0.0121$

Figure 7.13: Theoretical and experimental mode shapes of the octet modes used in iteration towards State 2; modes 1 and 2; ———— undisplaced frame; ———— theoretical mode shape; ———— experimental mode shape; note that convergence is achieved with the inclusion of the modal tagging strategy.

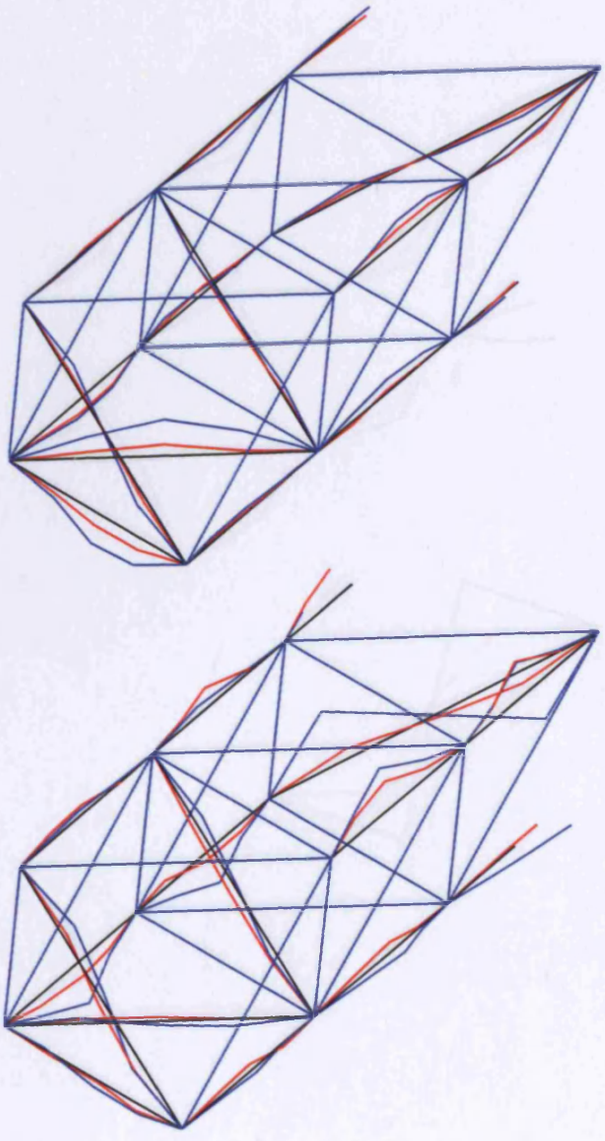

$\frac{1}{2\pi}\omega^{®} = 176.4$ Hz
$\frac{1}{2\pi}\sqrt{\lambda^{*}} = 179.0$ Hz
$mac(\phi^{®}, \phi^{*}) = 0.661$
$mac(\phi^{®}, \phi^{k=0}) = 0.634$
$mac(\phi^{k=0}, \phi^{*}) = 0.953$
$mac(\phi^{k=0}_{101\times1}, \phi^{*}_{101\times1}) = 0.978$
$\xi = 0.0208$

$\frac{1}{2\pi}\omega^{®} = 245.3$ Hz
$\frac{1}{2\pi}\sqrt{\lambda^{*}} = 247.9$ Hz
$mac(\phi^{®}, \phi^{*}) = 0.492$
$mac(\phi^{®}, \phi^{k=0}) = 0.543$
$mac(\phi^{k=0}, \phi^{*}) = 0.917$
$mac(\phi^{k=0}_{101\times1}, \phi^{*}_{101\times1}) = 0.954$
$\xi = 0.0105$

Figure 7.14: Theoretical and experimental mode shapes of the octet modes used in iteration towards State 2; modes 3 and 4; ———— undisplaced frame; ———— theoretical mode shape; ———— experimental mode shape; note that convergence is achieved with the inclusion of the modal tagging strategy.

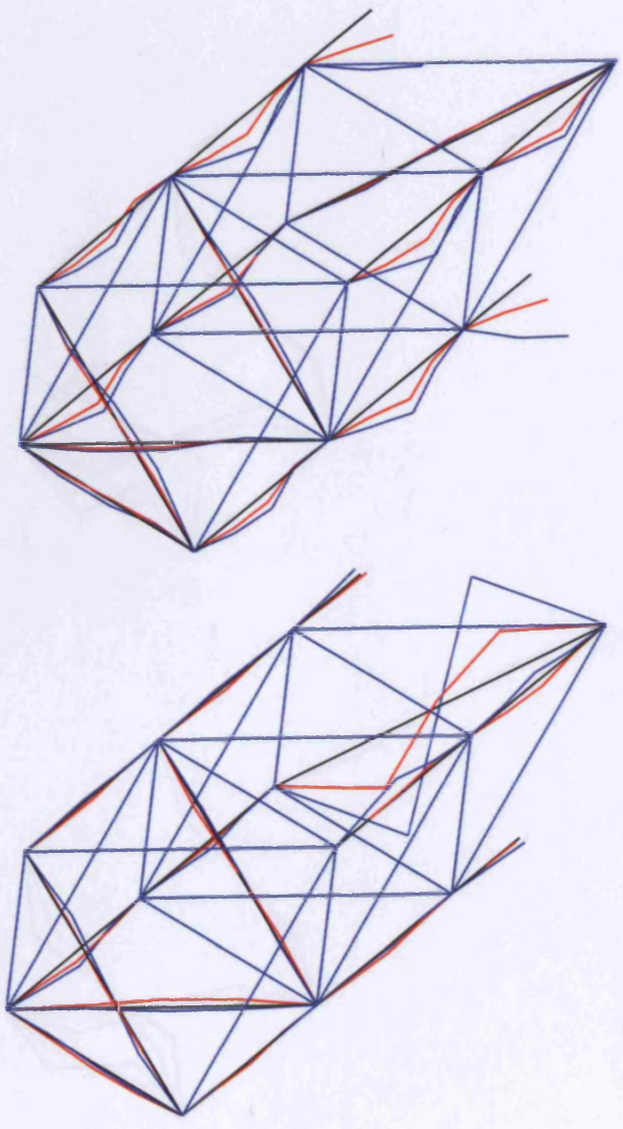

$\frac{1}{2\pi}\omega^{\circledR} = 247.6$ Hz
$\frac{1}{2\pi}\sqrt{\lambda^*} = 245.9$ Hz
$mac(\phi^{\circledR}, \phi^*) = 0.907$
$mac(\phi^{\circledR}, \phi^{k=0}) = 0.867$
$mac(\phi^{k=0}, \phi^*) = 0.900$
$mac(\phi^{k=0}_{101\times1}, \phi^*_{101\times1}) = 0.966$
$\xi = 0.0079$

$\frac{1}{2\pi}\omega^{\circledR} = 266.1$ Hz
$\frac{1}{2\pi}\sqrt{\lambda^*} = 265.8$ Hz
$mac(\phi^{\circledR}, \phi^*) = 0.778$
$mac(\phi^{\circledR}, \phi^{k=0}) = 0.805$
$mac(\phi^{k=0}, \phi^*) = 0.976$
$mac(\phi^{k=0}_{101\times1}, \phi^*_{101\times1}) = 0.992$
$\xi = 0.0173$

Figure 7.15: Theoretical and experimental mode shapes of the octet modes used in iteration towards State 2; modes 5 and 6; ———— undisplaced frame; ———— theoretical mode shape; ———— experimental mode shape; note that convergence is achieved with the inclusion of the modal tagging strategy.

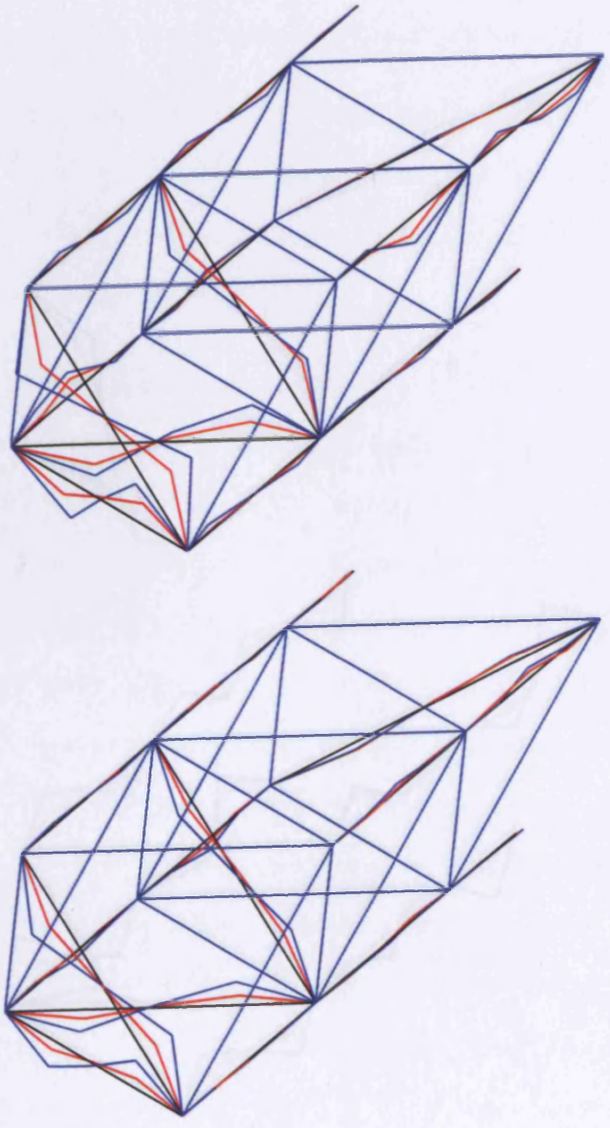

$\frac{1}{2\pi}\omega^{®} = 313.4$ Hz
$\frac{1}{2\pi}\sqrt{\lambda^*} = 314.1$ Hz
$mac(\phi^{®}, \phi^*) = 0.937$
$mac(\phi^{®}, \phi^{k=0}) = 0.905$
$mac(\phi^{k=0}, \phi^*) = 0.972$
$mac(\phi^{k=0}_{101\times1}, \phi^*_{101\times1}) = 0.965$
$\xi = 0.0107$

$\frac{1}{2\pi}\omega^{®} = 358.7$ Hz
$\frac{1}{2\pi}\sqrt{\lambda^*} = 358.2$ Hz
$mac(\phi^{®}, \phi^*) = 0.889$
$mac(\phi^{®}, \phi^{k=0}) = 0.883$
$mac(\phi^{k=0}, \phi^*) = 0.982$
$mac(\phi^{k=0}_{101\times1}, \phi^*_{101\times1}) = 0.989$
$\xi = 0.0098$

Figure 7.16: Theoretical and experimental mode shapes of the octet modes used in iteration towards State 2; modes 7 and 8; ———— undisplaced frame; ———— theoretical mode shape; ———— experimental mode shape; note that convergence is achieved with the inclusion of the modal tagging strategy.

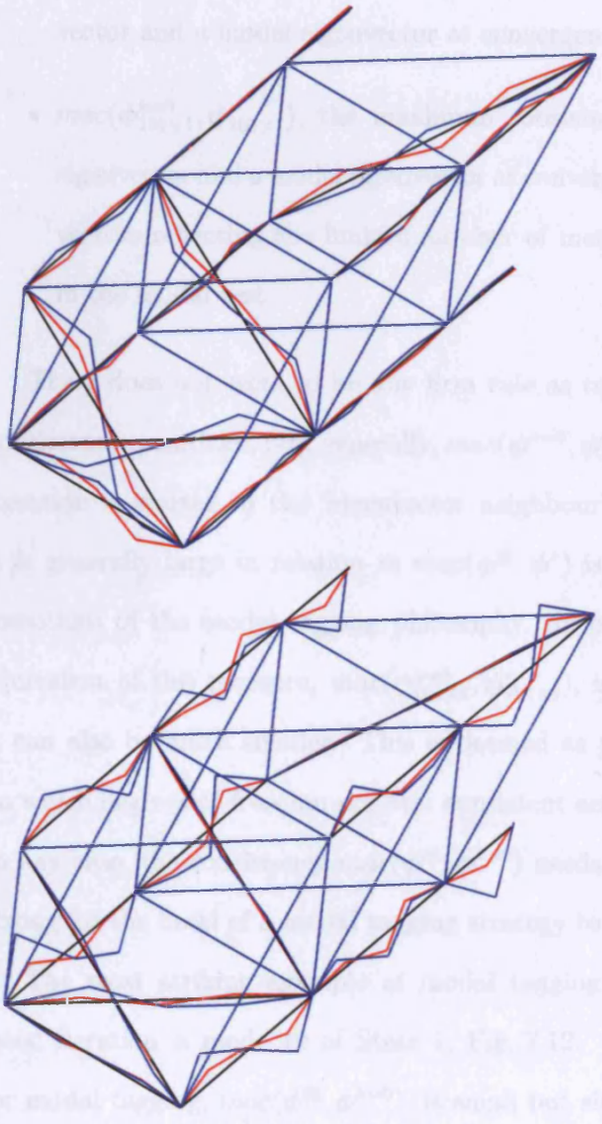

$\frac{1}{2\pi}\omega^{\circledR} = 433.7$ Hz
$\frac{1}{2\pi}\sqrt{\lambda^*} = 433.6$ Hz
$mac(\phi^{\circledR}, \phi^*) = 0.392$
$mac(\phi^{\circledR}, \phi^{k=0}) = 0.552$
$mac(\phi^{k=0}, \phi^*) = 0.882$
$mac(\phi^{k=0}_{101\times1}, \phi^*_{101\times1}) = 0.910$
$\xi = 0.0214$

$\frac{1}{2\pi}\omega^{\circledR} = 660.9$ Hz
$\frac{1}{2\pi}\sqrt{\lambda^*} = 660.8$ Hz
$mac(\phi^{\circledR}, \phi^*) = 0.724$
$mac(\phi^{\circledR}, \phi^{k=0}) = 0.738$
$mac(\phi^{k=0}, \phi^*) = 0.959$
$mac(\phi^{k=0}_{101\times1}, \phi^*_{101\times1}) = 0.991$
$\xi = 0.0058$

Figure 7.17: Theoretical and experimental mode shapes of the octet modes used in iteration towards State 2; modes 9 and 10; ———— undisplaced frame; ———— theoretical mode shape; ———— experimental mode shape; note that convergence is achieved with the inclusion of the modal tagging strategy.

- $mac(\boldsymbol{\phi}^{k=0}, \boldsymbol{\phi}^{*})$, the maximum consistency between the tagging eigenvector and a model eigenvector at convergence;

- $mac(\boldsymbol{\phi}^{k=0}_{101\times 1}, \boldsymbol{\phi}^{*}_{101\times 1})$, the maximum consistency between the tagging eigenvector and a model eigenvector at convergence, with reduced eigenvectors reflecting the limited number of measured degrees of freedom in the modal test.

There does not seem to be any firm rule as to the magnitudes of these consistency quantities, but, generally, $mac(\boldsymbol{\phi}^{k=0}, \boldsymbol{\phi}^{*})$ is large, suggesting that iteration is started in the 'eigenvector neighbourhood' of the root. That it is generally large in relation to $mac(\boldsymbol{\phi}^{\circledR}, \boldsymbol{\phi}^{*})$ is also encouraging for the intentions of the modal tagging philosophy. In certain cases, the reduced equivalent of this measure, $mac(\boldsymbol{\phi}^{k=0}_{101\times 1}, \boldsymbol{\phi}^{*}_{101\times 1})$, is much greater, although it can also be much smaller. This is deemed as pure chance and depends on which degrees of freedom are best consistent across a parameter interval. In any case, the consistency $mac(\boldsymbol{\phi}^{\circledR}, \boldsymbol{\phi}^{k=0})$ needs to be, and is seen to be, strong for the basis of a modal tagging strategy to be established at all.

The most striking example of modal tagging saving an otherwise ill-fated iteration is mode 10 of State 1, Fig. 7.12. For this mode, the basis for modal tagging, $mac(\boldsymbol{\phi}^{\circledR}, \boldsymbol{\phi}^{k=0})$, is small but significant and the tagging eigenvector returns a reasonable consistency with the converged eigenvector, $mac(\boldsymbol{\phi}^{k=0}, \boldsymbol{\phi}^{*}) = 0.668$. What is surprising is that the experimental mode shape is completely inconsistent with the converged eigenvector, $mac(\boldsymbol{\phi}^{\circledR}, \boldsymbol{\phi}^{*}) \approx 0$ (note that these values are the *maximum* consistencies

achieved), even though, to the nearest integer, iteration with the modal tagging strategy has brought the model frequency equal to the experimental frequency. Inspection of the mode shape plot reveals the reason for this. At first glance, the experimental and model mode shapes seem consistent, and indeed they are, except that roughly half of the members of the former are π radians out of phase with those of the latter but oscillating in the same local modes. It is understandable why, notwithstanding this fact, the experimental and converged model frequencies are almost the same, since two such mode shapes would be associated with the same vibration energy. Even though all indications suggest that these are the same mode, as far as the scrutiny of *mac* is concerned, they are almost orthogonal[1]. This is at least one mechanism by which mode shapes are susceptible to erratic change.

Damping factors for all modes were low and the octet frame, which is considerably larger than the bi-tetrahedral frame, was also known to resonate for lengthy periods following impact excitation. Fig. 7.7 shows that some damping is present, but the peaks are still well defined enough for damping not to become significant to the mathematical description.

It is necessary to investigate the attributes of the starting points for iteration to State 1 and State 2, and the modal tagging strategy further. Fig. 7.18 and Fig. 7.19 are parameter-*mac* maps illustrating the maximum consistency between each experimental mode shape and eigenvectors at various values of load parameters p_{u_1} and p_{u_2}, with the remaining four parameters constant.

[1]It is for the same reason why, for some angle θ defined regularly over $[0, 2\pi]$ and a vector defined by $\phi_i = \sin\theta_i$, $mac(\phi, \phi) = 1$ while $mac(\phi, |\phi|) = 0$.

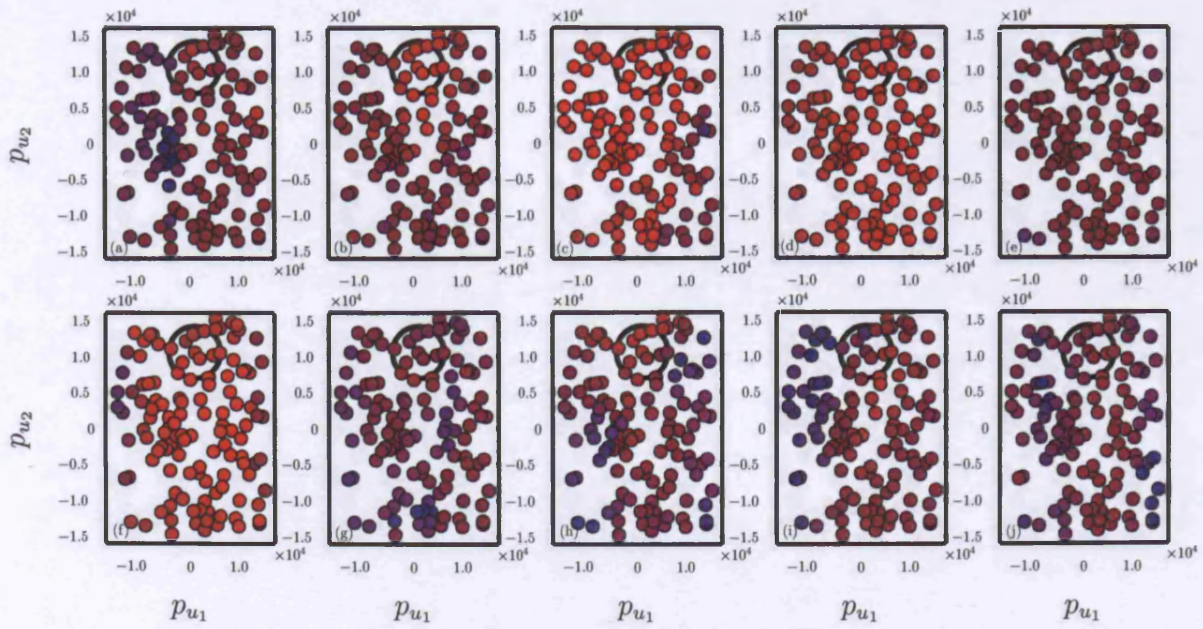

Figure 7.18: Parameter-$mac(\phi^{\circledR}, \phi(p_{u_1}, p_{u_2}))$ maps for octet frame State 1; $p_{u_3} = 2500$, $\eta_1 = 0.00$, $\eta_2 = 0.02$ and $L = 0.42$; 0 1 *mac* consistency scale; (a)-(j), experimental modes 1-10, respectively; starting point encircled.

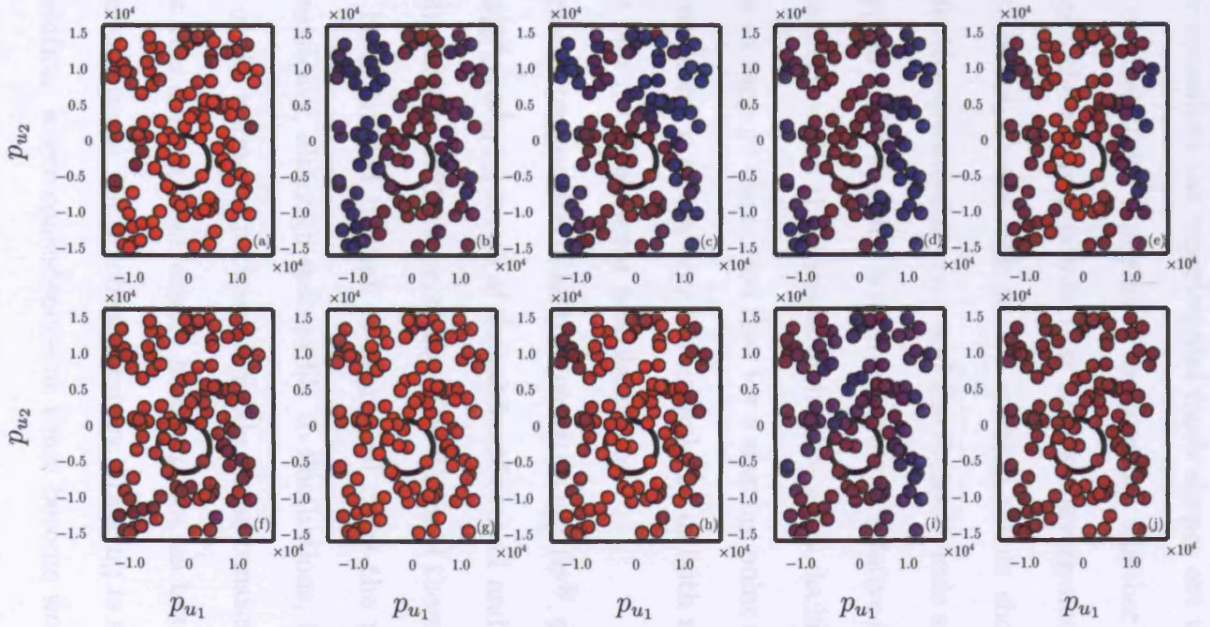

Figure 7.19: Parameter-$mac(\phi^{\circledR}, \phi(p_{u_1}, p_{u_2}))$ maps for octet frame State 2; $p_{u_3} = 5000$, $\eta_1 = 0.00$, $\eta_2 = 0.02$ and $L = 0.42$; 0 1 *mac* consistency scale; (a)-(j), experimental modes 1-10, respectively; starting point encircled.

The points of the figures have been generated by randomly varying p_{u_1} and p_{u_2} within the limits 1.5×10^4 and -1.5×10^4; the colour scale is indicative of how consistent the experimental mode shapes are with the randomly generated eigenvectors. The aim is to recognise whether there is anything special about the starting points that allows convergence to ensue. While consistency is not always high at the starting points chosen (this may be attributable to experimental error and the limited mode shape description), they do appear to be situated within hotspots of relative strength of consistency, away from which the maps demonstrate great declines in consistency. This serves to support the notion that for a starting point to succeed in leading to convergence, it at the very least should be in both the neighbourhood of the root *and* its 'eigenvector neighbourhood'.

The iterative progression of all the quantities $mac(\boldsymbol{\phi}^{\circledR}, \boldsymbol{\phi}^k)$, $mac(\boldsymbol{\phi}^{k=0}, \boldsymbol{\phi}^k)$ and $mac(\boldsymbol{\phi}^{k=0}_{101\times1}, \boldsymbol{\phi}^k_{101\times1})$ for all of the modes of State 1 and State 2 are shown in Fig. 7.20 and Fig. 7.21, respectively. The desire of the modal tagging proposal has been fulfilled in that in nearly all cases the progression of the tagged consistency, although susceptible to fluctuations, is at higher values than that of the normal experimental mode shape consistency during iteration. That this does not universally hold exposes, as has been anticipated, that modal tagging is not a robust strategy. Tagging is more useful in the State 1 iteration, where consistencies at times become worrying small. The tagged consistency that involves the reduced eigenvectors in some instances is greater than the tagged consistency with the full eigenvectors. As stated be-

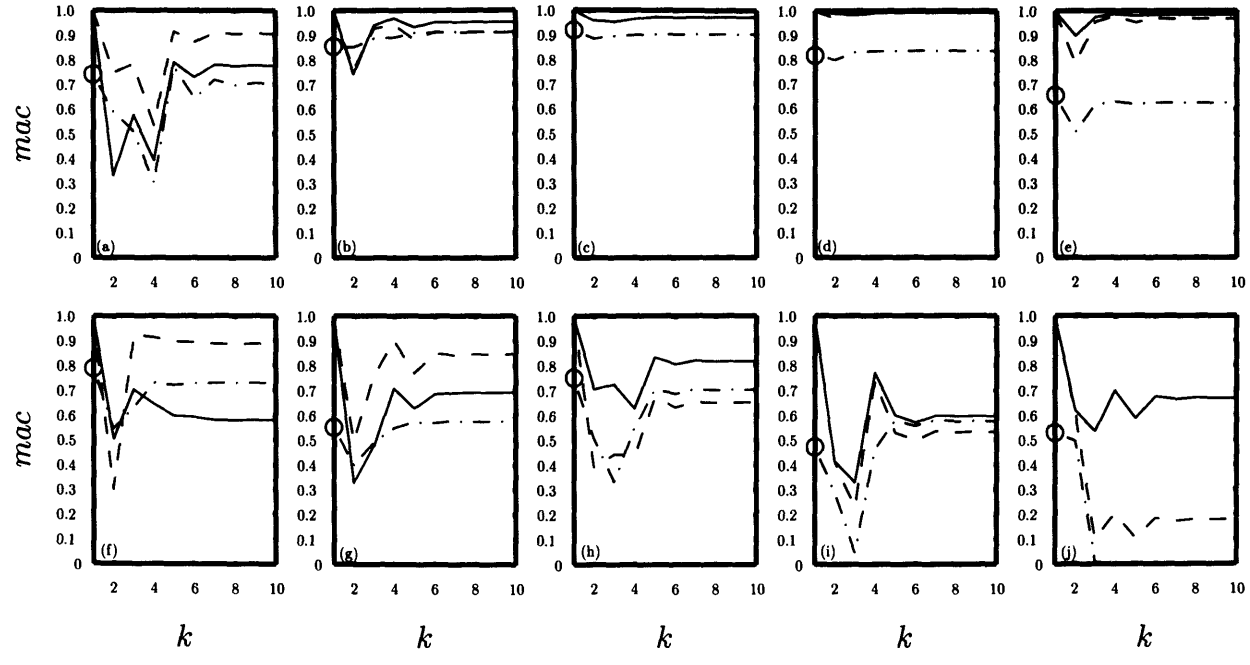

Figure 7.20: Iterative progression of maximum consistency values for octet frame State 1: O $mac(\phi^{\circledR}, \phi^{k=0})$; · – · – – · $mac(\phi^{\circledR}, \phi^{k})$; ———— $mac(\phi^{k=0}, \phi^{k})$; – – – – $mac(\phi^{k=0}_{101\times1}, \phi^{k}_{101\times1})$; (a)-(j), experimental modes 1-10, respectively; note that convergence is achieved with the inclusion of the modal tagging strategy.

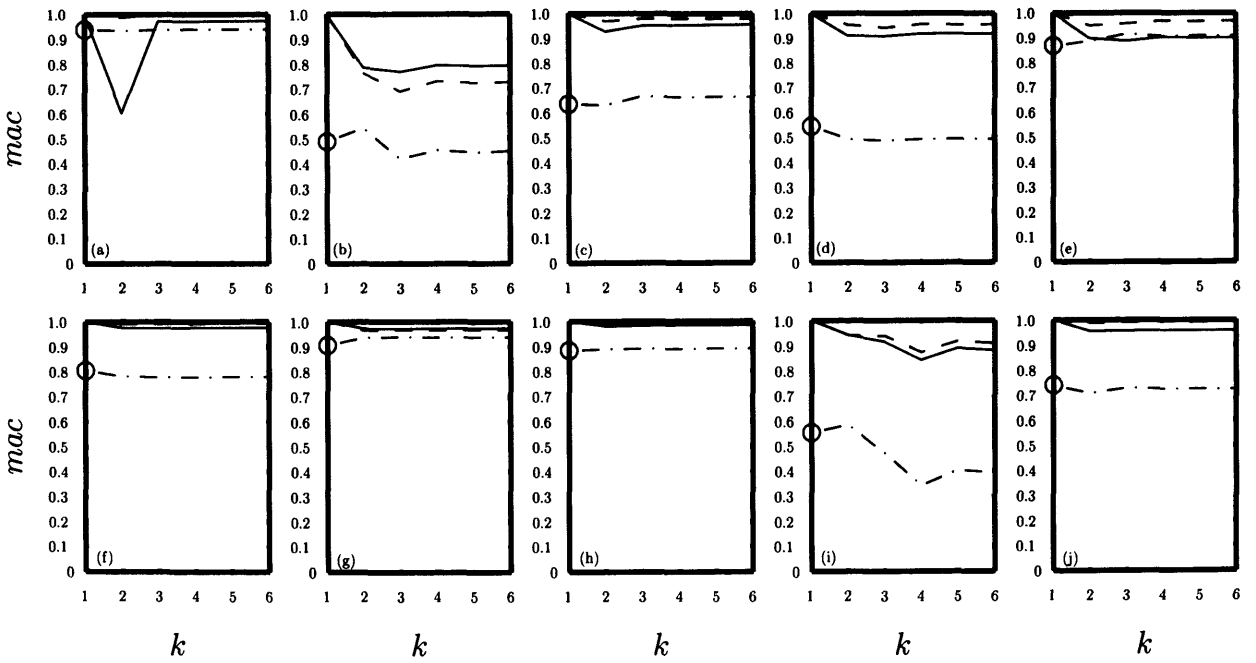

Figure 7.21: Iterative progression of maximum consistency values for octet frame State 2: O $mac(\phi^{\circledR}, \phi^{k=0})$; · — · — · $mac(\phi^{\circledR}, \phi^{k})$; ———— $mac(\phi^{k=0}, \phi^{k})$; — — — — $mac(\phi^{k=0}_{101\times1}, \phi^{k}_{101\times1})$; (a)-(j), experimental modes 1-10, respectively; note that convergence is achieved with the inclusion of the modal tagging strategy.

fore, this is deemed as pure chance and depends on which degrees of freedom are most consistent across a parameter interval. The fact that the reduced tagged measure is also, in other instances, troublingly below the unreduced tagged measure of consistency, suggests that if modal tagging is to be employed, it should be done so with all of the available degrees of freedom.

Overall, the identification of load in the thrice redundant octet frame has been a success, but whose solutions have been obscure and considerably demanding to find. The length, offset and load parameters that provided success for the bi-tetrahedral frame have been here employed to update the finite element model to be in very good agreement with physically observed measurements, in all aspects: mode shapes, frequencies and frequency response functions.

The issue of mode shape consistency has been investigated and the strategy of modal tagging has been seen to save an otherwise ill-fated iteration by artificially raising eigenvector consistency. Modal tagging is certainly not a robust measure and should be seen rather as an aid offering more insight into how eigenvectors should be paired between the current iterate and the root. It must be stressed that for such a large structure accommodating many members, the dynamic model is of such a nature as to make success of iteration the exception rather than the rule. What has been given here is two successful convergences, both of which presented obscure roots. The question of finding a global method of locating a starting point for Newton's method in the present context is still open to investigation. It would need

to take into account the volatility of the eigenvectors as well as the intricacy and erratic nature of the eigenvalue loci. What is encouraging is that roots to the force identification problem do exist, even for more complicated, multiply redundant space frames, and are easily found if iteration commences suitably close; it is locating the starting point that remains an issue.

Chapter 8

Epilogue

General conclusions for the work undertaken in this thesis are herein drawn, the potential uses of the title method noted and possible directions for future research suggested.

8.1 General Conclusions

A survey of the literature has revealed that, while the dynamics of axially loaded beams have long been understood, the way in which distributions of axial force affect the dynamics of frames is a relatively unexplored area of research. The finite element models of the frames in this thesis have served to show that the eigenvalue loci may be inferred as the coupled, individual, constituent member loci. Further, certain phenomena analogise with single beam characteristics, for example, the fundamental, global frame mode vanishes at buckling and rigid body modes have been seen to transform to flexural modes at high levels of predominantly tensile load.

It has been found that any state of frame equilibrium can be expressed through the superposition of a number of linearly independent distributions of axial force, equal to the degree of static redundancy. Enforcing such equilibrium constraints has greatly reduced the number of updating parameters compared to the approach of Greening (1999), which involves as many parameters as there are frame members. As well as iterating in a lower number of dimensions, there is a resulting improvement to the condition of Newton's method. Singular value decomposition of the equilibrium matrix has been a useful way to offer insight into the number of linearly independent force distributions necessary to describe any state of frame equilibrium. Although Maxwell's formula may be a more efficient way in which to determine this number, the decomposition further indicates the similarities between the force distributions and allows an orthogonal basis to be formed to describe

them.

Function discontinuity at points of eigenvalue coalescence means that evaluation of the eigenpair derivatives there needs particular attention for differentiability to be observed. Degeneracy associated with transitorily coalesced eigenvalues has been overcome, to make differentiability observable, through methods from the literature that anticipate the separation of the eigenvectors into distinct spaces along with the separation of the eigenvalues. The derivatives of eigenvectors of permanently degenerate eigenvalues are noted to be valid but non-unique, since the eigenvector spaces never separate. There are seen to be special cases of coalescence involving distinct and permanently degenerate loci, for which it is necessary to use usual methods in combination with methods of vector orthonormalisation.

The fact that eigenvalues coalesce, and that eigenpairs are ordered according to the magnitudes of the eigenvalues, means that the functions upon which Newton's method is formulated are generally non-smooth. Iteration is known to be encumbered by such discontinuous functions. Mode tracing, which makes use of the consistency of eigenvectors of the eigenvalue loci across coalescence, has been cited and experienced to be a measure of generally overcoming function discontinuity and preserving smoothness.

Eigenvalue locus veering is noted to be a detrimental mechanism of eigenvector consistency deterioration that can severely disrupt mode tracing, which relies on this consistency to discern function smoothness. When successful at veering, mode tracing causes iterates to transcend loci past veering events;

when unsuccessful, iteration can fail altogether because of erroneous mode pairings. The veerings, which relate to modal coupling, mark rapid changes in the eigenvectors so that they can become unrecognisable. An augmented modal assurance routine, which casts eigenvectors based on their derivatives and the parameter perturbation between iterates, has been proposed and seen to offer extra insight into how modes should be paired when consistency is deficient. Mode tracing in permanently degenerate loci requires that the eigenvectors be numerically aligned across parameter intervals since such eigenvectors are arbitrarily oriented.

Shortcomings of the modal assurance criterion have been brought to light by comparison to the more natural eigenvector consistency evaluation of cross-orthogonality or cross-mass-orthogonality. The unpredictability of the modal assurance criterion has been partly attributed to its artificial, scaling denominator. Unfortunately, since cross-mass-orthogonality involves the mass matrix by definition, it cannot be applied to experimental data, for which a limited number of degrees of freedom are measured, unless disruptive, artificial reduction or expansion techniques are applied.

Under certain conditions, eigenvector consistency has been seen to be quasi-linearly related to the eigenvalue derivative. These include the relative location of the datum eigenvector and the simplicity of the veering characteristic. This is a natural consequence of the variation of eigenvectors being related to the degree of non-linearity of their eigenvalue loci.

Overdeterminacy of Newton's method decreases the likelihood of converg-

ing upon an erroneous root and also generally decreases the error range at convergence.

Numerical simulations have served to show that the proposed method of force identification formulated on force distributions is successful for a variety of space frames. Locus plots for progressively more complicated frames show that, because the loci are the coupled systems of the constituent beams, with an increasing number of frame members the loci become more intricate and erratic. This is detrimental to Newton's method and is exemplified in a simulation of a frame with a large number of members. While simple frames are almost guaranteed convergence, for more complicated ones convergence is the exception rather than the rule and hinges largely on the proximity of the starting point to the root. What is meant by proximity is not only the eigenvalue neighbourhood of the root, but also the eigenvector neighbourhood because, for erratic loci, consistency has been seen to deteriorate very rapidly away from the root, making mode traces in some instances impossible.

For symmetric space frames with multiple axes of spatial periodicity, there will be interchangeable independent parameters of force that each affect the eigenvalues identically. If Newton's method is formulated upon these parameters, and even though the resulting set of equations is non-singular, there exist ambiguous roots that incorrectly ascribe member forces. Such an issue is wholly alleviated through employing mode tracing, which utilises the uniqueness of the force distribution to mode shape relation.

Newton's method has proved successful in identifying the level of load

in a real, physical, once redundant space frame. Following suggestions from the literature, offset and length parameters have been used to supplement a single load parameter to make the finite element model frequencies converge to a very good degree upon those measured for the frame. These physically meaningful, supplementary parameters are seen as a necessary inclusion in terms of both accuracy of identification and stabilising convergence; they may capture secondary effects of loading that Greening (1999) formerly accounted for with deformation. Experimentally determined modes are noted to exchange places in the spectrum, which is indicative of eigenvalue coalescence and veering phenomena. While identification has not been entirely accurate, tests at a number of different loads have indicated that iteration has converged to an encouraging degree. That an unconstrained Newton's method has resulted in convergence to physically determined data to identify load as well as it has is promising, especially considering that the literature shows little success of updating to experimental data.

The same success is met in identifying load in a more complicated space frame, with multiple force distributions, utilising load, offset and length parameters. Updating force distributions is seen not only to succeed, but not to be affected in terms of accuracy by the presence of more than one force parameter. Constraint is provided by the state of equilibrium, irrespective of the number of linearly independent force distributions required in describing it. Some beneficial strategies for more complicated frames have been suggested. Prudently, Newton's method should be formulated on an ortho-

normal basis for the distributions of force to ensure that the problem is well conditioned. Modal tagging, which tags experimental frequencies with mathematical eigenvectors based on consistency with experimental mode shapes in the neighbourhood of the root is seen to increase, generally, mode tracing confidence during iteration. In some instances, it can rescue an otherwise ill-fated iteration. It is again noted that the mode shape consistency greatly, and rapidly, deteriorates away from the root and that starting iteration in both the eigenvalue and eigenvector neighbourhood is crucial. It remains to find a global convergence strategy for the present context. Traditional global convergence strategies for Newton's method (e.g., line search) do not lend themselves because they cannot circumvent the eigenvector consistency deterioration problem.

One of the reasons for not using eigenvectors as the functions in Newton's method was the assumption that they are relatively insensitive to load, compared to the eigenvalues. This has been shown to be not always the case — at locus veering — and eigenvectors can undoubtedly become candidate functions at certain ranges of load to offer greater overdeterminacy.

The work in this thesis has highlighted the issue of defining a mode. When dependent upon such parameters as load, the definition of a mode becomes somewhat superficial as both the frequency and mode shape can change dramatically. In a landscape of varying dynamic characteristics, it is more sensible to speak of modes dying and being born as parameters are gradually perturbed; they can even resurrect, as seen following veering events.

8.2 Potential of Work Undertaken

The method of force identification outlined and described in this thesis has a number of potential uses. It is a useful way to account for load in a finite element model of a space frame that is susceptible to loading, particularly variable loading. There are also repercussions for monitoring the axial forces in space frames in a way that is, in a sense, more robust, albeit less accurate, compared to using strain gauges. The reason for this is that once gauges have failed, all knowledge of a load datum at which to configure new gauges is lost. Force identification from dynamic data could identify this load datum. For only a small number of gauge failures, Newton's method would have the potential of converging more accurately as extra information would be available from the functioning gauges. Finally, Newton's method could further be applied to the mathematically identical problem of determining the loads to be applied to a space frame to achieve a prescribed set of frequency magnitudes.

8.3 Future Research

There are some issues that remain to be addressed and would form areas of future research. Although there was success in identifying load in both singly and multiply redundant, real space frames, the accuracy of identification can still be improved. Ways in which to do so may include describing the set of offset parameters to greater detail or even parameterising with additional variables indicated by an error location technique. Updating deformation, as advocated by Greening (1999), may further help to obtain more accurate

solutions.

Another issue is the eigenvector consistency deterioration problem, which exists for complicated frames with a great number of constituent members. Some global convergence method needs to be sought that overcomes this predicament so that convergence can ensue from greater regions of the iteration space. This thesis has gone some way into viewing eigenvector consistency as a function of load. The augmented modal assurance routine was even seen to alleviate ambiguity of tracing modes at a veering event. Perhaps future work could investigate methods that involve perturbation expansions of the eigenproblem at a particular iterate and in this way attempt to approximate the eigenpairs at the proceeding iterate — consideration would of course need to be given to the associated computational cost. There may be merits in formulating the problem on frequency response function data rather than modal data.

Ultimately, future work should focus on making Newton's method for static force inference more mathematically robust and accurate.

Appendix A

Elemental Matrices and Their Derivatives

$$\mathbf{K}^e = \begin{bmatrix}
\frac{EA}{L} & 0 & 0 & 0 & 0 & 0 & -\frac{EA}{L} & 0 & 0 & 0 & 0 & 0 \\
0 & 12\frac{EI_z}{L^3} & 0 & 0 & 0 & 6\frac{EI_z}{L^2} & 0 & -12\frac{EI_z}{L^3} & 0 & 0 & 0 & 6\frac{EI_z}{L^2} \\
0 & 0 & 12\frac{EI_y}{L^3} & 0 & -6\frac{EI_y}{L^2} & 0 & 0 & 0 & -12\frac{EI_y}{L^3} & 0 & -6\frac{EI_y}{L^2} & 0 \\
0 & 0 & 0 & \frac{GJ}{L} & 0 & 0 & 0 & 0 & 0 & -\frac{GJ}{L} & 0 & 0 \\
0 & 0 & -6\frac{EI_y}{L^2} & 0 & 4\frac{EI_y}{L} & 0 & 0 & 0 & 6\frac{EI_y}{L^2} & 0 & 2\frac{EI_y}{L} & 0 \\
0 & 6\frac{EI_z}{L^2} & 0 & 0 & 0 & 4\frac{EI_z}{L} & 0 & -6\frac{EI_z}{L^2} & 0 & 0 & 0 & 2\frac{EI_z}{L} \\
-\frac{EA}{L} & 0 & 0 & 0 & 0 & 0 & \frac{EA}{L} & 0 & 0 & 0 & 0 & 0 \\
0 & -12\frac{EI_z}{L^3} & 0 & 0 & 0 & -6\frac{EI_z}{L^2} & 0 & 12\frac{EI_z}{L^3} & 0 & 0 & 0 & -6\frac{EI_z}{L^2} \\
0 & 0 & -12\frac{EI_y}{L^3} & 0 & 6\frac{EI_y}{L^2} & 0 & 0 & 0 & 12\frac{EI_y}{L^3} & 0 & 6\frac{EI_y}{L^2} & 0 \\
0 & 0 & 0 & -\frac{GJ}{L} & 0 & 0 & 0 & 0 & 0 & \frac{GJ}{L} & 0 & 0 \\
0 & 0 & -6\frac{EI_y}{L^2} & 0 & 2\frac{EI_y}{L} & 0 & 0 & 0 & 6\frac{EI_y}{L^2} & 0 & 4\frac{EI_y}{L} & 0 \\
0 & 6\frac{EI_z}{L^2} & 0 & 0 & 0 & 2\frac{EI_z}{L} & 0 & -6\frac{EI_z}{L^2} & 0 & 0 & 0 & 4\frac{EI_z}{L}
\end{bmatrix}$$

i. Elemental structural stiffness matrix

$$\mathbf{G}^e = \frac{e_{ij}}{L} \begin{bmatrix}
1 & 0 & 0 & 0 & 0 & 0 & -1 & 0 & 0 & 0 & 0 & 0 \\
0 & \frac{6}{5} & 0 & 0 & 0 & \frac{1}{10}L & 0 & -\frac{6}{5} & 0 & 0 & 0 & \frac{1}{10}L \\
0 & 0 & \frac{6}{5} & 0 & -\frac{1}{10}L & 0 & 0 & 0 & -\frac{6}{5} & 0 & -\frac{1}{10}L & 0 \\
0 & 0 & 0 & \frac{J}{A} & 0 & 0 & 0 & 0 & 0 & -\frac{J}{A} & 0 & 0 \\
0 & 0 & -\frac{1}{10}L & 0 & \frac{2}{15}L^2 & 0 & 0 & 0 & \frac{1}{10}L & 0 & -\frac{1}{30}L^2 & 0 \\
0 & \frac{1}{10}L & 0 & 0 & 0 & \frac{2}{15}L^2 & 0 & -\frac{1}{10}L & 0 & 0 & 0 & -\frac{1}{30}L^2 \\
-1 & 0 & 0 & 0 & 0 & 0 & 1 & 0 & 0 & 0 & 0 & 0 \\
0 & -\frac{6}{5} & 0 & 0 & 0 & -\frac{1}{10}L & 0 & \frac{6}{5} & 0 & 0 & 0 & -\frac{1}{10}L \\
0 & 0 & -\frac{6}{5} & 0 & \frac{1}{10}L & 0 & 0 & 0 & \frac{6}{5} & 0 & \frac{1}{10}L & 0 \\
0 & 0 & 0 & -\frac{J}{A} & 0 & 0 & 0 & 0 & 0 & \frac{J}{A} & 0 & 0 \\
0 & 0 & -\frac{1}{10}L & 0 & -\frac{1}{30}L^2 & 0 & 0 & 0 & \frac{1}{10}L & 0 & \frac{2}{15}L^2 & 0 \\
0 & \frac{1}{10}L & 0 & 0 & 0 & -\frac{1}{30}L^2 & 0 & -\frac{1}{10}L & 0 & 0 & 0 & \frac{2}{15}L^2
\end{bmatrix}$$

ii. Elemental geometric stiffness matrix

$$\mathbf{M}^e = \rho AL \begin{bmatrix}
\frac{1}{3} & 0 & 0 & 0 & 0 & 0 & \frac{1}{6} & 0 & 0 & 0 & 0 & 0 \\
0 & \frac{13}{35}+\frac{6}{5}\frac{I_z}{AL^2} & 0 & 0 & 0 & \frac{11}{210}L+\frac{1}{10}\frac{I_z}{AL} & 0 & \frac{9}{70}-\frac{6}{5}\frac{I_z}{AL^2} & 0 & 0 & 0 & -\frac{13}{420}L+\frac{1}{10}\frac{I_z}{AL} \\
0 & 0 & \frac{13}{35}+\frac{6}{5}\frac{I_y}{AL^2} & 0 & -\frac{11}{210}L-\frac{1}{10}\frac{I_y}{AL} & 0 & 0 & 0 & \frac{9}{70}-\frac{6}{5}\frac{I_y}{AL^2} & 0 & \frac{13}{420}L-\frac{1}{10}\frac{I_y}{AL} & 0 \\
0 & 0 & 0 & \frac{1}{3}\frac{J}{A} & 0 & 0 & 0 & 0 & 0 & \frac{1}{6}\frac{J}{A} & 0 & 0 \\
0 & 0 & -\frac{11}{210}L-\frac{1}{10}\frac{I_y}{AL} & 0 & \frac{1}{105}L^2+\frac{2}{15}I_yA & 0 & 0 & 0 & -\frac{13}{420}L+\frac{1}{10}\frac{I_y}{AL} & 0 & -\frac{1}{140}L^2-\frac{1}{30}\frac{I_y}{A} & 0 \\
0 & \frac{11}{210}L+\frac{1}{10}\frac{I_z}{AL} & 0 & 0 & 0 & \frac{1}{105}L^2+\frac{2}{15}I_zA & 0 & \frac{13}{420}L-\frac{1}{10}\frac{I_z}{AL} & 0 & 0 & 0 & -\frac{1}{140}L^2-\frac{1}{30}\frac{I_z}{A} \\
\frac{1}{6} & 0 & 0 & 0 & 0 & 0 & \frac{1}{3} & 0 & 0 & 0 & 0 & 0 \\
0 & \frac{9}{70}-\frac{6}{5}\frac{I_z}{AL^2} & 0 & 0 & 0 & \frac{13}{420}L-\frac{1}{10}\frac{I_z}{AL} & 0 & \frac{13}{35}+\frac{6}{5}\frac{I_z}{AL^2} & 0 & 0 & 0 & -\frac{11}{210}L-\frac{1}{10}\frac{I_z}{AL} \\
0 & 0 & \frac{9}{70}-\frac{6}{5}\frac{I_y}{AL^2} & 0 & -\frac{13}{420}L+\frac{1}{10}\frac{I_y}{AL} & 0 & 0 & 0 & \frac{13}{35}+\frac{6}{5}\frac{I_y}{AL^2} & 0 & \frac{11}{210}L+\frac{1}{10}\frac{I_y}{AL} & 0 \\
0 & 0 & 0 & \frac{1}{6}\frac{J}{A} & 0 & 0 & 0 & 0 & 0 & \frac{1}{3}\frac{J}{A} & 0 & 0 \\
0 & 0 & \frac{13}{420}L-\frac{1}{10}\frac{I_y}{AL} & 0 & -\frac{1}{140}L^2-\frac{1}{30}\frac{I_y}{A} & 0 & 0 & 0 & \frac{11}{210}L+\frac{1}{10}\frac{I_y}{AL} & 0 & \frac{1}{105}L^2+\frac{2}{15}I_yA & 0 \\
0 & -\frac{13}{420}L+\frac{1}{10}\frac{I_z}{AL} & 0 & 0 & 0 & -\frac{1}{140}L^2-\frac{1}{30}\frac{I_z}{A} & 0 & -\frac{11}{210}L-\frac{1}{10}\frac{I_z}{AL} & 0 & 0 & 0 & \frac{1}{105}L^2+\frac{2}{15}I_zA
\end{bmatrix}$$

iii. Elemental mass matrix

$$\mathbf{K}^e = \begin{bmatrix}
\frac{EA}{L} & 0 & 0 & 0 & 0 & 0 & -\frac{EA}{L} & 0 & 0 & 0 & 0 & 0 \\
0 & 12\frac{EI_z}{L^3} & 0 & 0 & 0 & 12\frac{\eta EI_z}{L^3} + 6\frac{EI_z}{L^2} & 0 & -12\frac{EI_z}{L^3} & 0 & 0 & 0 & 6\frac{EI_z}{L^2} \\
0 & 0 & 12\frac{EI_y}{L^3} & 0 & -12\frac{\eta EI_y}{L^3} - 6\frac{EI_y}{L^2} & 0 & 0 & 0 & -12\frac{EI_y}{L^3} & 0 & -6\frac{EI_y}{L^2} & 0 \\
0 & 0 & 0 & \frac{GJ}{L} & 0 & 0 & 0 & 0 & 0 & -\frac{GJ}{L} & 0 & 0 \\
0 & 0 & -12\frac{\eta EI_y}{L^3} - 6\frac{EI_y}{L^2} & 0 & 12\frac{\eta^2 EI_y}{L^3} + 12\frac{\eta EI_y}{L^2} + 4\frac{EI_y}{L} & 0 & 0 & 0 & 12\frac{\eta EI_y}{L^3} + 6\frac{EI_y}{L^2} & 0 & 6\frac{\eta EI_y}{L^2} + 2\frac{EI_y}{L} & 0 \\
0 & 12\frac{\eta EI_z}{L^3} + 6\frac{EI_z}{L^2} & 0 & 0 & 0 & 12\frac{\eta^2 EI_z}{L^3} + 12\frac{\eta EI_z}{L^2} + 4\frac{EI_z}{L} & 0 & -12\frac{\eta EI_z}{L^3} - 6\frac{EI_z}{L^2} & 0 & 0 & 0 & 6\frac{\eta EI_z}{L^2} + 2\frac{EI_z}{L} \\
-\frac{EA}{L} & 0 & 0 & 0 & 0 & 0 & \frac{EA}{L} & 0 & 0 & 0 & 0 & 0 \\
0 & -12\frac{EI_z}{L^3} & 0 & 0 & 0 & -12\frac{\eta EI_z}{L^3} - 6\frac{EI_z}{L^2} & 0 & 12\frac{EI_z}{L^3} & 0 & 0 & 0 & -6\frac{EI_z}{L^2} \\
0 & 0 & -12\frac{EI_y}{L^3} & 0 & 12\frac{\eta EI_y}{L^3} + 6\frac{EI_y}{L^2} & 0 & 0 & 0 & 12\frac{EI_y}{L^3} & 0 & 6\frac{EI_y}{L^2} & 0 \\
0 & 0 & 0 & -\frac{GJ}{L} & 0 & 0 & 0 & 0 & 0 & \frac{GJ}{L} & 0 & 0 \\
0 & 0 & -6\frac{EI_y}{L^2} & 0 & 6\frac{\eta EI_y}{L^2} + 2\frac{EI_y}{L} & 0 & 0 & 0 & 6\frac{EI_y}{L^2} & 0 & 4\frac{EI_y}{L} & 0 \\
0 & 6\frac{EI_z}{L^2} & 0 & 0 & 0 & 6\frac{\eta EI_z}{L^2} + 2\frac{EI_z}{L} & 0 & -6\frac{EI_z}{L^2} & 0 & 0 & 0 & 4\frac{EI_z}{L}
\end{bmatrix}$$

iv. Stiffness matrix of an element having rigid offset portion of length η from its first node

$$\mathbf{M}^e = \rho AL \begin{bmatrix}
\frac{1}{3} & 0 & 0 & 0 & 0 & 0 & \frac{1}{6} & 0 & 0 & 0 & 0 & 0 \\
0 & \frac{13}{35} & 0 & 0 & 0 & \frac{13}{35}\eta + \frac{11}{210}L & 0 & \frac{9}{70} & 0 & 0 & 0 & -\frac{13}{420}L \\
0 & 0 & \frac{13}{35} & 0 & -\frac{13}{35}\eta - \frac{11}{210}L & 0 & 0 & 0 & \frac{9}{70} & 0 & \frac{13}{420}L & 0 \\
0 & 0 & 0 & \frac{1}{3}\frac{J}{A} & 0 & 0 & 0 & 0 & 0 & \frac{1}{6}\frac{J}{A} & 0 & 0 \\
0 & 0 & -\frac{13}{35}\eta - \frac{11}{210}L & 0 & \frac{13}{35}\eta^2 + \frac{1}{105}\eta L + \frac{1}{105}L^2 & 0 & 0 & 0 & -\frac{9}{70}\eta - \frac{13}{420}L & 0 & -\frac{13}{420}\eta L - \frac{1}{140}L^2 & 0 \\
0 & \frac{13}{35}\eta + \frac{11}{210}L & 0 & 0 & 0 & \frac{13}{35}\eta^2 + \frac{1}{105}\eta L + \frac{1}{105}L^2 & 0 & \frac{9}{70}\eta + \frac{13}{420}L & 0 & 0 & 0 & -\frac{13}{420}\eta L - \frac{1}{140}L^2 \\
\frac{1}{6} & 0 & 0 & 0 & 0 & 0 & \frac{1}{3} & 0 & 0 & 0 & 0 & 0 \\
0 & \frac{9}{70} & 0 & 0 & 0 & \frac{9}{70}\eta + \frac{13}{420}L & 0 & \frac{13}{35} & 0 & 0 & 0 & -\frac{11}{210}L \\
0 & 0 & \frac{9}{70} & 0 & -\frac{9}{70}\eta - \frac{13}{420}L & 0 & 0 & 0 & \frac{13}{35} & 0 & \frac{11}{210}L & 0 \\
0 & 0 & 0 & \frac{1}{6}\frac{J}{A} & 0 & 0 & 0 & 0 & 0 & \frac{1}{3}\frac{J}{A} & 0 & 0 \\
0 & 0 & \frac{13}{420}L & 0 & -\frac{13}{420}\eta L - \frac{1}{140}L^2 & 0 & 0 & 0 & \frac{11}{210}L & 0 & \frac{1}{105}L^2 & 0 \\
0 & -\frac{13}{420}L & 0 & 0 & 0 & -\frac{13}{420}\eta L - \frac{1}{140}L^2 & 0 & -\frac{11}{210}L & 0 & 0 & 0 & \frac{1}{105}L^2
\end{bmatrix}$$

$$+\rho AL \begin{bmatrix}
0 & 0 & 0 & 0 & 0 & 0 & 0 & 0 & 0 & 0 & 0 & 0 \\
0 & \frac{6}{5}\frac{I_z}{AL^2} & 0 & 0 & 0 & \frac{1}{10}\frac{I_z}{AL} & 0 & -\frac{6}{5}\frac{I_z}{AL^2} & 0 & 0 & 0 & \frac{1}{10}\frac{I_z}{AL} \\
0 & 0 & \frac{6}{5}\frac{I_y}{AL^2} & 0 & -\frac{1}{10}\frac{I_y}{AL} & 0 & 0 & 0 & -\frac{6}{5}\frac{I_y}{AL^2} & 0 & -\frac{1}{10}\frac{I_y}{AL} & 0 \\
0 & 0 & 0 & 0 & 0 & 0 & 0 & 0 & 0 & 0 & 0 & 0 \\
0 & 0 & -\frac{1}{10}\frac{I_y}{AL} & 0 & \frac{2}{15}I_y A & 0 & 0 & 0 & \frac{1}{10}\frac{I_y}{AL} & 0 & \frac{1}{30}\frac{I_y}{A} & 0 \\
0 & \frac{1}{10}\frac{I_z}{AL} & 0 & 0 & 0 & \frac{2}{15}I_z A & 0 & -\frac{1}{10}\frac{I_z}{AL} & 0 & 0 & 0 & \frac{1}{30}\frac{I_z}{A} \\
0 & 0 & 0 & 0 & 0 & 0 & 0 & 0 & 0 & 0 & 0 & 0 \\
0 & -\frac{6}{5}\frac{I_z}{AL^2} & 0 & 0 & 0 & -\frac{1}{10}\frac{I_z}{AL} & 0 & \frac{6}{5}\frac{I_z}{AL^2} & 0 & 0 & 0 & -\frac{1}{10}\frac{I_z}{AL} \\
0 & 0 & -\frac{6}{5}\frac{I_y}{AL^2} & 0 & \frac{1}{10}\frac{I_y}{AL} & 0 & 0 & 0 & \frac{6}{5}\frac{I_y}{AL^2} & 0 & \frac{1}{10}\frac{I_y}{AL} & 0 \\
0 & 0 & 0 & 0 & 0 & 0 & 0 & 0 & 0 & 0 & 0 & 0 \\
0 & 0 & -\frac{1}{10}\frac{I_y}{AL} & 0 & -\frac{1}{30}\frac{I_y}{A} & 0 & 0 & 0 & \frac{1}{10}\frac{I_y}{AL} & 0 & \frac{2}{15}I_y A & 0 \\
0 & \frac{1}{10}\frac{I_z}{AL} & 0 & 0 & 0 & -\frac{1}{30}\frac{I_z}{A} & 0 & -\frac{1}{10}\frac{I_z}{AL} & 0 & 0 & 0 & \frac{2}{15}I_z A
\end{bmatrix}$$

v. Mass matrix of an element having rigid offset portion of length η from its first node

$$\frac{d\mathbf{K}^e}{d\eta} = \begin{bmatrix}
0 & 0 & 0 & 0 & 0 & 0 & 0 & 0 & 0 & 0 & 0 & 0 \\
0 & 0 & 0 & 0 & 0 & 12\frac{EI_y}{L^3} & 0 & 0 & 0 & 0 & 0 & 0 \\
0 & 0 & 0 & 0 & -12\frac{EI_y}{L^3} & 0 & 0 & 0 & 0 & 0 & 0 & 0 \\
0 & 0 & 0 & 0 & 0 & 0 & 0 & 0 & 0 & 0 & 0 & 0 \\
0 & 0 & -12\frac{EI_y}{L^3} & 0 & 24\frac{\eta EI_y}{L^3} + 12\frac{EI_y}{L^2} & 0 & 0 & 0 & 12\frac{EI_y}{L^3} & 0 & 6\frac{EI_y}{L^2} & 0 \\
0 & 12\frac{EI_z}{L^3} & 0 & 0 & 0 & 24\frac{\eta EI_z}{L^3} + 12\frac{EI_z}{L^2} & 0 & -12\frac{EI_z}{L^3} & 0 & 0 & 0 & 6\frac{EI_z}{L^2} \\
0 & 0 & 0 & 0 & 0 & 0 & 0 & 0 & 0 & 0 & 0 & 0 \\
0 & 0 & 0 & 0 & 0 & -12\frac{EI_z}{L^3} & 0 & 0 & 0 & 0 & 0 & 0 \\
0 & 0 & 0 & 0 & 12\frac{EI_y}{L^3} & 0 & 0 & 0 & 0 & 0 & 0 & 0 \\
0 & 0 & 0 & 0 & 0 & 0 & 0 & 0 & 0 & 0 & 0 & 0 \\
0 & 0 & 0 & 0 & 6\frac{EI_y}{L^2} & 0 & 0 & 0 & 0 & 0 & 0 & 0 \\
0 & 0 & 0 & 0 & 0 & 6\frac{EI_z}{L^2} & 0 & 0 & 0 & 0 & 0 & 0
\end{bmatrix}$$

vi. Derivative of the elemental structural stiffness matrix with respect to rigid offset η

$$\frac{d\mathbf{M}^e}{d\eta} = \rho AL \begin{bmatrix}
0 & 0 & 0 & 0 & 0 & 0 & 0 & 0 & 0 & 0 & 0 & 0 \\
0 & 0 & 0 & 0 & 0 & \frac{13}{35} & 0 & 0 & 0 & 0 & 0 & 0 \\
0 & 0 & 0 & 0 & -\frac{13}{35} & 0 & 0 & 0 & 0 & 0 & 0 & 0 \\
0 & 0 & 0 & 0 & 0 & 0 & 0 & 0 & 0 & 0 & 0 & 0 \\
0 & 0 & -\frac{13}{35} & 0 & \frac{26}{35}\eta + \frac{1}{105}L & 0 & 0 & 0 & -\frac{9}{70} & 0 & -\frac{13}{420}L & 0 \\
0 & \frac{13}{35} & 0 & 0 & 0 & \frac{26}{35}\eta + \frac{1}{105}L & 0 & \frac{9}{70} & 0 & 0 & 0 & -\frac{13}{420}L \\
0 & 0 & 0 & 0 & 0 & 0 & 0 & 0 & 0 & 0 & 0 & 0 \\
0 & 0 & 0 & 0 & 0 & \frac{9}{70} & 0 & 0 & 0 & 0 & 0 & 0 \\
0 & 0 & 0 & 0 & -\frac{9}{70} & 0 & 0 & 0 & 0 & 0 & 0 & 0 \\
0 & 0 & 0 & 0 & 0 & 0 & 0 & 0 & 0 & 0 & 0 & 0 \\
0 & 0 & 0 & 0 & -\frac{13}{420}L & 0 & 0 & 0 & 0 & 0 & 0 & 0 \\
0 & 0 & 0 & 0 & 0 & -\frac{13}{420}L & 0 & 0 & 0 & 0 & 0 & 0
\end{bmatrix}$$

vii. Derivative of the elemental mass matrix with respect to rigid offset η

$$\frac{d\mathbf{A}^e}{dL} = \begin{bmatrix}
-\frac{EA}{L^2} & 0 & 0 & 0 & 0 & 0 & \frac{EA}{L^2} & 0 & 0 & 0 & 0 & 0 \\
0 & -36\frac{EI_z}{L^4} & 0 & 0 & 0 & -36\frac{\eta EI_z}{L^4} - 12\frac{EI_z}{L^3} & 0 & 36\frac{EI_z}{L^4} & 0 & 0 & 0 & -12\frac{EI_z}{L^3} \\
0 & 0 & -36\frac{EI_y}{L^4} & 0 & 36\frac{\eta EI_y}{L^4} + 12\frac{EI_y}{L^3} & 0 & 0 & 0 & 36\frac{EI_y}{L^4} & 0 & 12\frac{EI_y}{L^3} & 0 \\
0 & 0 & 0 & -\frac{GJ}{L^2} & 0 & 0 & 0 & 0 & 0 & \frac{GJ}{L^2} & 0 & 0 \\
0 & 0 & 36\frac{\eta EI_y}{L^4} + 12\frac{EI_y}{L^3} & 0 & -36\frac{\eta^2 EI_y}{L^4} - 24\frac{\eta EI_y}{L^3} - 4\frac{EI_y}{L^2} & 0 & 0 & 0 & -36\frac{\eta EI_y}{L^4} - 12\frac{EI_y}{L^3} & 0 & -12\frac{\eta EI_y}{L^3} - 2\frac{EI_y}{L^2} & 0 \\
0 & -36\frac{\eta EI_z}{L^4} - 12\frac{EI_z}{L^3} & 0 & 0 & 0 & -36\frac{\eta^2 EI_z}{L^4} - 24\frac{\eta EI_z}{L^3} - 4\frac{EI_z}{L^2} & 0 & 36\frac{\eta EI_z}{L^4} + 12\frac{EI_z}{L^3} & 0 & 0 & 0 & -12\frac{\eta EI_z}{L^3} - 2\frac{EI_z}{L^2} \\
\frac{EA}{L^2} & 0 & 0 & 0 & 0 & 0 & -\frac{EA}{L^2} & 0 & 0 & 0 & 0 & 0 \\
0 & 36\frac{EI_z}{L^4} & 0 & 0 & 0 & 36\frac{\eta EI_z}{L^4} + 12\frac{EI_z}{L^3} & 0 & -36\frac{EI_z}{L^4} & 0 & 0 & 0 & 12\frac{EI_z}{L^3} \\
0 & 0 & 36\frac{EI_y}{L^4} & 0 & -36\frac{\eta EI_y}{L^4} - 12\frac{EI_y}{L^3} & 0 & 0 & 0 & -36\frac{EI_y}{L^4} & 0 & -12\frac{EI_y}{L^3} & 0 \\
0 & 0 & 0 & \frac{GJ}{L^2} & 0 & 0 & 0 & 0 & 0 & -\frac{GJ}{L^2} & 0 & 0 \\
0 & 0 & 12\frac{EI_y}{L^3} & 0 & -12\frac{\eta EI_y}{L^3} - 2\frac{EI_y}{L^2} & 0 & 0 & 0 & -12\frac{EI_y}{L^3} & 0 & -4\frac{EI_y}{L^2} & 0 \\
0 & -12\frac{EI_z}{L^3} & 0 & 0 & 0 & -12\frac{\eta EI_z}{L^3} - 2\frac{EI_z}{L^2} & 0 & 12\frac{EI_z}{L^3} & 0 & 0 & 0 & -4\frac{EI_z}{L^2}
\end{bmatrix}$$

$$+e_{ij}\begin{bmatrix}
-L^{-2} & 0 & 0 & 0 & 0 & 0 & L^{-2} & 0 & 0 & 0 & 0 & 0 \\
0 & -\frac{6}{5}L^{-2} & 0 & 0 & 0 & 0 & 0 & \frac{6}{5}L^{-2} & 0 & 0 & 0 & 0 \\
0 & 0 & -\frac{6}{5}L^{-2} & 0 & 0 & 0 & 0 & 0 & \frac{6}{5}L^{-2} & 0 & 0 & 0 \\
0 & 0 & 0 & -\frac{J}{AL^2} & 0 & 0 & 0 & 0 & 0 & \frac{J}{AL^2} & 0 & 0 \\
0 & 0 & 0 & 0 & \frac{2}{15} & 0 & 0 & 0 & 0 & 0 & -\frac{1}{30} & 0 \\
0 & 0 & 0 & 0 & 0 & \frac{2}{15} & 0 & 0 & 0 & 0 & 0 & -\frac{1}{30} \\
L^{-2} & 0 & 0 & 0 & 0 & 0 & -L^{-2} & 0 & 0 & 0 & 0 & 0 \\
0 & \frac{6}{5}L^{-2} & 0 & 0 & 0 & 0 & 0 & -\frac{6}{5}L^{-2} & 0 & 0 & 0 & 0 \\
0 & 0 & \frac{6}{5}L^{-2} & 0 & 0 & 0 & 0 & 0 & -\frac{6}{5}L^{-2} & 0 & 0 & 0 \\
0 & 0 & 0 & \frac{J}{AL^2} & 0 & 0 & 0 & 0 & 0 & -\frac{J}{AL^2} & 0 & 0 \\
0 & 0 & 0 & 0 & -\frac{1}{3}0 & 0 & 0 & 0 & 0 & 0 & \frac{2}{15} & 0 \\
0 & 0 & 0 & 0 & 0 & -\frac{1}{30} & 0 & 0 & 0 & 0 & 0 & \frac{2}{15}
\end{bmatrix}$$

viii. Derivative of the total elemental stiffness matrix with respect to elemental length L

$$\frac{dM^e}{dL} = \rho A \begin{bmatrix}
\frac{1}{3} & 0 & 0 & 0 & 0 & 0 & \frac{1}{6} & 0 & 0 & 0 & 0 & 0 \\
0 & \frac{13}{35} & 0 & 0 & 0 & \frac{13}{35}\eta + \frac{11}{105}L & 0 & \frac{9}{70} & 0 & 0 & 0 & -\frac{13}{210}L \\
0 & 0 & \frac{13}{35} & 0 & -\frac{13}{35}\eta - \frac{11}{105}L & 0 & 0 & 0 & \frac{9}{70} & 0 & \frac{13}{210}L & 0 \\
0 & 0 & 0 & \frac{1}{3}\frac{J}{A} & 0 & 0 & 0 & 0 & 0 & \frac{1}{6}\frac{J}{A} & 0 & 0 \\
0 & 0 & -\frac{13}{35}\eta - \frac{11}{105}L & 0 & \frac{13}{35}\eta^2 + \frac{2}{105}\eta L + \frac{1}{35}L^2 & 0 & 0 & 0 & -\frac{9}{70}\eta - \frac{13}{210}L & 0 & -\frac{13}{210}\eta L - \frac{3}{140}L^2 & 0 \\
0 & \frac{13}{35}\eta + \frac{11}{105}L & 0 & 0 & 0 & \frac{13}{35}\eta^2 + \frac{2}{105}\eta L + \frac{1}{35}L^2 & 0 & \frac{9}{70}\eta + \frac{13}{210}L & 0 & 0 & 0 & -\frac{13}{210}\eta L - \frac{3}{140}L^2 \\
\frac{1}{6} & 0 & 0 & 0 & 0 & 0 & \frac{1}{3} & 0 & 0 & 0 & 0 & 0 \\
0 & \frac{9}{70} & 0 & 0 & 0 & \frac{9}{70}\eta + \frac{13}{210}L & 0 & \frac{13}{35} & 0 & 0 & 0 & -\frac{11}{105}L \\
0 & 0 & \frac{9}{70} & 0 & -\frac{9}{70}\eta - \frac{13}{210}L & 0 & 0 & 0 & \frac{13}{35} & 0 & \frac{11}{105}L & 0 \\
0 & 0 & 0 & \frac{1}{6}\frac{J}{A} & 0 & 0 & 0 & 0 & 0 & \frac{1}{3}\frac{J}{A} & 0 & 0 \\
0 & 0 & \frac{13}{210}L & 0 & -\frac{13}{210}\eta L - \frac{3}{140}L^2 & 0 & 0 & 0 & \frac{11}{105}L & 0 & \frac{1}{35}L^2 & 0 \\
0 & -\frac{13}{210}L & 0 & 0 & 0 & -\frac{13}{210}\eta L - \frac{3}{140}L^2 & 0 & -\frac{11}{105}L & 0 & 0 & 0 & \frac{1}{35}L^2
\end{bmatrix}$$

$$+\rho A \begin{bmatrix}
0 & 0 & 0 & 0 & 0 & 0 & 0 & 0 & 0 & 0 & 0 & 0 \\
0 & -\frac{6}{5}\frac{I_z}{AL^2} & 0 & 0 & 0 & 0 & 0 & \frac{6}{5}\frac{I_z}{AL^2} & 0 & 0 & 0 & 0 \\
0 & 0 & -\frac{6}{5}\frac{I_y}{AL^2} & 0 & 0 & 0 & 0 & 0 & \frac{6}{5}\frac{I_y}{AL^2} & 0 & 0 & 0 \\
0 & 0 & 0 & 0 & 0 & 0 & 0 & 0 & 0 & 0 & 0 & 0 \\
0 & 0 & 0 & 0 & \frac{2}{15}I_yA & 0 & 0 & 0 & 0 & 0 & \frac{1}{30}\frac{I_y}{A} & 0 \\
0 & 0 & 0 & 0 & 0 & \frac{2}{15}I_zA & 0 & 0 & 0 & 0 & 0 & \frac{1}{30}\frac{I_z}{A} \\
0 & 0 & 0 & 0 & 0 & 0 & 0 & 0 & 0 & 0 & 0 & 0 \\
0 & \frac{6}{5}\frac{I_z}{AL^2} & 0 & 0 & 0 & 0 & 0 & -\frac{6}{5}\frac{I_z}{AL^2} & 0 & 0 & 0 & 0 \\
0 & 0 & \frac{6}{5}\frac{I_y}{AL^2} & 0 & 0 & 0 & 0 & 0 & -\frac{6}{5}\frac{I_y}{AL^2} & 0 & 0 & 0 \\
0 & 0 & 0 & 0 & 0 & 0 & 0 & 0 & 0 & 0 & 0 & 0 \\
0 & 0 & 0 & 0 & -\frac{1}{30}\frac{I_y}{A} & 0 & 0 & 0 & 0 & 0 & \frac{2}{15}I_yA & 0 \\
0 & 0 & 0 & 0 & 0 & -\frac{1}{30}\frac{I_z}{A} & 0 & 0 & 0 & 0 & 0 & \frac{2}{15}I_zA
\end{bmatrix}$$

ix. Derivative of the elemental mass matrix with respect to elemental length L

Appendix B

Photographic Material

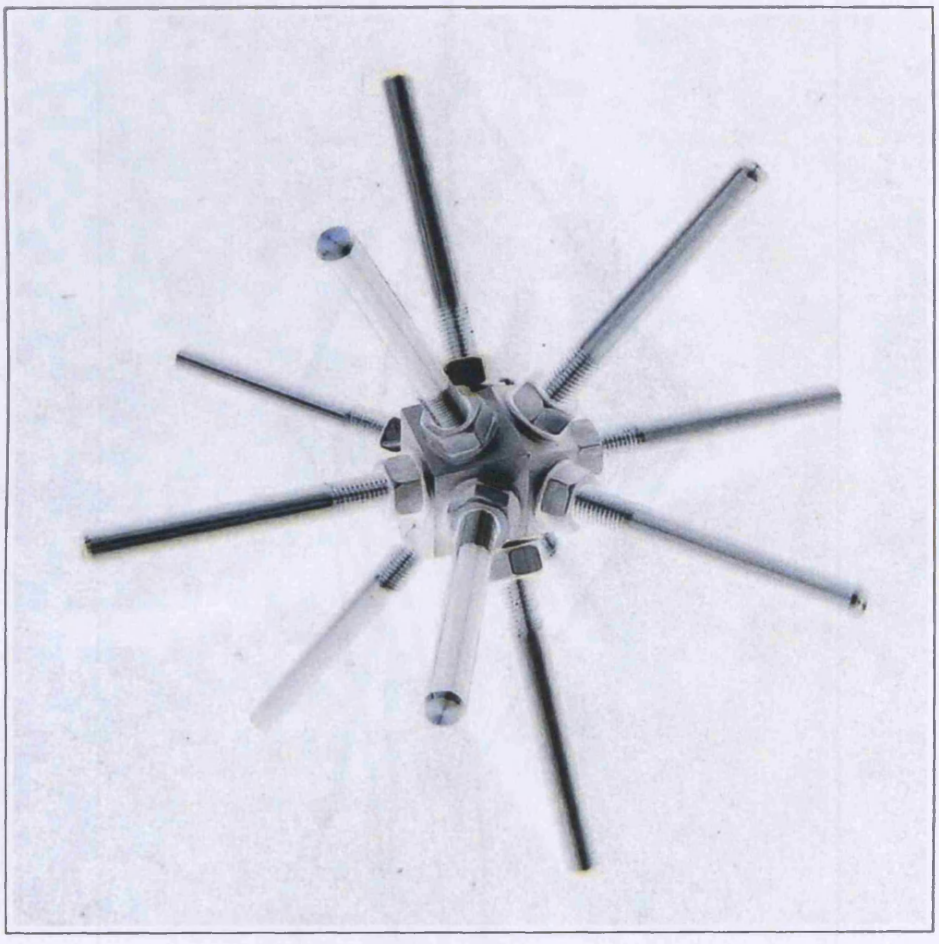

Figure B.1: Rhombic dodecahedral joint node.

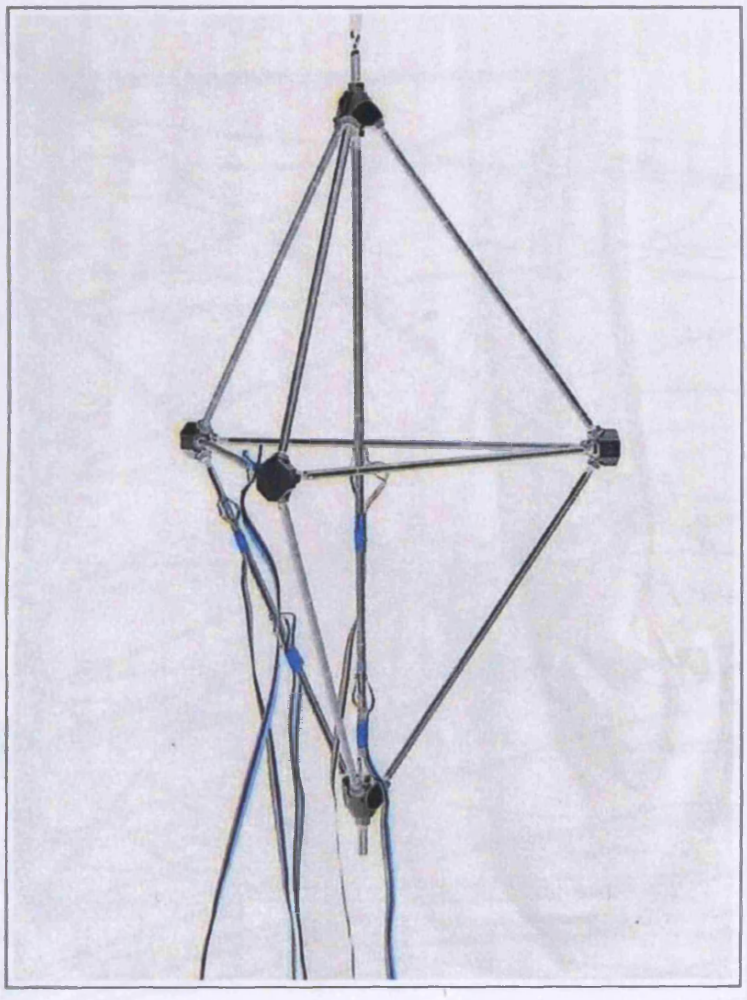

Figure B.2: Bi-tetrahedral space frame.

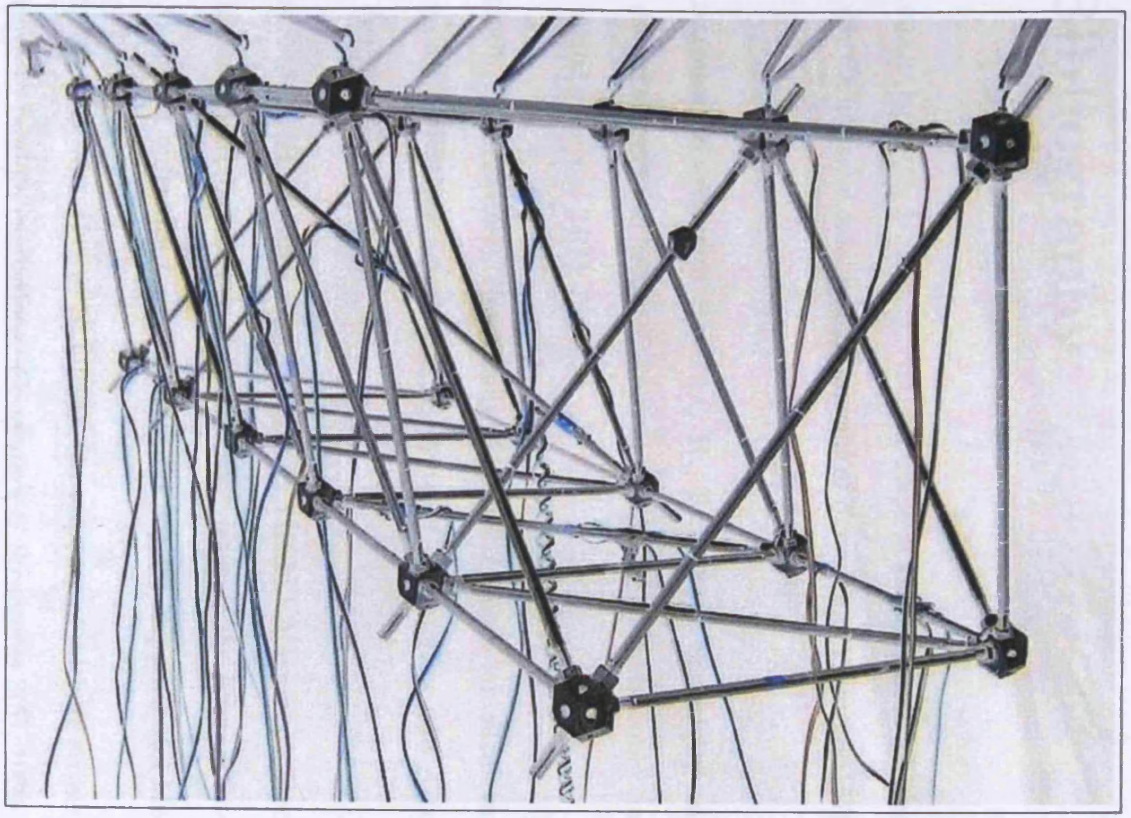

Figure B.3: Octet space frame.

Bibliography

ABRAHAMOVICH, H. (1992). Natural frequencies of Timoshenko beams under compressive axial loads. *Journal of Sound and Vibration* 157(1), 183–189.

ADELMAN, H. M. AND HAFTKA, R. T. (1986). Sensitivity analysis of discrete structural systems. *American Institute of Aeronautics and Astronautics Journal* 24(5), 823–832.

AKGÜN, M. A. (1994). New family of modal methods for calculating eigenvector derivatives. *American Institute of Aeronautics and Astronautics Journal* 32(2), 379–386.

ALLEMANG, R. J. AND BROWN, D. L. (1982). A correlation coefficient for modal vector analysis. In *The Proceedings of the International Modal Analysis Conference I.* pp. 110–116. Society for Experimental Mechanics.

ALPAY, I. B. AND UTKU, S. (1973). On response of initially stressed structures to random excitations. *Computers & Structures* 3(5), 1079–1097.

ANDERSON, M. AND NIMMO, N. A. (1985). Dynamic characteristics of statically determinate space-truss platforms. In *The Proceedings of the*

AIAA/ASME/ASCE/AHS Structures, Structural Dynamics and Materials Conference XXVI(II). pp. 723–728. New York.

ANDREW, A. L. (1978). Convergence of an iterative method for derivatives of eigensystems. *Journal of Computational Physics* 26, 107–112.

ANDREW, A. L. (1979). Iterative computation of derivatives of eigenvalues and eigenvectors. *Journal of the Institute of Mathematical Applications* 24, 209–218.

ANDREW, A. L. (1998). Finite and continuous perturbations of matrix eigenvalues. *Applied Mathematics Letters* 11(1), 47–51.

ANDREW, A. L. AND TAN, R. C. E. (1996). Computation of derivatives of repeated eigenvalues and corresponding eigenvectors by simultaneous iteration. *American Institute of Aeronautics and Astronautics Journal* 34(10), 2214–2216.

BAHRA, A. S. AND GREENING, P. D. 2005a. Mode traces in degenerate eigensystems and augmented assurance. *American Institute of Aeronautics and Astronautics Journal* 43(6), 1299–1305.

BAHRA, A. S. AND GREENING, P. D. 2005b. Particularities of Newton's method in space frame force determination, utilising eigenpair functions. *Journal of Sound and Vibration* 291(1-2), 462–490.

BAYCAN, C. M., UTKU, S., AND WADA, B. K. (1991). Control of resonant frequencies in adaptive structures by prestressing. In *The Proceedings of*

the Japan/USA Joint Conference on Adaptive Structures II. pp. 297–314. Nagoya, Japan.

BERNARD, M. L. AND BRONOWICKI, A. J. (1994). Modal expansion method for eigensensitivity with repeated roots. *American Institute of Aeronautics and Astronautics Journal* 32(7), 1500–1506.

BOKAIAN, A. 1988. Natural frequencies of beams under compressive axial load. *Journal of Sound and Vibration* 126(1), 49–65.

BOKAIAN, A. (1990). Natural frequencies of beams under tensile axial loads. *Journal of Sound and Vibration* 142(3), 481–498.

BRANDON, J. A. (1984). Derivation and significance of second-order modal design derivatives. *American Institute of Aeronautics and Astronautics Journal* 22(5), 723–724.

BRANDON, J. A. (1985). Author reply to A.H. Flax. *American Institute of Aeronautics and Astronautics Journal* 23(3), 479.

BRANDON, J. A. (1991). Second-order design sensitivities to assess the applicability of sensitivity analysis. *American Institute of Aeronautics and Astronautics Journal* 29(1), 135–139.

BUSHNELL, D. (1979)a. Control of surface configuration by application of concentrated loads. *American Institute of Aeronautics and Astronautics Journal* 17(1), 71–77.

BUSHNELL, D. (1979)b. Control of surface configuration of non-uniformly heated shells. *American Institute of Aeronautics and Astronautics Journal* 17(1), 78–84.

BĂLUŢ, N. AND GIONCU, V. (1990). The influence of geometrical tolerances on the behaviour of space structures. *International Journal of Space Structures* 15(3), 189–194.

CHEN, G. S., BRUNO, R., AND SALAMA, M. (1989). Selection of active member locations in adaptive structures. In *The Proceedings of the AIAA/ASME/ASCE/AHS Structures, Structural Dynamics And Materials Conference XXX.* pp. 1127–1135. Mobile, AL.

CHOI, K. M., CHO, S. W., KO, M. G., AND LEE, I. W. (2004). Higher order eigensensitivity analysis of damped systems with repeated eigenvalues. *Computers & Structures* 82(1), 63–69.

CHU, K. W. E. (1990). On multiple eigenvalues of matrices depending on several parameters. *SIAM Journal on Numerical Analysis* 27(October), 1368–1385.

CILLEY, F. H. (1900). The exact design of statically indeterminate frameworks, an exposition of its possibility, but futility. *Transactions of the ASCE* 43, 353–443.

COOK, R. D. 1974. *Concepts and Applications of Finite Element Analysis.* John Wiley & Sons, Inc.

DAILEY, R. L. (1989). Eigenvector derivatives with repeated eigenvalues. *American Institute of Aeronautics and Astronautics Journal* 27(4), 486–491.

D'AMBROGIO, W. AND FREGOLENT, A. (2003). Higher-order MAC for the correlation of close and multiple modes. *Mechanical Systems and Signal Processing* 17(3), 599–610.

DAS, S. K., UTKU, S., CHEN, G. S., AND WADA, B. K. (1991). Optimal placement of actuators in the precision control of truss structures. In *The Proceedings of the Biennial Conference on Mechanical Vibration and Noise XIII (ASME Design Technical Conferences)*. pp. 95–105. Miami, FL.

DOUGHTY, S. 1982. Eigenvalue derivatives of damped torsional vibrations. *Journal of Mechanical Design* 104, 463–465.

ELDRED, M. S., LERNER, P. B., AND ANDERSON, W. J. (1992). Improvement of normalization methods for eigenvector derivatives. *American Institute of Aeronautics and Astronautics Journal* 30(6), 1609–1616.

ELDRED, M. S., LESTARI, W., AND ANDERSON, W. J. (1992). Higher order eigenpair perturbations. *American Institute of Aeronautics and Astronautics Journal* 30(7), 1870–1876.

ELDRED, M. S., VENKAYYA, V. B., AND ANDERSON, W. J. (1995)a. Mode tracking issues in structural optimization. *American Institute of Aeronautics and Astronautics Journal* 33(10), 1926–1933.

ELDRED, M. S., VENKAYYA, V. B., AND ANDERSON, W. J. (1995)b. New mode tracking methods in aeroelastic analysis. *American Institute of Aeronautics and Astronautics Journal* 33(7), 1292–1299.

FLAX, A. H. (1985). Comment on 'Derivation and significance of second-order modal design sensitivities'. *American Institute of Aeronautics and Astronautics Journal* 23(3), 478.

FOX, R. L. AND KAPOOR, M. P. (1968). Rates of change of eigenvalues and eigenvectors. *American Institute of Aeronautics and Astronautics Journal* 6(12), 2426–2429.

FRISWELL, M. I. (1994). Calculation of second order eigenvector derivatives. *Journal of Guidance, Control and Dynamics* 18(4), 919–921.

FRISWELL, M. I. (1996). The derivatives of repeated eigenvalues and their associated eigenvectors. *Journal of Vibration and Acoustics* 118, 390–397.

GALEF, A. E. (1968). Bending frequencies of compressed beams. *Journal of the Acoustical Society of America* 44, 643.

GAO, W., CHEN, J. J., MA, H. B., AND MA, X. S. (2003). Optimal placement of active bars in active vibration control for piezoelectric intelligent truss structures with random parameters. *Computers & Structures* 81(1), 53–60.

GARG, S. (1973). Derivatives of eigensolutions for a general matrix. *American Institute of Aeronautics and Astronautics Journal* 11(8), 1191–1194.

GIBSON, W. 1992. *ASTROS-ID: Software for System Identification using Mathematical Programming*, Wright Lab TR WL-TR-92-3100 ed. Wright-Patterson AFB, Ohio.

GOLUB, G. H. AND VAN LOAN, C. F. 1983. *Matrix Computations*, First ed. The John Hopkins University Press, Baltimore, Maryland 21218.

GREENE, W. H. (1983). Effects of random member length errors on the accuracy and internal loads of truss antennas. In *The Proceedings of the AIAA/ASME/ASCE/AHS Structures, Structural Dynamics and Materials Conference XXIV.* pp. 697–704. Lake Tahoe Nevada.

GREENING, P. D. (1999). Dynamic finite element modelling and updating of loaded structures. *University of Bristol* Ph.D. thesis.

GREENING, P. D. AND LIEVEN, N. A. J. (2003). Identification and updating of loading in frameworks using dynamic measurements. *Journal of Sound and Vibration* 260(1), 101–115.

HAFTKA, R. T. 1984. Optimum placement of controls for static deformations of space structures. *American Institute of Aeronautics and Astronautics Journal* 22(9), 1293–1298.

HAFTKA, R. T. AND ADELMAN, H. M. (1985). An analytical investigation of shape control of large space structures by applied temperatures. *American Institute of Aeronautics and Astronautics Journal* 23(3), 450–457.

HANAOR, A. (1988). Prestressed pin-jointed structures — flexibility analysis and prestress design. *Computers & Structures* 28(6), 757–769.

HANAOR, A. AND LEVY, R. (1985). Imposed lack of fit as a means of enhancing space truss design. *Journal of Space Structures* 1(1), 147–154.

HAUG, E. J. AND ROUSSELET, B. (1980). Design sensitivity analysis in structural mechanics ii: Eigenvalue variations. *Journal of Structural Mechanics* 8(2), 161–186.

HEDGEPETH, J. M. (1982). Influence of fabrication tolerances on the surface accuracy of large antenna structures. *American Institute of Aeronautics and Astronautics Journal* 20(5), 680–686.

HOLNICKI-SZULC, J. (1979). Prestressing of truss and frame structures. *Journal of the Structural Division* 105(1), 601–616.

HOLNICKI-SZULC, J. AND HAFTKA, R. T. (1992). Vibration mode shape control by prestressing. *American Institute of Aeronautics and Astronautics Journal* 30(7), 1924–1927.

HOU, J. W. AND KENNY, S. (1992). Eigenvalue and eigenvector approximate analysis for repeated eigenvalue problems. *American Institute of Aeronautics and Astronautics Journal* 30(9), 2317–2324.

HOWSON, W. P. AND WILLIAMS, F. W. (1973). Natural frequencies of frames with axially loaded Timoshenko members. *Journal of Sound and Vibration* 26(4), 503–515.

IRSCHIK, H. (2002). A review on static and dynamic shape control of structures by piezoelectric actuation. *Engineering Structures* 24(1), 5–11.

IRWANTO, B., HARDTKE, H.-J., AND PAWANDENAT, D. (2003). An efficient technique for the computation of eigenvalue and eigenvector derivatives of cyclic structures. *Computers & Structures* 81(24-25), 2395–2400.

JACOBI, C. G. J. (1846). Uber ein leichtes verfahren die in der theorie der saecularstoerungen vorkommenden gleichung numerische aufzuloesen. *Zeitschrift für Reine unde Angewandte Mathematik* 30, 51–95.

JALIHAL, P., UTKU, S., AND WADA, B. K. (1996). Optimal location of redundants for prestressing adaptive structures. *Journal of Intelligent Material Systems and Structures* 7(4), 420–426.

JANKOVIC, M. S. 1994. Exact n^{th} derivatives of eigenvalues and eigenvectors. *Journal of Guidance, Control and Dynamics* 17(1), 136–144.

JENSEN, J. S. (2000). Buckling of an elastic beam with added high-frequency excitation. *International Journal of Nonlinear Mechanics* 35(2), 217–227.

KATO, T. 1976. *Perturbation Theory for Linear Operators*, Second ed. Springer-Verlag Berlin Heidelberg, New York.

KIM, K. O. AND WALLERSTEIN, D. V. (1987). Modal design sensitivities for multiple eigenvalues. *Computers & Structures* 29(5), 755–762.

KIM, T. S. AND KIM, Y. Y. (2000). MAC-based mode-tracking in structural topology optimization. *Computers & Structures* 74(3), 375–383.

KOLLO, T. AND NEUDECKER, H. (1997). The derivative of an orthogonal matrix of eigenvectors of a symmetric matrix. *Linear Algebra and its Applications* 264(1-3), 489–493.

KUTTLER, J. R. AND SIGILLITO, V. G. (1981). On curve veering. *Journal of Sound and Vibration* 75(4), 585–588.

LALLEMENT, G. AND KOSANEK, J. (1993). Parametric correction of self adjoint finite element models in the presence of multiple eigenvalues. In *The Proceedings of the Modern Practice in Stress and Vibration Analysis Conference.* pp. 593–603. Sheffield, England.

LANCASTER, P. (1960). Free vibrations of lightly damped systems by perturbation methods. *Quarterly Journal of Mechanics and Applied Mathematics* 13(2), 138–155.

LANCASTER, P. (1963). Some applications of the Newton-Raphson method to nonlinear matrix problems. *Proceedings of the Royal Society* 271, 324–331.

LANCASTER, P. (1964). On eigenvalues of matrices dependent on a parameter. *Numerische Mathematik* 6, 377–387.

LAURA, P. A. A. (1992). Comment on 'Natural frequencies of beams under tensile axial load'. *Journal of Sound and Vibration* 152(2), 381.

LAURA, P. A. A., DE IRASSAR, V., P., AND FICCADENTI, G. M. (1983). A note on transverse vibrations of continuous beams subject to an axial force

and carrying concentrated masses. *Journal of Sound and Vibration* 86(2), 279–284.

LEE, I. W. AND JUNG, G. H. (1997). An efficient algebraic method for the computation of natural frequency and mode shape sensitivities — part ii: multiple natural frequencies. *Computers & Structures* 62(3), 437–443.

LEE, I.-W., KIM, D.-O., AND JUNG, G.-H. (1999). Natural frequency and mode shape sensitivities of damped systems: part ii, multiple natural frequencies. *Journal of Sound and Vibration* 223(3), 413–424.

LEE, I.-W., J. G.-H. AND LEE, J.-W. (1996). Numerical method for sensitivity analysis of eigensystems with non-repeated and repeated eigenvalues. *Journal of Sound and Vibration* 195(1), 17–32.

LEISSA, A. W. (1974). On a curve veering aberration. *Journal of Applied Mathematics and Physics (ZAMP)* 25, 99–111.

LEVY, R. AND HANAOR, A. (1991). Optimal design of prestressed trusses. *Computers & Structures* 43(4), 741–744.

LIEVEN, N. A. J. AND GREENING, P. D. (2001). Effect of experimental prestress and residual stress on modal behaviour. *Philosophical Transactions of the Royal Society* 359, 97–111.

LIM, K. AND JUANG, J. N. (1989). Eigenvector derivatives of repeated eigenvalues using singular value decomposition. *Journal of Guidance, Control and Dynamics* 12(2), 282–283.

LIM, K. B., JUNKINS, J. L., AND WANG, B. P. (1987). Re-examination of eigenvector derivatives. *Journal of Guidance, Control and Dynamics* 10(6), 581–587.

LIN, R. M., WANG, Z., AND LIM, M. K. (1996). A practical algorithm for the efficient computation of eigenvector sensitivities. *Computer Methods in Applied Mechanics and Engineering* 130(3-4), 355–367.

LIU, C. Q., LIU, X. B., AND CHANG, C. C. (1995). On sensitivity analysis of discrete structural systems. *Computers & Structures* 56(1), 141–145.

LIU, X. L. (2002). Behavior of derivatives of eigenvalues and eigenvectors in curve veering and mode localization and their relation to close eigenvalues. *Journal of Sound and Vibration* 256(3), 551–564.

LIU, X. Q., ERTEKIN, R. C., AND RIGGS, H. R. (1996). Vibration of a free-free beam under tensile axial loads. *Journal of Sound and Vibration* 190(2), 273–282.

LIU, Z., CHEN, S., YU, M., AND ZHAO, Y. (1994). Contribution of the truncated modes to eigenvector derivatives. *American Institute of Aeronautics and Astronautics Journal* 32(7), 1551–1553.

LIU, Z., CHEN, S., AND ZHAO, Y. (1994). An accurate method for computing eigenvector derivatives for free-free structures. *Computers & Structures* 52(6), 1135–1143.

LORD RAYLEIGH, J. W. S. 1877. *The Theory of Sound*, Second ed. Dover Publications , Inc., New York, 1945.

LU, L. Y., BAIN, J. J., AND CHUNG, L. L. (1999). Use of the active member concept in vibration mitigation of seismic structures. *Engineering Structures* 21(4), 341–351.

LURIE, H. (1951). Effective end restraint of columns by frequency measurements. *Journal of the Acoustical Society of America* 19, 21–22.

MA, F. AND NG, C. H. (2004). On the orthogonality of natural modes of vibration. *Mechanics Research Communications* 31(3), 295–299.

MACKIEWICZ, A., HOLNICKI-SZULC, J., AND LOPEZ-ALMANSA, F. (1995). Optimal sensor location in active control of flexible structures. *American Institute of Aeronautics and Astronautics Journal* 34(4), 857–859.

MEAD, D. J. (2002). Free vibrations of self-strained assemblies of beams. *Journal of Sound and Vibration* 249(1), 101–127.

MEAD, D. J. (2003). Vibration and buckling of flat free-free plates under non-uniform in-plane thermal stresses. *Journal of Sound and Vibration* 260(1), 141–165.

MILLS-CURRAN, W. C. (1988). Calculation of eigenvector derivatives for structures with repeated eigenvalues. *American Institute of Aeronautics and Astronautics Journal* 26(7), 867–871.

MILLS-CURRAN, W. C. (1989). Comment on 'Eigenvector derivatives with repeated eigenvalues'. *American Institute of Aeronautics and Astronautics Journal* 28(10), 1846.

MOTTERSHEAD, J. E., FRISWELL, M. I., AND BRANDON, J. A. (1996). Geometric parameters for finite element model updating of joints and constraints. *Mechanical Systems and Signal Processing* 10(2), 171–182.

MOTTERSHEAD, J. E. AND JAMES, S. (1998). Updating parameters for the model of a three storey aluminium space frame. In *The Proceedings of the International Modal Analysis Conference XVI.* pp. 8–11. The Society for Experimental Mechanics.

MOTTERSHEAD, J. E., MARES, C., FRISWELL, M. I., AND JAMES, S. (2000). Selection and updating of parameters for an aluminium space-frame model. *Mechanical Systems and Signal Processing* 6(14), 923–944.

MURTHY, D. V. AND HAFTKA, R. T. (1988). Derivatives of eigenvalues and eigenvectors of a general complex matrix. *International Journal for Numerical Methods in Engineering* 26, 293–311.

NAGULESWARAN, S. (2004). Transverse vibration of an uniform Euler-Bernoulli beam under linearly varying axial force. *Journal of Sound and Vibration* 275(1-2), 47–57.

NATORI, M. AND IWASAKI, K. (1987). Adaptive planar trusses and their vibration characteristics. In *The Proceedings of the*

AIAA/ASME/ASCE/AHS Structures, Structural Dynamics and Materials Conference XXVIII. pp. 143–151. Monterey, CA.

NATSIAVAS, S. (1993). Mode localization and frequency veering in a non-conservative mechanical system with dissimilar components. *Journal of Sound and Vibration* 165(1), 137–147.

NELSON, R. B. (1976). Simplified calculation of eigenvector derivatives. *American Institute of Aeronautics and Astronautics Journal* 14(9), 1201–1205.

NEWTON, I. (1711). *De analysi per aequationes numero terminorum infinitas, 1669.*

NEWTON, I. (1736). *Methodus fluxionum et serierum infinitarum, 1671.*

OJALVO, I. U. (1988). Efficient computation of modal sensitivities for systems with repeated frequencies. *American Institute of Aeronautics and Astronautics Journal* 26(3), 361–365.

OVUNC, B. A. (1980). Effect of axial force on framework dynamics. *Computers & Structures* 11, 389–395.

PERKINS, N. C. AND MOTE, C. D. (1986). Comments on curve veering problems in eigenvalue problems. *Journal of Sound and Vibration* 106(3), 451–463.

PEŜEK, L. (1995). An extension of the inverse sensitivity method to systems with repeated eigenvalues. *Journal of Sound and Vibration* 182(4), 623–635.

PETYT, M. AND FLEISCHER, C. C. (1971). Free vibration of a curved beam. *Journal of Sound and Vibration* 18(1), 17–30.

PIERRE, C. (1988). Mode localization and eigenvalue loci veering phenomena in disordered structures. *Journal of Sound and Vibration* 126(3), 485–502.

PIERRE, C. AND CHA, P. D. (1989). Strong mode localization in nearly periodic disordered structures. *American Institute of Aeronautics and Astronautics Journal* 27(2), 227–241.

PIERRE, C. AND DOWELL, E. H. (1987). Localization of vibrations by structural irregularity. *Journal of Sound and Vibration* 114(3), 549–564.

PLAUT, R. H. AND HUSEYIN, K. (1973). Derivatives of eigenvalues and eigenvectors in non-self-adjoint systems. *American Institute of Aeronautics and Astronautics Journal* 11(2), 250–251.

PRZEMIENIECKI, J. S. 1968. *Theory of Matrix Structural Analysis.* McGraw Hill, Inc.

PRZYBYLSKI, J. (2000). The role of prestressing in establishing regions of instability for a compound column under conservative or non-conservative load. *Journal of Sound and Vibration* 231(2), 291–305.

PRZYBYLSKI, J., TOMSKI, L., AND GOLEBIOWSKA-ROZANOW, M. (1996). Free vibration of an axially loaded prestressed planar frame. *Journal of Sound and Vibration* 189(5), 609–624.

RAMESH, A. V., UTKU, S., AND WADA, B. K. (1991). Real-time control of geometry and stiffness in adaptive structures. *Computer Methods in Applied Mechanics and Engineering* 90(1-3), 761–779.

RAPHSON, J. (1690). *Analysis aequationum universalis.*

ROGERS, L. C. 1970. Derivatives of eigenvalues and eigenvectors. *American Institute of Aeronautics and Astronautics Journal* 8(5), 943–944.

RONG, J. H., XIE, Y. M., YANG, X. Y., AND LIANG, Q. Q. (2000). Topology optimization of structures under dynamic response constraints. *Journal of Sound and Vibration* 234(2), 177–189.

RUDISILL, C. S. (1974). Derivatives of eigenvalues and eigenvectors for a general matrix. *American Institute of Aeronautics and Astronautics Journal* 12(5), 721–722.

RUDISILL, C. S. AND CHU, Y.-Y. (1975). Numerical methods for evaluating the derivatives of eigenvalues and eigenvectors. *American Institute of Aeronautics and Astronautics Journal* 13(9), 834–837.

SHAKER, F. J. (1975). Effect of axial load on mode shapes and frequencies of beams. Tech. Rep. NASA-TN-8109, NASA. 30 Pages.

SHAW, J. AND JAYASURIYA, S. (1991). Modal sensitivities for repeated eigenvalues and eigenvalue derivatives. *American Institute of Aeronautics and Astronautics Journal* 30(3), 850–852.

SIMPSON, A. (1976). On the rates of change of sets of equal eigenvalues. *Journal of Sound and Vibration* 44(1), 83–102.

SONG, D., W-Z, H., S-H., C., AND QUI, Z. (1995). Simplified calculation of eigenvector derivatives with repeated eigenvalues. *American Institute of Aeronautics and Astronautics Journal* 34(4), 859–862.

SPILLERS, W. R. AND LEVY, R. (1984). Truss design: two loading conditions with prestress. *Journal of Structural Engineering* 110(1), 677–687.

STEPHEN, N. G. (1989). Beam vibration under compressive axial load: upper and lower bound approximation. *Journal of Sound and Vibration* 131(2), 345–350.

STEPHENS, B. C. 1936. Natural vibration frequencies of structural members as an indication of end fixity and magnitude of stress. *Journal of the Aeronautical Sciences* 4, 54–60.

STEWART, G. W. (1972). On the sensitivity of the eigenvalue problem $\mathbf{Ax} = \lambda \mathbf{Bx}$. *SIAM Journal on Numerical Analysis* 9(4), 669–686.

SUNDARARAJAN, C. (1992). Frequency analysis of axially loaded structures. *American Institute of Aeronautics and Astronautics Journal* 30(4), 1139–1141.

SUTTER, T. R., CAMARDA, C. J., WALSH, J. L., AND ADELMAN, H. M. (1988). Comparison of several methods for calculating vibration mode shape derivatives. *American Institute of Aeronautics and Astronautics Journal* 26(12), 1506–1511.

TANG, J. AND WANG, W.-L. (1999). On calculation of sensitivity for non-defective eigenproblems with repeated roots. *Journal of Sound and Vibration* 225(4), 611–631.

TARNAI, T. (1980). Simultaneous static and kinematic indeterminacy of space trusses with cyclic symmetry. *International Journal of Solids and Structures* 16(4), 347–359.

TAYLOR, D. L. AND KANE, T. R. (1975). Multiparameter quadratic eigenproblems. *Journal of Applied Mechanics* June, 478–483.

TING, T., CHEN, T. L. C., AND TWOMEY, W. J. (1995). Automated mode tracking strategy. *American Institute of Aeronautics and Astronautics Journal* 33(1), 183–185.

TOMSKI, L., PRZYBYLSKI, J., GOLEBIOWSKA-ROZANOW, M., AND SZMIDLA, J. (1998). Vibration and stability of a cantilever column subject to a follower force passing through a fixed point. *Journal of Sound and Vibration* 214(1), 67–81.

UTKU, S., RAMESH, A. V., DAS, S. K., WADA, B. K., AND CHEN, G. S. (1991). Control of a slow-moving space crane as an adaptive structure.

American Institute of Aeronautics and Astronautics Journal 29(6), 961–967.

VIRGIN, L. N. (1985). The dynamics of symmetric post-buckling. *International Journal of Mechanical Science* 27(4), 235–248.

VIRGIN, L. N. AND PLAUT, R. H. (1993). Effect of axial load on forced vibrations of beams. *Journal of Sound and Vibration* 168(3), 395–405.

WALTHER, H., KMETYK, L., HOLZMANN, W., AND SEGALMAN, D. (2004). Model correlation with closely spaced modes. In *The Proceedings of the International Modal Analysis Conference XXII.* pp. 1–8. The Society For Experimental Mechanics.

WANG, B. P. (1991). Improved approximate methods for computing eigenvector derivatives in structural dynamics. *American Institute of Aeronautics and Astronautics Journal* 29(6), 1018–1020.

WANXIE, Z. AND GENGDONG, C. (1986). Second-order sensitivity analysis of multimodal eigenvalues and related optimization techniques. *Journal of Structural Mechanics* 14(4), 421–436.

WITTRICK, W. H. (1962). Rates of change of eigenvalues, with reference to buckling and vibration problems. *Journal of the Royal Aeronautical Society* 66, 590–591.

XIAOCHENG, X. (1999). Random response analysis of prestressed structures using MSC/NASTRAN. In *The Proceedings of the MSC Aerospace Users' Conference*. pp. 1–5. MSC.

YU, M., LIU, Z. S., AND WANG, D. J. (1997). Comparison of several approximate modal methods for computing mode shape derivatives. *Computers & Structures* 62(2), 381–393.

ZHAO, Y. Q., LIU, Z. S., CHEN, S. H., AND ZHANG, G. Y. (1999). An accurate modal truncation method for eigenvector derivatives. *Computers & Structures* 73(6), 609–614.